

*Midwest States' Regional Pooled Fund Research Program
Fiscal Years 2003-2005 (Years 14 and 15)
Research Project Number SPR-3(017)
NDOR Sponsoring Agency Code RFPF-04-03 and RFPF-05-05*

EVALUATION OF CRITICAL FLARE RATES FOR THE MIDWEST GUARDRAIL SYSTEM (MGS)

Submitted by

Cody S. Stolle
Undergraduate Research Assistant

Karla A. Polivka, M.S.M.E., E.I.T.
Research Associate Engineer

John D. Reid, Ph.D.
Professor

Ronald K. Faller, Ph.D., P.E.
Research Assistant Professor

Dean L. Sicking, Ph.D., P.E.
Professor and MwRSF Director

Robert W. Bielenberg, M.S.M.E., E.I.T.
Research Associate Engineer

John R. Rohde, Ph.D., P.E.
Associate Professor

MIDWEST ROADSIDE SAFETY FACILITY

University of Nebraska-Lincoln
527 Nebraska Hall
Lincoln, Nebraska 68588-0529
(402) 472-0965

Submitted to

MIDWEST STATES' REGIONAL POOLED FUND PROGRAM

Nebraska Department of Roads
1500 Nebraska Highway 2
Lincoln, Nebraska 68502

MwRSF Research Report No. TRP-03-191-08

July 15, 2008

Technical Report Documentation Page

1. Report No. TRP-03-191-08	2.	3. Recipient's Accession No.	
4. Title and Subtitle EVALUATION OF CRITICAL FLARE RATES FOR THE MIDWEST GUARDRAIL SYSTEM (MGS)		5. Report Date July 15, 2008	
		6.	
7. Author(s) Stolle, C.S., Polivka, K.A., Reid, J.D., Faller, R.K., Sicking, D.L., Bielenberg, R.W., and Rohde, J.R.		8. Performing Organization Report No. TRP-03-191-08	
9. Performing Organization Name and Address Midwest Roadside Safety Facility (MwRSF) University of Nebraska-Lincoln 527 Nebraska Hall Lincoln, Nebraska 68588-0529		10. Project/Task/Work Unit No.	
		11. Contract © or Grant (G) No. SPR-3(017)	
12. Sponsoring Organization Name and Address Midwest States' Regional Pooled Fund Program Nebraska Department of Roads 1500 Nebraska Highway 2 Lincoln, Nebraska 68502		13. Type of Report and Period Covered Final Report 2003-2008	
		14. Sponsoring Agency Code RPFP-04-03, RPFP-05-05	
15. Supplementary Notes Prepared in cooperation with U.S. Department of Transportation, Federal Highway Administration			
16. Abstract (Limit: 200 words) <p>The potential to increase suggested flare rates for strong post, W-beam guardrail systems, and thus reduce guardrail installation lengths, is investigated. This reduction in length would result in decreased guardrail construction and maintenance costs, and reduced impact frequency. If the W-beam guardrail can withstand the higher impact angles, with only modest increases in accident severity, total accident costs can be reduced. Computer simulation and five full-scale crash tests were completed to evaluate increased flare rates up to, and including, 5:1. Computer simulations indicated that conventional G4(1S) guardrail modified to incorporate a routed wood block could not successfully meet NCHRP Report 350 crash test criteria when installed at any steeper flare rates than the 15:1 recommended in the Roadside Design Guide. However, computer modeling and full-scale crash testing showed that the Midwest Guardrail System (MGS) could meet NCHRP Report 350 impact criteria when installed at a 5:1 flare rate. Impact severities during testing were found to be greater than intended, yet the MGS passed all NCHRP 350 requirements. Hence, flaring the MGS guardrail as much as 5:1 will still provide acceptable safety performance for the full range of passenger vehicles. Increasing guardrail flare rates will reduce the overall number of guardrail crashes without significantly increasing risks of injury or fatality during the remaining crashes. Therefore, it is recommended that, whenever guardrail is outside of the shy line for adjacent traffic and the roadside terrain is sufficiently flat, flare rates should be increased to as high as 5:1 when using the MGS guardrail.</p>			
17. Document Analysis/Descriptors Highway Safety, Longitudinal Barriers, Guardrail, MGS, Flare Rates, Roadside Appurtenances, Crash Test, Compliance Test		18. Availability Statement No restrictions. Document available from: National Technical Information Services, Springfield, Virginia 22161	
19. Security Class (this report) Unclassified	20. Security Class (this page) Unclassified	21. No. of Pages 294	22. Price

DISCLAIMER STATEMENT

The contents of this report reflect the views of the authors who are responsible for the facts and the accuracy of the data presented herein. The contents do not necessarily reflect the official views nor policies of the State Highway Departments participating in the Midwest States' Regional Pooled Fund Research Program nor the Federal Highway Administration. This report does not constitute a standard, specification, or regulation.

ACKNOWLEDGMENTS

The authors wish to acknowledge several sources that made a contribution to this project:(1) the Midwest Regional States' Pooled Fund Program funded by the Connecticut Department of Transportation, Illinois Department of Transportation, Iowa Department of Transportation, Kansas Department of Transportation, Minnesota Department of Transportation, Missouri Department of Transportation, Nebraska Department of Roads, New Jersey Department of Transportation, Ohio Department of Transportation, South Dakota Department of Transportation, Wisconsin Department of Transportation, and Wyoming Department of Transportation for funding this project; and (2) MwRSF staff for constructing the barriers and conducting the crash tests.

Acknowledgment is also given to the following individuals who made a contribution to the completion of this research project.

Midwest Roadside Safety Facility

J.C. Holloway, Research Manager
C.L. Meyer, B.S.M.E., E.I.T., Research Engineer II
S.K. Rosenbaugh, M.S.C.E., E.I.T., Research Associate Engineer
A.T. Russell, B.S.B.A., Laboratory Mechanic II
K.L. Krenk, B.S.M.A., Field Operations Manager
A.T. McMaster, Laboratory Mechanic I
Undergraduate and Graduate Assistants

Connecticut Department of Transportation

Dionysia Oliveira, Transportation Engineer 3

Illinois Department of Transportation

David Piper, P.E., Highway Policy Engineer

Iowa Department of Transportation

David Little, P.E., Assistant District Engineer
Deanna Maifield, P.E., Methods Engineer
Chris Poole, Transportation Engineer Specialist

Kansas Department of Transportation

Ron Seitz, P.E., Bureau Chief
Rod Lacy, P.E., Road Design Leader
Scott W. King, P.E., Road Design Leader

Minnesota Department of Transportation

Mohammed Dehdashti, P.E., Design Standard Engineer
Michael Elle, P.E., Technical Support Engineer

Missouri Department of Transportation

Joseph G. Jones, P.E., Technical Support Engineer

Nebraska Department of Roads

Amy Starr, P.E., Research Engineer
Phil TenHulzen, P.E., Design Standards Engineer
Jodi Gibson, Research Coordinator

New Jersey Department of Transportation

Kiran Patel, P.E., P.M.P, C.P.M, Deputy State Transportation Engineer

Ohio Department of Transportation

Dean Focke, P.E., Roadway Safety Engineer

South Dakota Department of Transportation

David Huft, Research Engineer
Bernie Clocksin, Lead Project Engineer
Paul Oien, Project Engineer

Wisconsin Department of Transportation

John Bridwell, P.E., Standards Development Engineer
Erik Emerson, P.E., Standards Development Engineer

Wyoming Department of Transportation

William Wilson, P.E., Standards Engineer

Federal Highway Administration

John Perry, P.E., Nebraska Division Office
Danny Briggs, Nebraska Division Office

Dunlap Photography

James Dunlap, President and Owner

TABLE OF CONTENTS

	Page
TECHNICAL REPORT DOCUMENTATION PAGE	i
DISCLAIMER STATEMENT	ii
ACKNOWLEDGMENTS	iii
TABLE OF CONTENTS	vi
List of Figures	ix
List of Tables	xv
1 INTRODUCTION	1
1.1 Problem Statement	1
1.2 Objective	2
1.3 Scope	2
2 TEST REQUIREMENTS AND EVALUATION CRITERIA	3
2.1 Test Requirements	3
2.2 Evaluation Criteria	4
3 TEST CONDITIONS	6
3.1 Test Facility	6
3.2 Vehicle Tow and Guidance Systems	6
3.3 Test Vehicles	6
3.4.1 Accelerometers	23
3.4.2 Rate Transducers	23
3.4.3 High-Speed Photography	24
3.4.4 Pressure Tape Switches	25
4 DESIGN DETAILS - DESIGN NO. 1	31
5 CRASH TEST NO. 1	43
5.1 Test FR-1	43
5.2 Test Description	43
5.3 Barrier Damage	45
5.4 Vehicle Damage	46
5.5 Occupant Risk Values	47
5.6 Discussion	47
6 DESIGN DETAILS - DESIGN NO. 2	68

7 CRASH TEST NO. 2	73
7.1 Test FR-2	73
7.2 Test Description	73
7.3 Barrier Damage	74
7.4 Vehicle Damage	76
7.5 Occupant Risk Values	76
7.6 Discussion	77
8 CRASH TEST NO. 3	100
8.1 Test FR-3	100
8.2 Test Description	100
8.3 Barrier Damage	102
8.4 Vehicle Damage	103
8.5 Occupant Risk Values	104
8.6 Discussion	104
9 DESIGN DETAILS - DESIGN NO. 3	128
10 CRASH TEST NO. 4	133
10.1 Test FR-4	133
10.2 Test Description	133
10.3 Barrier Damage	135
10.4 Vehicle Damage	136
10.5 Occupant Risk Values	137
10.6 Discussion	138
11 CRASH TEST NO. 5	162
11.1 Test FR-5	162
11.2 Test Description	162
11.3 Barrier Damage	163
11.4 Vehicle Damage	165
11.5 Occupant Risk Values	165
11.6 Discussion	166
13 RECOMMENDATIONS	192
14 REFERENCES	195
15 APPENDICES	197
APPENDIX A	
ENGLISH-UNIT SYSTEM DRAWINGS - DESIGN NO. 1	198
APPENDIX B	
TEST SUMMARY SHEETS IN ENGLISH UNITS	205

APPENDIX C	
OCCUPANT COMPARTMENT DEFORMATION DATA, TEST FR-1	211
APPENDIX D	
ACCELEROMETER AND RATE TRANSDUCER DATA ANALYSIS,	
TEST FR-1	215
APPENDIX E	
SYSTEM DRAWINGS - DESIGN NO. 2	223
APPENDIX F	
OCCUPANT COMPARTMENT DEFORMATION DATA, TEST FR-2	236
APPENDIX G	
ACCELEROMETER AND RATE TRANSDUCER DATA ANALYSIS,	
TEST FR-2	240
APPENDIX H	
OCCUPANT COMPARTMENT DEFORMATION DATA, TEST FR-3	248
APPENDIX I	
ACCELEROMETER AND RATE TRANSDUCER DATA ANALYSIS,	
TEST FR-3	250
APPENDIX J	
SYSTEM DRAWINGS - DESIGN NO. 3	258
APPENDIX K	
OCCUPANT COMPARTMENT DEFORMATION DATA, TEST FR-4	273
APPENDIX L	
ACCELEROMETER AND RATE TRANSDUCER DATA ANALYSIS,	
TEST FR-4	277
APPENDIX M	
OCCUPANT COMPARTMENT DEFORMATION DATA, TEST FR-5	285
APPENDIX N	
ACCELEROMETER AND RATE TRANSDUCER DATA ANALYSIS,	
TEST FR-5	287

List of Figures

	Page
1. Test Vehicle, Test FR-1	7
2. Vehicle Dimensions, Test FR-1	8
3. Test Vehicle, Test FR-2	10
4. Vehicle Dimensions, Test FR-2	11
5. Test Vehicle, Test FR-3	12
6. Vehicle Damage, Test FR-3	13
7. Test Vehicle, Test FR-4	14
8. Vehicle Dimensions, Test FR-4	15
9. Test Vehicle, Test FR-5	16
10. Vehicle Dimensions, Test FR-5	17
11. Vehicle Target Locations, Test FR-1	18
12. Vehicle Target Locations, Test FR-2	19
13. Vehicle Target Locations, Test FR-3	20
14. Vehicle Target Locations, Test FR-4	21
15. Vehicle Target Locations, Test FR-5	22
16. Camera Locations, Test FR-1	26
17. Camera Locations, Test FR-2	27
18. Camera Locations, Test FR-3	28
19. Camera Locations, Test FR-4	29
20. Camera Locations, Test FR-5	30
21. System Details, Design No. 1	33
22. Rail Detail, Design No. 1	34
23. Post Details, Design No. 1	35
24. Anchorage Details, Design No. 1	36
25. Anchorage Details, Design No. 1	37
26. Anchorage Details, Design No. 1	38
27. System Details, Design No. 1	39
28. System Details, Design No. 1	40
29. Post Details, Design No. 1	41
30. Splice Details, Design No. 1	42
31. Summary of Test Results and Sequential Photographs, Test FR-1	49
32. Additional Sequential Photographs, Test FR-1	50
33. Additional Sequential Photographs, Test FR-1	51
34. Additional Sequential Photographs, Test FR-1	52
35. Documentary Photographs, Test FR-1	53
36. Documentary Photographs, Test FR-1	54
37. Impact Location, Test FR-1	55
38. Vehicle Trajectory and Final Position, Test FR-1	56
39. System Damage, Test FR-1	57
40. System Damage, Test FR-1	58
41. Post Nos. 11 and 12 Damage, Test No. FR-1	59

42. Post Nos. 13 and 14 Damage, Test No. FR-1	60
43. Post Nos. 15 and 16 Damage, Test No. FR-1	61
44. Post Nos. 17 and 18 Damage, Test FR-1	62
45. Upstream Anchorage Damage, Test FR-1	63
46. Vehicle Damage, Test FR-1	64
47. Vehicle Damage, Test FR-1	65
48. Vehicle Damage, Test FR-1	66
49. Vehicle Undercarriage Damage, Test FR-1	67
50. System Details, Design No. 2	69
51. System Details, Design No. 2	70
52. Post Details, Design No. 2	71
53. Splice Details, Design No. 2	72
54. Summary of Test Results and Sequential Photographs, Test FR-2	79
55. Additional Sequential Photographs, Test FR-2	80
56. Additional Sequential Photographs, FR-2	81
57. Documentary Photographs, Test FR-2	82
58. Documentary Photographs, Test FR-2	83
59. Impact Location, Test FR-2	84
60. Vehicle Trajectory and Final Position, Test FR-2	85
61. System Damage, Test FR-2	86
62. System Damage, Test FR-2	87
63. Post Nos. 9 and 10 Damage, Test FR-2	88
64. Post No. 11 Damage, Test FR-2	89
65. Post No. 12 Damage, Test FR-2	90
66. Post Nos. 13 and 14 Damage, Test FR-2	91
67. Post Nos. 15 and 16 Damage, Test FR-2	92
68. Post No. 17 Damage, Test FR-2	93
69. Post Nos. 18 and 19 Damage, Test FR-2	94
70. Anchorage Damage, Test FR-2	95
71. Vehicle Damage, Test FR-2	96
72. Vehicle Damage, Test FR-2	97
73. Undercarriage Damage, Test FR-2	98
74. Occupant Compartment Deformation, Test FR-2	99
75. Summary of Test Results and Sequential Photographs, Test FR-3	106
76. Additional Sequential Photographs, Test FR-3	107
77. Additional Sequential Photographs, Test FR-3	108
78. Additional Sequential Photographs, Test FR-3	109
79. Documentary Photographs, Test FR-3	110
80. Documentary Photographs, Test FR-3	111
81. Impact Location, Test FR-3	112
82. Vehicle Trajectory and Final Position, Test FR-3	113
83. System Damage, Test FR-3	114
84. Post Nos. 9 and 10 Damage, Test FR-3	115
85. Post Nos. 11 and 12 Damage, Test FR-3	116

86. Post Nos. 13 and 14 Damage, Test FR-3	117
87. Post No. 15 Damage, Test FR-3	118
88. Post Nos. 16 and 17 Damage, Test FR-3	119
89. Post Nos. 18 and 19 Damage, Test FR-3	120
90. Downstream Anchorage Damage, Test FR-3	121
91. Vehicle Damage, Test FR-3	122
92. Vehicle Damage, Test FR-3	123
93. Vehicle Damage, Test FR-3	124
94. Vehicle Damage, Test FR-3	125
95. Suspension Damage, Test FR-3	126
96. Occupant Compartment Damage, Test FR-3	127
97. System Details, Design No. 3	129
98. System Details, Design No. 3	130
99. System Details, Design No. 3	131
100. Post Details, Design No. 3	132
101. Summary of Test Results and Sequential Photographs, Test FR-4	139
102. Additional Sequential Photographs, FR-4	140
103. Additional Sequential Photographs, Test FR-4	141
104. Additional Sequential Photographs, Test FR-4	142
105. Documentary Photographs, Test FR-4	143
106. Documentary Photographs, Test FR-4	144
107. Impact Location, Test FR-4	145
108. Vehicle Trajectory and Final Position, Test FR-4	146
109. System Damage, Test FR-4	147
110. System Damage, Test FR-4	148
111. System Damage, Test FR-4	149
112. Post Nos. 9 and 10 Damage, Test FR-4	150
113. Post Nos. 11 and 12 Damage, Test FR-4	151
114. Post Nos. 13 and 14 Damage, Test FR-4	152
115. Post Nos. 15 and 16 Damage, Test FR-4	153
116. Post Nos. 17 and 18 Damage, Test FR-4	154
117. Post Nos. 19 and 20 Damage, Test FR-4	155
118. Upstream Anchorage Damage, Test FR-4	156
119. Downstream Anchorage Damage, Test FR-4	157
120. Vehicle Damage, Test FR-4	158
121. Vehicle Damage, Test FR-4	159
122. Undercarriage Damage, Test FR-4	160
123. Occupant Compartment Deformation, Test FR	161
124. Summary of Test Results and Sequential Photographs, Test FR-5	167
125. Additional Sequential Photographs, Test FR-5	168
126. Additional Sequential Photographs, Test FR-5	169
127. Additional Sequential Photographs, Test FR-5	170
128. Documentary Photographs, Test FR-5	171
129. Documentary Photographs, Test FR-5	172

130. Impact Location, Test FR-5	173
131. Vehicle Trajectory and Final Position, Test FR-5	174
132. System Damage, Test FR-5	175
133. System Damage, Test FR-5	176
134. Rail Damage, Test FR-5	177
135. Post Nos. 9 and 10 Damage, Test FR-5	178
136. Post Nos. 11 and 12 Damage, Test FR-5	179
137. Post Nos. 13 and 14 Damage, Test FR-5	180
138. Post Nos. 15 and 16 Damage, Test FR-5	181
139. Post Nos. 17 and 18 Damage, Test FR-5	182
140. Post Nos. 19 and 20 Damage, Test FR-5	183
141. Vehicle Damage, Test FR-5	184
142. Vehicle Damage, Test FR-5	185
143. Windshield Damage, Test FR-5	186
144. Undercarriage Damage, Test FR-5	187
145. Occupant Compartment Deformation, Test FR-5	188
A-1. System Layout, Design No. 1 (English)	199
A-2. Rail Details, Design No. 1 (English)	200
A-3. Post Details, Design No. 1 (English)	201
A-4. Anchorage Details, Design No. 1 (English)	202
A-5. Anchorage Details, Design No. 1 (English)	203
A-6. Anchorage Details, Design No. 1 (English)	204
B-1. Summary of Test Results and Sequential Photographs (English), Test No. FR-1	206
B-2. Summary of Test Results and Sequential Photographs (English), Test FR-2	207
B-3. Summary of Test Results and Sequential Photographs (English), Test FR-3	208
B-4. Summary of Test Results and Sequential Photographs (English), Test FR-4	209
B-5. Summary of Test Results and Sequential Photographs (English), Test FR-5	210
C-1. Occupant Compartment Deformation Data - Set 1, Test FR-1	212
C-2. Occupant Compartment Deformation - Set 2, Test FR-1	213
C-3. Occupant Compartment Deformation Index (OCDI), Test FR-1	214
D-1. Graph of Longitudinal Occupant Deceleration, Test FR-1	216
D-2. Graph of Longitudinal Occupant Impact Velocity (OIV), Test FR-1	217
D-3. Graph of Longitudinal Occupant Displacement, Test FR-1	218
D-4. Graph of Lateral Occupant Deceleration, Test FR-1	219
D-5. Graph of Lateral Occupant Impact Velocity (OIV), Test FR-1	220
D-6. Graph of Lateral Occupant Displacement, Test FR-1	221
D-7. Graph of Lateral Occupant Displacement, Test FR-1	222
E-1. System Layout, Design No. 2 (Metric)	224
E-2. Rail Details, Design No. 2 (Metric)	225
E-3. Post Details, Design No. 2 (Metric)	226
E-4. Anchorage Details, Design No. 2 (Metric)	227
E-5. Anchorage Details, Design No. 2 (Metric)	228
E-6. Anchorage, Design No. 2 (Metric)	229
E-7. System Layout, Design No. 2 (English)	230

E-8. Rail Details, Design No. 2 (English)	231
E-9. Post Details, Design No. 2 (English)	232
E-10. Anchorage Details, Design No. 2 (English)	233
E-11. Anchorage Details, Design No. 2 (English)	234
E-12. Anchorage Details, Design No. 2 (English)	235
F-1. Occupant Compartment Deformation Data - Set 1, Test FR-2	237
F-2. Occupant Compartment Deformation Data - Set 2, Test FR-2	238
F-3. Occupant Compartment Deformation Index (OCDI), Test FR-2	239
G-1. Graph of Longitudinal Deceleration, Test FR-2	241
G-2. Graph of Longitudinal Occupant Impact Velocity (OIV), Test FR-2	242
G-3. Graph of Longitudinal Occupant Displacement, Test FR-2	243
G-4. Graph of Lateral Deceleration, Test FR-2	244
G-5. Graph of Lateral Occupant Impact Velocity (OIV), Test FR-2	245
G-6. Graph of Lateral Occupant Displacement, Test FR-2	246
G-7. Graph of Roll, Pitch, and Yaw Angular Displacements, Test FR-2	247
H-1. Occupant Compartment Deformation Index (OCDI), Test FR-3	249
I-1. Graph of Longitudinal Deceleration, Test FR-3	251
I-2. Graph of Longitudinal Occupant Impact Velocity (OIV), Test FR-3	252
I-3. Graph of Longitudinal Occupant Displacement, Test FR-3	253
I-4. Graph of Lateral Deceleration, Test FR-3	254
I-5. Graph of Lateral Occupant Impact Velocity (OIV), Test FR-3	255
I-6. Graph of Lateral Occupant Displacement, Test FR-3	256
I-7. Graph of Roll, Pitch, and Yaw Angular Displacements, Test FR-3	257
J-1. System Layout, Design No. 3 (Metric)	259
J-2. Rail Details, Design No. 3 (Metric)	260
J-3. Post Details, Design No. 3 (Metric)	261
J-4. Anchorage Details, Design No. 3 (Metric)	262
J-5. Anchorage Details, Design No. 3 (Metric)	263
J-6. Anchorage Details, Design No. 3 (Metric)	264
J-7. Rail Bend Details, Design No. 3 (Metric)	265
J-8. System Layout, Design No. 3 (English)	266
J-9. Rail Details, Design No. 3 (English)	267
J-10. Post Details, Design No. 3 (English)	268
J-11. Anchorage Details, Design No. 3 (English)	269
J-12. Anchorage Details, Design No. 3 (English)	270
J-13. Anchorage Details, Design No. 3 (English)	271
J-14. Rail Bend Details, Design No. 3 (English)	272
K-1. Occupant Compartment Deformation Data - Set 1, Test FR-4	274
K-2. Occupant Compartment Deformation Data - Set 2, Test FR-4	275
K-3. Occupant Compartment Deformation Index (OCDI), Test FR-4	276
L-1. Graph of Longitudinal Deceleration, Test FR-4	278
L-2. Graph of Longitudinal Occupant Impact Velocity (OIV), Test FR-4	279
L-3. Graph of Longitudinal Occupant Displacement, Test FR-4	280
L-4. Graph of Lateral Deceleration, Test FR-4	281

L-5. Graph of Lateral Occupant Impact Velocity (OIV), Test FR-4	282
L-6. Graph of Lateral Occupant Displacement, Test FR-4	283
L-7. Graph of Roll, Pitch, and Yaw Angular Displacements, Test FR-4	284
M-1. Occupant Compartment Deformation Index (OCDI), Test FR-5	286
N-1. Graph of Longitudinal Deceleration, Test FR-5	288
N-2. Graph of Longitudinal Occupant Impact Velocity (OIV), Test FR-5	289
N-3. Graph of Longitudinal Occupant Displacement, Test FR-5	290
N-4. Graph of Lateral Deceleration, Test FR-5	291
N-5. Graph of Lateral Occupant Impact Velocity (OIV), Test FR-5	292
N-6. Graph of Lateral Occupant Displacement, Test FR-5	293
N-7. Graph of Roll and Yaw Angular Displacements, Test FR-5	294

List of Tables

	Page
1. NCHRP Report No. 350 Test Level 3 Crash Test Conditions	3
2. NCHRP Report No. 350 Evaluation Criteria for Crash Tests	5
3. Summary of Safety Performance Evaluation Results	190
4. Summary of Test Results, Test Nos. FR-1 through FR-5	191

1 INTRODUCTION

1.1 Problem Statement

The National Cooperative Highway Research Program (NCHRP) Report No. 350, *Recommended Procedures for the Safety Performance Evaluation of Highway Features*, defines crash testing standards that roadside hardware must satisfy in order to be approved for installation on the National Highway System (NHS) (1). In the case of strong-post, W-beam guardrail systems this does not mean, however, that the installation of the guardrail must be identical to the crash testing conditions. For example, such guardrail systems are allowed to be installed with a flare up to a rate of 15:1 for high-speed applications; as opposed to the tangent installations used during crash test evaluation. This flare rate is justified because of an overall reduction in crash frequency due to the flare (2). Reducing the number of crashes can offset modest increases in crash severity, such that the total accident costs, measured in terms of injuries and fatalities, go down.

Utilizing a flared guardrail configuration effectively raises the impact severity of all roadside collisions by increasing the relative impact angle between the encroaching vehicle and the guardrail installation. The maximum flare rates currently recommended in the American Association of State Highway and Transportation Officials (AASHTO) Roadside Design Guide (RDG) are based on the performance of conventional strong-post, W-beam guardrail (3). The strong-post, W-beam guardrail has long been recognized as having very little reserve capacity to contain and redirect heavy passenger vehicles when impact severities increase (4). The Midwest Guardrail System (MGS) has been shown to have significantly greater capacity than conventional strong-post guardrail and should provide improved performance when installed in a flared configuration (5-11).

In recognition of the need to update the flare rate guidelines, the Midwest States' Pooled

Fund Program and the National Cooperative Highway Research Program (Project 17-20(3)) sponsored the research project to develop updated flare rate guidelines. Previously, the Midwest Roadside Safety Facility (MwRSF) reviewed previous research and current standards for flare rates and conducted detailed simulation to identify a critical flare rate to be full-scale vehicle crash tested (12).

1.2 Objective

The objective of the research project was to evaluate the safety performance of the critical flare rates for the MGS, determined from a previous study (12), in order to identify the maximum flare rate at which the MGS could provide acceptable safety performance. The systems were to be evaluated according to the Test Level 3 (TL-3) safety performance criteria presented in the NCHRP Report No. 350 guidelines.

1.3 Scope

In order to complete the research objective, several tasks were undertaken. Five full-scale crash-tests were performed on various flare rates. The first, second, and fourth tests utilized $\frac{3}{4}$ -ton pickup trucks weighing approximately 2,000 kg (4,409 lbs), with a target impact speed and angle of 100.0 km/h (62.1 mph) and 25 degrees, respectively. The third and fifth tests utilized a small compact car weighing approximately 820 kg (1,808 lbs) with an impact speed and angle of 100 km/h (62.1 mph) and 20 degrees, respectively. The test results were then analyzed, evaluated, and documented. Conclusions and recommendations were made that pertained to the safety performance of the flared versions of the MGS. In addition, recommendations for flare rate guidelines for the MGS were presented.

2 TEST REQUIREMENTS AND EVALUATION CRITERIA

2.1 Test Requirements

Longitudinal barriers, such as W-beam guardrail systems, must satisfy the requirements provided in NCHRP Report No. 350 to be accepted for use on NHS construction projects or as a replacement for existing systems not meeting current safety standards. According to TL-3 of NCHRP Report No. 350, the longitudinal barriers must be subjected to two full-scale vehicle crash tests. The two crash tests are as follows:

1. Test Designation 3-10, consisting of an 820-kg (1,808-lb) small car impacting the guardrail at a nominal speed and angle of 100.0 km/h (62.1 mph) and 20 degrees, respectively.
2. Test Designation 3-11, consisting of a 2,000-kg (4,409-lb) pickup truck impacting the guardrail at a nominal speed and angle of 100.0 km/h (62.1 mph) and 25 degrees, respectively.

The test conditions for TL-3 longitudinal barriers are summarized in Table 1.

Table 1. NCHRP Report No. 350 Test Level 3 Crash Test Conditions

Test Article	Test Designation	Test Vehicle	Impact Conditions			Evaluation Criteria ¹
			Speed		Angle (degrees)	
			(km/h)	(mph)		
Longitudinal Barrier	3-10	820C	100	62.1	20	A,D,F,H,I,K,M
	3-11	2000P	100	62.1	25	A,D,F,K,L,M

¹ Evaluation criteria explained in Table 2.

2.2 Evaluation Criteria

Evaluation criteria for full-scale vehicle crash testing are based on three appraisal areas: (1) structural adequacy; (2) occupant risk; and (3) vehicle trajectory after collision. Criteria for structural adequacy are intended to evaluate the ability of the barrier to contain, redirect, or allow controlled vehicle penetration in a predictable manner. Occupant risk evaluates the degree of hazard to occupants in the impacting vehicle. Vehicle trajectory after collision is a measure of the potential for the post-impact trajectory of the vehicle to cause subsequent multi-vehicle accidents. This criterion also indicates the potential safety hazard for the occupants of other vehicles or the occupants of the impacting vehicle when subjected to secondary collisions with other fixed objects. These three evaluation criteria are defined in Table 2. The full-scale vehicle crash tests were conducted and reported in accordance with the procedures provided in NCHRP Report No. 350.

Table 2. NCHRP Report No. 350 Evaluation Criteria for Crash Tests

Structural Adequacy	A. Test article should contain and redirect the vehicle; the vehicle should not penetrate, underride, or override the installation although controlled lateral deflection of the test article is acceptable.
Occupant Risk	D. Detached elements, fragments or other debris from the test article should not penetrate or show potential for penetrating the occupant compartment, or present an undue hazard to other traffic, pedestrians, or personnel in a work zone. Deformations of, or intrusions into, the occupant compartment that could cause serious injuries should not be permitted.
	F. The vehicle should remain upright during and after collision although moderate roll, pitching, and yawing are acceptable.
	H. Longitudinal and lateral occupant impact velocities should fall below the preferred value of 9 m/s (29.53 ft/s), or at least below the maximum allowable value of 12 m/s (39.37 ft/s).
	I. Longitudinal and lateral occupant ridedown accelerations should fall below the preferred value of 15 g's, or at least below the maximum allowable value of 20 g's.
Vehicle Trajectory	K. After collision it is preferable that the vehicle's trajectory not intrude into adjacent traffic lanes.
	L. The occupant impact velocity in the longitudinal direction should not exceed 12 m/s (39.37 ft/s), and the occupant ridedown acceleration in the longitudinal direction should not exceed 20 g's.
	M. The exit angle from the test article preferably should be less than 60 percent of test impact angle measured at time of vehicle loss of contact with test device.

3 TEST CONDITIONS

3.1 Test Facility

The testing facility is located at the Lincoln Air-Park on the northwest (NW) side of the Lincoln Municipal Airport and is approximately 8.0 km (5 mi.) NW of the University of Nebraska-Lincoln.

3.2 Vehicle Tow and Guidance Systems

A reverse cable tow system with a 1:2 mechanical advantage was used to propel the test vehicle. The distance traveled and the speed of the tow vehicle were one-half that of the test vehicle. The test vehicle was released from the tow cable before impact with the guardrail system. A digital speedometer was located on the tow vehicle to increase the accuracy of the test vehicle impact speed.

A vehicle guidance system developed by Hinch ([13](#)) was used to steer the test vehicle. A guide-flag, attached to the front-right wheel and the guide cable, was sheared off before impact with the guardrail system. The 9.5-mm (0.375-in.) diameter guide cable was tensioned to approximately 15.6 kN (3,500 lbf), and supported laterally and vertically every 30.48 m (100 ft) by hinged stanchions. The hinged stanchions stood upright while holding up the guide cable, but as the vehicle was towed down the line, the guide-flag struck and knocked each stanchion to the ground. For tests FR-1 and FR-2, the vehicle guidance system was approximately 189 m (1,080 ft) long. For test nos. FR-3 and FR-5, the vehicle guidance system was approximately 239 m (784 ft) long, while for test FR-4, the vehicle guidance system was approximately 189 m (621 ft) long.

3.3 Test Vehicles

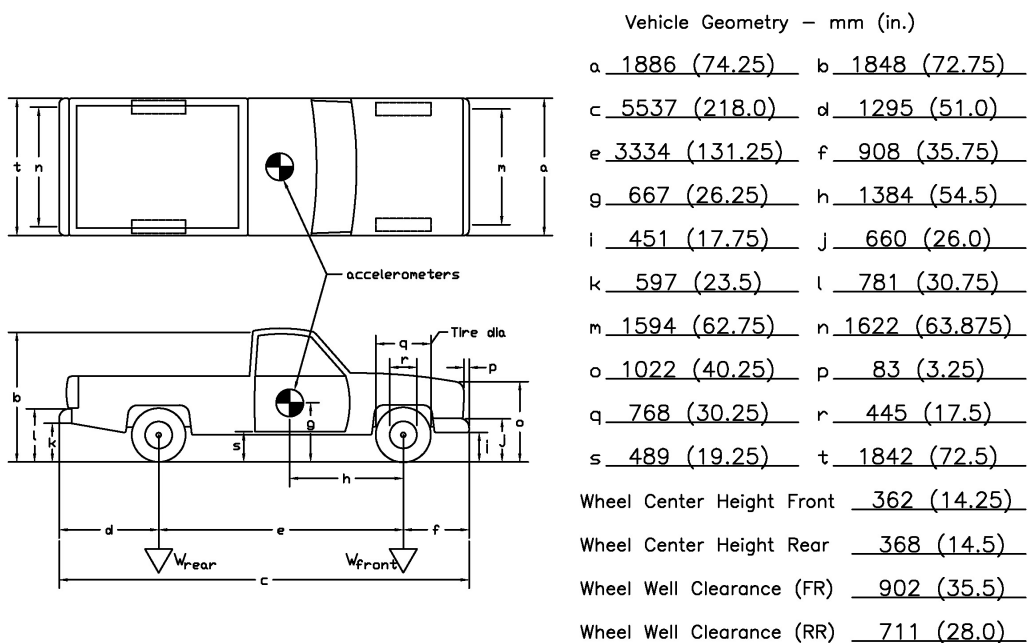
For test FR-1, a 2000 Chevrolet C2500 $\frac{3}{4}$ -ton pickup truck was used as the test vehicle. The test inertial and gross static weights were 2,025 kg (4,466 lbs). The test vehicle is shown in Figure 1, and vehicle dimensions are shown in Figure 2.



Figure 1. Test Vehicle, Test FR-1

Date: 5/24/2005 Test Number: FR-1 Model: C2500
 Make: Chevrolet Vehicle I.D.#: 1GCGC24R9YF475956
 Tire Size: LT 245/75 R16 Year: 2000 Odometer: 176941

*(All Measurements Refer to Impacting Side)



Weights kg (lbs)	Curb	Test Inertial	Gross Static
W_{front}	<u>1148 (2531)</u>	<u>1181 (2603)</u>	<u>1181 (2603)</u>
W_{rear}	<u>825 (1819)</u>	<u>845 (1163)</u>	<u>845 (1163)</u>
W_{total}	<u>1973 (4350)</u>	<u>2026 (4466)</u>	<u>2026 (4466)</u>

Engine Type 8 CYL. GAS
 Engine Size 5.7 L 350 CID
 Transmission Type:
☒ Automatic or Manual
 FWD or ☒ RWD or 4WD

Note any damage prior to test: None

Figure 2. Vehicle Dimensions, Test FR-1

For test FR-2, a 1999 Chevrolet C2500 $\frac{3}{4}$ -ton pickup truck was used as the test vehicle. The test inertial and gross static weights were 2,023 kg (4,461 lbs). The test vehicle is shown in Figure 3, and vehicle dimensions are shown in Figure 4.

For test FR-3, a 1998 Geo Metro was used as the test vehicle. The test inertial and gross static weights were 818 kg (1,804 lbs) and 894 kg (1,970 lbs), respectively. The test vehicle is shown in Figure 5, and vehicle dimensions are shown in Figure 6.

For test FR-4, a 1999 Chevrolet C2500 $\frac{3}{4}$ -ton pickup truck was used as the test vehicle. The test inertial and gross static weights were 2,014 kg (4,441 lbs). The test vehicle is shown in Figure 7, and vehicle dimensions are shown in Figure 8.

For test FR-5, a 1998 Geo Metro was used as the test vehicle. The test inertial and gross static weights were 833 kg (1,836 lbs) and 908 kg (2002 lbs), respectively. The test vehicle is shown in Figure 9, and vehicle dimensions are shown in Figure 10.

The longitudinal component of the center of gravity was determined using the measured axle weights. The location of the final centers of gravity are shown in Figures 1 through 10.

Square black and white-checkered targets were placed on the vehicle to aid in the analysis of the high-speed E/cam, Photron and AOS videos, as shown in Figures 11 through 15. Round, checkered targets were placed on the center of gravity, on the driver's side door, on the passenger's side door, and on the roof of the vehicle. The remaining targets were located for reference so that they could be viewed from the high-speed cameras for film analysis.

The front wheels of the test vehicles were aligned for camber, caster, and toe-in values of zero so that the vehicle would track properly along the guide cable. A 5B flash bulb was mounted on the left side of the vehicle's dash to pinpoint the time of impact with the test article on the high-



Figure 3. Test Vehicle, Test FR-2

Date: 8/2/2005 Test Number: FR-2 Model: C2500
 Make: Chevrolet Vehicle I.D.#: 1GCGC24R7XR705460
 Tire Size: LT 245/75 R16 Year: 1999 Odometer: 132,645

*(All Measurements Refer to Impacting Side)

Diagram labels: a, b, c, d, e, f, g, h, i, j, k, l, m, n, o, p, q, r, s, t. Accelerometers, Tire dia, W_{rear}, W_{front}.

Vehicle Geometry - mm (in.)

a 1886 (74.25) b 1829 (72.0)
 c 5537 (218.0) d 1308 (51.5)
 e 3334 (131.25) f 895 (35.25)
 g 667 (26.25) h 1400 (55.1)
 i 457 (18.0) j 660 (26.0)
 k 600 (23.63) l 794 (31.25)
 m 1600 (63.0) n 1626 (64.0)
 o 1022 (40.25) p 69.85 (2.75)
 q 756 (29.75) r 438 (17.25)
 s 476 (18.75) t 1845 (72.63)

Wheel Center Height Front 368 (14.5)
 Wheel Center Height Rear 371 (14.625)
 Wheel Well Clearance (FR) 905 (35.625)
 Wheel Well Clearance (RR) 949 (37.375)

Frame Height (FR) 356 (14.0)
 Frame Height (RR) 679 (26.75)
 Engine Type 8 CYL. GAS
 Engine Size 5.7 L 350 CID
 Transmission Type: (Automatic) or Manual
 FWD or (RWD) or 4WD

Weights

kg (lbs)	Curb	Test Inertial	Gross Static
W _{front}	<u>1220 (2690)</u>	<u>1174 (2588)</u>	<u>1174 (2588)</u>
W _{rear}	<u>870 (1919)</u>	<u>850 (1873)</u>	<u>850 (1873)</u>
W _{total}	<u>2090 (4609)</u>	<u>2023 (4461)</u>	<u>2023 (4461)</u>

GVWR Ratings

Front 1860 (4100)

Back 2722 (6000)

Total 3901 (8600)

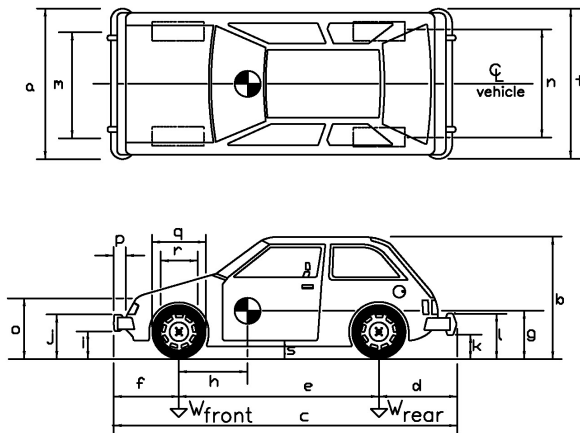
Note any damage prior to test: None

Figure 4. Vehicle Dimensions, Test FR-2



Figure 5. Test Vehicle, Test FR-3

Date: 8/17/05 Test Number: FR-3 Model: 820C Metro
 Make: Geo Vehicle I.D.#: 2C1MR2260W6708220
 Tire Size: P155/80 R13 Year: 1998 Odometer: 74637



Vehicle Geometry - mm (in.)

a 1562 (61.5) b 1403 (55.25)
 c 3778 (148.75) d 610 (24.0)
 e 2369 (93.25) f 800 (31.5)
 g 546 (21.5) h 933 (36.75)
 i 222 (8.75) j 533 (21.0)
 k 279 (11.0) l 635 (25.0)
 m 1378 (54.25) n 1365 (53.75)
 o 559 (22.0) p 76 (3.0)
 q 565 (22.25) r 362 (14.25)
 s 286 (11.25) t 1581 (62.25)

Wheel Center Height 264 (10.375)

Engine Type 3 CYL. GAS

Engine Size 1.0 L

Transmission Type:

Automatic or Manual

FWD or RWD or 4WD

Weights			
kg (lbs)	Stripped	Test Inertial	Gross Static
W _{front}	<u>468 (1031)</u>	<u>495 (1092)</u>	<u>532 (1173)</u>
W _{rear}	<u>295 (651)</u>	<u>323 (712)</u>	<u>362 (797)</u>
W _{total}	<u>763 (1682)</u>	<u>818 (1804)</u>	<u>894 (1970)</u>

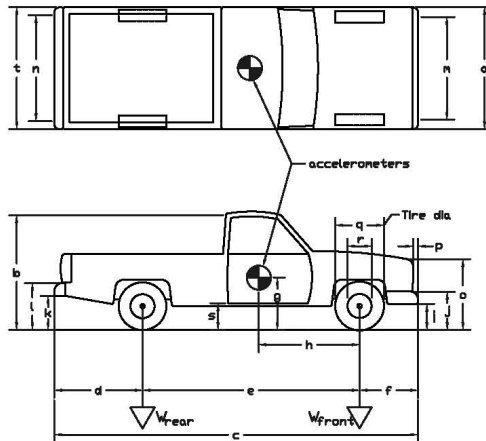
Note any damage prior to test: None

Figure 6. Vehicle Damage, Test FR-3



Figure 7. Test Vehicle, Test FR-4

Date: 5/17/2006 Test Number: FR-4 Model: 2000P
 Make: Chevrolet Vehicle I.D.#: 1GCGC24R8XR722686
 Tire Size: LT 245/75 R16 Year: 1999 Odometer: 94,673
 *(All Measurements Refer to Impacting Side)



Vehicle Geometry - mm (in.)

a 1905 (75.0) b 1864 (73.375)
 c 5556 (218.75) d 1270 (50.0)
 e 3343 (131.625) f 943 (37.125)
 g 667 (26.25) h 1410 (55.5)
 i 457 (18.0) j 660 (26.0)
 k 610 (24.0) l 797 (31.375)
 m 1594 (62.75) n 1626 (64.0)
 o 1035 (40.75) p 102 (4.0)
 q 756 (29.75) r 445 (17.5)
 s 495 (19.5) t 1867 (73.5)
 Wheel Center Height Front 368 (14.5)
 Wheel Center Height Rear 371 (14.625)
 Wheel Well Clearance (FR) 914 (36.0)
 Wheel Well Clearance (RR) 959 (37.75)
 Frame Height (FR) 419 (16.5)
 Frame Height (RR) 686 (27.0)

Weights kg (lbs)	Curb	Test Inertial	Gross Static
W_{front}	<u>1134 (2501)</u>	<u>1163 (2564)</u>	<u>1163 (2564)</u>
W_{rear}	<u>839 (1849)</u>	<u>851 (1877)</u>	<u>851 (1877)</u>
W_{total}	<u>1973 (4350)</u>	<u>2014 (4441)</u>	<u>2014 (4441)</u>

GVWR Ratings
 Front 1860 (4100)
 Back 2722 (6000)
 Total 3901 (8600)

Engine Type 8 CYL. GAS
 Engine Size 5.7 L 350 CID
 Transmission Type:
☒ Automatic or Manual
 FWD or ☒ RWD or 4WD

Note any damage prior to test: None

Figure 8. Vehicle Dimensions, Test FR-4



Figure 9. Test Vehicle, Test FR-5

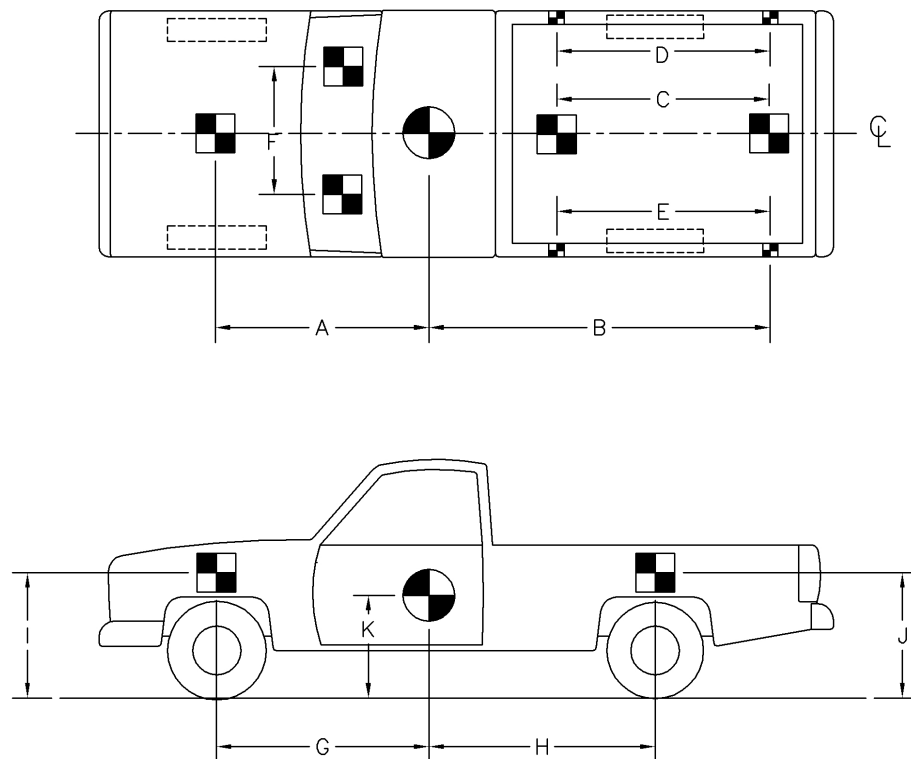
Date: 7-6-06 Test Number: FR-5 Model: Metro
 Make: Geo Vehicle I.D.#: 2C1MR2227W6728901
 Tire Size: 155/80 R13 Year: 1998 Odometer: 89,214

		Vehicle Geometry - mm (in)	
		a <u>1556 (61.25)</u> b <u>1435 (56.5)</u> c <u>3753 (147.75)</u> d <u>622 (24.5)</u> e <u>2292 (90.25)</u> f <u>838 (33.0)</u> g <u>546 (21.5)</u> h <u>884 (34.8)</u> i <u>432 (17.0)</u> j <u>533 (21.0)</u> k <u>298 (11.75)</u> l <u>616 (24.25)</u> m <u>1397 (55.0)</u> n <u>1372 (54.0)</u> o <u>565 (22.25)</u> p <u>102 (4.0)</u> q <u>559 (22.0)</u> r <u>362 (14.25)</u> s <u>330 (13.0)</u> t <u>1565 (61.625)</u>	height of wheel center <u>267 (10.5)</u> Engine Type <u>4 cyl. Gas</u> Engine size <u>1.3 L</u> Transmission Type: <input checked="" type="checkbox"/> Automatic or Manual <input type="checkbox"/> FWD or RWD or 4WD

Weight kg (lbs)	Curb	Test Inertial	Gross Static
w_{front}	<u>541 (1192)</u>	<u>526 (1160)</u>	<u>564 (1243)</u>
w_{rear}	<u>299 (660)</u>	<u>307 (676)</u>	<u>344 (759)</u>
w_{total}	<u>840 (1852)</u>	<u>833 (1836)</u>	<u>908 (2002)</u>

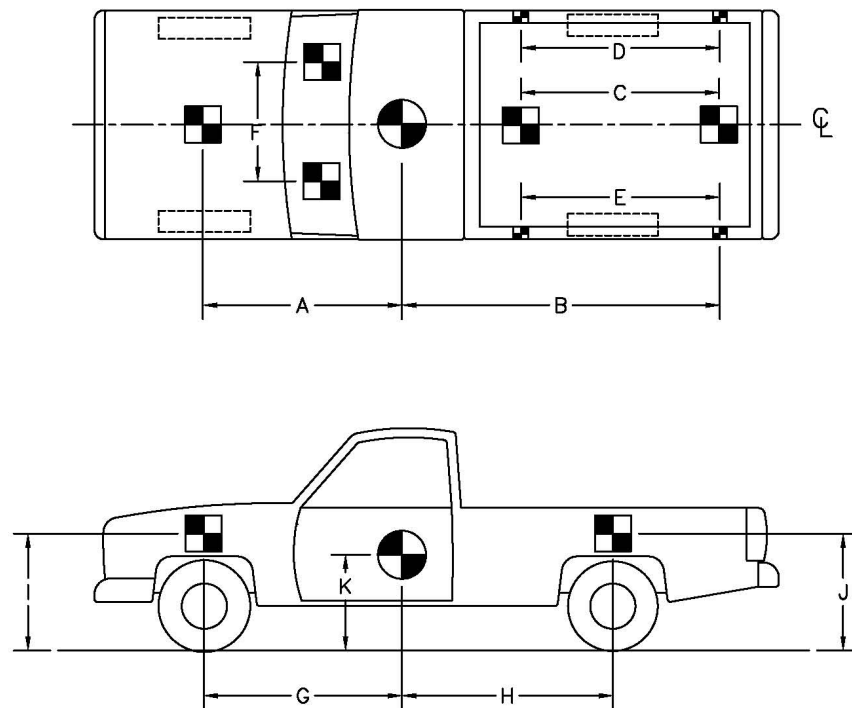
Damage prior to test: None

Figure 10. Vehicle Dimensions, Test FR-5



TEST #: <u>FR-1</u>			
TARGET GEOMETRY -- mm (in.)			
A <u>1581 (62.25)</u>	D <u>2153 (84.75)</u>	G <u>1394 (54.5)</u>	J <u>1067 (42.0)</u>
B <u>2667 (105.0)</u>	E <u>2153 (84.75)</u>	H <u>1949 (76.75)</u>	K <u>667 (26.25)</u>
C <u>1581 (62.25)</u>	F <u>845 (33.25)</u>	I <u>1016 (40.0)</u>	

Figure 11. Vehicle Target Locations, Test FR-1

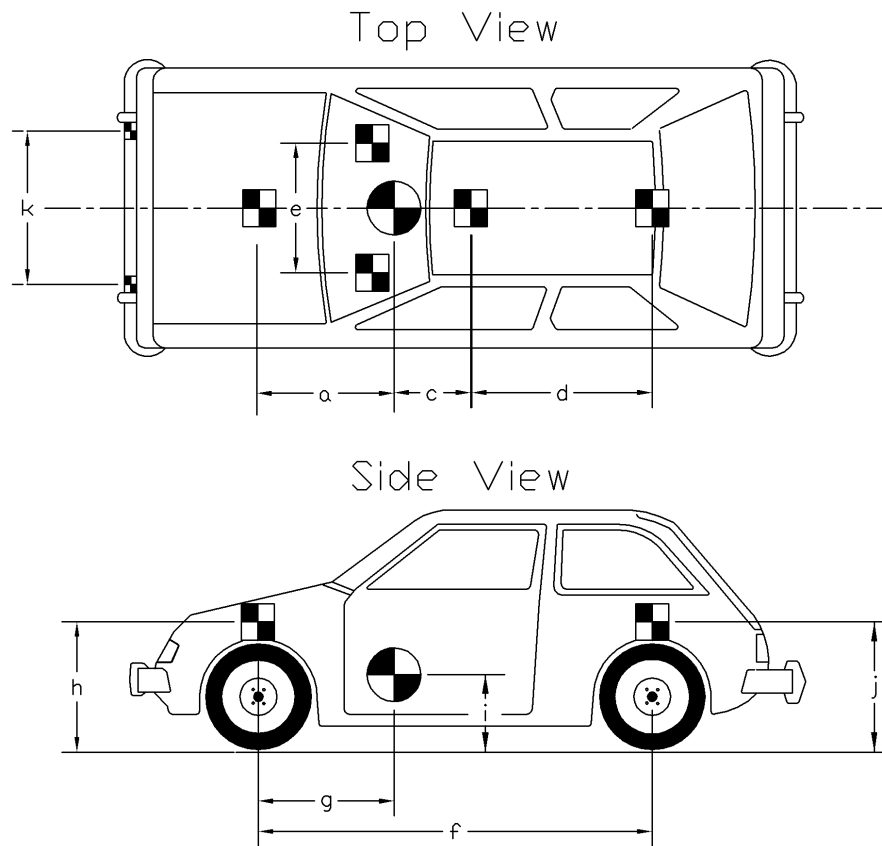


TEST #: FR-2

TARGET GEOMETRY -- mm (in.)

A	<u>1588 (62.5)</u>	D	<u>2146 (84.5)</u>	G	<u>1397 (55.0)</u>	J	<u>1054 (41.5)</u>
B	<u>2581 (101.625)</u>	E	<u>2146 (84.5)</u>	H	<u>1937 (76.25)</u>	K	<u>667 (26.25)</u>
C	<u>1562 (61.5)</u>	F	<u>911 (35.875)</u>	I	<u>1010 (39.75)</u>		

Figure 12. Vehicle Target Locations, Test FR-2

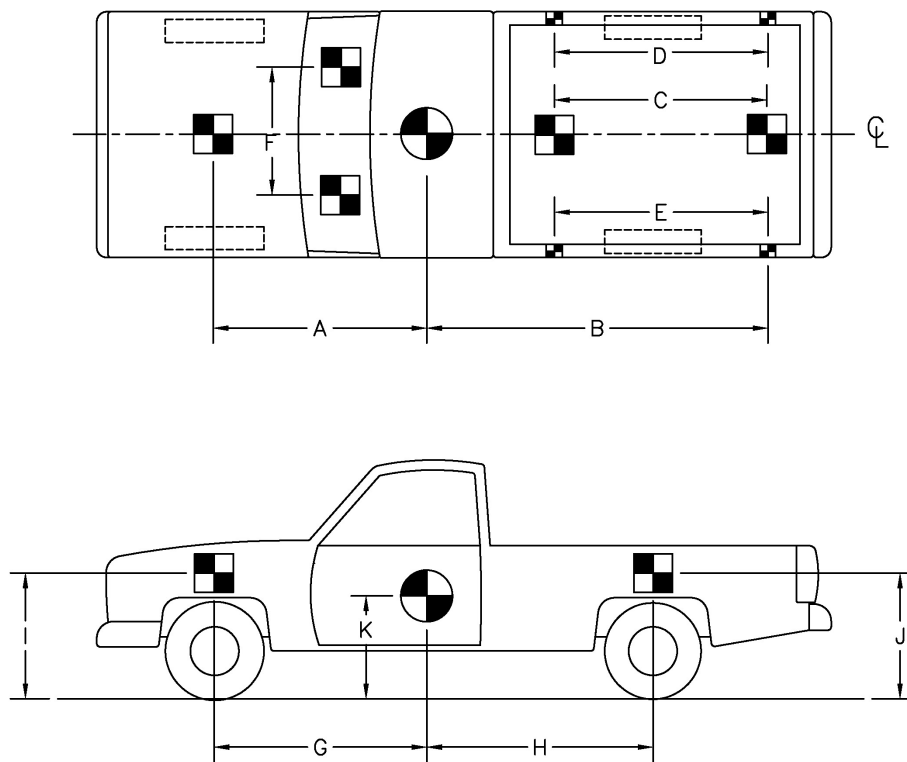


TEST #: FR-3

TARGET GEOMETRY -- mm (in.)

a	<u>1140 (44.875)</u>	b	<u>NA</u>	c	<u>416 (16.375)</u>	d	<u>810 (31.875)</u>
e	<u>876 (34.5)</u>	f	<u>2369 (93.25)</u>	g	<u>933 (36.75)</u>	h	<u>714 (28.125)</u>
		i	<u>546 (21.5)</u>	j	<u>740 (29.125)</u>	k	<u>NA</u>

Figure 13. Vehicle Target Locations, Test FR-3

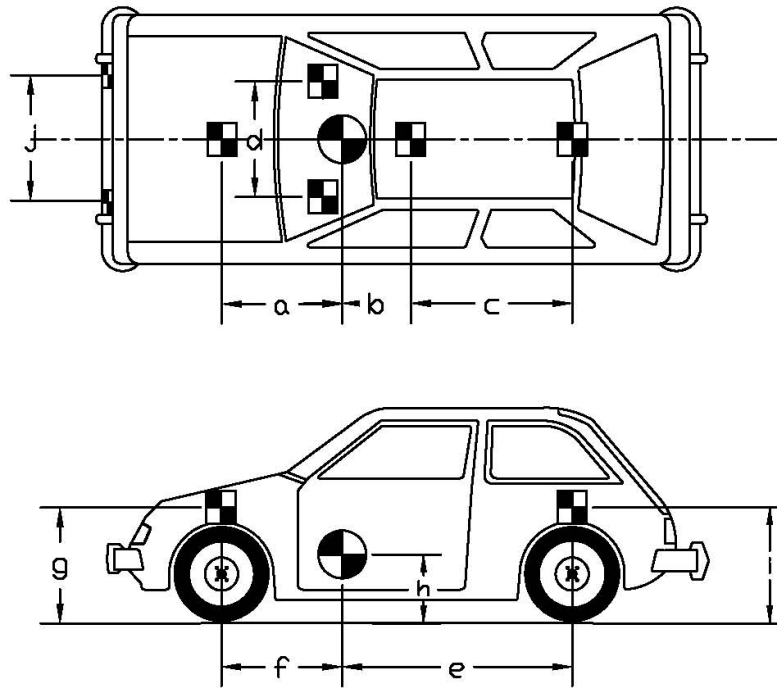


TEST #: FR-4

TARGET GEOMETRY -- mm (in.)

A	<u>1588 (62.5)</u>	D	<u>2153 (84.75)</u>	G	<u>1410 (55.5)</u>	J	<u>1080 (42.5)</u>
B	<u>2553 (100.5)</u>	E	<u>2153 (84.75)</u>	H	<u>1934 (76.125)</u>	K	<u>667 (26.25)</u>
C	<u>1562 (61.5)</u>	F	<u>908 (35.75)</u>	I	<u>1035 (40.75)</u>		

Figure 14. Vehicle Target Locations, Test FR-4



TEST #: <u>FR-5</u>			
TARGET GEOMETRY -- mm (in.)			
a <u>1127 (44.375)</u>	b <u>330 (13.0)</u>	c <u>972 (38.25)</u>	d <u>756 (29.75)</u>
e <u>1410 (55.5)</u>	f <u>884 (34.8)</u>	g <u>762 (30.0)</u>	h <u>546 (21.5)</u>
i <u>781 (30.75)</u>	j <u>N/A</u>		

Figure 15. Vehicle Target Locations, Test FR-5

speed video footage. The flash bulbs were fired by a pressure tape switch mounted at the right corner of the bumper. A remote-controlled brake system was installed in the test vehicle so the vehicle could be brought safely to a stop after the test.

3.4 Data Acquisition Systems

Three data acquisition systems, two accelerometers and one rate transducer were used to measure the motion of the vehicle. The results of all three were analyzed and plotted using “Dyna Max 1 (DM-1)” and “DADiSP” computer software programs.

3.4.1 Accelerometers

One triaxial piezoresistive accelerometer system with a range of ± 200 Gs was used to measure the acceleration in the longitudinal, lateral and vertical directions at a sample rate of 10,000 Hz. The environmental shock and vibration sensor/recorder system, Model EDR-4M6, was developed by Instrumented Sensor Technology (IST) of Okemos, Michigan and includes three differential channels as well as three single-ended channels. The EDR-4 was configured with 6 MB of RAM memory and a 1,500 Hz lowpass filter.

Another triaxial piezoresistive accelerometer system with a range of ± 200 Gs was also used to measure the acceleration in the longitudinal, lateral, and vertical directions at a sample rate of 3,200 Hz. The environmental shock and vibration sensor/recorder system, Model EDR-3, was developed by the Instrumental Sensor Technologies (IST) of Okemos, Michigan. The EDR-3 was configured with 256 kB of RAM memory and 1,120 Hz lowpass filter.

3.4.2 Rate Transducers

An Analog Systems 3-axis rate transducer with a range of 1,200 degrees/sec in each of the three directions (pitch, roll, and yaw) was used to measure the rates of motion of the test vehicle.

The rate transducer was mounted inside the body of the EDR-4M6 and recorded data at 10,000 Hz to a second data acquisition board inside the EDR-4M6 housing. The raw data measurements were then downloaded, converted to the appropriate Euler angles for analysis, and plotted.

3.4.3 High-Speed Photography

For test FR-1, two high-speed Photron digital video cameras, two high-speed AOS VITcam digital video cameras, and three high-speed RedLake E/cam digital video cameras, all with operating speeds of 500 frames/sec, were used to film the crash test. Six Canon digital video cameras, with standard operating speed of 29.97 frames/sec, were also used to film the crash test. Camera details and a schematic of all thirteen camera locations for test FR-1 is shown in Figure 16.

For test FR-2, two high-speed Photron digital video cameras, two high-speed AOS VITcam digital video cameras, and two high-speed RedLake E/cam digital video cameras, all with operating speeds of 500 frames/sec, were used to film the crash test. Six Canon digital video cameras and one JVC digital video camera, all with operating speeds of 29.97 frames/sec, were also used to film the crash test. Camera details and a schematic showing the locations of all thirteen cameras for test FR-2 is shown in Figure 17.

For test FR-3, two high-speed Photron digital video cameras, two high-speed AOS VITcam digital video cameras, and two high-speed RedLake E/cam digital video cameras, with operating speeds of 500 frames/sec, were used to film the crash test. Five Canon digital video cameras and one JVC digital video camera, all with standard operating speeds of 29.97 frames/sec, were also used to film the crash test. Camera details and a schematic of all twelve camera locations for test FR-3 is shown in Figure 18.

For test FR-4, four high-speed AOS VITcam digital video cameras and two high-speed

RedLake E/cam digital video cameras, all with operating speeds of 500 frames/sec, were used to film the crash test. Four Canon digital video cameras and two JVC digital video cameras, all with standard operating speeds of 29.97 frames/sec, were also used to film the crash test. Camera details and a schematic of all twelve camera locations for test FR-4 are shown in Figure 19.

For test FR-5, four high-speed AOS VITcam digital video cameras, with operating speeds of 500 frames/sec, were used to film the crash test. Five Canon digital video cameras and two JVC digital video cameras, with standard operating speeds of 29.97 frames/sec, were also used to film the crash test. Camera details and a schematic of all eleven camera locations for test FR-5 is shown in Figure 20.

The Photron and AOS videos and E/cam videos were analyzed using ImageExpress MotionPlus software and RedLake Motion Scope software, respectively. Actual camera divergence factors were considered in the analysis of the high-speed videos.

3.4.4 Pressure Tape Switches

For test FR-1 through FR-5, five pressure-activated tape switches, spaced at 2-m (6.56-ft) intervals, were used to determine the speed of the vehicle before impact. Each tape switch fired a strobe light which sent an electronic timing signal to the data acquisition system as the right-front tire of the test vehicle passed over it. Test vehicle speed was determined from electronic timing mark data recorded using TestPoint software. Strobe lights and high-speed video analysis are used only as a backup in the event that the vehicle speed cannot be determined from the electronic data.

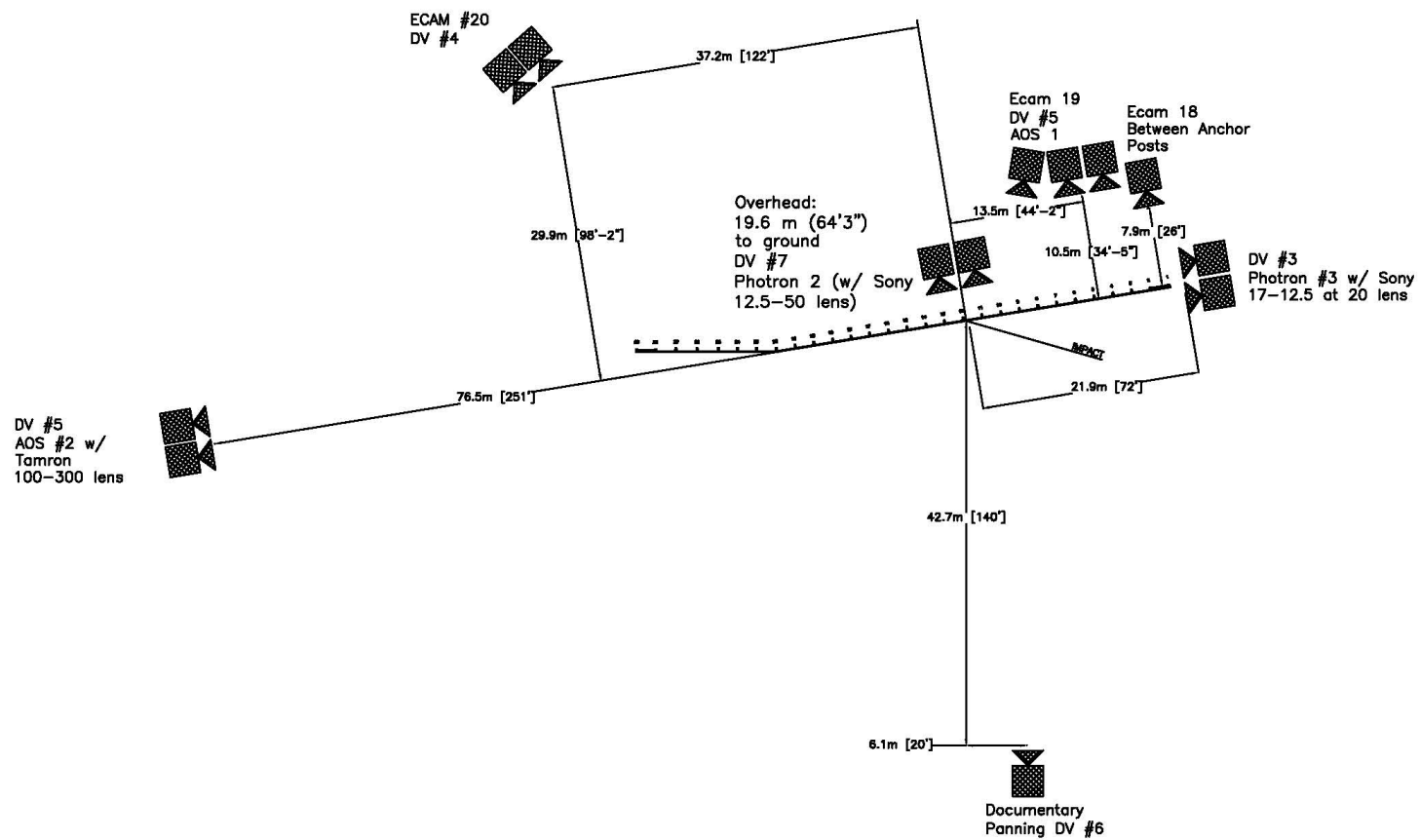


Figure 16. Camera Locations, Test FR-1

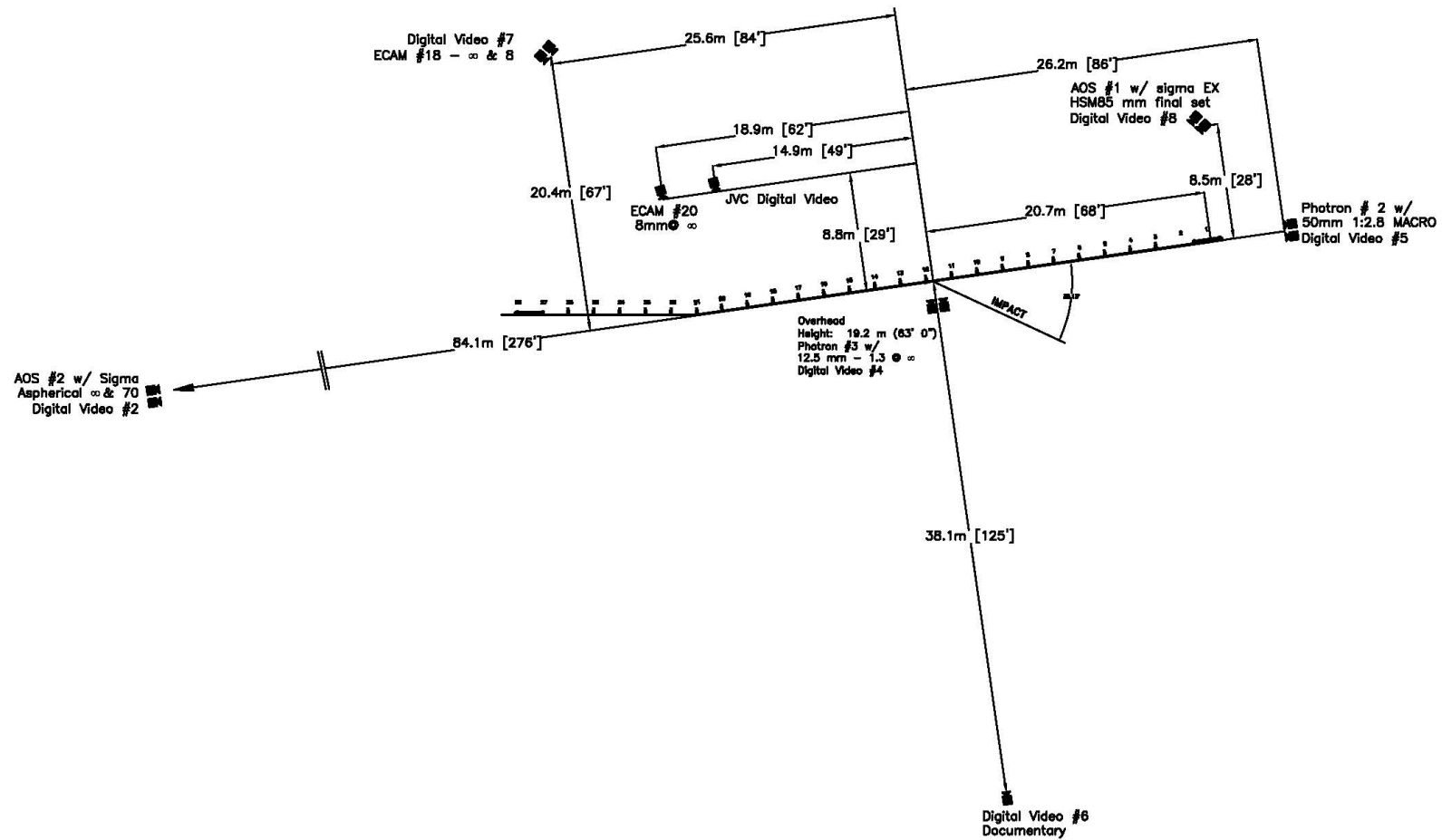


Figure 17. Camera Locations, Test FR-2

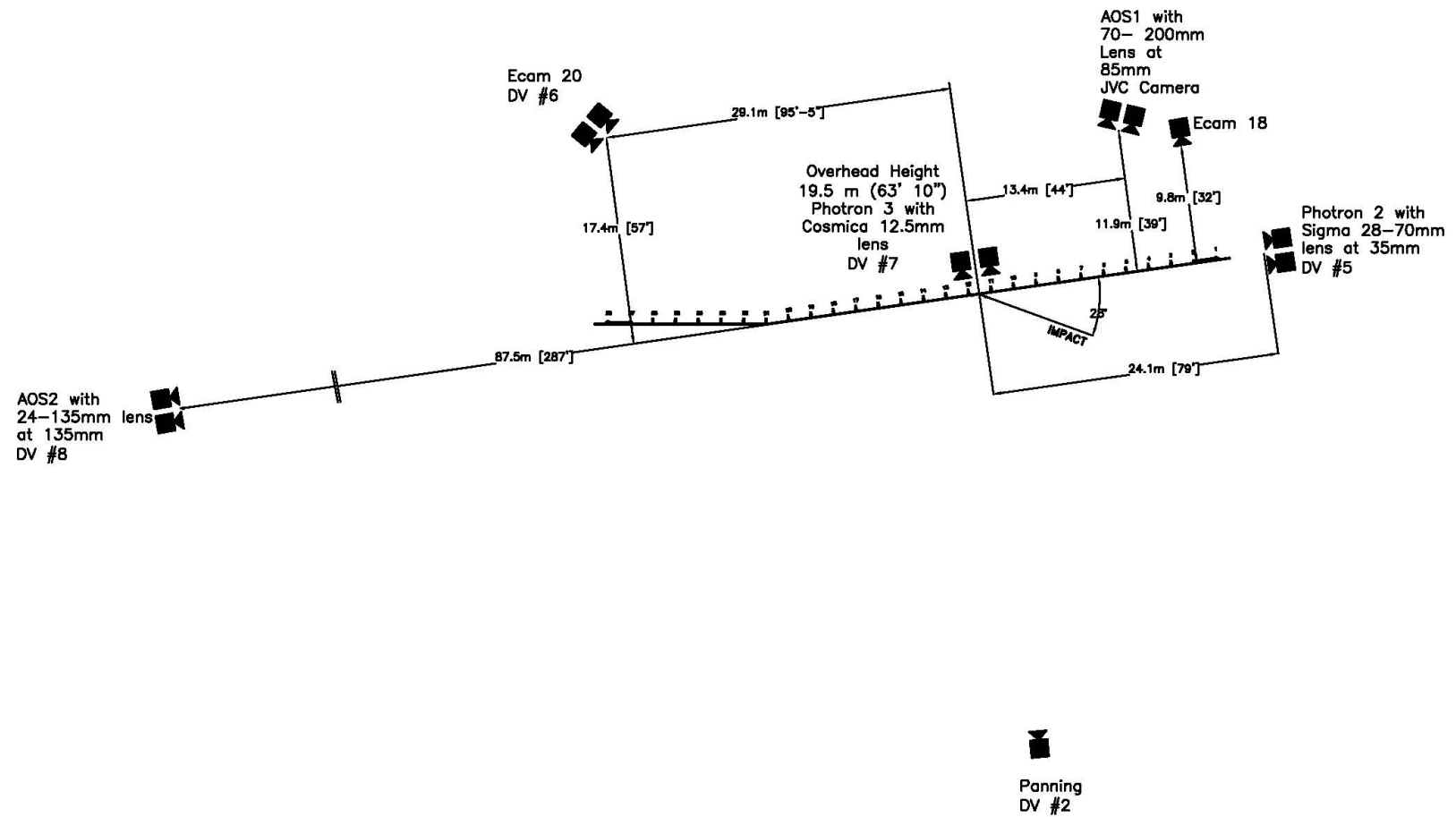


Figure 18. Camera Locations, Test FR-3

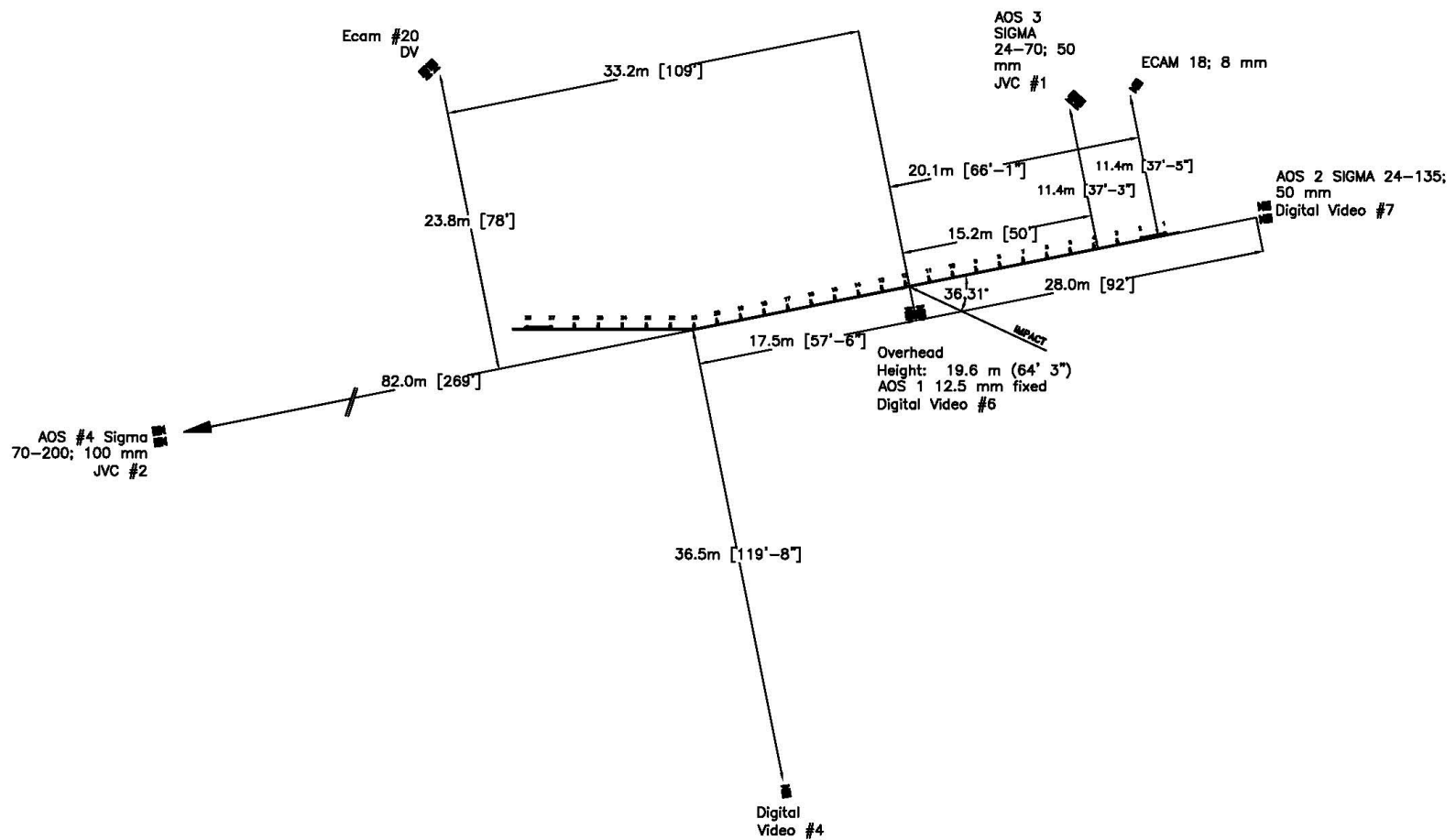


Figure 19. Camera Locations, Test FR-4

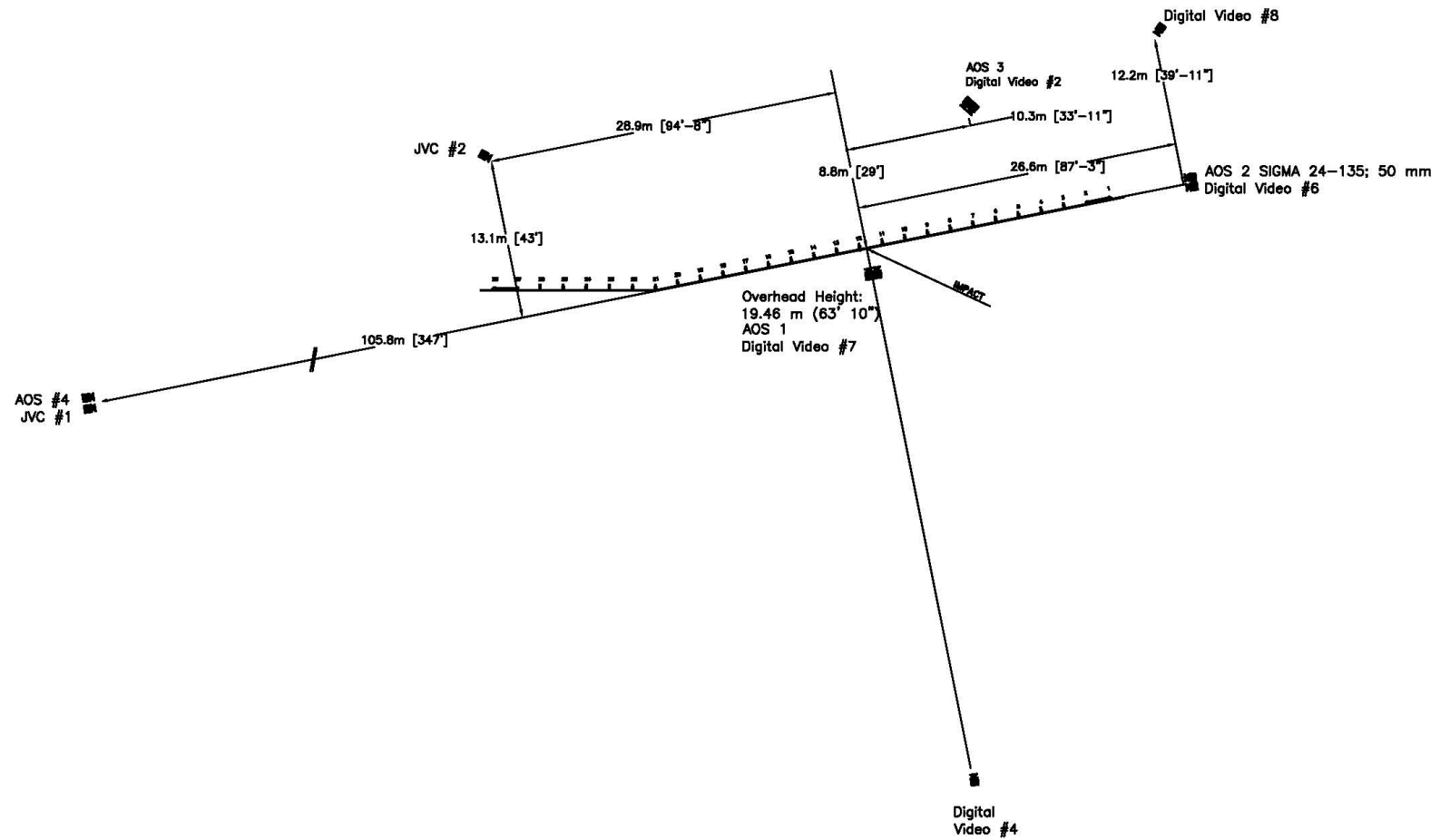


Figure 20. Camera Locations, Test FR-5

4 DESIGN DETAILS - DESIGN NO. 1

The test installation measured 55.25 m (181 ft - 3 in.) long along the length of guardrail, or 55.13 m (180 ft - 10.375 in.) long tangent to the roadway. It consisted of standard 2.66-mm (12-gauge) W-beam supported by steel posts, as shown in Figures 21, 27, and 28. Anchorage systems similar to those used on tangent guardrail terminals were utilized on both the upstream and downstream ends of the guardrail system. Design details are shown in Figures 21 through 26. The corresponding English-unit drawings are shown in Appendix A. Photographs of the test installation are shown in Figures 27 through 30.

The entire system was constructed with twenty-nine guardrail posts. Post nos. 3 through 27 were galvanized ASTM A36 steel W152x13.4 (W6x9) sections measuring 1,829 mm (6 ft) long. Post nos. 1, 2, 28, and 29 were timber posts measuring 140 mm wide x 190 mm deep x 1,080 mm long (5.5 in. x 7.5 in. x 42.5 in.) and were placed in 1,829 mm (6 ft) long steel galvanized foundation tubes, as shown in Figures 22 and 24. The timber posts and foundation tubes were part of anchor systems designed to replicate the capacity of a tangent guardrail terminal.

Post nos. 1 through 29 were spaced 1,905 mm (75 in.) on center with a soil embedment depth of 1,016 mm (40 in.), as shown in Figure 21. The posts were placed in a compacted course, crushed limestone material that met Grading B of AASHTO M147-65 (1990) as found in NCHRP Report No. 350. For post nos. 3 through 27, 152 mm wide x 305 mm deep x 362 mm long (6 in. x 12 in. x 14.25 in.) wood spacer blockouts were used to block the rail away from the front face of the steel posts, as shown in Figure 29.

Standard 2.66-mm (12-gauge) W-beam rails with additional post bolt slots at half post spacing intervals were placed between post nos. 1 and 29, as shown in Figures 21 and 22. The W-

beam top rail height was 787 mm (31 in.), with 632-mm (24.875-in.) center mounting height. The rail splices have been moved to the center of the span locations, as shown in Figures 21 and 22. All lap-splice connections between the rail sections were configured to reduce vehicle snag at splices during the crash test.

The W-beam rail was bent around post no. 22 such that the guardrail was flared to a 13:1 flare which corresponds to an angle of 4.4 degrees away from the travelway. Post nos. 1 through 21 were located along a 40 m (131 ft - 3 in.) length of flared guardrail, while post nos. 22 through 29 were located along the length of tangent guardrail, as shown in Figures 21, 27, and 28.

Figure 21. System Details, Design No. 1

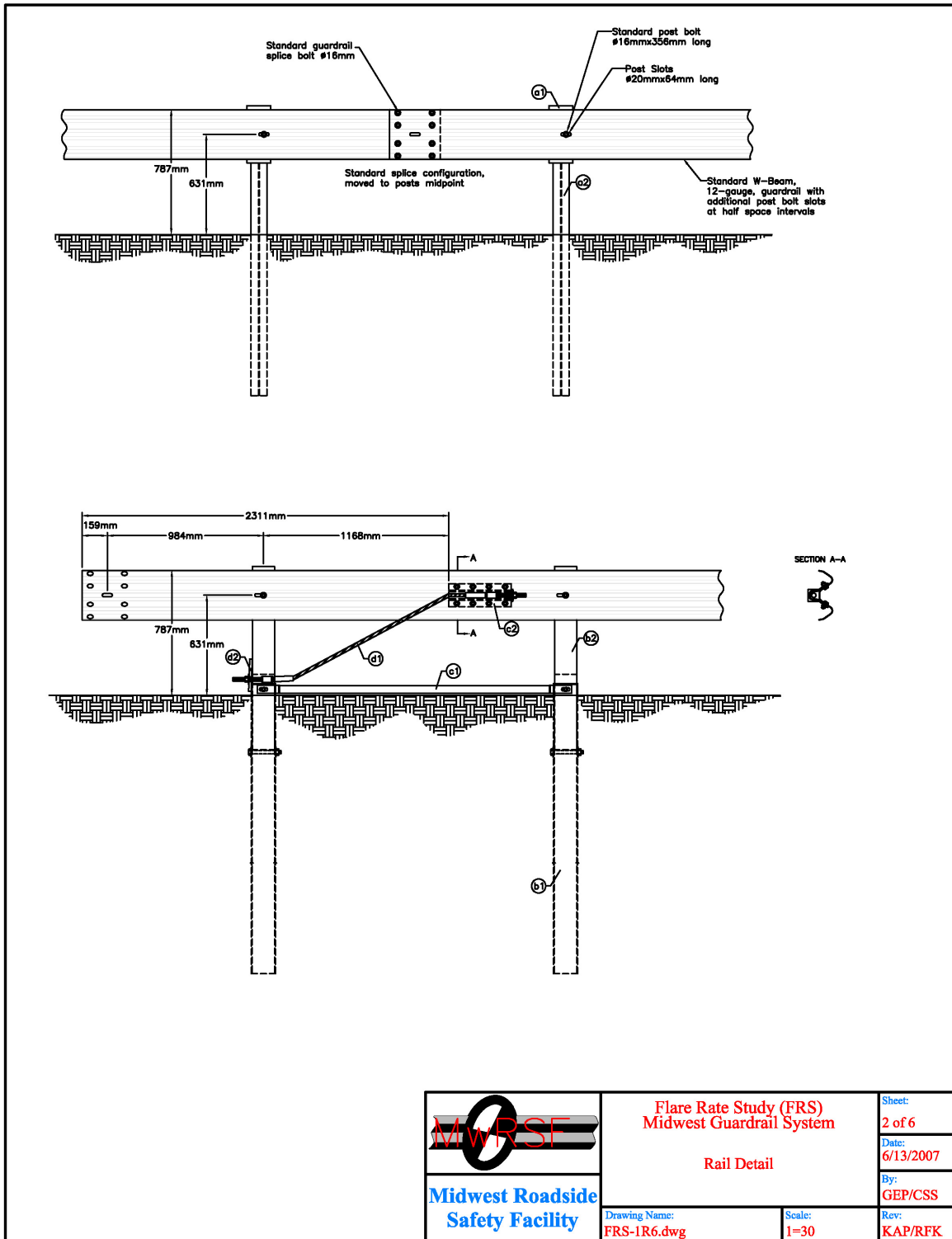


Figure 22. Rail Detail, Design No. 1

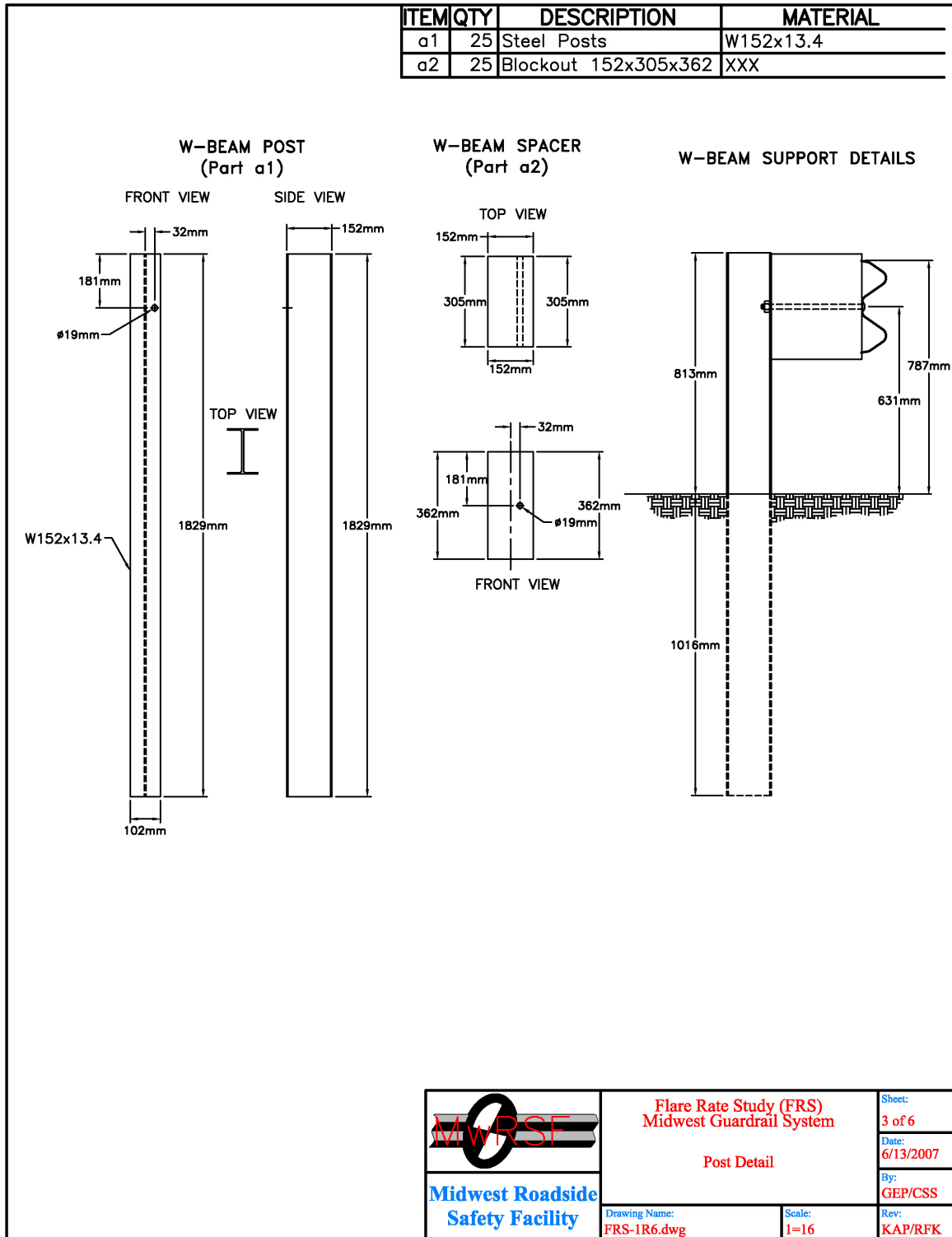


Figure 23. Post Details, Design No. 1

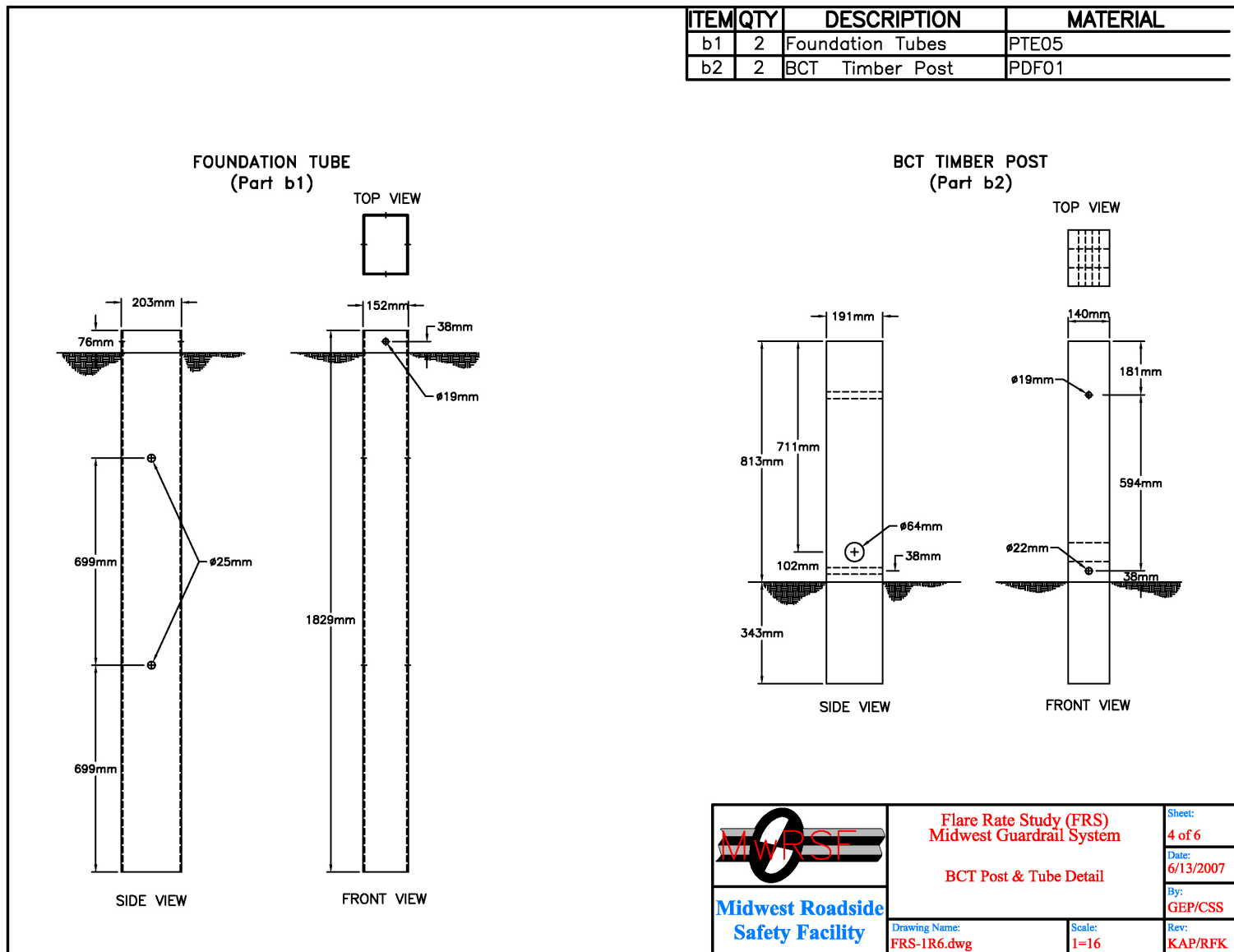


Figure 24. Anchorage Details, Design No. 1

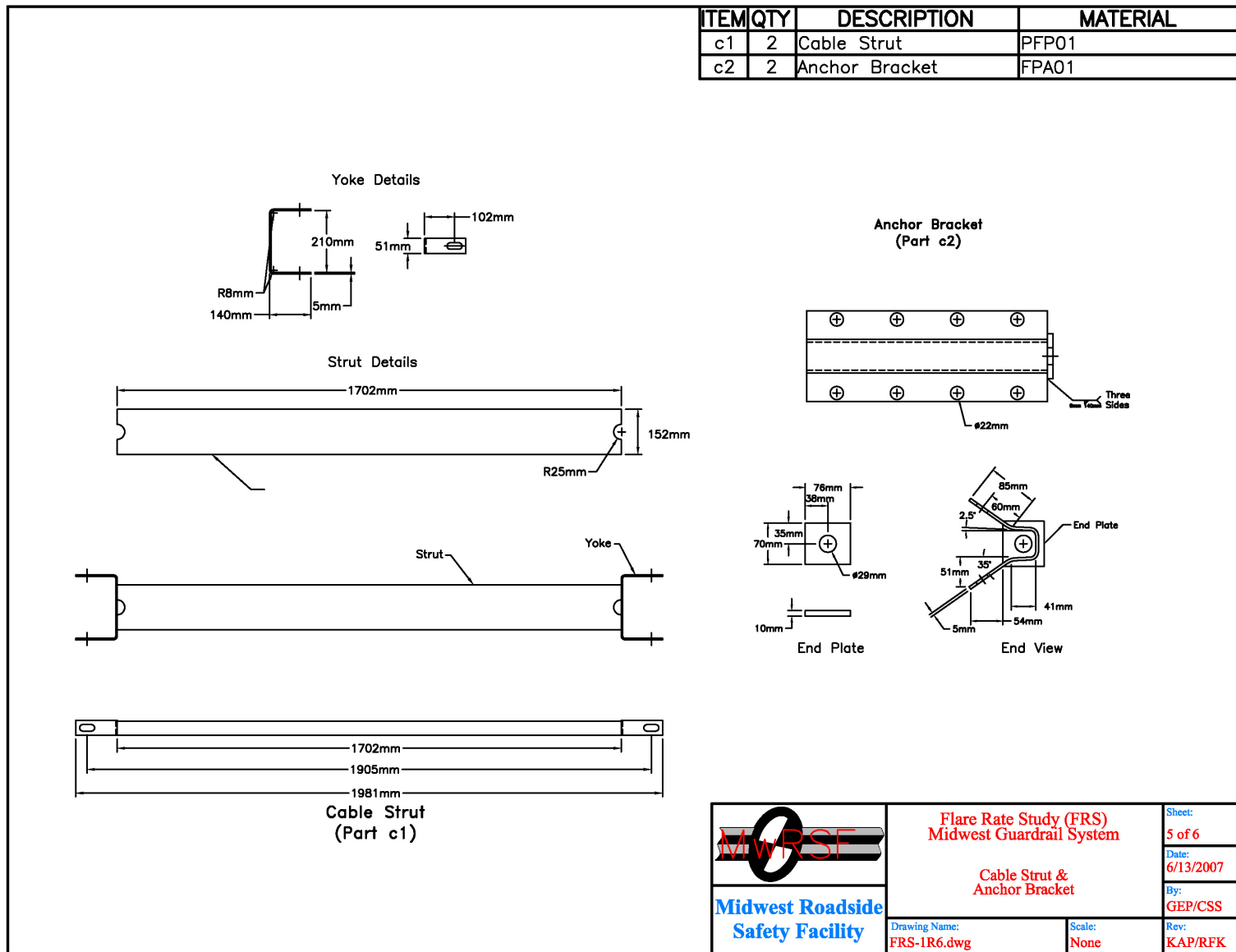


Figure 25. Anchorage Details, Design No. 1

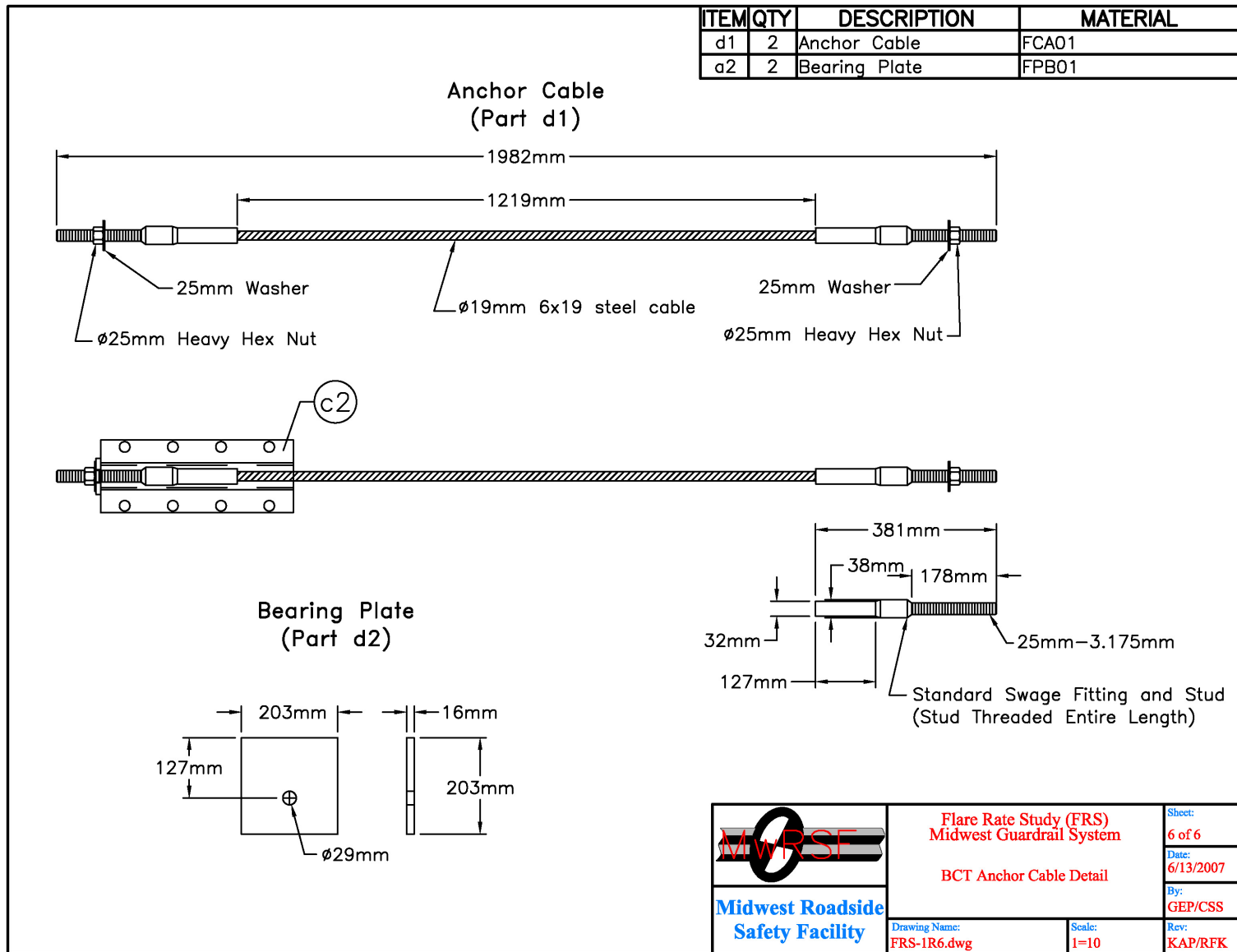


Figure 26. Anchorage Details, Design No. 1



Figure 27. System Details, Design No. 1



Figure 28. System Details, Design No. 1



Figure 29. Post Details, Design No. 1



Figure 30. Splice Details, Design No. 1

5 CRASH TEST NO. 1

5.1 Test FR-1

The 2,026-kg (4,466-lb) pickup truck impacted the MGS installed with a 13:1 flare at a speed of 102.9 km/h (63.9 mph) and at an angle of 30.6 degrees relative to the guardrail (or 26.2 degrees relative to the roadway). A summary of the test results and the sequential photographs are shown in Figure 31. The summary of the test results and sequential photographs in English units is shown in Appendix B. Additional sequential photographs are shown in Figures 32 through 34. Documentary photographs of the crash test are shown in Figures 35 and 36.

5.2 Test Description

Initial impact was to occur between post nos. 11 and 12, or 4.97-m (16 ft - 3.625 in.) upstream from the centerline of the splice between post nos. 14 and 15, as shown in Figure 37. Actual vehicle impact occurred at post no. 12, or 4.76 m (15 ft - 7.5 in.) upstream from the centerline of the splice between post nos. 14 and 15. At 0.014 sec after impact, post no. 12 rotated backwards, and a dent appeared in the vehicle's right-front quarter panel. At 0.020 sec, post nos. 11 and 13 deflected backwards. At 0.030 sec, the rail flattened, and the right-front headlight disengaged and protruded over the rail. At 0.042 sec, the hood protruded over the top of the system, and post no. 14 deflected backwards. At 0.064 sec, the right-front headlight contacted post no. 13, and post nos. 10 and 15 deflected. At this same time, the vehicle's right-front tire twisted. At 0.078 sec, as the right-front quarter panel was crushed into the wheel well, post no. 13 deflected toward the ground, and the blockout at post no. 13 disengaged from the system. At 0.092 sec, the vehicle's right-front tire contacted post no. 13. At 0.100 sec, buckle points appeared in the rail at post no. 13, and the rail flattened around the vehicle. At this same time, the center of the vehicle's bumper bent upwards and

the grill deformed into the radiator. At 0.122 sec, the vehicle approached post no. 14, and post no. 13 twisted and deflected. At 0.130 sec, post no. 14 disengaged from the system, and the blackout at post no. 13 detached from the post. At 0.136 sec, post no. 12 twisted at ground level and buckle points formed at post nos. 19 and 20. At 0.154 sec, post no. 14 contacted the ground. At this same time, the right-front tire deformed the W-beam's bottom corrugation. At 0.196 sec, the front bumper was located at the midspan between post nos. 14 and 15. At this same time, the blackout at post no. 12 disengaged from the system. At 0.228 sec, the front of the vehicle pitched downward and contacted the deformed posts. At this same time, the vehicle's right-rear tire became airborne. At 0.256 sec, post no. 15 disengaged from the system and bent toward the ground. At 0.278 sec, post nos. 16 through 18 deflected. At 0.310 sec, the right-front tire contacted post no. 15, with the rail in contact with the entire right side of the vehicle. At 0.326 sec, excessive tensile forces were encountered by the rail. At this same time, the blackout at post no. 14 disengaged from the post. At 0.382 sec, the vehicle became parallel to the flared portion of the system with a resultant velocity of 54.3 km/h (33.8 mph). At 0.400 sec, the vehicle overrode post no. 16. At 0.456 sec, the bumper was located at post no. 17. At this same time, the blackout at post no. 10 disengaged from the system as the post twisting ceased. At 0.524 sec, the right-front tire overrode post no. 17. At 0.564 sec, the rail disengaged from post nos. 1 through 9. At 0.670 sec, the vehicle was located at post no. 18 without impacting it. At 1.040 sec, the vehicle exited the system at an angle of 28.9 degrees with respect to the flared section and at a resultant velocity of 19.3 km/h (12.0 mph). The vehicle came to rest 12.9 m (42 ft - 4 in.) downstream from impact and 1.9 m (6 ft - 2 in.) laterally away from the traffic-side face of the flared rail. The vehicle trajectory and final position are shown in Figures 31 and 38.

5.3 Barrier Damage

Barrier damage was moderate, as shown in Figures 39 through 44. Barrier damaged consisted of deformed guardrail posts, deformed W-beam rail, deformed and disengaged blockouts, and contact marks on a guardrail section. The length of vehicle contact along the system was approximately 11.4 m (37 ft - 6 in.), which spanned from the centerline of post no. 12 through the centerline of post no. 18.

Moderate deformation and flattening of the impacted section of W-beam rail occurred between post nos. 12 and 18. Contact marks were found on the rail between post nos. 12 and 18. The guardrail buckled at nearly every post location between post nos. 12 and 18. Major buckling of the guardrail occurred at the upstream side of post no. 19. The W-beam was pulled off of post nos. 1 through 19. The W-beam rail sustained significant yielding around the post bolt slots at post nos. 1 through 11, 13, 14, 18, and 19. Minor tearing of the W-beam rail occurred around the post bolt slots at post nos. 12 and 15, while the tearing of the W-beam rail around the post bolt slots at post nos. 16 and 17 was very significant. No significant guardrail damage occurred downstream of post no. 20.

Post nos. 10 and 11 rotated downstream and bend backward slightly. Post no. 12 also rotated downstream, but more significantly. Post no. 13 deformed completely to the ground, with twisting of the front flange. Post no. 14 deformed downstream and backwards with the top of the post 203 mm (8 in.) above the ground. Post nos. 15 through 17 were twisted and deformed downstream and backwards with the tops of the posts 356 mm (14 in.), 305 mm (12 in.), and 152 mm (6 in.) above the ground, respectively. Post nos. 18 and 19 were twisted and bent backwards slightly. The upstream and downstream anchorage systems moved longitudinally 51 mm (2 in.) and 19 mm (0.75

in.), respectively, and pulled up out of the ground slightly. The two wood BCT posts in the upstream anchor were split vertically, but remained with the rest of the anchorage system.

The wooden blockouts at post nos. 3 through 10 and 19 rotated slightly while still attached to the post. The wooden blockouts at post nos. 11, 12, and 18 encountered damage on the front face due to W-beam rail contact, but remained attached to the posts. The wooden blockouts at post nos. 13 through 17 were fractured and removed from the posts.

The permanent set of the barrier system is shown in Figure 39. The maximum lateral permanent set rail and post deflections were 1,140 mm (44.875 in.) at the midspan between post nos. 15 and 16 and 813 mm (32 in.) at the centerline of post no. 13, respectively, as measured in the field. The maximum lateral dynamic rail and post deflections were 1,684 mm (66.3 in.) at the centerline of post no. 15 and 853 mm (33.6 in.) at the centerline of post no. 13, respectively, as determined from high-speed video analysis. The working width of the system was found to be 1,794 mm (70.6 in.).

5.4 Vehicle Damage

Exterior vehicle damage was moderate, as shown in Figures 46 through 49. Occupant compartment deformations to the right side and center of the floorboard were judged insufficient to cause serious injury to the vehicle occupants. Maximum longitudinal deflections of 6 mm (0.25 in.) were located near the front and left sides of the right-side floorpan. Maximum lateral deflections of 13 mm (0.5 in.) were located near the center of the right-side floorpan. Maximum vertical deflections of 19 mm (0.75 in.) were located near the right side of the right-side floorpan. Complete occupant compartment deformations and the corresponding locations are provided in Appendix C.

Damage was concentrated on the right-front corner of the vehicle. The right-front bumper

had a buckle point at the center. Scrape marks and deformations were found along the entire right side. The right-rear corner of the box was dented. The right-side suspension, ball joint, and control arm connections were broken. The front grill was shifted toward the left, and the right side of the grill was fractured. The hood was ajar. The right-side headlight and turn signal assembly were fractured and disengaged from the vehicle. The left side, rear, roof, and all window glass remained undamaged.

5.5 Occupant Risk Values

The longitudinal and lateral occupant impact velocities were determined to be 6.51 m/s (21.36 ft/s) and 4.12 m/s (13.52 ft/s), respectively. The maximum 0.010-sec average occupant ridedown decelerations in the longitudinal and lateral directions were 8.08 g's and 10.41 g's, respectively. It is noted that the occupant impact velocities (OIVs) and occupant ridedown decelerations (ORDs) were within the suggested limits provided in NCHRP Report No. 350. The THIV and PHD values were determined to be 7.45 m/s (24.43 ft/s) and 12.15 g's, respectively. The results of the occupant risk, determined from the accelerometer data, are summarized in Figure 31. Results are shown graphically in Appendix D. The results from the rate transducer are also shown graphically in Appendix D.

5.6 Discussion

The analysis of the test results for test no. FR-1 showed that the MGS installed with a 13:1 flare, impacted with the 2000P vehicle, adequately contained and redirected the vehicle with controlled lateral displacements of the barrier system. There were no detached elements nor fragments which showed potential for penetrating the occupant compartment nor presented undue hazard to other traffic. Deformations of, or intrusion into, the occupant compartment that could have

caused serious injury did not occur. The test vehicle did not penetrate nor ride over the guardrail system and remained upright during and after collision. Vehicle roll, pitch, and yaw angular displacements were noted, but they were deemed acceptable because they did not adversely influence occupant risk safety criteria nor cause rollover. After collision, the vehicle's trajectory revealed minimum intrusion into adjacent traffic lanes. In addition, the vehicle's exit angle of 28.9 degrees was greater than 60 percent of the impact angle of 30.6 degrees. However, it should be noted that this evaluation criterion is only preferred and not required. Therefore, test no. FR-1 conducted on the MGS installed with a 13:1 flare was determined to be acceptable according to TL-3 safety performance criteria of test designation 3-11 found in NCHRP Report No. 350.

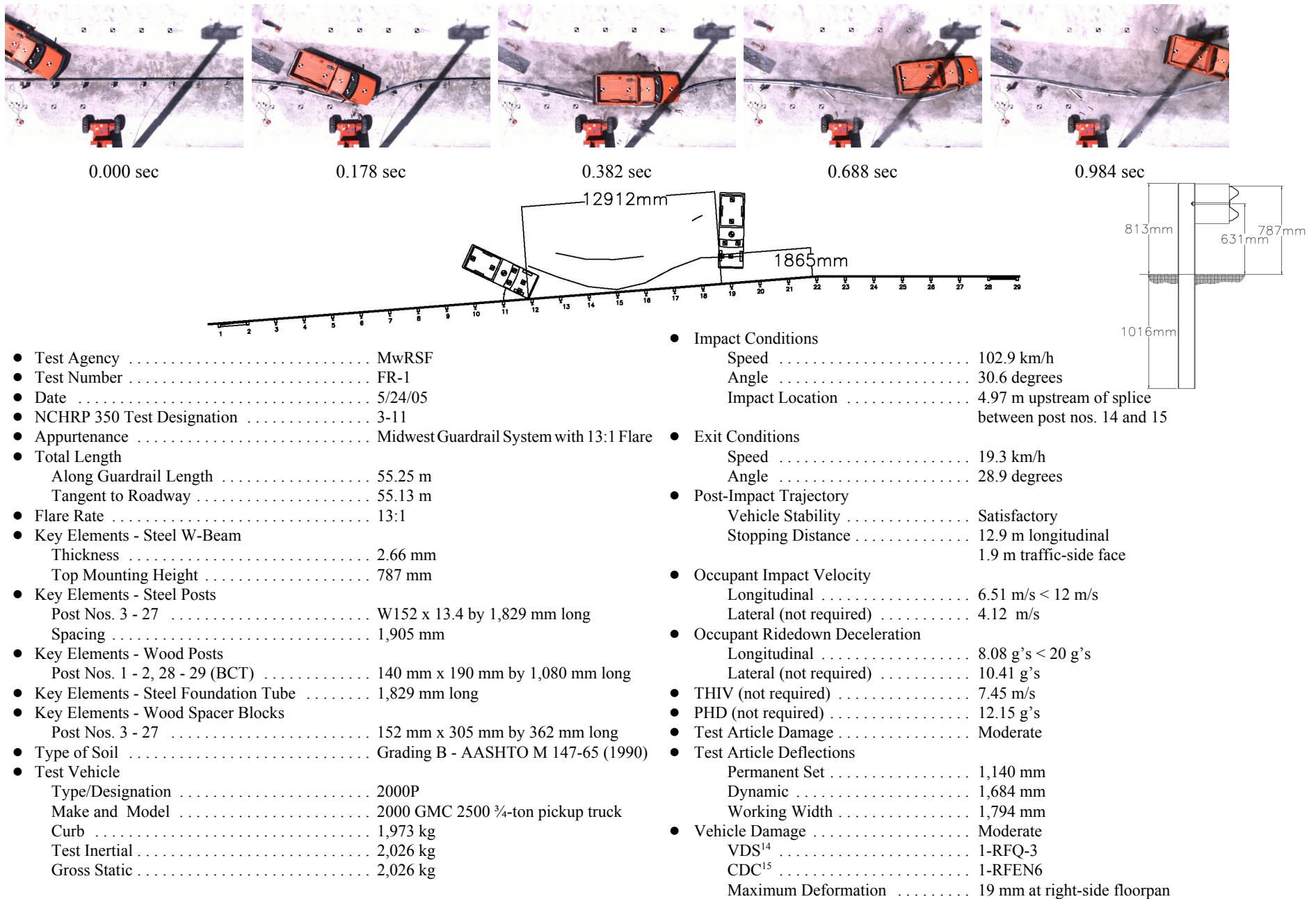
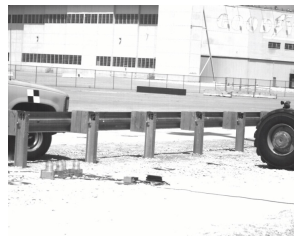


Figure 31. Summary of Test Results and Sequential Photographs, Test FR-1



0.000 sec



0.096 sec



0.228 sec



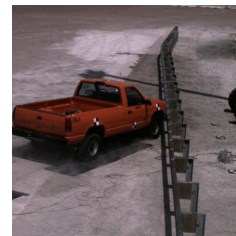
0.326 sec



0.494 sec



1.082 sec



0.000 sec



0.136 sec



0.338 sec



0.504 sec



0.746 sec



0.982 sec

Figure 32. Additional Sequential Photographs, Test FR-1



0.000 sec



0.118 sec



0.292 sec



0.510 sec



0.854 sec



1.246 sec



0.000 sec



0.154 sec



0.266 sec



0.432 sec



0.660 sec



0.922 sec

Figure 33. Additional Sequential Photographs, Test FR-1



0.000 sec



0.104 sec



0.207 sec



0.345 sec



0.621 sec



0.897 sec

Figure 34. Additional Sequential Photographs, Test FR-1



Figure 35. Documentary Photographs, Test FR-1



Figure 36. Documentary Photographs, Test FR-1



Figure 37. Impact Location, Test FR-1



Figure 38. Vehicle Trajectory and Final Position, Test FR-1



Figure 39. System Damage, Test FR-1



58

Figure 40. System Damage, Test FR-1



Figure 41. Post Nos. 11 and 12 Damage, Test No. FR-1



Figure 42. Post Nos. 13 and 14 Damage, Test No. FR-1



Figure 43. Post Nos. 15 and 16 Damage, Test No. FR-1



Figure 44. Post Nos. 17 and 18 Damage, Test FR-1



Figure 45. Upstream Anchorage Damage, Test FR-1



Figure 46. Vehicle Damage, Test FR-1



Figure 47. Vehicle Damage, Test FR-1

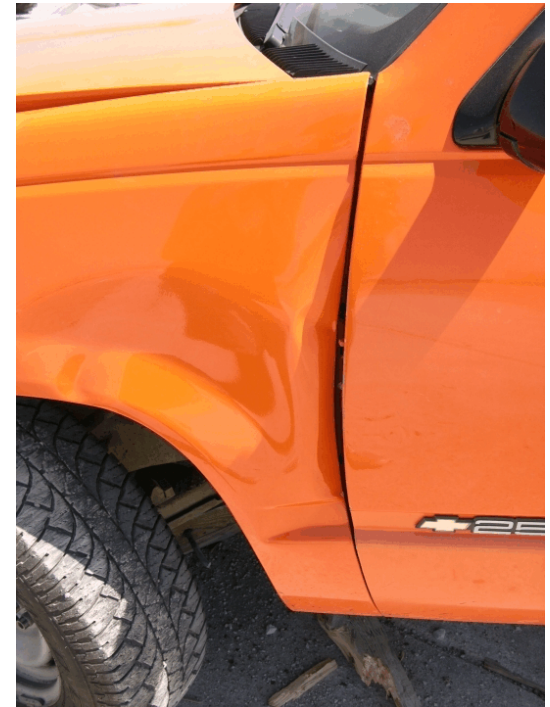


Figure 48. Vehicle Damage, Test FR-1



Figure 49. Vehicle Undercarriage Damage, Test FR-1

6 DESIGN DETAILS - DESIGN NO. 2

Due to testing deviations, the actual impact of test no. FR-1 had a higher impact speed and angle than those specified in NCHRP Report No. 350. As a result, the impact severity (IS) was 15% higher than targeted and an effective flare rate can be calculated for this test. The effective flare rate was calculated to be 8.4:1 for test no. FR-1. Thus, due to the desire to determine the flare rate performance limits for the MGS, it was decided to increase the flare of the system.

The second design was identical to the first design except for the flare rate of the system. The first installation's flare was set at 13:1, or 4.4 degrees away from the travelway. However, the second installation's flare was increased to 7:1 which corresponds to an angle of 8.1 degrees away from the travelway. Post nos. 1 through 20 were located along a 38.1 m (125 ft) length of guardrail, while post nos. 21 through 28 were located along the length of tangent guardrail, as shown in Figure 50.

The test installation measured 53.34 m (175 ft) long along the length of guardrail, but measured 52.93 m (173 ft - 8 in.) long tangent to the roadway. This system also consisted of standard 2.66-mm (12-gauge) W-beam guardrail supported by steel posts. Anchorage systems similar to those used on tangent guardrail terminals were also utilized on both the upstream and downstream ends of the system, as shown in Figures 50 and 51. Similarly, the rail splices have been moved to the center of the span locations. In addition, all lap splice connections between the rail sections were configured to reduce vehicle snag at the splices during the crash test. Photographs of the installation are shown in Figures 51 through 53. The complete set of system drawings, along with the corresponding English-unit drawings, are shown in Appendix E.

Figure 50. System Details, Design No. 2



Figure 51. System Details, Design No. 2



Figure 52. Post Details, Design No. 2

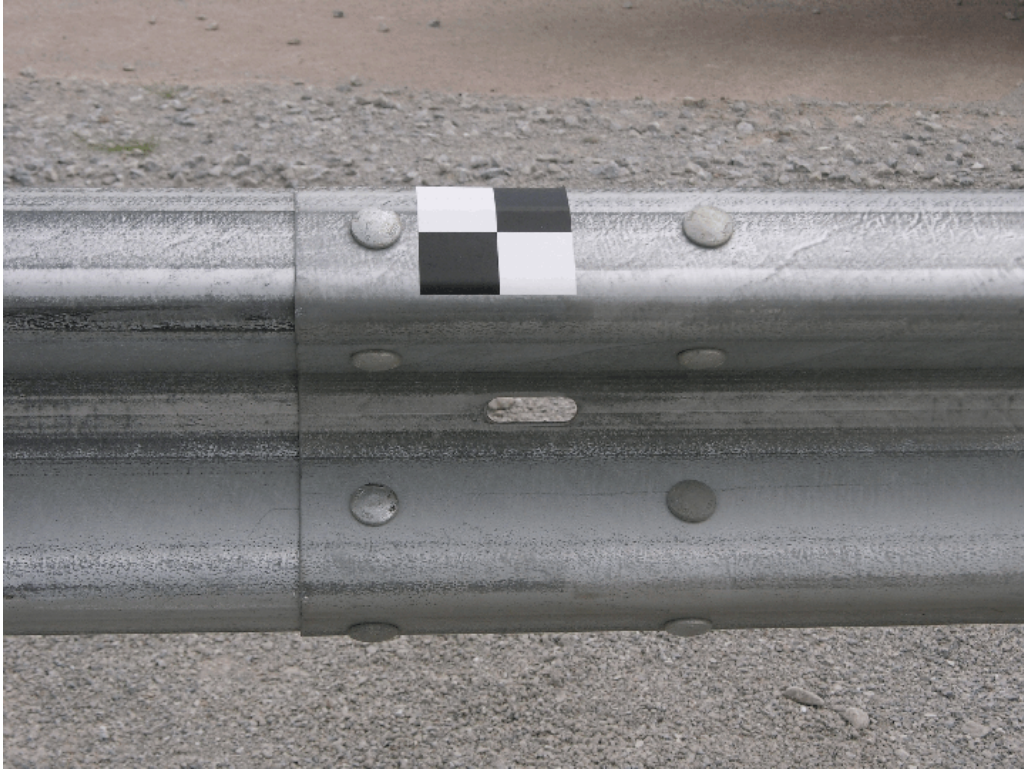


Figure 53. Splice Details, Design No. 2

7 CRASH TEST NO. 2

7.1 Test FR-2

The 2,023-kg (4,461-lb) pickup truck impacted the MGS installed with a 7:1 flare at a speed of 101.6 km/h (63.1 mph) and at an angle of 34.0 degrees relative to the guardrail (or 25.9 degrees relative to the roadway). A summary of the test results and the sequential photographs are shown in Figure 54. The summary of the test results and sequential photographs in English units is shown in Appendix B. Additional sequential photographs are shown in Figures 55 and 56. Documentary photographs of the crash test are shown in Figures 57 and 58.

7.2 Test Description

Initial impact was to occur between post nos. 11 and 12, or 5.24 m (17 ft - 2.25 in.) upstream from the centerline of the splice between post nos. 14 and 15, as shown in Figure 59. Actual vehicle impact occurred 5.21 m (17 ft - 1 in.) upstream from the centerline of the splice between post nos. 14 and 15. Immediately following impact, the front bumper and the rail deformed. At 0.010 sec, post no. 12 deflected backward. At 0.018 sec, post no. 13 deflected, and a gap formed between the vehicle's hood and body. At 0.042 sec, post nos. 3 through 11 twisted clockwise towards impact, and post no. 14 deflected slightly. At 0.078 sec, the vehicle contacted the blockout and traffic-side flange of post no. 13. At 0.086 sec, cracks propagated throughout the blockout at post no. 13. At 0.100 sec, the blockout at post no. 13 disengaged from the system. At 0.122 sec, post no. 14 twisted counter-clockwise, and post no. 13 contacted the ground. At 0.132 sec, post no. 16 deflected backwards. At 0.150 sec, the vehicle contacted the blockout on post no. 14, and the vehicle's right-front tire protruded under the rail. At 0.182 sec, post no. 17 deflected backwards, and the hood rose slightly. At 0.216 sec, the blockout at post no. 15 disengaged from the rail. At 0.242 sec, the vehicle

contacted the traffic-side flange of post no. 15. At 0.262 sec, the blockout at post no. 16 disengaged from the system, and the right-rear tire became airborne. At 0.286 sec, post no. 17 twisted counter-clockwise toward the vehicle as the rear of the vehicle pitched downward. At 0.302 sec, the right-rear corner of the vehicle contacted the guardrail. At 0.364 sec, the vehicle contacted the upstream edge of the traffic-side flange of post no. 16. At 0.392 sec, the rail disengaged from the blockout at post no. 17 and twisted. At 0.478 sec, the vehicle became parallel to the system with a resultant velocity of 41.4 km/h (25.7 mph). At this same time, the vehicle contacted post no. 17. At 0.490 sec, the right-rear corner of the vehicle rode on top of the guardrail section. At 0.562 sec, post nos. 8 through 10 ceased twisting as the rail rebounded. At 0.960 sec, the vehicle yawed while in contact with post no. 18. At 1.360 sec, the vehicle exited the system with a resultant velocity of 23.2 km/h (14.4 mph) and at an angle of 8.7 degrees relative to the tangent section. At 2.410 sec, the vehicle came to rest in contact with the “knee joint” between the flare and the tangent guardrail sections. The vehicle came to rest 16.9 m (55 ft - 4 in.) downstream from impact and 2.5 m (8 ft - 2 in.) laterally away from the traffic-side face of the tangent rail. The trajectory and final position of the pickup truck are shown in Figure 60.

7.3 Barrier Damage

Damage to the barrier system was moderate, as shown in Figures 61 through 69. Barrier damage consisted of deformed guardrail posts, deformed W-beam rail, deformed and disengaged blockouts, and contact marks on a guardrail section. The length of vehicle contact along the system was approximately 16.3 m (53 ft - 6.75 in.), which spanned from 451 mm (17.75 in.) upstream from the centerline of post no. 12 through 635 mm (25 in.) downstream from the centerline of post no. 20.

Contact marks were found along the length of vehicle contact with the system. Minor guardrail deformation was found between post nos. 21 and 28. The W-beam rail was deformed and flattened between post nos. 13 and 17. The guardrail buckled at post nos. 2 and 17 through 19 and at the midspan between post nos. 11 and 12. Other guardrail buckle points were found at 432 mm (17 in.) upstream of post no. 19, 470 mm (18.5 in.) downstream of post no. 19, 203 mm (8 in.) upstream of post no. 21, and at post no. 28. The W-beam rail pulled off of post nos. 12 through 24 and 26. The W-beam rail sustained major tearing and significant yielding around the post bolt slots at post nos. 12, 15, and 26, while only minor yielding occurred around the post bolt slots at post nos. 13, 14, and 16 through 24.

Steel post no. 3 through 11 encountered minor twisting downstream. Post nos. 8 through 11 were also bent slightly. Post no. 12 encountered significant twisting and was bent backwards. Post nos. 13 through 17 were bent longitudinally and twisted clockwise. Post nos. 18 through 20 rotated backward and twisted clockwise. The upstream and downstream anchorage systems moved longitudinally 25 mm (1 in.) downstream and 25 mm (1 in.) upstream, respectively. The second wood BCT post in the upstream anchor, post no. 2, split vertically but remained with the rest of the anchorage system.

The wooden blockouts at post nos. 3 through 11 rotated slightly, while still attached to the post. The wooden blockouts at post nos. 12 and 18 through 21 encountered moderate damage, but remained attached to the posts. The wooden blockouts at post nos. 13 through 17 were fractured and removed from the posts.

The permanent set of the barrier system is shown in Figures 61 and 62. The maximum lateral permanent set rail and post deflections were 1,156 mm (45.5 in.) at the midspan between post nos.

16 and 17 and 756 mm (29.75 in.) at the centerline of post no. 15, respectively, as measured in the field. The maximum lateral dynamic rail and post deflectionsn were 1,925 mm (75.8 in.) at the centerline of post no. 15 and 798 mm (31.4 in.) at the centerline of post no. 15, respectively, as determined from high-speed digital video analysis. The working width of the system was found to be 2,232 mm (87.9 in.).

7.4 Vehicle Damage

Exterior vehicle damage was moderate, as shown in Figures 71 through 74. Occupant compartment deformations to the right side and center of the floorboard were judged insufficient to cause serious injury to the vehicle occupants. Maximum longitudinal deflections of 6 mm (0.25 in.) were located along the left side of the right-side floorpan. Maximum lateral deflections of 13 mm (0.5 in.) were located near the left-front corner of the right-side floorpan. Maximum vertical deflections of 6 mm (0.25 in.) were located near the center of the right-side floorpan. Complete occupant compartment deformations and the corresponding locations are provided in Appendix F.

Damage was concentrated on the right-front corner of the vehicle. The right-front quarter panel was deformed and crushed inward toward the engine compartment. Contact marks were found along the entire right side. The right side of the front bumper was crushed inward and torn. The front bumper was twisted, shifted to the left and deformed in toward the radiator. The radiator mounts were deformed backward into the engine. The top of the right-side door was ajar. The right-front corner of the frame was crushed and deformed upward. The right-front tie rod was fractured, and the control arm was bent inward toward the frame. The right-front tire was deflated, and a gouge was found on the inside of the steel rim. The left side, rear, roof, hood, and all window glass remained undamaged.

a 7:1 flare was determined to be acceptable according to the TL-3 safety performance criteria of test designation no. 3-11 found in NCHRP Report No. 350.

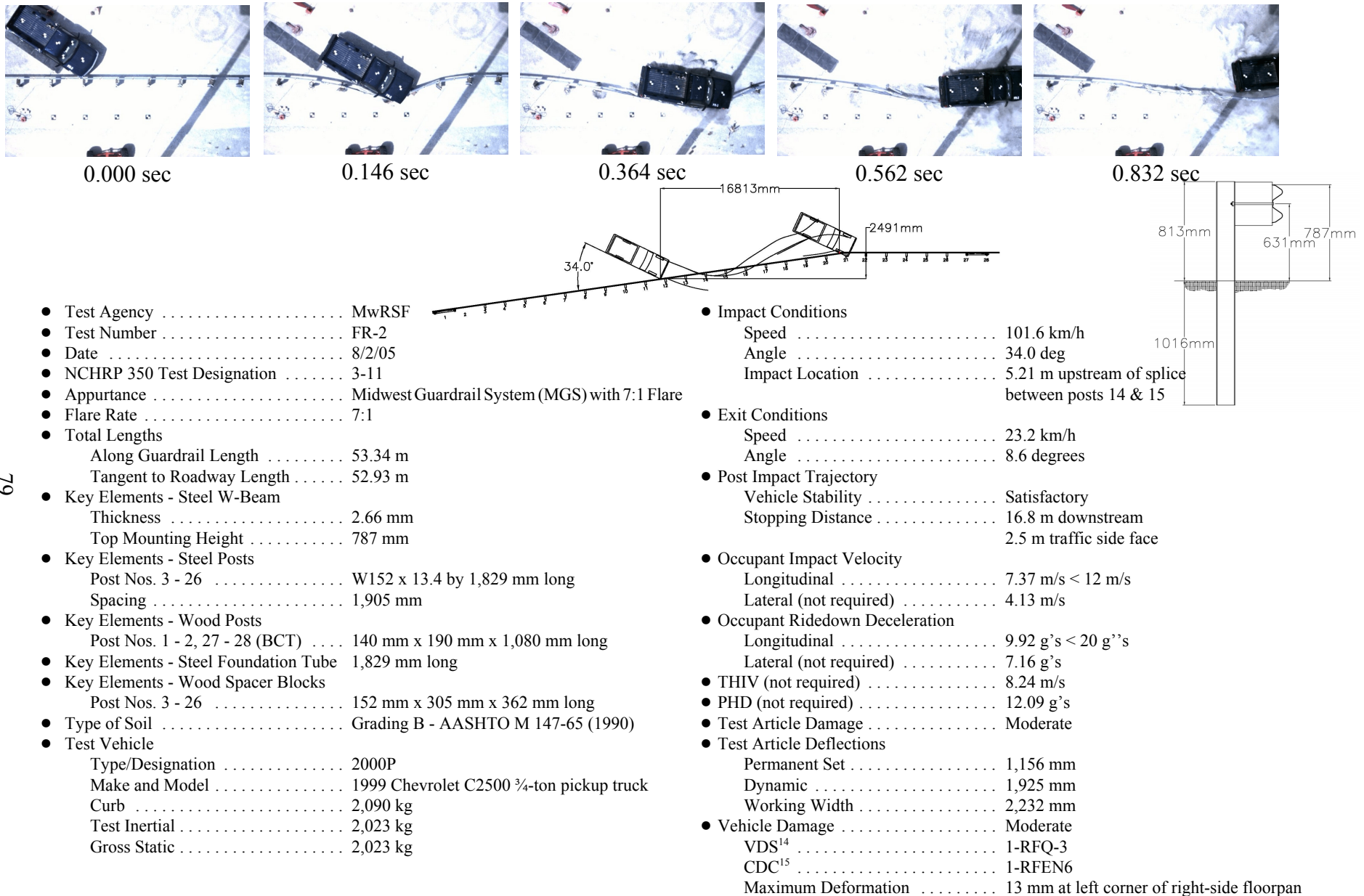


Figure 54. Summary of Test Results and Sequential Photographs, Test FR-2



0.000 sec



0.180 sec



0.452 sec



0.606 sec



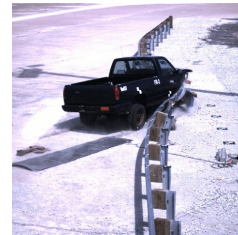
0.890 sec



1.210 sec



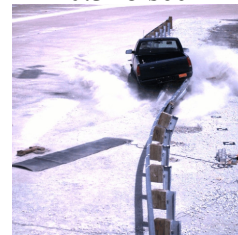
0.000 sec



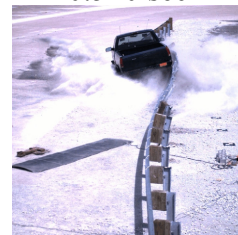
0.154 sec



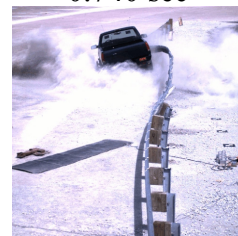
0.318 sec



0.510 sec



0.740 sec



0.970 sec

Figure 55. Additional Sequential Photographs, Test FR-2



0.000 sec



0.118 sec



0.318 sec



0.492 sec



0.630 sec



1.158 sec



0.000 sec



0.172 sec



0.312 sec



0.472 sec



0.662 sec



0.964 sec

Figure 56. Additional Sequential Photographs, FR-2



Figure 57. Documentary Photographs, Test FR-2

7.5 Occupant Risk Values

The longitudinal and lateral occupant impact velocities were determined to be 7.37 m/s (24.18 ft/s) and 4.13 m/s (13.55 ft/s), respectively. The maximum 0.010-sec average occupant ridedown decelerations in the longitudinal and lateral directions were 9.92 g's and 7.16 g's, respectively. It is noted that the occupant impact velocities (OIVs) and occupant ridedown decelerations (ORDs) were within the suggested limits provided in NCHRP Report No. 350. The THIV and PHD values were determined to be 8.24 m/s (27.03 ft/s) and 12.09 g's, respectively. The results of the occupant risk, determined from the accelerometer data, are summarized in Figure 54. Results are shown graphically in Appendix G. The results from the rate transducer are also shown graphically in Appendix G.

7.6 Discussion

The analysis of the test results for test no. FR-2 showed that the MGS installed with a 7:1 flare, impacted with the 2000P vehicle, adequately contained and redirected the vehicle with controlled lateral displacements of the barrier system. There were no detached elements nor fragments which showed potential for penetrating the occupant compartment nor presented undue hazard to other traffic. Deformations of, or intrusion into, the occupant compartment that could have caused serious injury did not occur. The test vehicle did not penetrate nor ride over the guardrail system and remained upright during and after the collision. Vehicle roll, pitch, and yaw angular displacements were noted, but they were deemed acceptable because they did not adversely influence occupant risk safety criteria nor cause rollover. After collision, the vehicle's trajectory revealed minimum intrusion into adjacent traffic lanes. In addition, the vehicle's exit angle was less than 60 percent of the impact angle. Therefore, test no. FR-2 conducted on the MGS installed with



Figure 58. Documentary Photographs, Test FR-2



Figure 59. Impact Location, Test FR-2



Figure 60. Vehicle Trajectory and Final Position, Test FR-2



Figure 61. System Damage, Test FR-2



Figure 62. System Damage, Test FR-2



Figure 63. Post Nos. 9 and 10 Damage, Test FR-2



Figure 64. Post No. 11 Damage, Test FR-2



Figure 65. Post No. 12 Damage, Test FR-2



Figure 66. Post Nos. 13 and 14 Damage, Test FR-2



92

Figure 67. Post Nos. 15 and 16 Damage, Test FR-2



Figure 68. Post No. 17 Damage, Test FR-2



Figure 69. Post Nos. 18 and 19 Damage, Test FR-2



Figure 70. Anchorage Damage, Test FR-2



Figure 71. Vehicle Damage, Test FR-2



Figure 72. Vehicle Damage, Test FR-2



Figure 73. Undercarriage Damage, Test FR-2



Figure 74. Occupant Compartment Deformation, Test FR-2

8 CRASH TEST NO. 3

8.1 Test FR-3

The 894-kg (1,970-lb) small car impacted the MGS installed with a 7:1 flare at a speed of 102.2 km/h (63.5 mph) and at an angle of 28.7 degrees relative to the guardrail (or 20.6 degrees relative to the roadway). A summary of the test results and the sequential photographs are shown in Figure 75. The summary of the test results and sequential photographs in English units is shown in Appendix B. Additional sequential photographs are shown in Figures 76 through 78. Documentary photographs of the crash test are shown in Figures 79 and 80.

8.2 Test Description

Initial impact was to occur between post nos. 11 and 12, or 1.80 m (5 ft - 10.8125 in.) upstream from the centerline of the splice between post nos. 12 and 13, as shown in Figure 81. Actual vehicle impact occurred 1.80 m (5 ft - 10.9375 in.) upstream from the centerline of the splice between post nos. 12 and 13. Immediately following impact, the front quarter panel deformed and crushed inward toward the engine compartment. At 0.010 sec, the right-front corner of the bumper protruded under the rail, deforming the rail upward. At 0.016 sec, the right-front corner of the bumper contacted the bottom edge of the blockout at post no. 12. At 0.020 sec, post nos. 11 and 12 rotated backward and the rail deformed around the vehicle. At 0.024 sec, post no. 12 twisted clockwise, and the right-front corner of the vehicle's bumper contacted the traffic-side face of post no. 12. At 0.034 sec, the vehicle's hood deformed upward, and post no. 13 deflected. At 0.044 sec, the hood deformed toward the windshield, the right-front tire contacted the upstream edge of the traffic-side face of post no. 12, and the blockout at post no. 12 twisted. At 0.068 sec, the blockout at post no. 12 split vertically. At this same time, the right-front tire was located at the splice between

post nos. 12 and 13, and a buckle formed at post no. 13. At 0.072 sec, the posts upstream of post no. 11 twisted toward impact, and the top corrugation on the W-beam slid upward around the right side and contacted the right-side mirror. At 0.084 sec, the blockouts at post nos. 12 and 13 fractured, and the right-front corner contacted post no. 13. At this same time, the rail was positioned over the right-front tire, and the right-side mirror disengaged from the vehicle. At 0.100 sec, the rail disengaged from post no. 13, which twisted clockwise. At this same time, the blockout at post no. 13 fractured and disengaged from the system. At 0.118 sec, the right-front tire contacted the deflecting post no. 13. At 0.134 sec, the bumper cover disengaged from the vehicle, and the top of the right-side door became ajar. At 0.140 sec, the right-side door was dented, and a buckle was found at post no. 15. At this same time, the occupant's head contacted the right-side window and shattered it. At 0.164 sec, the rail slid across the right-side quarter panel and hood, and the detached bumper contacted post no. 14. At 0.170 sec, the guardrail contacted the right-side A-pillar, and the right-front tire contacted post no. 14. At 0.190 sec, kinking and buckling was found in the deformed guardrail sections. At 0.198 sec, the right-front corner was located downstream of the deformed post no. 14. At 0.202 sec, the right-front tire contacted post no. 14. At 0.226 sec, the vehicle became parallel to the flared guardrail with a velocity of 67.0 km/h (41.6 mph). At 0.256 sec, post no. 15 deflected, and post no. 14 contacted the ground. At 0.296 sec, the hood folded under, and the front of the vehicle redirected away from the system. At 0.300 sec, the right-front tire contacted post no. 15. At 0.342 sec, the hood lost contact with the guardrail. At 0.396 sec the vehicle yawed toward the system, while redirecting away from the system. At 0.408 sec, the guardrail buckled at the post bolt slot at post no. 14. At 0.472 sec, the hood fractured at the attachment. At 0.540 sec, the vehicle exited the system at a trajectory angle of 18.2 degrees relative to the tangent section and at a resultant velocity

of 40.8 km/h (25.3 mph). At 0.664 sec, the vehicle yawed toward the system. At 2.106 sec, the vehicle recontacted the barrier near post no. 26. At 2.188 sec, the right-front tire snagged on post no. 26. The vehicle came to rest 34.4 m (112 ft - 11 in.) downstream from impact and 2.4 m (8 ft - 9 in.) laterally away from the traffic-side face of the rail at impact. The trajectory and final position of the small car are shown in Figures 75 and 82.

8.3 Barrier Damage

Barrier damage was moderate, as shown in Figure 83. Barrier damage consisted of deformed guardrail posts, deformed and disengaged blockouts, deformed W-beam guardrail, and contact marks on a guardrail section. The length of vehicle contact along the system was approximately 9.6 m (31 ft - 4.1875 in.), which spanned from 849 mm (33.4375 in.) downstream upstream from the centerline of post no. 12 through 1,086 mm (42.75 in.) downstream from the centerline of post no. 16.

Contact marks were found along the length of vehicle contact with the system. The W-beam rail was deformed and flattened between post nos. 11 and 15. The guardrail buckled at the midspan between post nos. 10 and 11, at post nos. 12 and 15, and at the midspan between post nos. 13 and 14. The guardrail also buckled at 648 mm (25.5 in.) downstream of post no. 12, at 254 mm (10 in.) and 356 mm (14 in.) upstream of post no. 13, and at 191 mm (7.5 in.) and 419 mm (16.5 in.) downstream of post no. 13. Guardrail buckle points were also found at 227 mm (9 in.) upstream of post no. 14, at 286 mm (11.25 in.) and 184 mm (7.25 in.) upstream of post no. 15, and 483 mm (19 in.) downstream of post no. 15. The W-beam was pulled off of post nos. 13 and 14. Minor yielding occurred around the post bolt slots at post nos. 12 through 15. No significant damage occurred downstream of post no. 16, except for slight deflection and minor contact marks between post nos. 25 and 28 due to the secondary vehicle contact with the system before coming to rest.

Post nos. 3 through 11 encountered minor twisting downstream, and post nos. 9 through 17 rotated backward in the soil. Post nos. 13 and 14 were also bent longitudinally downstream. The upstream and downstream end anchorage systems moved longitudinally approximately 13 mm (0.5 in.) downstream and 13 mm (0.5 in.) upstream, respectively, and the posts deflected downstream. However, all four wood BCT posts remained undamaged. The blockouts at post nos. 12 through 14 were fractured and removed from the system.

The permanent set of the barrier system is shown in Figure 83. The maximum lateral permanent set rail and post deflections were 527 mm (20.75 in.) at the midspan between post nos. 13 and 14 and 483 mm (19 in.) at the centerline of post no. 13, as measured in the field. The maximum lateral dynamic rail and post deflections 925 mm (36.4 in.) at the centerline of post no. 13 and 693 mm (27.3 in.) at the centerline of post no. 13, as determined from high-speed digital video analysis. The working width of the system was found to be 1,107 mm (43.6 in.).

8.4 Vehicle Damage

Exterior vehicle damage was moderate, as shown in Figures 91 through 96. Occupant compartment deformations to the right side and center of the floorboard were judged insufficient to cause serious injury to the vehicle occupants. Complete occupant compartment deformations and the corresponding locations are provided in Appendix H.

Damage was concentrated on the right-front corner of the vehicle. Contact marks and dents were found along the entire right side of the vehicle. The right-front quarter panel deformed and crushed inward toward the engine compartment. The right-front tire bead was broken, and the tire deflated. Dents were found on the right-side door, the right-front and right-rear quarter panels, and the right-side suspension housing, strut and shock absorbers. A hole was found in the right-rear

taillight. The right-side mirror was disengaged from the vehicle. The right-side frame horn was bent. The right-front bumper mount and right-side headlight were fractured. The radiator, air intake, and grill were crushed and bent. The windshield washer fluid tank disengaged. The suspension and tie rod were fractured and deformed. The hood shifted toward the right and the right-front corner was torn. The lower-right corner of the windshield was cracked, and the windshield vents were dislodged. The left side, rear, roof, and all window glass except the windshield remained undamaged.

8.5 Occupant Risk Values

The longitudinal and lateral occupant impact velocities were determined to be 6.65 m/s (21.83 ft/s) and 5.42 m/s (17.80 ft/s), respectively. The maximum 0.010-sec average occupant ridedown decelerations in the longitudinal and lateral directions were 8.20 g's and 9.70 g's, respectively. It is noted that the occupant impact velocities (OIVs) and occupant ridedown decelerations (ORDs) were within the suggested limits provided in NCHRP Report No. 350. The THIV and PHD values were determined to be 8.30 m/s (27.23 ft/s) and 11.33 g's, respectively. The results of the occupant risk, determined from the accelerometer data, are summarized in Figure 75. Results are shown graphically in Appendix I. The results from the rate transducer are also shown graphically in Appendix I.

8.6 Discussion

The analysis of the test results for test no. FR-3 showed that the MGS installed with a 7:1 flare, impacted with the 820C vehicle, adequately contained and redirected the vehicle with controlled lateral displacements of the barrier system. There were no detached elements nor fragments which showed potential for penetrating the occupant compartment nor presented undue

hazard to other traffic. Deformations of, or intrusion into, the occupant compartment that could have caused serious injury did not occur. The test vehicle did not penetrate nor ride over the guardrail system and remained upright during and after the collision. Vehicle roll, pitch, and yaw angular displacements were noted, but they were deemed acceptable because they did not adversely influence occupant risk safety criteria nor cause rollover. After collision, the vehicle's trajectory revealed minimum intrusion into adjacent traffic lanes. In addition, the vehicle's exit angle of 18.2 degrees was greater than 60 percent of the impact angle of 28.7 degrees. However, it should be noted that this evaluation criterion is only preferred and not required. Therefore, it was determined that test no. FR-3 conducted on the MGS installed with a 7:1 flare was determined to be acceptable according to the TL-3 safety performance criteria of test designation no. 3-10 found in NCHRP Report No. 350.

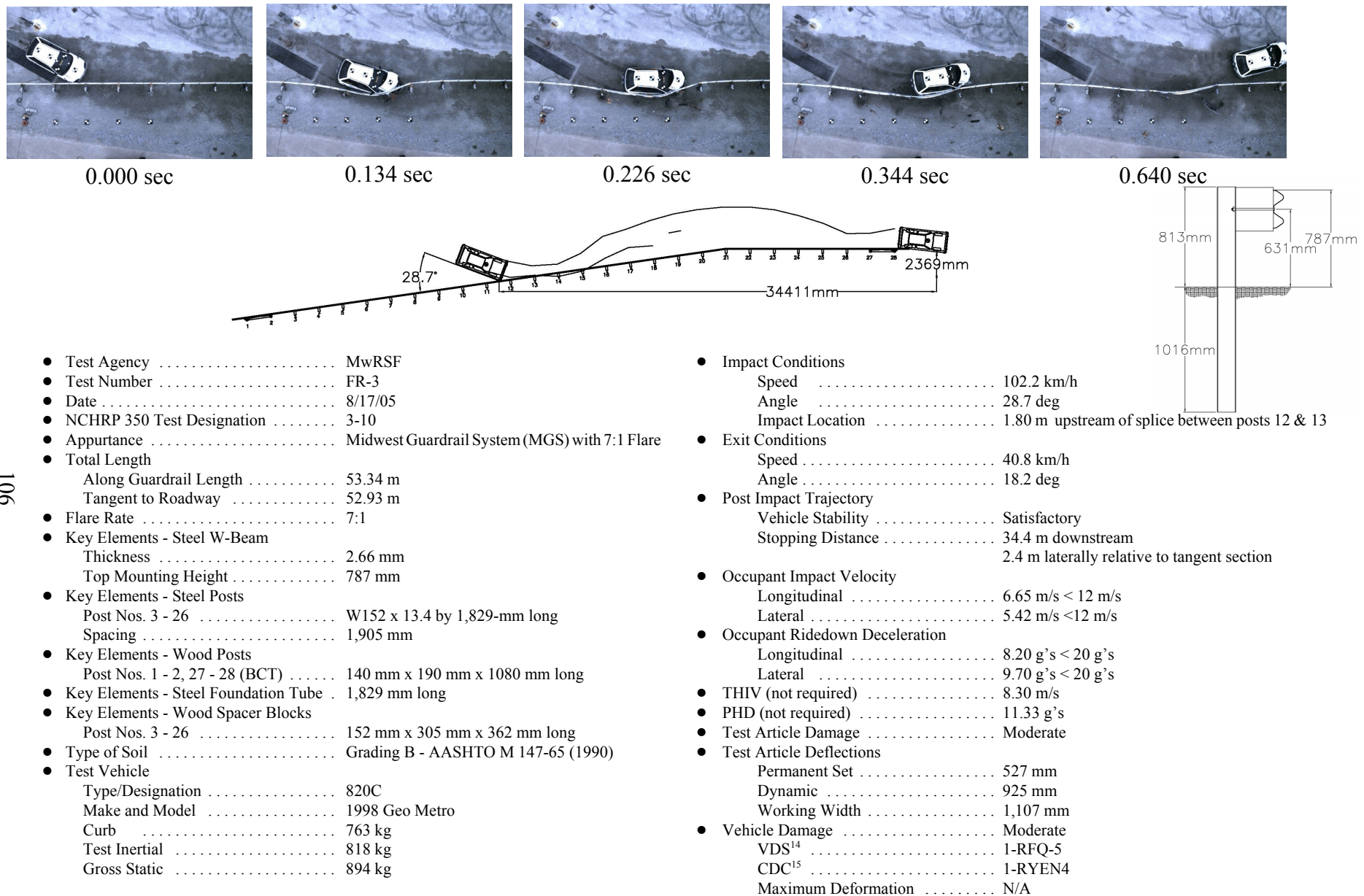


Figure 75. Summary of Test Results and Sequential Photographs, Test FR-3



0.000 sec



0.106 sec



0.180 sec



0.292 sec



0.396 sec



0.564 sec



0.000 sec



0.082 sec



0.154 sec



0.256 sec



0.408 sec



0.718 sec

Figure 76. Additional Sequential Photographs, Test FR-3



0.000 sec



0.068 sec



0.184 sec



0.304 sec



0.438 sec



0.614 sec



0.000 sec



0.088 sec



0.188 sec



0.254 sec



0.444 sec



0.676 sec

Figure 77. Additional Sequential Photographs, Test FR-3



0.000 sec



0.138 sec



0.311 sec



0.483 sec



0.724 sec



1.001 sec



0.000 sec



0.069 sec



0.173 sec



0.242 sec



0.483 sec



0.656 sec

Figure 78. Additional Sequential Photographs, Test FR-3



Figure 79. Documentary Photographs, Test FR-3



Figure 80. Documentary Photographs, Test FR-3



Figure 81. Impact Location, Test FR-3



Figure 82. Vehicle Trajectory and Final Position, Test FR-3



Figure 83. System Damage, Test FR-3



Figure 84. Post Nos. 9 and 10 Damage, Test FR-3



Figure 85. Post Nos. 11 and 12 Damage, Test FR-3



Figure 86. Post Nos. 13 and 14 Damage, Test FR-3



Figure 87. Post No. 15 Damage, Test FR-3



Figure 88. Post Nos. 16 and 17 Damage, Test FR-3



Figure 89. Post Nos. 18 and 19 Damage, Test FR-3



Figure 90. Downstream Anchorage Damage, Test FR-3



Figure 91. Vehicle Damage, Test FR-3



Figure 92. Vehicle Damage, Test FR-3



Figure 93. Vehicle Damage, Test FR-3



Figure 94. Vehicle Damage, Test FR-3



Figure 95. Suspension Damage, Test FR-3



Figure 96. Occupant Compartment Damage, Test FR-3

9 DESIGN DETAILS - DESIGN NO. 3

Once again due to testing deviations, the actual impacts of test nos. FR-2 and FR-3 had higher impact speeds and angles than those specified in NCHRP Report No. 350. As a result, the IS was 9% higher than targeted for test no. FR-2. The effective flare rate was calculated to be 5.8:1 for test FR-2. Thus, due to the desire to determine the limits of the MGS with a flare, it was decided to increase the flare of the system again.

The third design was identical to the first and second designs except for the flare rate of the system. The first installation's flare was increased to 5:1 which corresponds to an angle of 11.3 degrees away from the travelway. Post nos. 1 through 20 were located along a 38.1 m (125 ft) length of guardrail, while post nos. 21 through 28 were located along the length of tangent guardrail, as shown in Figure 97.

For this design, the test installation measured 53.34 m (175 ft) long along the length of the guardrail, but measured 52.57 m (172 ft - 5.75 in.) long tangent to the roadway. This system also consisted of standard 2.66-mm (12-gauge) W-beam guardrail supported by steel posts. Anchorage systems similar to those used on tangent guardrail terminals were also utilized on both the upstream and downstream ends of the system, as shown in Figures 97 and 98. Similarly, the rail splices have been moved to the center of the span locations. In addition, all lap splice connections between the rail sections were configured to reduce vehicle snag at the splices during the crash test. Photographs of the installation are shown in Figures 98 through 100. A complete set of system drawings, along with the corresponding English-unit drawings, are shown in Appendix J.

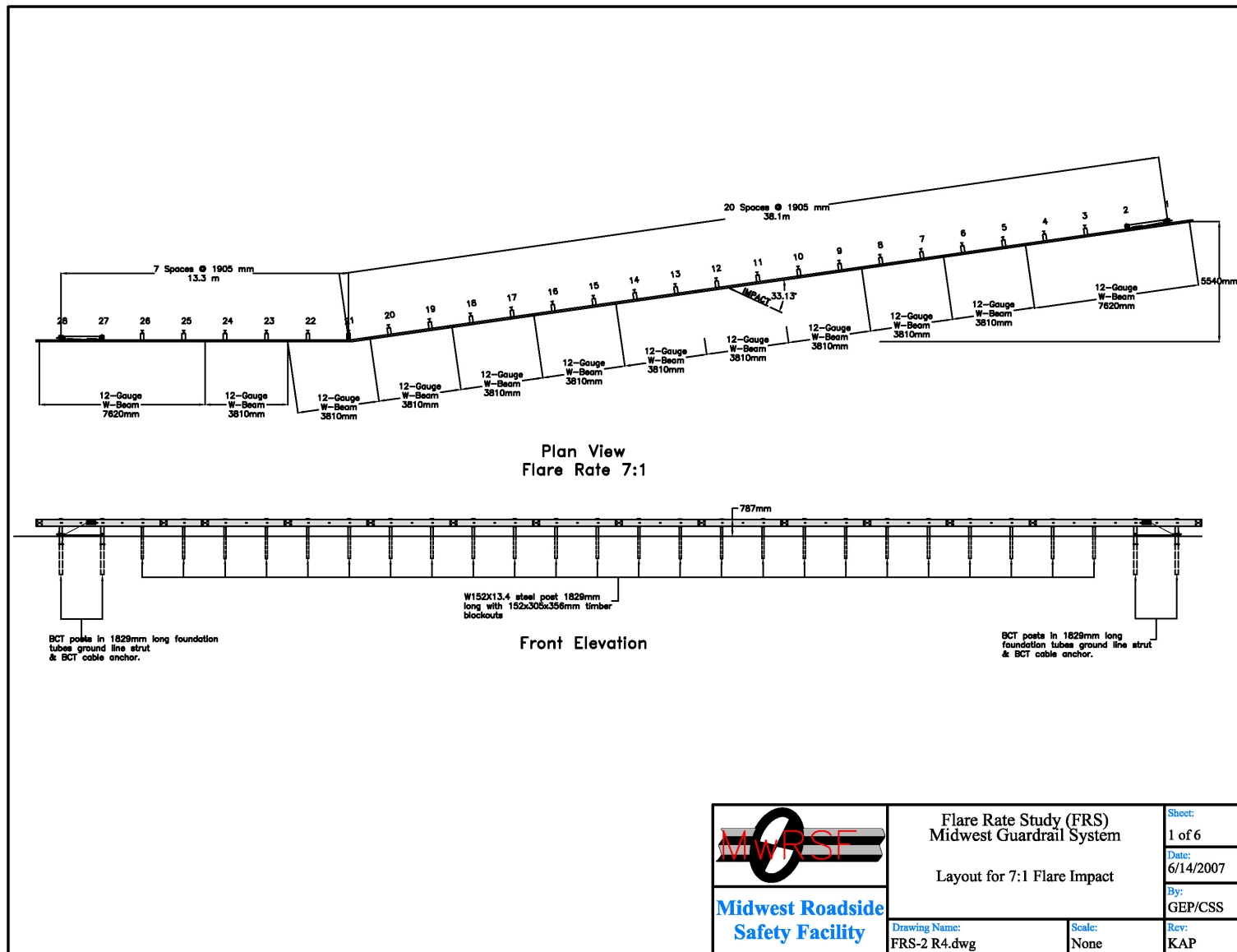


Figure 97. System Details, Design No. 3



Figure 98. System Details, Design No. 3



Figure 99. System Details, Design No. 3



Figure 100. Post Details, Design No. 3

10 CRASH TEST NO. 4

10.1 Test FR-4

The 2,014-kg (4,441-lb) pickup truck impacted the MGS installed with a 5:1 flare at a speed of 104.7 km/h (65.0 mph) and at an angle of 36.8 degrees relative to the guardrail (or 25.5 degrees relative to the roadway). A summary of the test results and the sequential photographs are shown in Figure 101. The summary of the test results and sequential photographs in English units is shown in Appendix B. Additional sequential photographs are shown in Figures 102 through 104. Documentary photographs of the crash test are shown in Figures 105 and 106.

10.2 Test Description

Initial impact was to occur between post nos. 11 and 12, or 5.00 m (16 ft - 4.825 in.) upstream from the centerline of the splice between post nos. 14 and 15, as shown in Figure 107. Actual vehicle impact occurred 4.76 m (15 ft - 7.5 in.) upstream from the centerline of the splice between post nos. 14 and 15. Immediately following impact, the bumper crushed and deformed into the engine compartment and wheel well. At 0.014 sec, post nos. 12 and 13 deflected, and the right-side headlight housing deformed. At 0.030 sec, the right-front quarter panel dented, the rail near the right-front corner of the bumper buckled, the W-beam's bottom corrugation twisted and deflected, and the hood separated from the right-front corner of the vehicle. At 0.054 sec, the guardrail buckled between post nos. 13 and 14, and post no. 12 twisted, bent, and rotated with the rail. At 0.068 sec, the bumper deformed downward, and the rail disengaged from post no. 13. At 0.080 sec, post no. 15 deflected, and rail buckling continued. At 0.086 sec, the rail disengaged from post no. 12. At 0.096 sec, the right-front tire traversed over post no. 13, twisting and deforming it. At 0.120 sec, the rail disengaged from post no. 14, and post no. 16 deflected. At 0.128 sec, post no. 28 and the

foundation tube raised upward out of the ground. At this same time, the right-front tire lodged under the rail, and the roll angle increased negatively. At 0.140 sec, the right-front tire contacted the upstream edge of the traffic-side face of post no. 15. At 0.162 sec, post nos. 16 through 20 twisted counterclockwise toward impact, and the rail buckled between post nos. 27 and 28. At 0.182 sec, post no. 16 twisted clockwise toward impact, and the right-front tire contacted the blockout at post no. 16. At 0.204 sec, the rail disengaged from post no. 16. At 0.236 sec, the rail raised up over the top of post no. 16, and the bottom corrugation bent toward the traffic side. At 0.245 sec, post nos. 16 through 18 disengaged from the rail. At 0.276 sec, post nos. 17 through 21 deflected. At 0.338 sec, the grill deformed, and the right-front headlight protruded over the rail. At 0.342 sec, the guardrail was positioned in the right-front wheel well, causing deformation to the right-front corner of the bumper. At 0.362 sec, post no. 17 twisted counterclockwise, and post no. 28 ceased rising out of the ground. At 0.394 sec, the right-rear corner of the bumper was positioned on top of the deformed guardrail. At 0.426 sec, the guardrail lost contact with the inside of the right-front wheel well. At 0.476 sec, the vehicle became parallel to the flared section of guardrail with a resultant velocity of 40.2 km/h (25.0 mph). At this same time, the right-front tire snagged on post no. 17. At 0.514 sec, the right side of the vehicle became airborne. At 0.632 sec, the right-front corner of the vehicle was located at post no. 18. At 0.704 sec, the rail disengaged from post nos. 19 through 27. At 0.778 sec, the right-front corner of the hood raised upward, and the right-front quarter panel crushed into the wheel well. At 0.954 sec, the vehicle twisted in the air. At 1.080 sec, the right-front tire protruded under the rail, and the left-rear corner of the vehicle pitched upward and yawed away from the system. At 1.306 sec, the vehicle encountered an increased negative roll, and the left-front tire became airborne. At this same time, the rail was wrapped around the right-front wheel, and rose

with the right-front tire. At 1.458 sec, the left-front tire contacted the ground, and the vehicle's roll and pitch ceased. At 2.388 sec, the vehicle came to rest 11.84 m (38 ft - 10 in.) downstream and in contact with the system. The trajectory and final position of the pickup truck are shown in Figures 101 and 108.

10.3 Barrier Damage

Barrier damage was moderate, as shown in Figures 109 through 119. Barrier damage consisted of deformed guardrail posts, deformed and disengaged blockouts, deformed W-beam guardrail, and contact marks on a guardrail section. The length of vehicle contact along the system was approximately 11.8 m (38 ft - 10 in.), which spanned from the centerline of post no. 12 through 406 mm (16 in.) downstream from the centerline of post no. 18.

Contact marks were found along the length of vehicle contact with the system, which spanned from post nos. 12 through 19. The W-beam rail was deformed and flattened between post nos. 13 and 19. The guardrail buckled at post nos. 11, 13, 17, 19, 20, and between post nos. 19 and 22. The guardrail was deformed upward between post nos. 14 and 17, and reached a maximum height of 775 mm (30.5 in.) above the ground at post no. 17. Minor yielding occurred around the post bolt slots at post nos. 12 through 27. The W-beam was pulled off of post nos. 6 and 12 through 28. No significant damage occurred upstream of post no. 11.

Post nos. 3 through 12 rotated backward and longitudinally downstream. Post no. 12 also twisted downstream approximately 90 degrees. Post nos. 13, 14, 17, and 18 were bent to 191 mm (7.5 in.), 229 mm (9 in.), 356 mm (14 in.), and 229 mm (9 in.) above the ground, respectively. Post nos. 15 and 16 twisted upstream approximately 90 degrees and bent downstream 45 degrees and 35 degrees, respectively. Post nos. 19 through 26 were rotated backward and twisted upstream toward

impact. The upstream and downstream anchorage systems moved longitudinally 25 mm (1 in.) downstream and 37 mm (1.5 in.) upstream, respectively. The upstream and downstream anchor posts deflected downstream and upstream, respectively. The foundation tube at post no. 28 was uprooted 254 mm (10 in.). All four wood BCT posts remained undamaged, except for the bending fracture found on post no. 27 at the top of the foundation tube.

The wooden blockouts at post nos. 3 through 12 and 19 through 26 rotated slightly, while still attached to the post. The wooden blockout at post no. 7 was partially fractured. The wooden blockout at post nos. 11 and 12 also encountered moderate deformations, while the blockout at post nos. 16 through 19 encountered minor deformations. The wooden blockout at post nos. 13 through 17 were fractured and removed from the post, while a portion of the blockout at post no. 18 was removed from the post.

The permanent set of the barrier system is shown in Figure 109. The maximum lateral permanent set rail and post deflections were 1,753 mm (69 in.) at the midspan between post nos. 16 and 17 and 737 mm (29 in.) at the centerline of post no. 14, respectively, as measured in the field. The maximum lateral dynamic rail and post deflections were 1,919 mm (75.6 in.) at the centerline of post no. 16 and 834 mm (32.8 in.) at the centerline of post no. 14, respectively, as determined from high-speed digital video analysis. The working width of the system was found to be 2,475 mm (97.4 in.).

10.4 Vehicle Damage

Exterior vehicle damage was moderate, as shown in Figures 120 through 122. Occupant compartment deformations to the right side and center of the floorboard were judged insufficient to cause serious injury to the vehicle occupants. Maximum longitudinal deflections of 6 mm (0.25 in.)

were located along the center and right side of the right-side floorpan. Maximum lateral deflections of 19 mm (0.75 in.) were located along the firewall and near the left center of the right-side floorpan. Maximum vertical deflections of 13 mm (0.5 in.) were located near the left-rear corner of the right-side floorpan. The occupant compartment deformation is shown in Figure 123. Complete occupant compartment deformations and the corresponding locations are provided in Appendix K.

Damage was concentrated on the right-front corner of the vehicle. The right-front and right-rear quarter panels and the right-side door were crushed and deformed. The right side of the bumper was crushed, deformed back into the engine compartment, and torn. The bumper was also detached from the left-front bumper mount. Contact marks and scratches occurred to the entire right side. A significant gouge occurred to the center of the right-side door. The right side of the grill was fractured and detached from the front of the vehicle. The frame was deformed near the engine. The right-rear exhaust pipe was dented and scratched. The right-side control arm was deformed. Minor contact marks were found on the underside of the vehicle. The left side, rear, roof, and all window glass remained undamaged.

10.5 Occupant Risk Values

The longitudinal and lateral occupant impact velocities were determined to be 8.00 m/s (26.23 ft/s) and 4.06 m/s (13.31 ft/s), respectively. The maximum 0.010-sec average occupant ridedown decelerations in the longitudinal and lateral directions were 7.15 g's and 6.35 g's, respectively. It is noted that the occupant impact velocities (OIVs) and occupant ridedown decelerations (ORDs) were within the suggested limits provided in NCHRP Report No. 350. The THIV and PHD values were determined to be 8.67 m/s (28.44 ft/s) and 7.60 g's, respectively. The results of the occupant risk, determined from the accelerometer data, are summarized in Figure 101.

Results are shown graphically in Appendix L. The results from the rate transducer are also shown graphically in Appendix L.

10.6 Discussion

The analysis of the test results for test no. FR-4 showed that the MGS installed with a 5:1 flare, impacted with the 2000P vehicle, adequately contained and redirected the vehicle with controlled lateral displacements of the barrier system. There were no detached elements nor fragments which showed potential for penetrating the occupant compartment nor presented undue hazard to other traffic. Deformations of, or intrusion into, the occupant compartment that could have caused serious injury did not occur. The test vehicle did not penetrate nor ride over the guardrail system and remained upright during and after collision. Vehicle roll, pitch, and yaw angular displacements were noted, but they were deemed acceptable because they did not adversely influence occupant risk safety criteria nor cause rollover. After collision, the vehicle's trajectory revealed no intrusion into adjacent traffic lanes. In addition, the vehicle never exited the system. Therefore, test no. FR-4 conducted on MGS installed with a 5:1 flare was determined to be acceptable according to the TL-3 safety performance criteria of test designation 3-11 found in NCHRP Report No. 350.



0.000 sec



0.140 sec



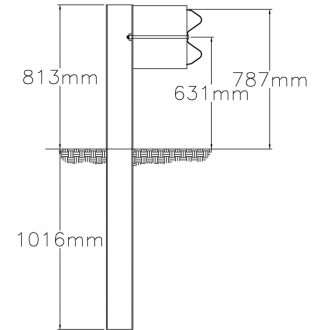
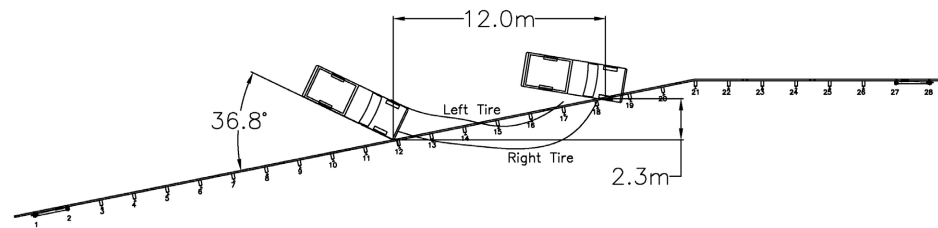
0.348 sec



0.632 sec



1.230 sec



- Test Agency MwRSF
- Test Number FR-4
- Date 5/17/06
- NCHRP 350 Test Designation 3-11
- Appurtenance Midwest Guardrail System (MGS) with 5:1 Flare
- Flare Rate 5:1
- Total Length
 - Along Guardrail Length 53.34 m
 - Tangent to Roadway 52.57 m
- Key Elements - Steel W-Beam
 - Thickness 2.66 mm
 - Top Mounting Height 787 mm
- Key Elements - Steel Posts
 - Post Nos. 3 - 26 W152 x 13.4 by 1,829 mm long
 - Spacing 1,905 mm
- Key Elements - Wood Posts
 - Post Nos. 1 - 2, 27 - 28 (BCT) 140 mm x 190 mm x 1,080 mm long
- Key Elements - Steel Foundation Tube 1,829 mm long
- Key Elements - Wood Spacer Blocks
 - Post Nos. 3 - 26 152 mm x 305 mm x 362 mm long
- Type of Soil Grading B - AASHTO M 147-65 (1990)
- Test Vehicle
 - Type/Designation 2000P
 - Make and Model 1999 Chevrolet C2500 ¾-ton Pickup
 - Curb 1,973 kg
 - Test Inertial 2,014 kg
 - Gross Static 2,014 kg

- Impact Conditions
 - Speed 104.7 km/h
 - Angle 36.8 deg
 - Impact Location 4.76 m upstream of splice between posts 14 & 15
- Exit Conditions
 - Speed N/A
 - Angle N/A
- Post Impact Trajectory
 - Vehicle Stability Satisfactory
 - Stopping Distance 12.0 m downstream
2.3 m laterally relative to tangent section
- Occupant Impact Velocity
 - Longitudinal 8.00 m/s < 12 m/s
 - Lateral (not required) 4.06 m/s
- Occupant Ridedown Deceleration
 - Longitudinal 7.15 g's < 20 g's
 - Lateral (not required) 6.35 g's
- THIV (not required) 8.67 m/s
- PHD (not required) 7.60 g's
- Test Article Damage Moderate
- Test Article Deflections
 - Permanent Set 1,753 mm
 - Dynamic 1,919 mm
 - Working Width 2,475 mm
- Vehicle Damage Moderate
 - VDS¹⁴ 1-RFQ-4
 - CDC¹⁵ 1-RYEN5
 - Maximum Deformation 19 mm at firewall

Figure 101. Summary of Test Results and Sequential Photographs, Test FR-4



0.000 sec



0.124 sec



0.254 sec



0.394 sec



0.514 sec



0.764 sec



0.000 sec



0.096 sec



0.204 sec



0.292 sec



0.364 sec



0.534 sec

Figure 102. Additional Sequential Photographs, FR-4



0.000 sec



0.152 sec



0.390 sec



0.590 sec



0.842 sec



1.062 sec



0.000 sec



0.138 sec



0.310 sec



0.552 sec



0.759 sec



1.105 sec

Figure 103. Additional Sequential Photographs, Test FR-4



0.000 sec



0.069 sec



0.138 sec



0.207 sec



0.276 sec



0.345 sec



0.000 sec



0.192 sec



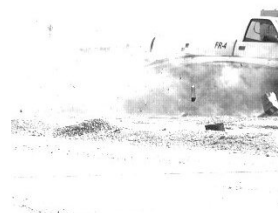
0.304 sec



0.464 sec



0.644 sec



0.884 sec

Figure 104. Additional Sequential Photographs, Test FR-4



Figure 105. Documentary Photographs, Test FR-4



Figure 106. Documentary Photographs, Test FR-4

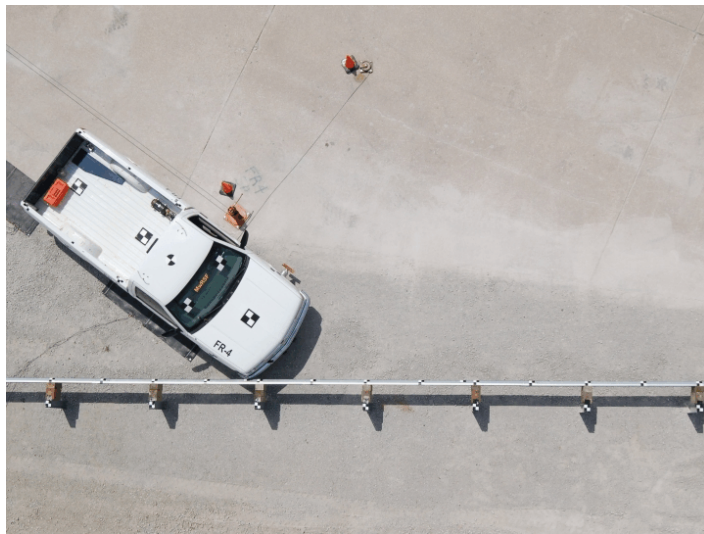


Figure 107. Impact Location, Test FR-4



Figure 108. Vehicle Trajectory and Final Position, Test FR-4



Figure 109. System Damage, Test FR-4



Figure 110. System Damage, Test FR-4



Figure 111. System Damage, Test FR-4



Figure 112. Post Nos. 9 and 10 Damage, Test FR-4



Figure 113. Post Nos. 11 and 12 Damage, Test FR-4



Figure 114. Post Nos. 13 and 14 Damage, Test FR-4



Figure 115. Post Nos. 15 and 16 Damage, Test FR-4



154

Figure 116. Post Nos. 17 and 18 Damage, Test FR-4



Figure 117. Post Nos. 19 and 20 Damage, Test FR-4



Figure 118. Upstream Anchorage Damage, Test FR-4



Figure 119. Downstream Anchorage Damage, Test FR-4



Figure 120. Vehicle Damage, Test FR-4



Figure 121. Vehicle Damage, Test FR-4



Figure 122. Undercarriage Damage, Test FR-4



Figure 123. Occupant Compartment Deformation, Test FR-4

11 CRASH TEST NO. 5

11.1 Test FR-5

The 908-kg (2,002-lb) small car impacted the MGS installed with a 5:1 flare at a speed of 95.5 km/h (59.4 mph) and at an angle of 31.8 degrees relative to the guardrail (or 20.5 degrees relative to the roadway). A summary of the test results and the sequential photographs are shown in Figure 124. The summary of the test results and sequential photographs in English units is shown in Appendix B. Additional sequential photographs are shown in Figures 125 through 127. Documentary photographs of the crash test are shown in Figures 128 and 129.

11.2 Test Description

Initial impact was to occur between post nos. 11 and 12, or 1.43 m (4 ft - 8.25 in.) upstream from the centerline of the splice between post nos. 12 and 13, as shown in Figure 130. Actual vehicle impact occurred 1.38 m (4 ft - 6.25 in.) upstream from the centerline of the splice between post nos. 12 and 13. Immediately after impact, the bumper deformed, and the rail deflected backwards. At 0.008 sec, post no. 12 deflected backwards, and the front of the hood jarred open. At 0.014 sec, the rail deformed and flattened, and post no. 11 deflected. At 0.024 sec, the bumper cover protruded under the rail, and post no. 13 deflected. At 0.038 sec, the right-front corner of the bumper protruded under the rail. At this same time, post no. 14 deflected backwards. At 0.062 sec, the bumper, right-front quarter panel, and hood deformed, and the midpoint of the grill deformed and cracked. At 0.074 sec, the guardrail buckled both upstream and downstream of post no. 14, and the bumper contacted the edge of the upstream flange of post no. 13 and disengaged from the right-side mounting clips. At 0.096 sec, post no. 15 deflected. At 0.108 sec, the blockout at post no. 13 fractured. At 0.114 sec, the right-front tire contacted post no. 13. At 0.132 sec, the right-front tire

protruded under the guardrail as the vehicle redirected. At 0.194 sec, the bumper deformed as it contacted post no. 14. At 0.202 sec, the entire right side of the vehicle was in contact with the barrier. At 0.218 sec, the right-front tire contacted post no. 14. At 0.232 sec, the rear tires became airborne, and post no. 17 deflected. At 0.268 sec, the W-beam deformed under the right-rear corner of the vehicle. At this same time, the right-rear corner of the bumper contacted the top corrugation of W-beam. At 0.286 sec, the vehicle became parallel with the system with a resultant velocity of 42.0 km/h (26.1 mph). At 0.338 sec, the blockout at post no. 15 fractured, and the vehicle contacted the upstream edge of the front flange of post no. 15. At 0.386 sec, the right-front tire snagged on post no. 15 and yawed the rear of the vehicle away from the system. At 0.690 sec, the right-front corner of the vehicle protruded under the rail between post nos. 15 and 16. At 0.774 sec, the vehicle exited the system at a trajectory angle of 35.9 degrees relative to the flared section and at a resultant velocity of 22.4 km/h (13.9 mph). The vehicle came to rest 9.2 m (30 ft - 2.75 in.) downstream from impact and 4.2 m (13 ft - 8 in.) laterally away from the traffic-side face of the rail at impact. The trajectory and final position of the small car are shown in Figures 124 and 131.

11.3 Barrier Damage

Damage to the barrier system was minimal, as shown in Figures 132 through 140. Barrier damage consisted of deformed guardrail posts, deformed and disengaged blockouts, deformed guardrail, and contact marks on a guardrail section. The length of vehicle contact along the system was approximately 6.14 m (20 ft - 4.75 in.), which spanned from 425 mm (16.75 in.) upstream from the centerline of post no. 12 through the centerline of post no. 15.

Contact marks were found along the length of vehicle contact with the system. The W-beam guardrail was deformed and flattened between post nos. 12 and 15. The guardrail buckled at post

nos. 11 through 16 and at the midspan between post nos. 13 and 14. The W-beam was pulled off of post nos. 13 through 16. Significant yielding occurred around the post bolt slots at post nos. 12 through 16. No significant damage occurred downstream of post no. 16, except for slight rail deflection and post rotation.

Post nos. 1 and 2 were pulled downstream, and were leaning with the rail. Post nos. 3 through 11 encountered twisting downstream, and post nos. 8 through 11 rotated backward. Post nos. 12 was twisted clockwise and rotated backwards. Post nos. 13 through 15 were bent downstream and rotated backward. Post no. 16 rotated backward in the soil slightly. Post nos. 17 through 21 twisted toward impact. The upstream and downstream anchorage systems moved longitudinally 25 mm (1 in.) downstream and 51 mm (2 in.) upstream, respectively, but the four wood BCT posts remained undamaged.

The wooden blockouts at post nos. 3 through 12 and 16 were rotated slightly, while still attached to the post. The wooden blockouts at post nos. 13 and 14 were fractured and removed from the posts, while the blockout at post no. 15 was fractured but remained attached to the post.

The permanent set of the barrier system is shown in Figure 132. The maximum lateral permanent set and post deflections were 660 mm (26 in.) at the midspan between post nos. 13 and 14 and 470 mm (18.5 in.) at the centerline of post no. 13, respectively, as measured in the field. The maximum lateral dynamic rail and post deflections were 908 mm (35.7 in.) at the midspan between post nos. 13 and 14 and 670 mm (26.4 in.) at the centerline of post no. 14, respectively, as determined from high-speed digital video analysis. The working width of the system was found to be 1,270 mm (50 in.).

11.4 Vehicle Damage

Exterior vehicle damage was moderate, as shown in Figures 141 through 145. Occupant compartment deformations to the right side and center of the floorboard were judged insufficient to cause serious injury to the vehicle occupants. The occupant compartment deformation is shown in Figure 145. Complete occupant compartment deformations and the corresponding locations are provided in Appendix M.

Damage was concentrated on the right-front corner of the vehicle. The right-front quarter panel, bumper, and radiator were deformed and crushed inward toward the engine compartment. Significant sheet metal tears occurred to the right-front corner of the hood, the right-front quarter panel, and the right door panel. The right-side door could not be opened. The front of the hood was crushed, deformed, and shifted to the right side, causing the right-side hood clips to fracture. Dents and scratches occurred to the entire right side of the vehicle and the exhaust system. The bumper cover disengaged from the vehicle. The right-side headlight was fractured and removed from the housing. The right-front tire was twisted at the wheel attachment and deformed into the wheel well. The right-side lower control arm and steering arm were fractured. The right-side sway bar was bent at the connection to the wheel. The lower-right corner of the windshield encountered “spider-web” cracking due to hood contact. The left side, rear, roof, and all window glass except the windshield remained undamaged.

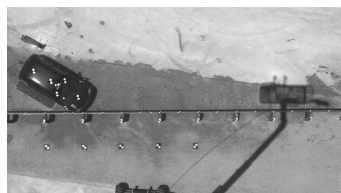
11.5 Occupant Risk Values

The longitudinal and lateral occupant impact velocities were determined to be -6.86 m/s (-22.52 ft/s) and -4.89 m/s (-16.04 ft/s), respectively. The maximum 0.010-sec average occupant ridedown decelerations in the longitudinal and lateral directions were -9.27 g's and -7.98 g's,

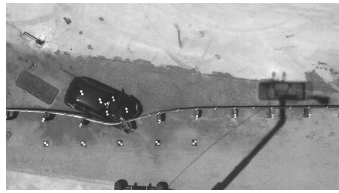
respectively. It is noted that the occupant impact velocities (OIVs) and occupant ridedown decelerations (ORDs) were within the suggested limits provided in NCHRP Report No. 350. The THIV and PHD values were determined to be 8.45 m/s (27.71 ft/s) and 11.69 g's, respectively. The results of the occupant risk, determined from the accelerometer data, are summarized in Figure 124. Results are shown graphically in Appendix N. The results of the rate transducer are also shown graphically in Appendix N.

11.6 Discussion

The analysis of the test results for test no. FR-5 showed that the MGS installed with a 5:1 flare, impacted with the 820C vehicle, adequately contained and redirected the vehicle with controlled lateral displacements of the barrier system. There were no detached elements nor fragments which showed potential for penetrating the occupant compartment nor presented undue hazard to other traffic. Deformations of, or intrusion into, the occupant compartment that could have caused serious injury did not occur. The test vehicle did not penetrate nor ride over the guardrail system and remained upright during and after the collision. Vehicle roll, pitch, and yaw angular displacements were noted, but they were deemed acceptable because they did not adversely influence occupant risk safety criteria nor cause rollover. After collision, the vehicle's trajectory revealed minimum intrusion into adjacent traffic lanes. In addition, the vehicle's exit angle of 35.8 degrees was greater than 60 percent of the impact angle of 31.8 degrees. However, it should be noted that this evaluation criterion is only preferred and not required. Therefore, test no. FR-5 conducted on the MGS installed with a 5:1 flare was determined to be acceptable according to the TL-3 safety performance criteria of test designation no. 3-10 found in NCHRP Report No. 350.



0.000 sec



0.110 sec



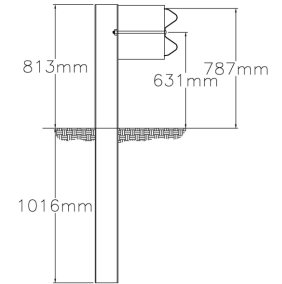
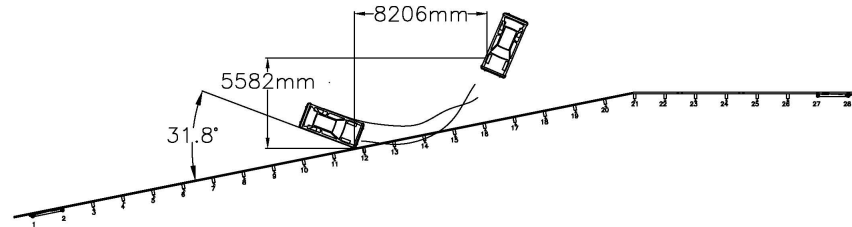
0.226 sec



0.420 sec



0.604 sec



- Test Agency MwRSF
- Test Number FR-5
- Date 7/6/06
- NCHRP 350 Test Designation 3-10
- Appurtenance Midwest Guardrail System (MGS) with 5:1 Flare
- Total Length
 - Along Guardrail Length 53.34 m
 - Tangent to Roadway 52.57 m
- Flare Rate 5:1
- Key Elements - Steel W-Beam
 - Thickness 2.66 mm
 - Top Mounting Height 787 mm
- Key Elements - Steel Posts
 - Post Nos. 3 - 26 W152 x 13.4 by 1,829 mm long
 - Spacing 1,905 mm
- Key Elements - Wood Posts
 - Post Nos. 1 - 2, 27 - 28 (BCT) 140 mm x 190 mm x 1,080 mm long
- Key Elements - Steel Foundation Tube 1,829 mm long
- Key Elements - Wood Spacer Blocks
 - Post Nos. 3 - 26 152 mm x 305 mm x 362 mm long
- Type of Soil Grading B - AASHTO M 147-65 (1990)
- Test Vehicle
 - Type/Designation 820C
 - Make and Model 1998 Chevrolet Metro
 - Curb 840 kg
 - Test Inertial 833 kg
 - Gross Static 908 kg

- Impact Conditions
 - Speed 95.5 km/h
 - Angle 31.8 deg
 - Impact Location 1.38 m upstream of splice between posts 14 & 15
- Exit Conditions
 - Speed 22.4 km/h
 - Exit 35.8 deg
- Post Impact Trajectory
 - Vehicle Stability Satisfactory
 - Stopping Distance 9.2 m downstream
 - 4.2 m laterally away from impact
- Occupant Impact Velocity
 - Longitudinal -6.86 m/s < 12 m/s
 - Lateral -4.89 m/s < 12 m/s
- Occupant Ridedown Deceleration
 - Longitudinal -9.27 g's < 20 g's
 - Lateral -7.98 g's < 20 g's
- THIV (not required) 8.43 m/s
- PHD (not required) 11.69 g's
- Test Article Damage Moderate
- Test Article Deflections
 - Permanent Set 660 mm
 - Dynamic 908 mm
 - Working Width 1,270 mm
- Vehicle Damage Moderate
 - VDS¹⁴ 1-RFQ-5
 - CDC¹⁵ 1-RYEN5
 - Maximum Deformation N/A

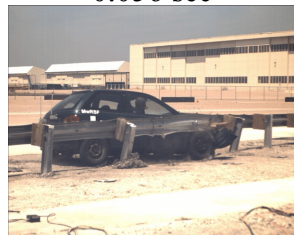
Figure 124. Summary of Test Results and Sequential Photographs, Test FR-5



0.000 sec



0.056 sec



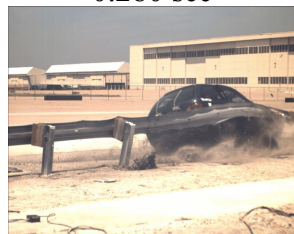
0.126 sec



0.196 sec



0.280 sec



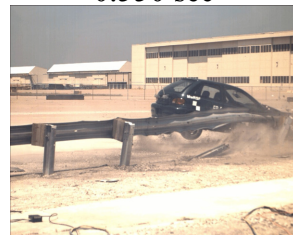
0.338 sec



0.426 sec



0.550 sec



0.612 sec



0.736 sec



0.888 sec



1.112 sec

Figure 125. Additional Sequential Photographs, Test FR-5



0.000 sec



0.108 sec



0.252 sec



0.396 sec



0.578 sec



0.790 sec



0.000 sec



0.138 sec



0.310 sec



0.414 sec



0.587 sec



0.863 sec

Figure 126. Additional Sequential Photographs, Test FR-5



0.000 sec



0.104 sec



0.276 sec



0.518 sec



0.759 sec



0.897 sec



0.000 sec



0.130 sec



0.286 sec



0.432 sec



0.616 sec



0.834 sec

Figure 127. Additional Sequential Photographs, Test FR-5



Figure 128. Documentary Photographs, Test FR-5



Figure 129. Documentary Photographs, Test FR-5



Figure 130. Impact Location, Test FR-5



Figure 131. Vehicle Trajectory and Final Position, Test FR-5



Figure 132. System Damage, Test FR-5



Figure 133. System Damage, Test FR-5



Figure 134. Rail Damage, Test FR-5



Figure 135. Post Nos. 9 and 10 Damage, Test FR-5



Figure 136. Post Nos. 11 and 12 Damage, Test FR-5



Figure 137. Post Nos. 13 and 14 Damage, Test FR-5



Figure 138. Post Nos. 15 and 16 Damage, Test FR-5



Figure 139. Post Nos. 17 and 18 Damage, Test FR-5



Figure 140. Post Nos. 19 and 20 Damage, Test FR-5



Figure 141. Vehicle Damage, Test FR-5



Figure 142. Vehicle Damage, Test FR-5



Figure 143. Windshield Damage, Test FR-5



Figure 144. Undercarriage Damage, Test FR-5



Figure 145. Occupant Compartment Deformation, Test FR-5

12 SUMMARY AND CONCLUSIONS

Whenever roadside or median slopes are relatively flat (10:1 or flatter), increasing the flare rate on guardrail installations becomes practical and has some major advantages including significantly reducing guardrail lengths and associated costs. Hence, a revised flare rate design has the potential to decrease construction, maintenance, and overall accident costs, provided guardrail accident severities are not increased significantly.

Although computer simulations indicate that conventional G4(1S)M guardrail cannot perform effectively when installed at flare rates higher than 15:1, the MGS has been shown to provide adequate protection for motorists when installed at flare rates of up to 5:1. Crash testing results, as well as LS-DYNA simulations, for both the 2000P pickup truck and 820C small car on the MGS installed with multiple flare rates demonstrated excellent performance. All tests conducted up to, and including, a flare rate of 5:1 passed all NCHRP Report No. 350 safety performance evaluation requirements, including occupant risk measures that are not specifically required for Test 3-11, as shown in Table 3. Additionally, all tests had higher impact angles and speeds than those specified in NCHRP Report No. 350, resulting in even higher effective flare rates than intended, as shown in Table 4. These tests indicate that the MGS is a very robust system when installed in a flared configuration.

Based upon the series of full-scale crash tests described herein, it is recommended that, whenever roadside topography permits, much steeper flare rates, up to 5:1, should be considered for MGS installations. These steeper flare rates will reduce overall accident frequencies, overall accident costs, and total construction costs, without sacrificing guardrail redirective capacity. Hence, implementing findings from this study should not only improve roadside safety, but also reduce guardrail construction and repair costs.

Table 3. Summary of Safety Performance Evaluation Results

Evaluation Factors	Evaluation Criteria	Test FR-1	Test FR-2	Test FR-3	Test FR-4	Test FR-5
Structural Adequacy	A	S	S	S	S	S
Occupant Risk	D	S	S	S	S	S
	F	S	S	S	S	S
	H	N/A	N/A	S	N/A	S
	I	N/A	N/A	S	N/A	S
Vehicle Trajectory	K	S	S	S	S	S
	L	S	S	N/A	S	N/A
	M	U	S	U	S	U
NCHRP Report No. 350 Test Level		TL-3	TL-3	TL-3	TL-3	TL-3
NCHRP Report No. 350 Test Designation		3-11	3-11	3-10	3-11	3-10
Pass/Marginal/Fail		Pass	Pass	Pass	Pass	Pass

S - Satisfactory
 M - Marginal
 U - Unsatisfactory
 N/A - Not Applicable

Table 4. Summary of Test Results, Test Nos. FR-1 through FR-5

Test	Installation Flare Rate		Impact Angle Relative to Roadway (deg)		Impact Angle Relative to Guardrail (deg)		Impact Speed (km/h)		Total Vehicle Mass (kg)		Impact Severity (kJ)		Effective Flare Rate	
	(a:b)	(deg)	Target	Actual	Target	Actual	Target	Actual	Target	Actual	Target	Actual	(deg)	(a:b)
FR-1	13:1	4.4	25.0	26.2	29.4	30.5	100.0	102.9	2000	2026	186	214	6.8	8.4:1
FR-2	7:1	8.1	25.0	25.9	33.1	34.0	100.0	101.6	2000	2023	230	252	9.7	5.8:1
FR-3	7:1	8.1	20.0	20.6	28.1	28.7	100.0	102.2	895	894	77	83	9.4	6.1:1
FR-4	5:1	11.3	25.0	25.5	36.3	36.8	100.0	104.7	2000	2014	270	306	14.0	4.0:1
FR-5	5:1	11.3	20.0	20.5	31.3	31.8	100.0	95.5	895	908	93	89	10.5	5.4:1

13 RECOMMENDATIONS

Some concern has been expressed that there may be a potential weak point in a flared guardrail associated with the beginning of the flare. The theory is that there is some delay in the development of tension as the hinge point is pushed backward and that this delay may cause the guardrail to disengage from the impacting vehicle. This behavior arises whenever there is a portion of the impact during which the lateral stiffness of the barrier is essentially zero. Although this type of delayed tension has been shown to be a problem for weak-post guardrails, including cables and weak-post W-beam guardrails, the high post stiffness of a strong-post guardrail assures that there is significant lateral stiffness of the barrier throughout the impact. In fact, the effective impact severity of a crash is significantly reduced when a vehicle encounters the end of the flared section. For such an impact, the vehicle does not need to be redirected to be parallel to the flared section, but instead needs only to become parallel to the tangent portion of the barrier. This reduction in effective IS for impacts just upstream of the hinge point greatly reduces the degree of barrier loading during a high energy impact. Some researchers have expressed concern regarding the potential for a vehicle to pocket behind the hinge point. However, a review of historical testing wherein pocketing caused a test failure indicates that this problem appears to be limited to installations with a significant stiffness transition or an inadequate anchor. Because the flared installations do not incorporate a stiffness transition and the tests described previously demonstrate adequacy of the barrier anchor, pocketing upstream of the start of the flared section is not believed to be very likely.

Another concern that has been expressed regarding implementation of the research described herein is the presence of roadside slopes. Clearly W-beam guardrail cannot be used on roadside

slopes steeper than 8:1. Steeper flare rates cannot be utilized when the flare would extend onto such a slope. Never-the-less, the steeper flare rates recommended herein will provide improved safety performance at a reduced cost whenever roadside slopes are 10:1 or flatter. Note that recent crash testing has indicated that the MGS can be safely installed on 8:1 slopes (16). However, sufficient study has not been undertaken to determine whether it is appropriate to install a flared MGS guardrail on an 8:1 slope.

As described above, the effective impact angle increases as the guardrail flare rate increases. A vehicle encroaching at an angle of 25 degrees from the roadway would strike 15:1 and 5:1 flared guardrail terminals at effective impact angles of 28 and 36 degrees, respectively. It is generally believed that no existing guardrail terminals will be capable of sustaining an impact near the beginning of LON at either of these effective impact angles. In fact, NCHRP Report No. 350 only requires terminals to be tested at an impact angle of 20 degrees, instead of the 25 degree impact angle required for the guardrail itself. This reduced requirement for redirective capacity at the beginning of the LON for guardrail terminals is, in part, based upon recognition of the small window of vulnerability associated with this type of impact. Hence, increasing the recommended flare rate does not introduce a new inconsistency in guardrail terminal testing and installed configuration.

The concept behind using high flare rates has always been that the reduction in impacts obtained by reducing the barrier length will outweigh the increase in accident costs associated with a modest increase in barrier penetrations. Research into the cost-effectiveness of flaring temporary concrete barriers clearly indicated that reducing the number of barrier crashes more than outweighed a relatively significant increase in both impact severities and barrier penetrations (2). Research findings presented above clearly indicate that both impact severities and barrier penetration rates

will not increase greatly, even with guardrail flare rates as high as 5:1. Note that there may be a significant increase in penetration rates for impacts very near the beginning of the LON for the terminal. However, this region of vulnerability is small in comparison to the overall guardrail installation and cannot be considered to represent a major increase in overall barrier penetration rate.

Additional research for flare rates could include a more thorough investigation into the topics listed in this section along with research into flare rates for other types of barrier systems.

14 REFERENCES

1. Ross, H.E., Sicking, D.L., Zimmer, R.A., and Michie, J.D., *Recommended Procedures for the Safety Performance Evaluation of Highway Features*, National Cooperative Research Program (NCHRP) Report No. 350, Transportation Research Board, Washington, D.C., 1993.
2. Ross, H.E. Jr., Krammes, R. A., Sicking, D. L., Tyer, K. D., and Perera, H. S., *Traffic Barriers and Control Treatments for Restricted Work Zones*, National Cooperative Highway Research Program (NCHRP) Report No. 358, Transportation Research Board, Washington, D.C., 1994.
3. *Roadside Design Guide, Chapter 5 Roadside Barrier, Section 5.6.3 Flare Rate*, American Association of State Highway and Transportation Officials (AASHTO), Washington, D.C., 2002.
4. Reid, J.D., Sicking, D.L., Faller, R.K., and Pfeifer, B.G., *Development of a New Guardrail System*, Transportation Research Record 1599, Transportation Research Board, National Research Council, Washington, D.C., September 1997, pp. 72-80.
5. Sicking, D.L., Reid, J.D., and Rohde, J.R., *Development of the Midwest Guardrail System*, Transportation Research Record 1797, Transportation Research Board, National Research Council, Washington, D.C., November 2002, pp. 44-52.
6. Faller, R.K., Polivka, K.A., Kuipers, B.D., Bielenberg, B.W., Reid, J.D., Rohde, J.R., and Sicking, D.L., *Midwest Guardrail System for Standard and Special Applications*, Paper No. 04-4778, Transportation Research Record No. 1890, Journal of the Transportation Research Board, Best Paper Award - TRB AFB20 Committee on Roadside Safety Design, Transportation Research Board, Washington D.C., January 2004.
7. Faller, R.K., Sicking, D.L., Bielenberg, R.W., Rohde, J.R., Polivka, K.A., and Reid, J.D., *Performance of Steel-Post W-Beam Guardrail Systems*, Paper No. 07-2642, Transportation Research Record No. 2025, Journal of the Transportation Research Board, TRB AFB20 Committee on Roadside Safety Design, Transportation Research Board, Washington D.C., January 2007.
8. Polivka, K.A., Faller, R.K., Sicking, D.L., Reid, J.D., Rohde, J.R., Holloway, J.C., Bielenberg, B.W., and Kuipers, B.D., *Development of the Midwest Guardrail System (MGS) for Standard and Reduced Post Spacing and in Combination with Curbs*, Final Report to the Midwest States' Regional Pooled Fund Program, Transportation Research Report No. TRP-03-139-04, Midwest Roadside Safety Facility, University of Nebraska-Lincoln, Lincoln, Nebraska, September 1, 2004.
9. Polivka, K.A., Faller, R.K., Sicking, D.L., Rohde, J.R., Bielenberg, B.W., and Reid, J.D., *Performance Evaluation of the Midwest Guardrail System - Update to NCHRP 350 Test No. 3-11 (2214MG-1)*, Final Report to the National Cooperative Highway Research Program

- (NCHRP), Transportation Research Report No. TRP-03-170-06, Midwest Roadside Safety Facility, University of Nebraska-Lincoln, Lincoln, Nebraska, October 10, 2006.
10. Polivka, K.A., Faller, R.K., Sicking, D.L., Rohde, J.R., Bielenberg, B.W., and Reid, J.D., *Performance Evaluation of the Midwest Guardrail System - Update to NCHRP 350 Test No. 3-11 With 28" C.G. Height (2214MG-2)*, Final Report to the National Cooperative Highway Research Program (NCHRP), Transportation Research Report No. TRP-03-171-06, Midwest Roadside Safety Facility, University of Nebraska-Lincoln, Lincoln, Nebraska, October 11, 2006.
 11. Polivka, K.A., Faller, R.K., Sicking, D.L., Rohde, J.R., Bielenberg, B.W., and Reid, J.D., *Performance Evaluation of the Midwest Guardrail System - Update to NCHRP 350 Test No. 3-10 (2214MG-3)*, Final Report to the National Cooperative Highway Research Program (NCHRP), Transportation Research Report No. TRP-03-172-06, Midwest Roadside Safety Facility, University of Nebraska-Lincoln, Lincoln, Nebraska, October 11, 2006.
 12. Kuipers, B.D., Faller, R.K., and Reid, J.D., *Critical Flare Rates for W-Beam Guardrail - Determining Maximum Capacity Using Computer Simulation*, Project NCHRP 17-20(3), Final Report to the National Cooperative Highway Research Program (NCHRP), Transportation Research Report No. TRP-03-157-04, Midwest Roadside Safety Facility, University of Nebraska-Lincoln, Lincoln, Nebraska, January 24, 2005.
 13. Hinch, J., Yang, T.L., and Owings, R., *Guidance Systems for Vehicle Testing*, ENSCO Inc., Springfield, VA, 1986.
 14. *Vehicle Damage Scale for Traffic Investigators*, Second Edition, Technical Bulletin No. 1, Traffic Accident Data (TAD) Project, National Safety Council, Chicago, Illinois, 1971.
 15. *Collision Deformation Classification - Recommended Practice J224 March 1980*, Handbook Volume 4, Society of Automotive Engineers (SAE), Warrendale, Pennsylvania, 1985.
 16. Allison, E.M., Polivka, K.A., Reid, J.D., Sicking, D.L., Faller, R.K., Bielenberg, R.W., and Rohde, J.R., *Approach Slope for Midwest Guardrail System*, Draft Report to the Midwest States' Regional Pooled Fund Program, Transportation Research Report TRP-03-188-08, Midwest Roadside Safety Facility, University of Nebraska-Lincoln, Lincoln, Nebraska, 2008.

15 APPENDICES

APPENDIX A

ENGLISH-UNIT SYSTEM DRAWINGS - DESIGN NO. 1

- Figure A-1. System Details, Design No. 1 (English)
- Figure A-2. Rail Details, Design No. 1 (English)
- Figure A-3. Post Details, Design No. 1 (English)
- Figure A-4. Anchorage Details, Design No. 1 (English)
- Figure A-5. Anchorage Details, Design No. 1 (English)
- Figure A-6. Anchorage Details, Design No. 1 (English)

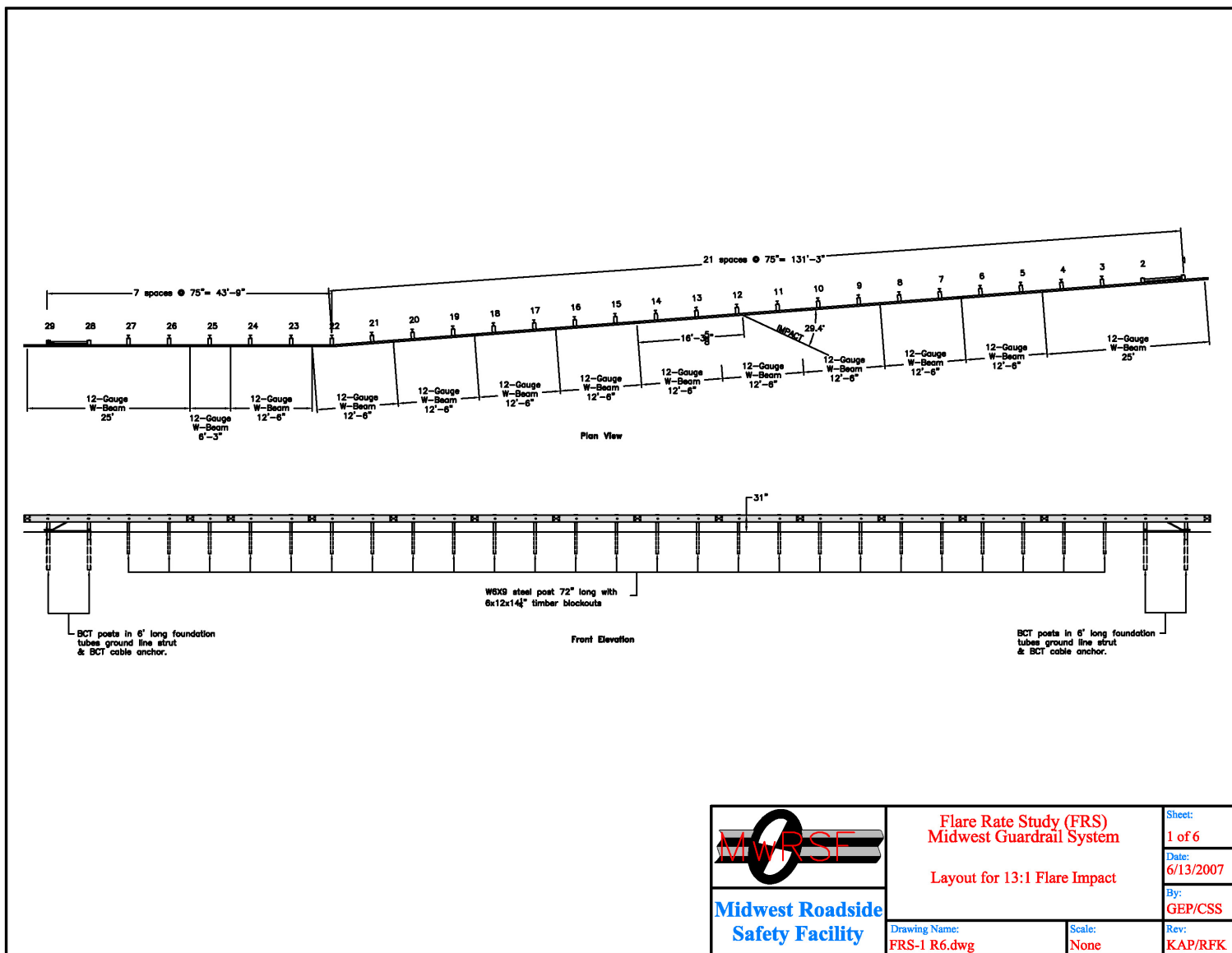


Figure A-1. System Layout, Design No. 1 (English)

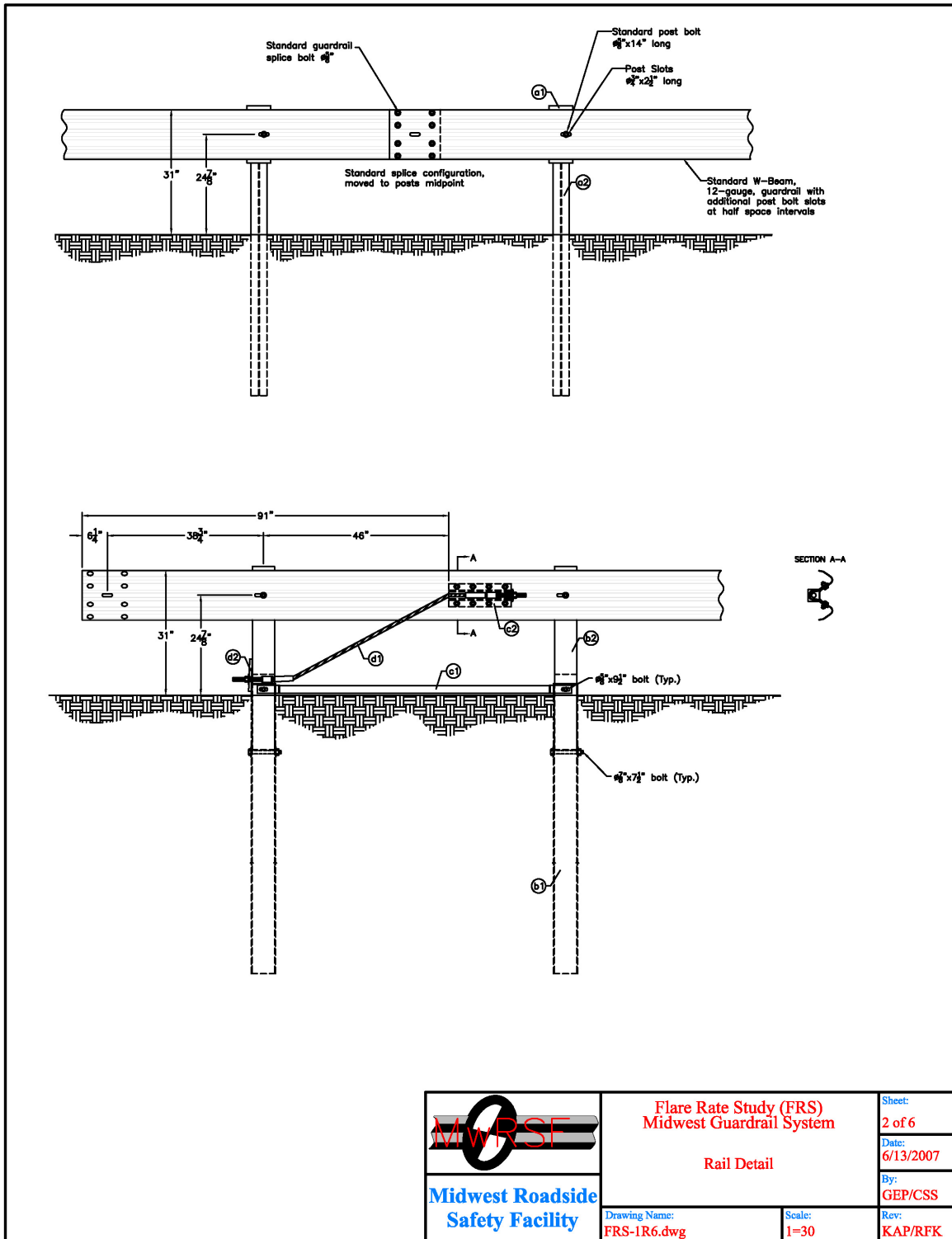


Figure A-2. Rail Details, Design No. 1 (English)

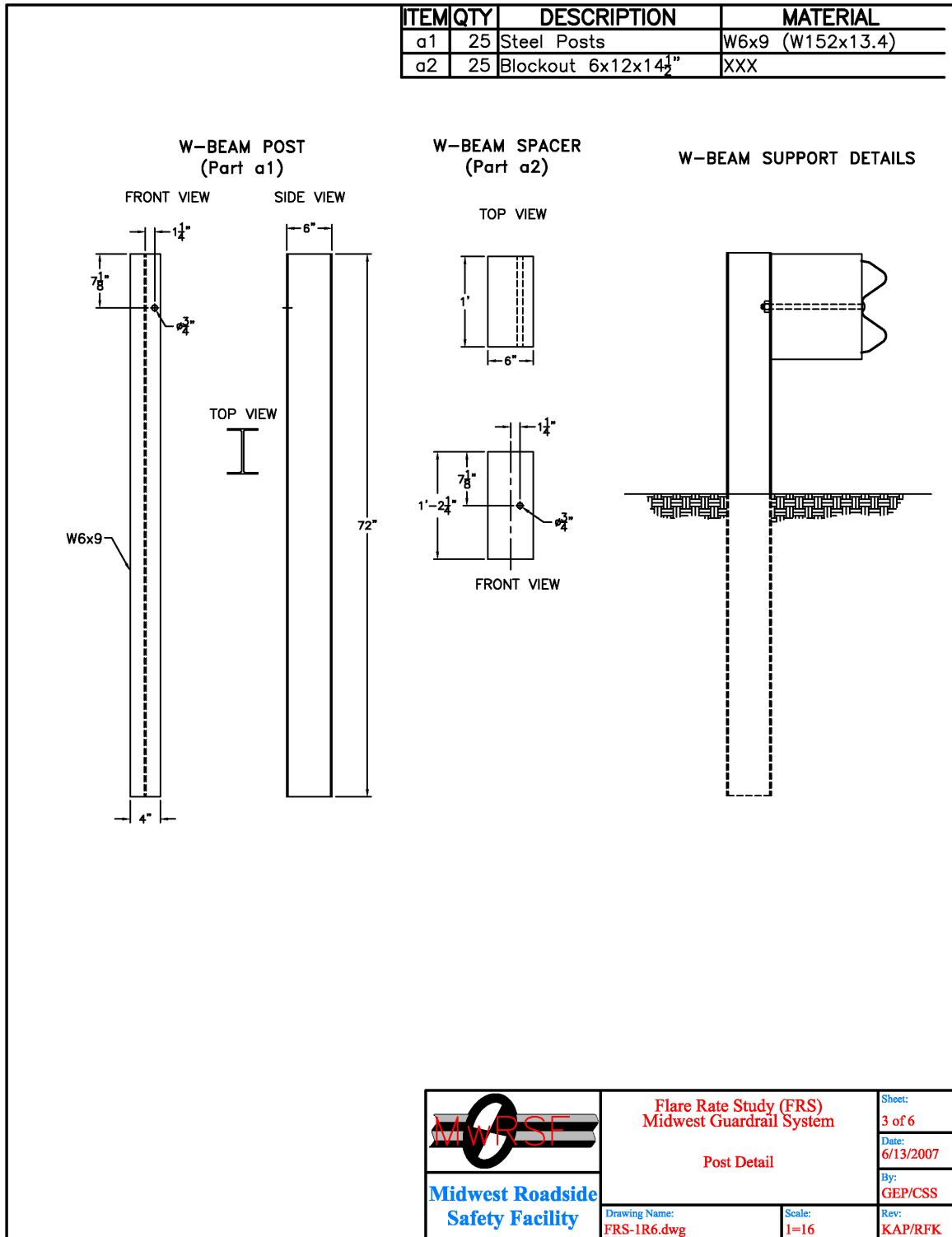


Figure A-3. Post Details, Design No. 1 (English)

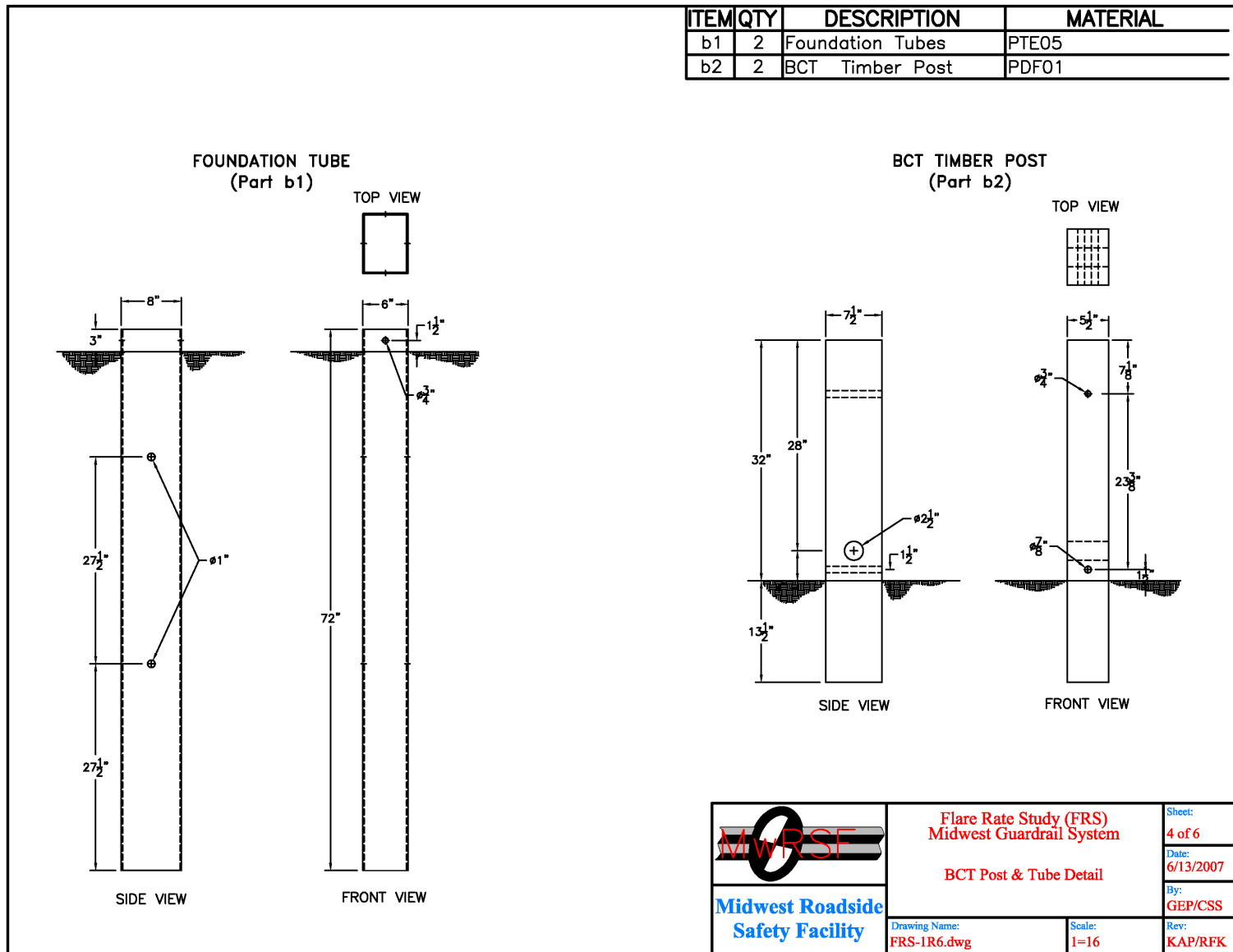


Figure A-4. Anchorage Details, Design No. 1 (English)

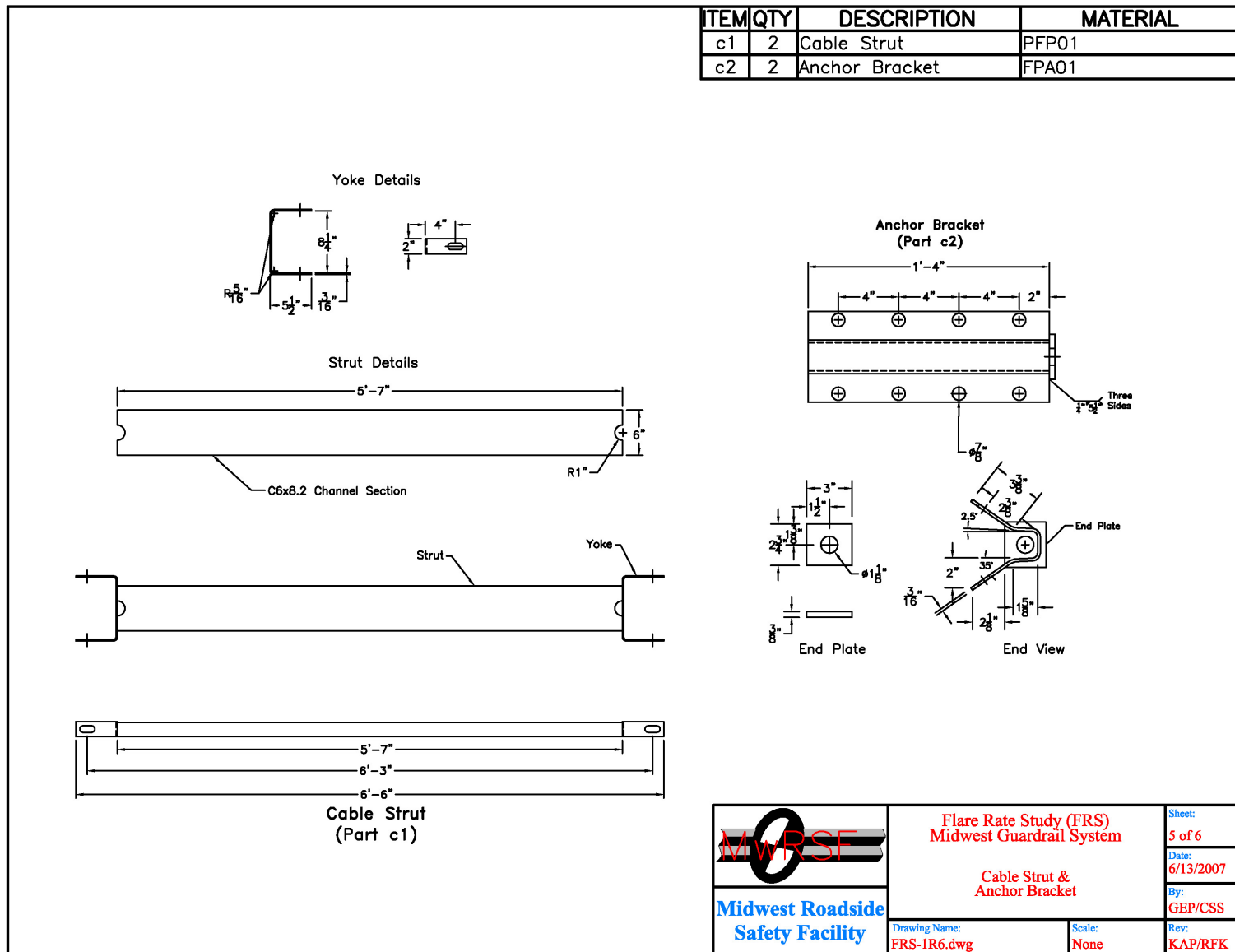


Figure A-5. Anchorage Details, Design No. 1 (English)

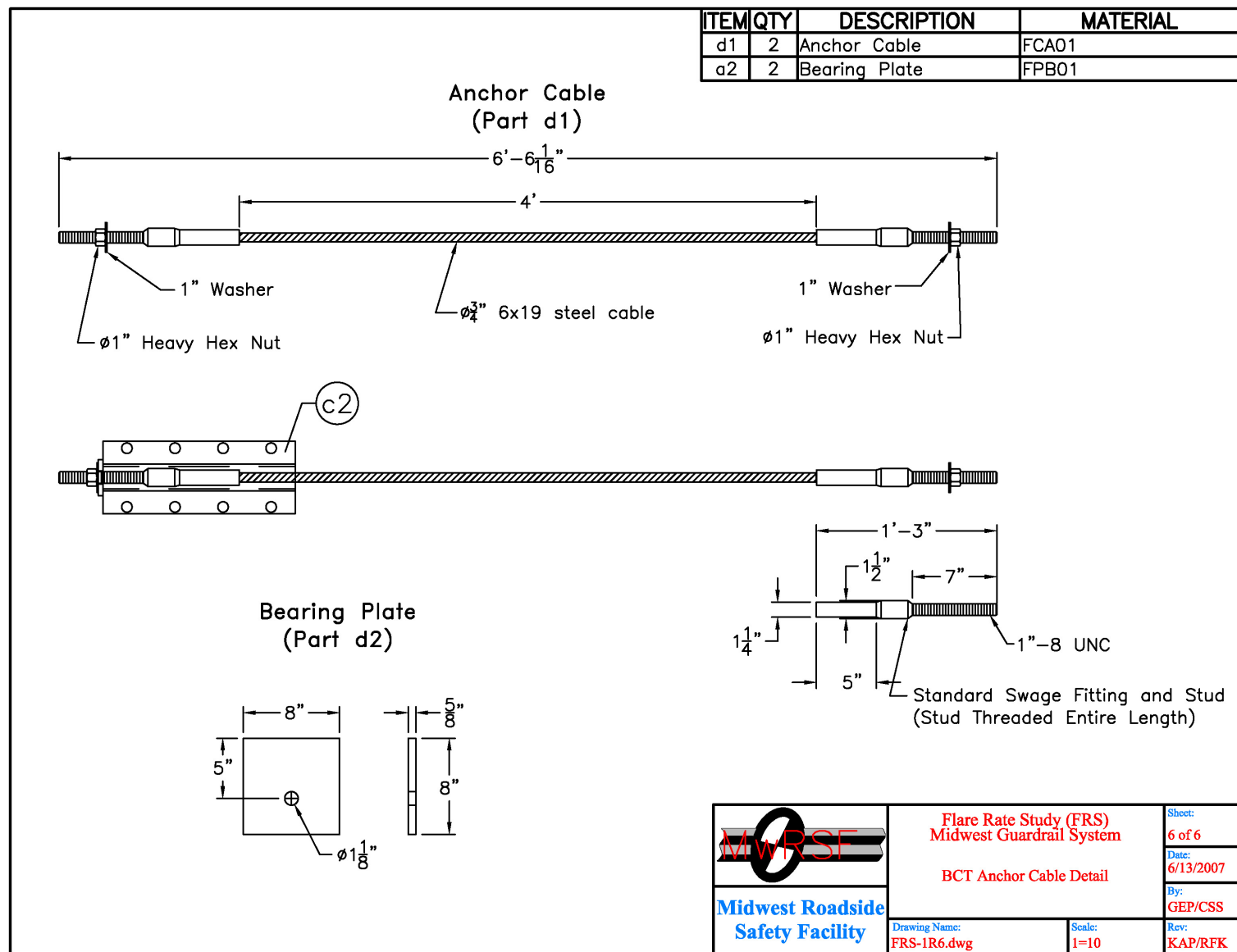


Figure A-6. Anchorage Details, Design No. 1 (English)

APPENDIX B

TEST SUMMARY SHEETS IN ENGLISH UNITS

- Figure B-1. Summary of Test Results and Sequential Photographs (English), Test No. FR-1
Figure B-2. Summary of Test Results and Sequential Photographs (English), Test No. FR-2
Figure B-3. Summary of Test Results and Sequential Photographs (English), Test No. FR-3
Figure B-4. Summary of Test Results and Sequential Photographs (English), Test No. FR-4
Figure B-5. Summary of Test Results and Sequential Photographs (English), Test No. FR-5

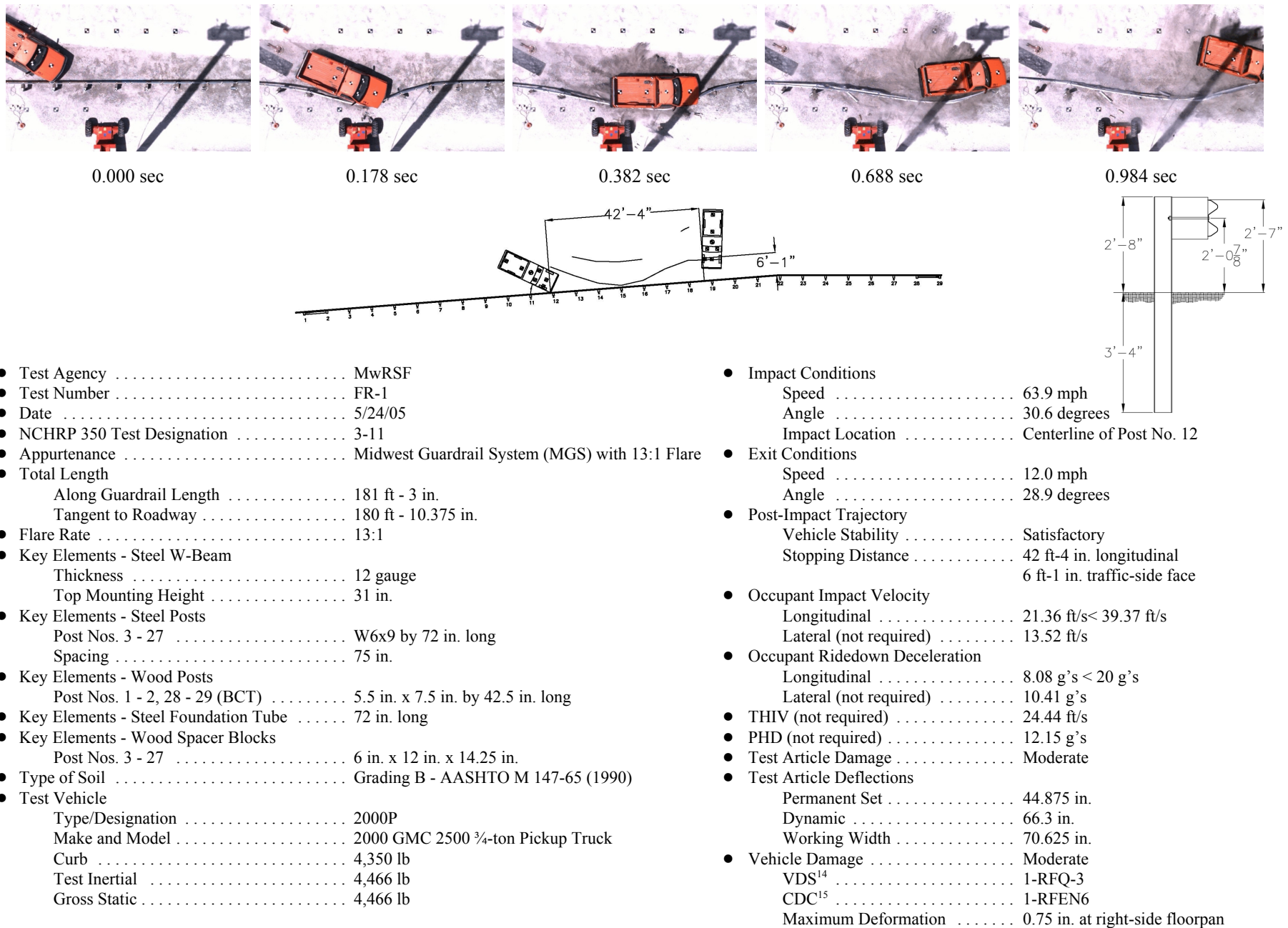


Figure B-1. Summary of Test Results and Sequential Photographs (English), Test No. FR-1

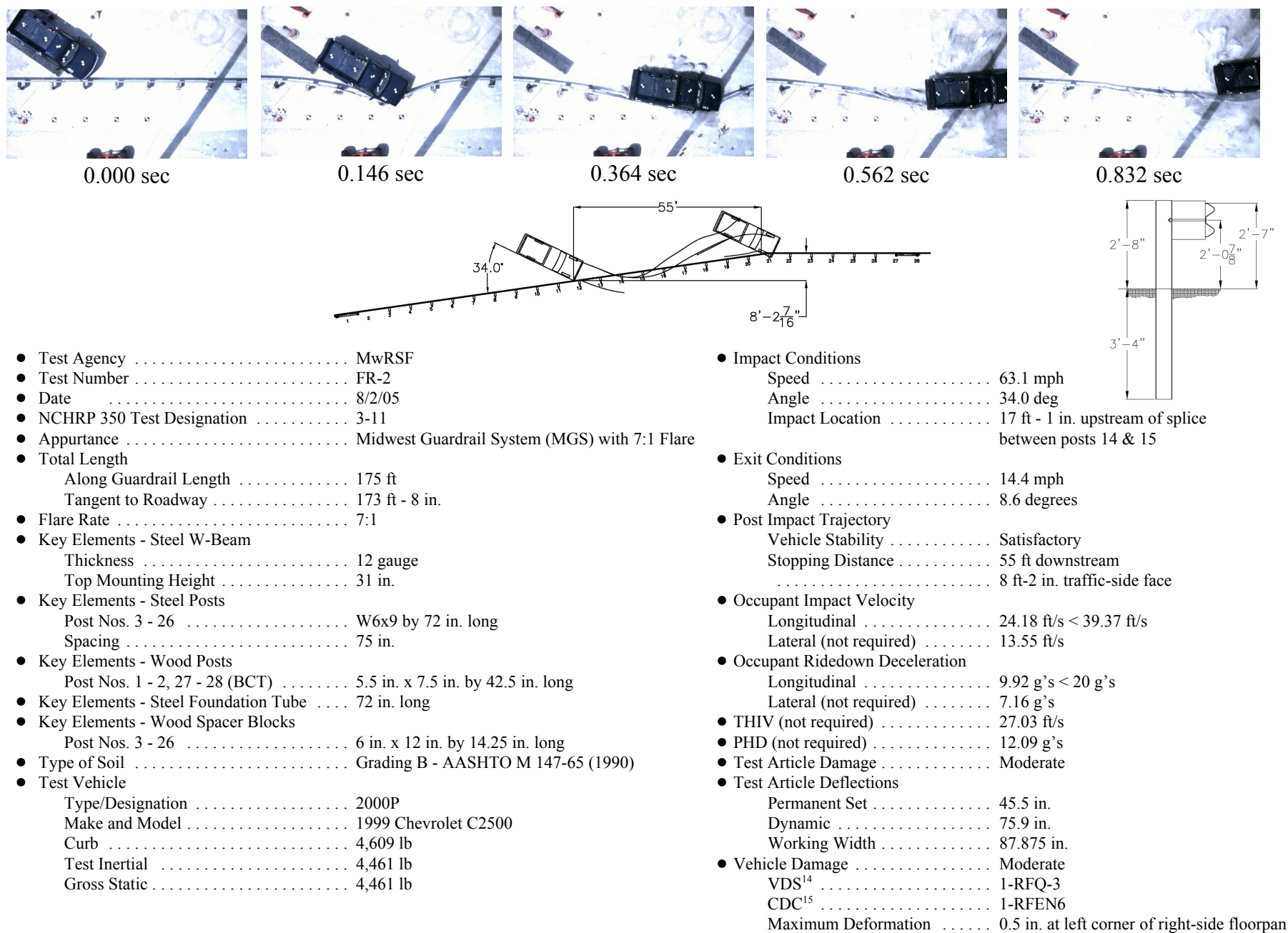


Figure B-2. Summary of Test Results and Sequential Photographs (English), Test FR-2

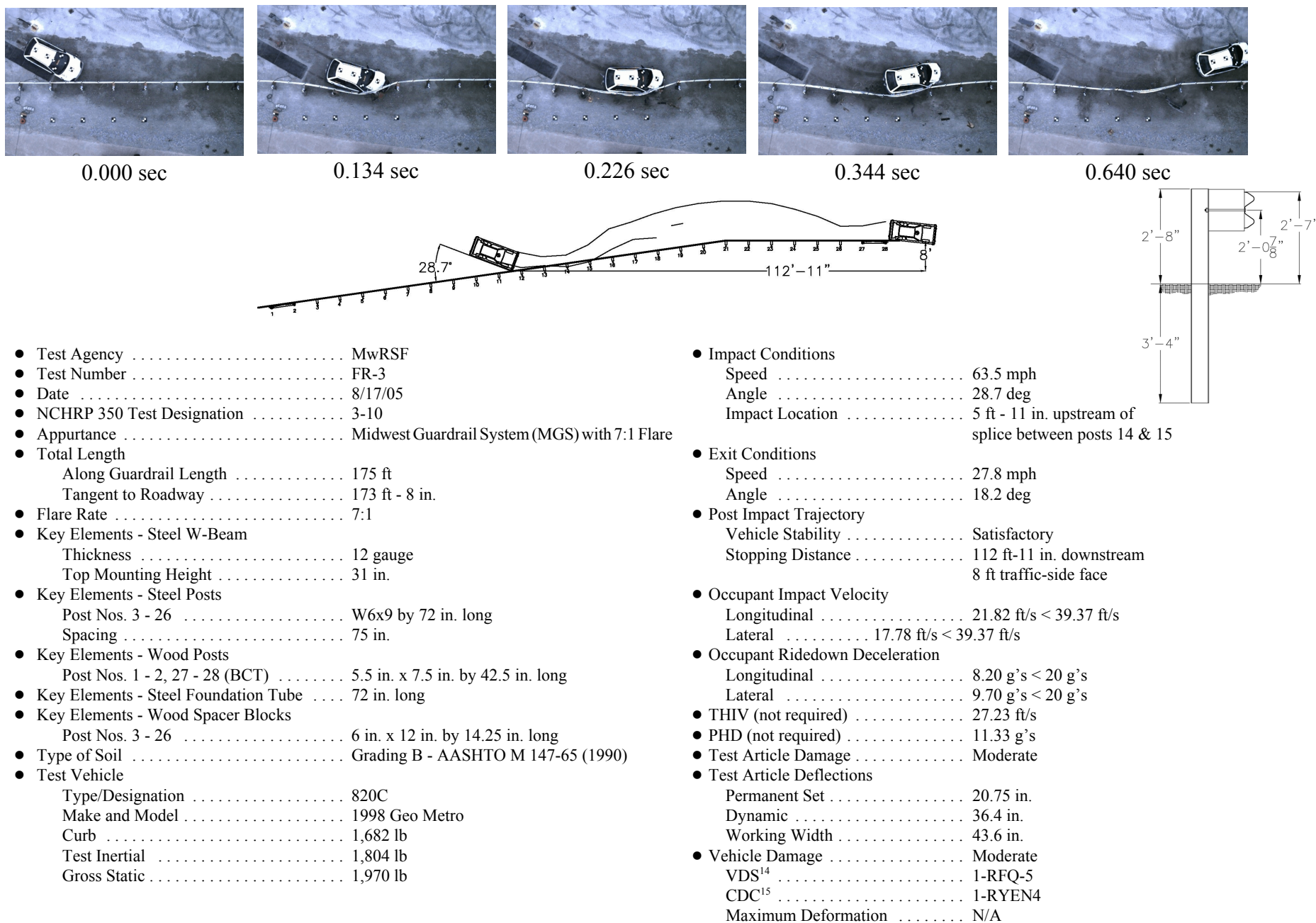


Figure B-3. Summary of Test Results and Sequential Photographs (English), Test FR-3

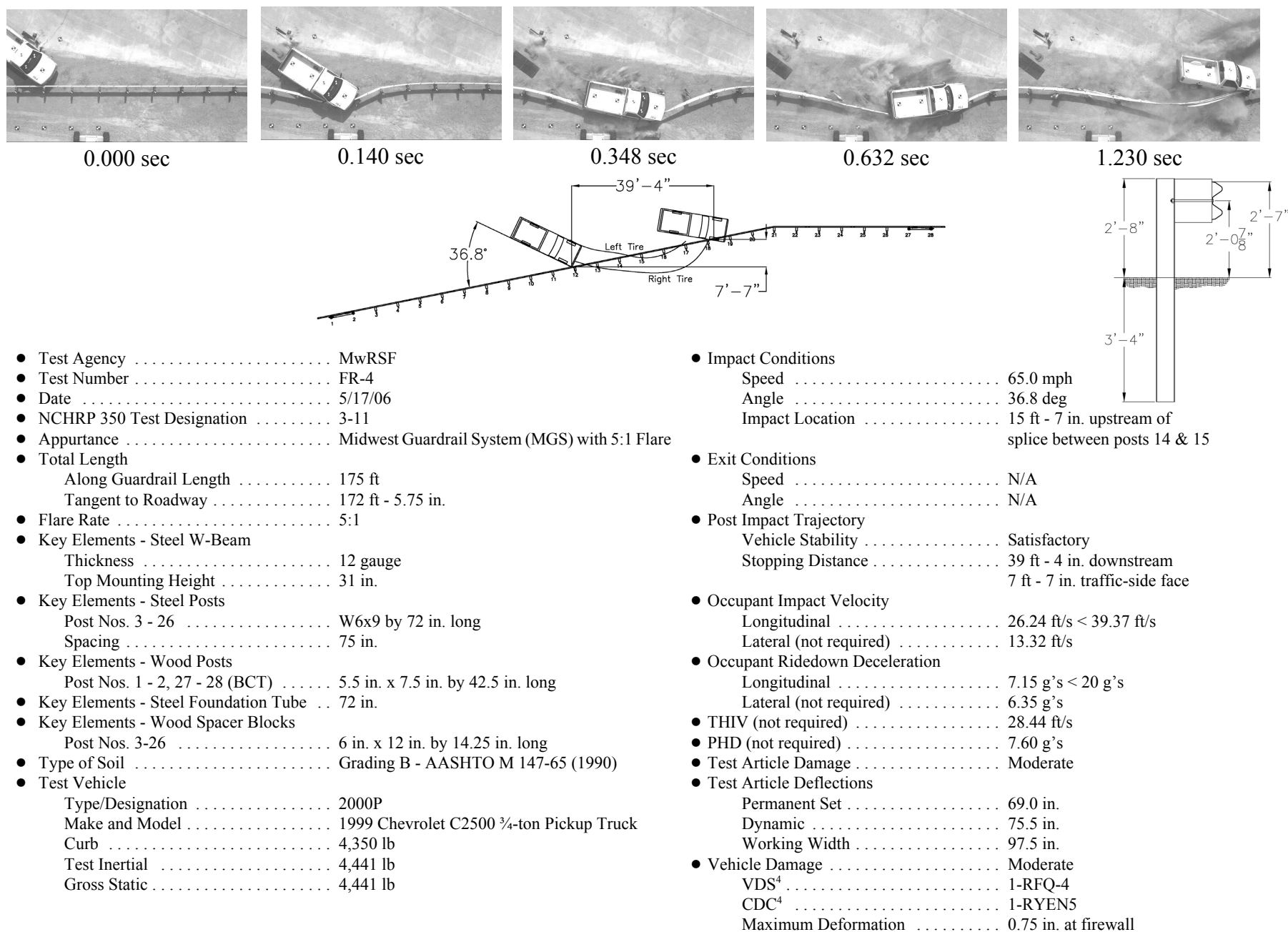


Figure B-4. Summary of Test Results and Sequential Photographs (English), Test FR-4

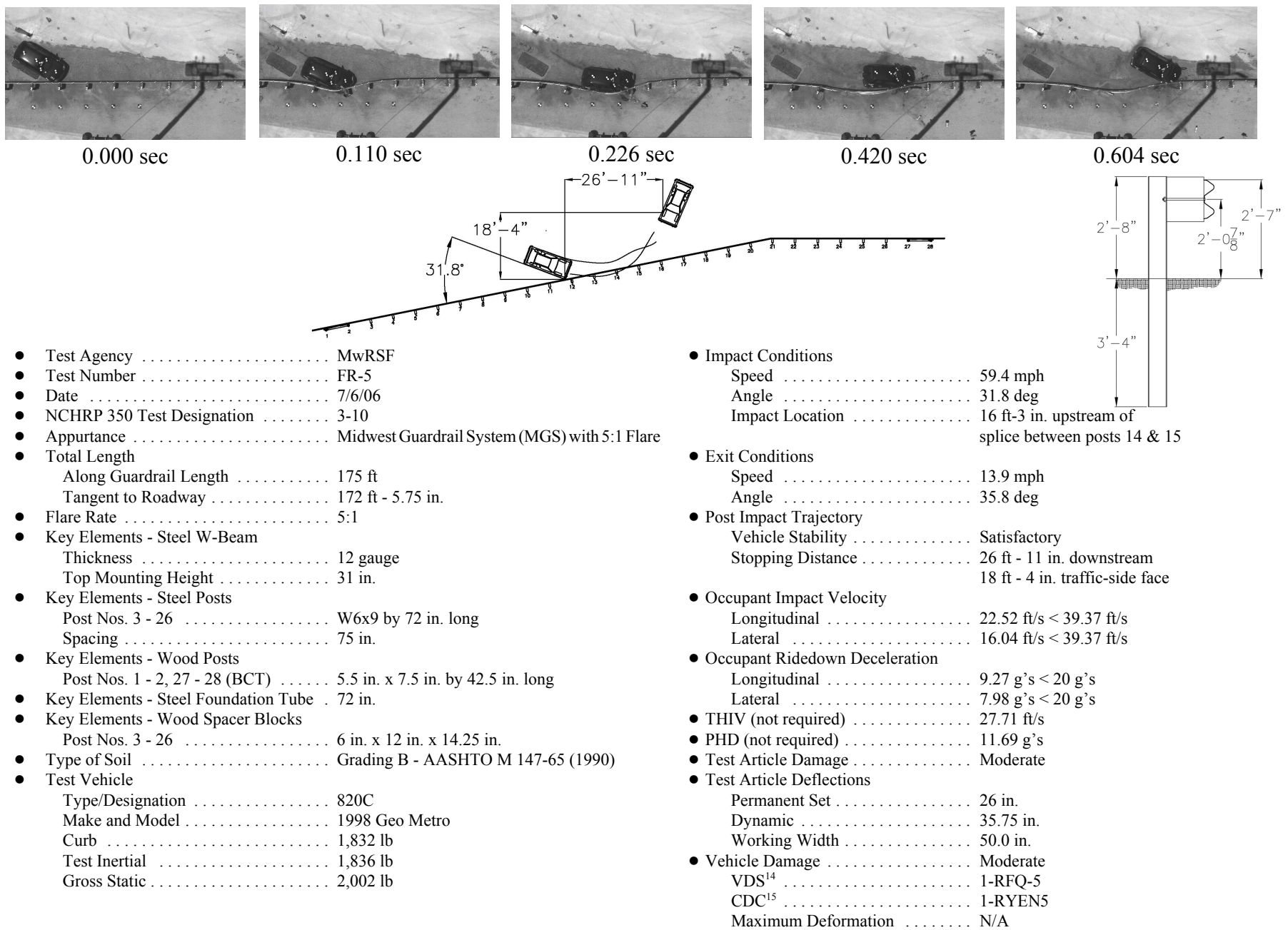


Figure B-5. Summary of Test Results and Sequential Photographs (English), Test FR-5

APPENDIX C

OCCUPANT COMPARTMENT DEFORMATION DATA, TEST FR-1

Figure C-1. Occupant Compartment Deformation Data - Set 1, Test FR-1

Figure C-2. Occupant Compartment Deformation Data - Set 2, Test FR-1

Figure C-3. Occupant Compartment Deformation Index (OCDI), Test FR-1

VEHICLE PRE/POST CRUSH INFO
Set-1

TEST: FR-1
VEHICLE: 2000p

POINT	X	Y	Z	X'	Y'	Z'	DEL X	DEL Y	DEL Z
1	52	3.5	0.25	51.75	3.5	0.25	-0.25	0	0
2	54.75	11	-3	54.75	11	-3	0	0	0
3	55.25	16.5	-3	55	16.25	-3	-0.25	-0.25	0
4	55.25	23.25	-3	55	23.25	-3	-0.25	0	0
5	55	27.75	-2.5	55	27.75	-2.75	0	0	-0.25
6	47	4	-1	47	3.75	-0.75	0	-0.25	0.25
7	47.75	11.5	-6.5	48	11.25	-6.25	0.25	-0.25	0.25
8	48.25	18	-6.25	48	18.25	-6.25	-0.25	0.25	0
9	47.5	23.5	-6.5	47.5	23.75	-5.75	0	0.25	0.75
10	46	29.5	-6	46	29.5	-6	0	0	0
11	42.5	4	-1.75	42.5	4.25	-1.5	0	0.25	0.25
12	43.25	11.25	-6.5	43.25	11.5	-6.25	0	0.25	0.25
13	43.5	18.5	-6.25	43.5	18.25	-6.25	0	-0.25	0
14	42.75	24.5	-5.75	42.75	24.5	-6	0	0	-0.25
15	42.5	29.75	-6	42.5	29.5	-6	0	-0.25	0
16	38.25	4.25	-2.5	38.25	4.25	-2.25	0	0	0.25
17	38.5	11.75	-6.75	38.5	11.75	-6.5	0	0	0.25
18	38.5	18.5	-6.25	38.5	18.5	-6.25	0	0	0
19	38.25	24	-6	38.25	23.75	-6	0	-0.25	0
20	38.25	29.25	-6	38.25	28.75	-6.25	0	-0.5	-0.25
21	33.25	4.5	-3	33.25	4.5	-2.75	0	0	0.25
22	33	12.5	-7	32.75	12.25	-6.5	-0.25	-0.25	0.5
23	32.25	20.75	-6.25	32.25	20.5	-6	0	-0.25	0.25
24	32.75	28.5	-6	33	28.25	-6	0.25	-0.25	0
25	27.75	3.5	-3.75	27.75	3.5	-3.5	0	0	0.25
26	27	12.5	-6.75	26.75	12.25	-6.5	-0.25	-0.25	0.25
27	26.25	21.25	-6	26.5	20.75	-6	0.25	-0.5	0
28	26.5	28.5	-6	26.5	28	-6	0	-0.5	0
29									
30									

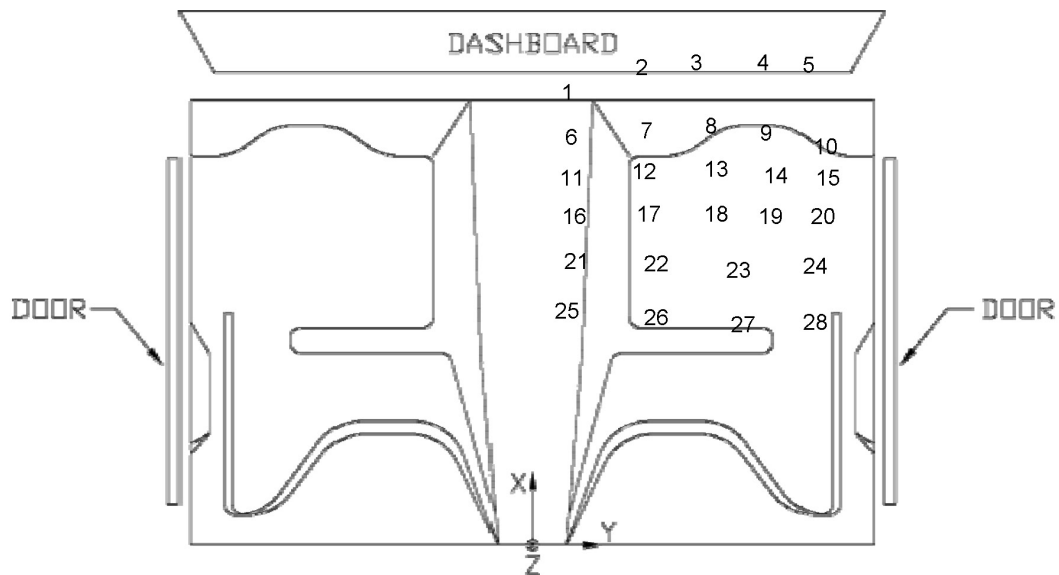


Figure C-1. Occupant Compartment Deformation Data - Set 1, Test FR-1

VEHICLE PRE/POST CRUSH INFO
Set-2

TEST: FR-1
VEHICLE: 2000p

POINT	X	Y	Z	X'	Y'	Z'	DEL X	DEL Y	DEL Z
1	45.25	11.75	-0.5	45	12.25	-0.5	-0.25	0.5	0
2	48	19.25	-4	48.25	19.25	-4	0.25	0	0
3	48.5	24.75	-4	48.5	24.5	-4	0	-0.25	0
4	48.5	31.5	-4	48.5	31.5	-4	0	0	0
5	48.25	36	-3.5	48.25	36	-3.5	0	0	0
6	40.25	12.25	-1.5	40.25	12	-1.5	0	-0.25	0
7	41	19.75	-7	41.25	19.5	-7.25	0.25	-0.25	-0.25
8	41.5	26.25	-7	41.25	26.75	-7	-0.25	0.5	0
9	40.75	31.75	-6.5	40.75	32.25	-6.75	0	0.5	-0.25
10	39.25	37.75	-6.75	39.25	37.75	-7	0	0	-0.25
11	35.75	12.25	-2.25	35.75	12.25	-2.25	0	0	0
12	36.5	19.5	-7.25	36.5	19.75	-7.25	0	0.25	0
13	36.75	26.75	-7.25	36.75	26.75	-7	0	0	0.25
14	36	32.75	-6.75	36.5	32.75	-6.75	0.5	0	0
15	35.75	38	-7	35.75	38	-7	0	0	0
16	31.5	12.5	-3	31.5	12.75	-2.75	0	0.25	0.25
17	31.75	20	-7.5	31.75	20.25	-7.25	0	0.25	0.25
18	31.75	26.75	-7.25	31.75	27.25	-7.25	0	0.5	0
19	31.5	32.25	-7	31.75	32.75	-7	0.25	0.5	0
20	31.5	37.5	-7.25	31.5	37.5	-7.25	0	0	0
21	26.5	12.75	-3.75	26.5	13	-3.5	0	0.25	0.25
22	26.25	20.75	-7.75	26	20.75	-7.5	-0.25	0	0.25
23	25.5	29	-7.25	25.75	29	-7	0.25	0	0.25
24	26	36.75	-7	26.25	36.75	-7	0.25	0	0
25	21	11.75	-4.5	21	12	-4.25	0	0.25	0.25
26	20.25	20.75	-7.75	20.25	20.75	-7.5	0	0	0.25
27	19.5	29.5	-7.25	19.75	29.5	-7	0.25	0	0.25
28	19.75	36.75	-7.25	20	36.75	-7.25	0.25	0	0
29									
30									

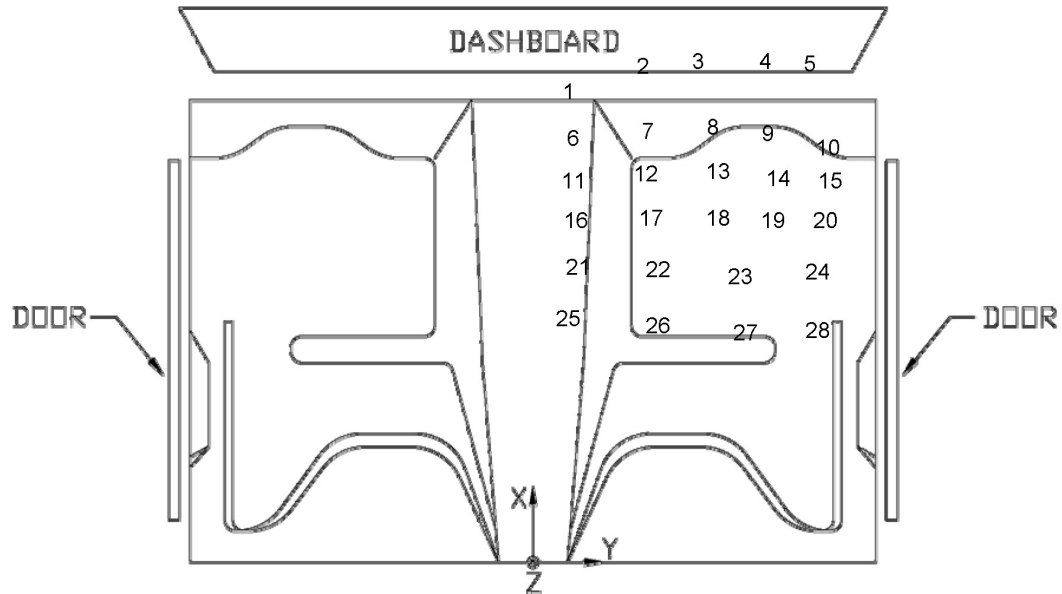


Figure C-2. Occupant Compartment Deformation - Set 2, Test FR-1

Occupant Compartment Deformation Index (OCDI)

Test No. FR-1
Vehicle Type: 2000p

OCDI = XXABCDEFGHI

XX = location of occupant compartment deformation

A = distance between the dashboard and a reference point at the rear of the occupant compartment, such as the top of the rear seat or the rear of the cab on a pickup

B = distance between the roof and the floor panel

C = distance between a reference point at the rear of the occupant compartment and the motor panel

D = distance between the lower dashboard and the floor panel

E = interior width

F = distance between the lower edge of right window and the upper edge of left window

G = distance between the lower edge of left window and the upper edge of right window

H = distance between bottom front corner and top rear corner of the passenger side window

I = distance between bottom front corner and top rear corner of the driver side window

Severity Indices

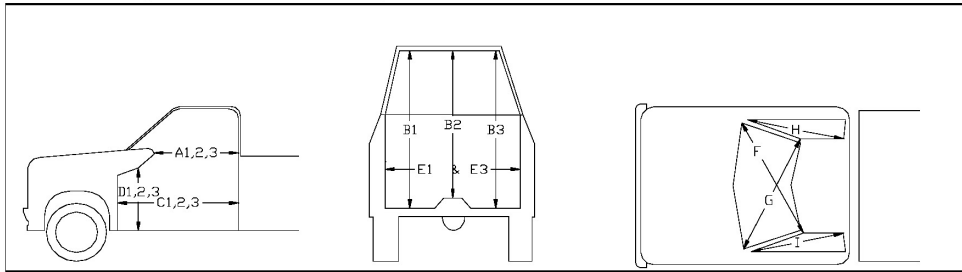
0 - if the reduction is less than 3%

1 - if the reduction is greater than 3% and less than or equal to 10 %

2 - if the reduction is greater than 10% and less than or equal to 20 %

3 - if the reduction is greater than 20% and less than or equal to 30 %

4 - if the reduction is greater than 30% and less than or equal to 40 %



where,
1 = Passenger Side
2 = Middle
3 = Driver Side

Location:

Measurement	Pre-Test (in.)	Post-Test (in.)	Change (in.)	% Difference	Severity Index
A1	39.75	40.00	0.25	0.63	0
A2	41.25	41.50	0.25	0.61	0
A3	40.25	40.50	0.25	0.62	0
B1	45.50	45.50	0.00	0.00	0
B2	42.25	42.00	-0.25	-0.59	0
B3	46.00	45.75	-0.25	-0.54	0
C1	56.75	56.50	-0.25	-0.44	0
C2	52.00	52.00	0.00	0.00	0
C3	57.00	57.25	0.25	0.44	0
D1	19.75	19.75	0.00	0.00	0
D2	16.50	16.50	0.00	0.00	0
D3	19.50	19.50	0.00	0.00	0
E1	62.50	62.00	-0.50	-0.80	0
E3	63.75	63.50	-0.25	-0.39	0
F	57.50	57.50	0.00	0.00	0
G	57.75	58.00	0.25	0.43	0
H	42.50	42.25	-0.25	-0.59	0
I	42.25	42.25	0.00	0.00	0

Note: Maximum severity index for each variable (A-I) is used for determination of final OCDI value

Final OCDI: XX A B C D E F G H I
RF 0 0 0 0 0 0 0 0 0

Figure C-3. Occupant Compartment Deformation Index (OCDI), Test FR-1

APPENDIX D

ACCELEROMETER AND RATE TRANSDUCER DATA ANALYSIS, TEST FR-1

Figure D-1. Graph of Longitudinal Deceleration, Test FR-1

Figure D-2. Graph of Longitudinal Occupant Impact Velocity (OIV), Test FR-1

Figure D-3. Graph of Longitudinal Occupant Displacement, Test FR-1

Figure D-4. Graph of Lateral Deceleration, Test FR-1

Figure D-5. Graph of Lateral Occupant Impact Velocity (OIV), Test FR-1

Figure D-6. Graph of Lateral Occupant Displacement, Test FR-1

Figure D-7. Graph of Roll, Pitch, and Yaw Angular Displacements, Test FR-1

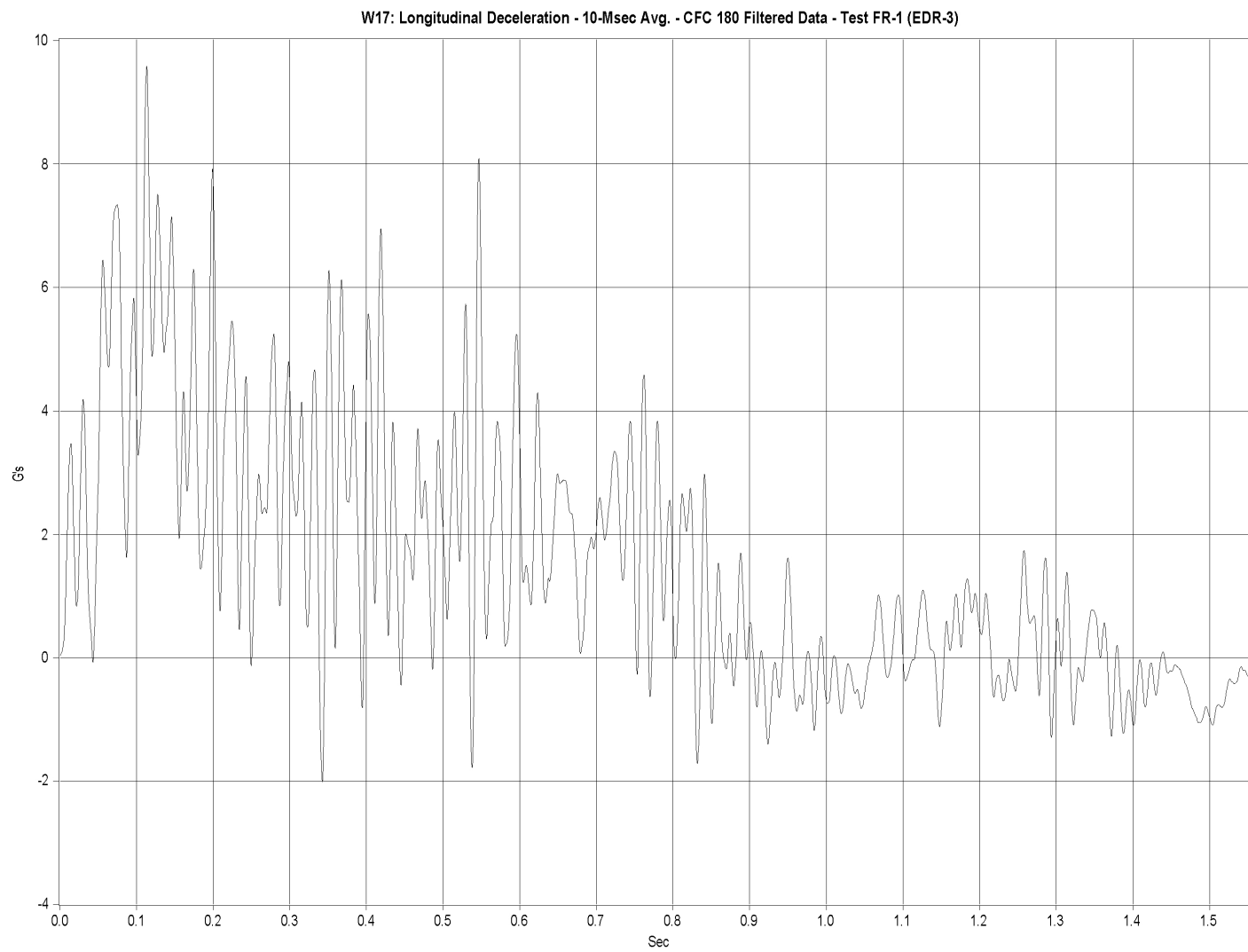


Figure D-1. Graph of Longitudinal Occupant Deceleration, Test FR-1

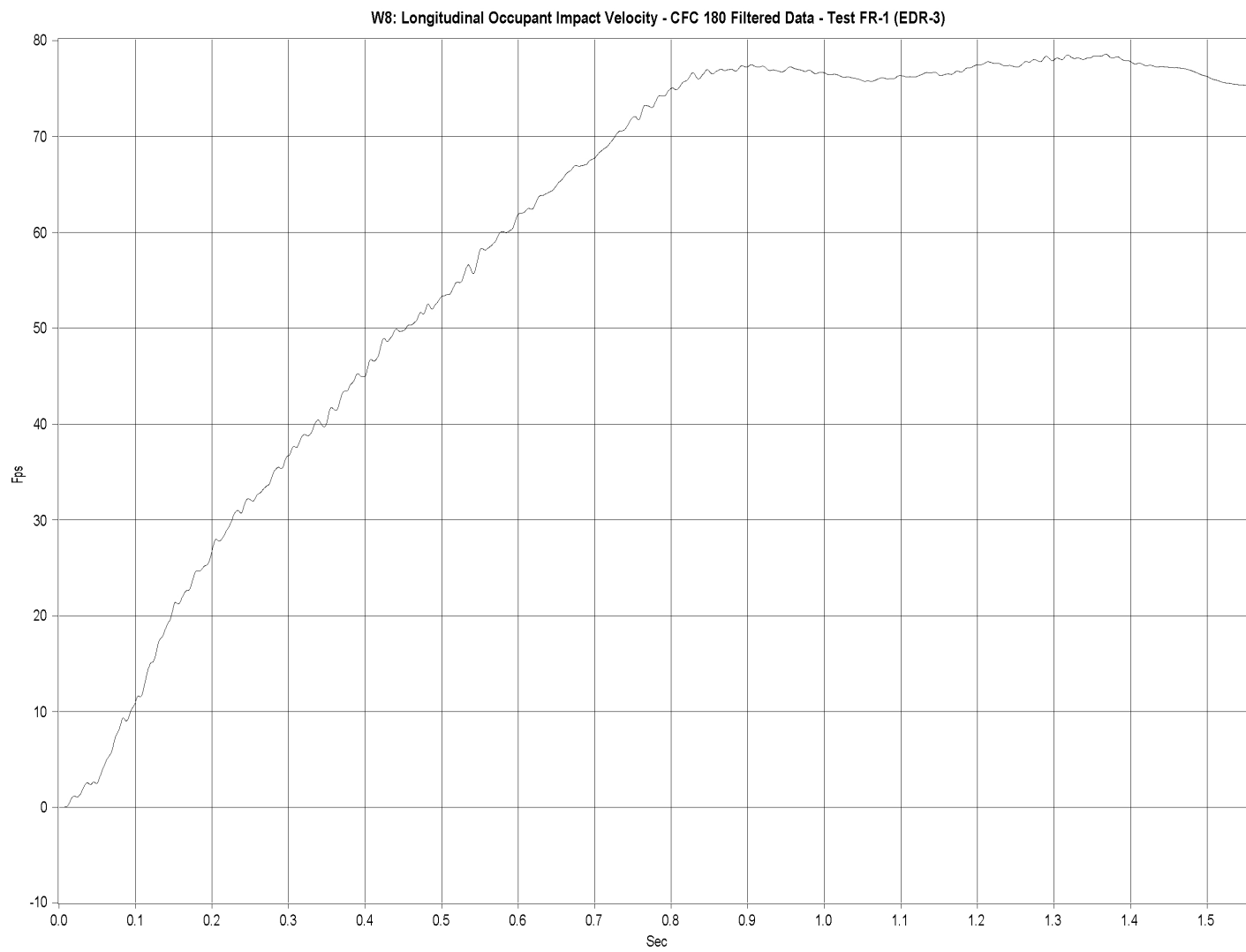


Figure D-2. Graph of Longitudinal Occupant Impact Velocity (OIV), Test FR-1

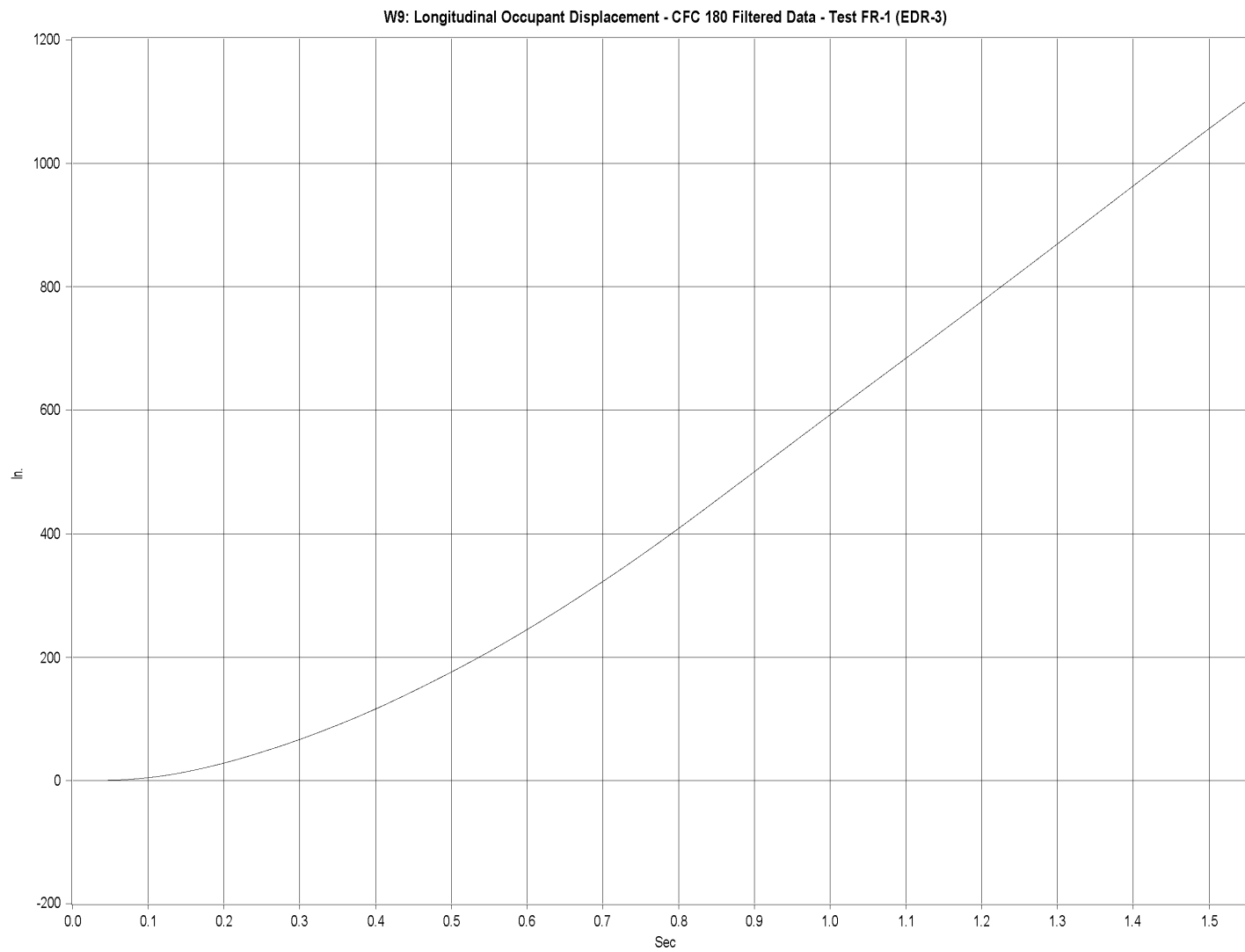


Figure D-3. Graph of Longitudinal Occupant Displacement, Test FR-1

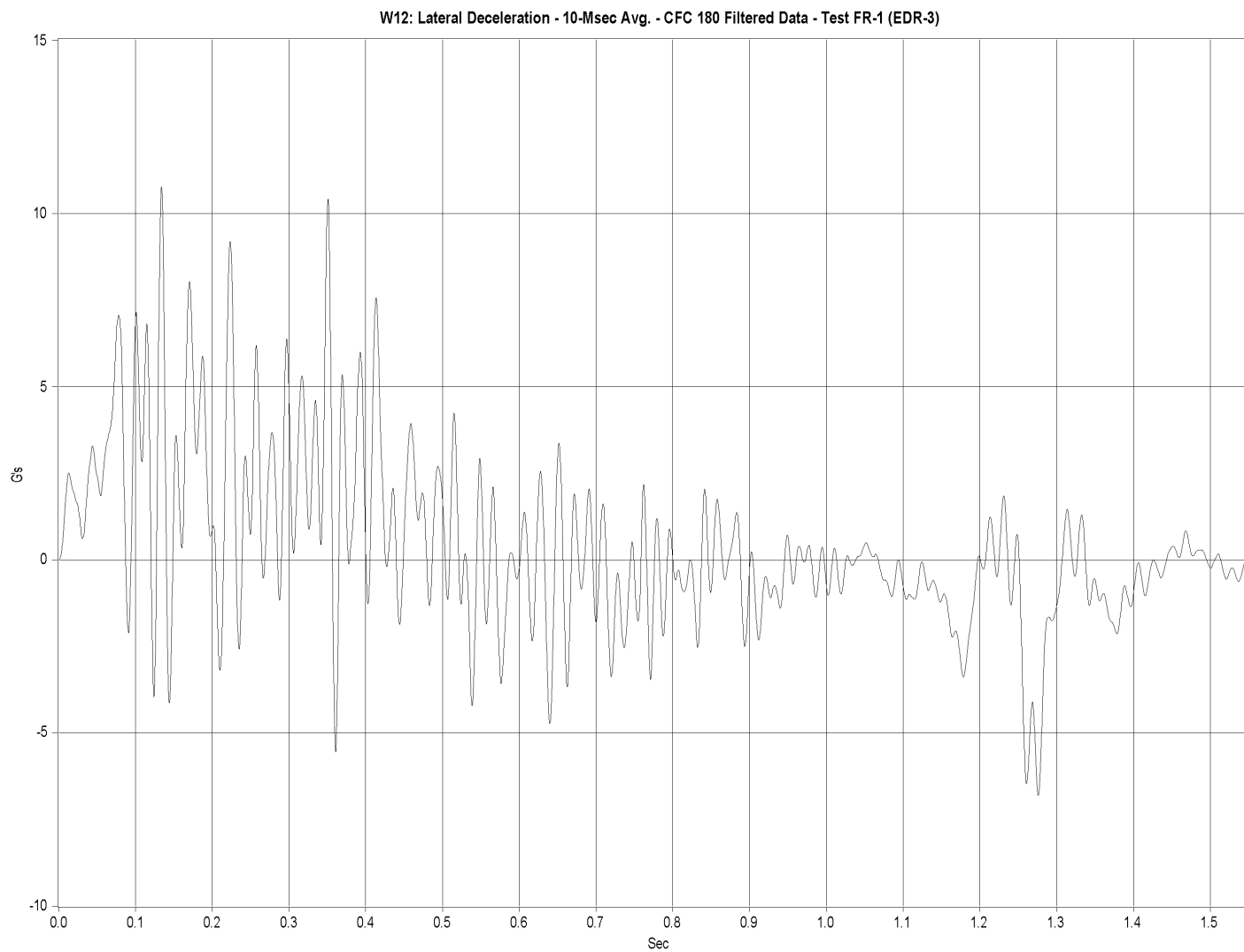


Figure D-4. Graph of Lateral Occupant Deceleration, Test FR-1

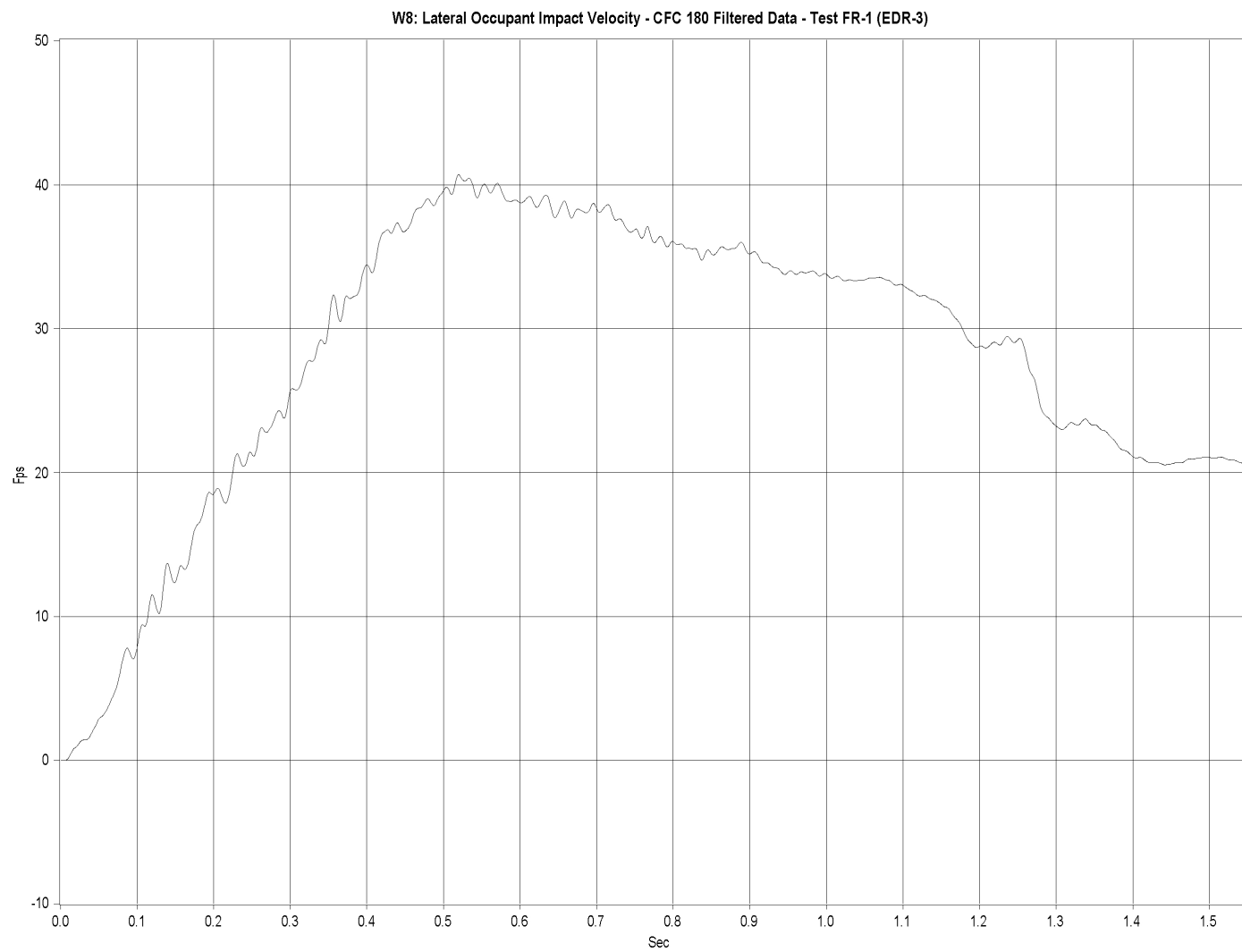


Figure D-5. Graph of Lateral Occupant Impact Velocity (OIV), Test FR-1

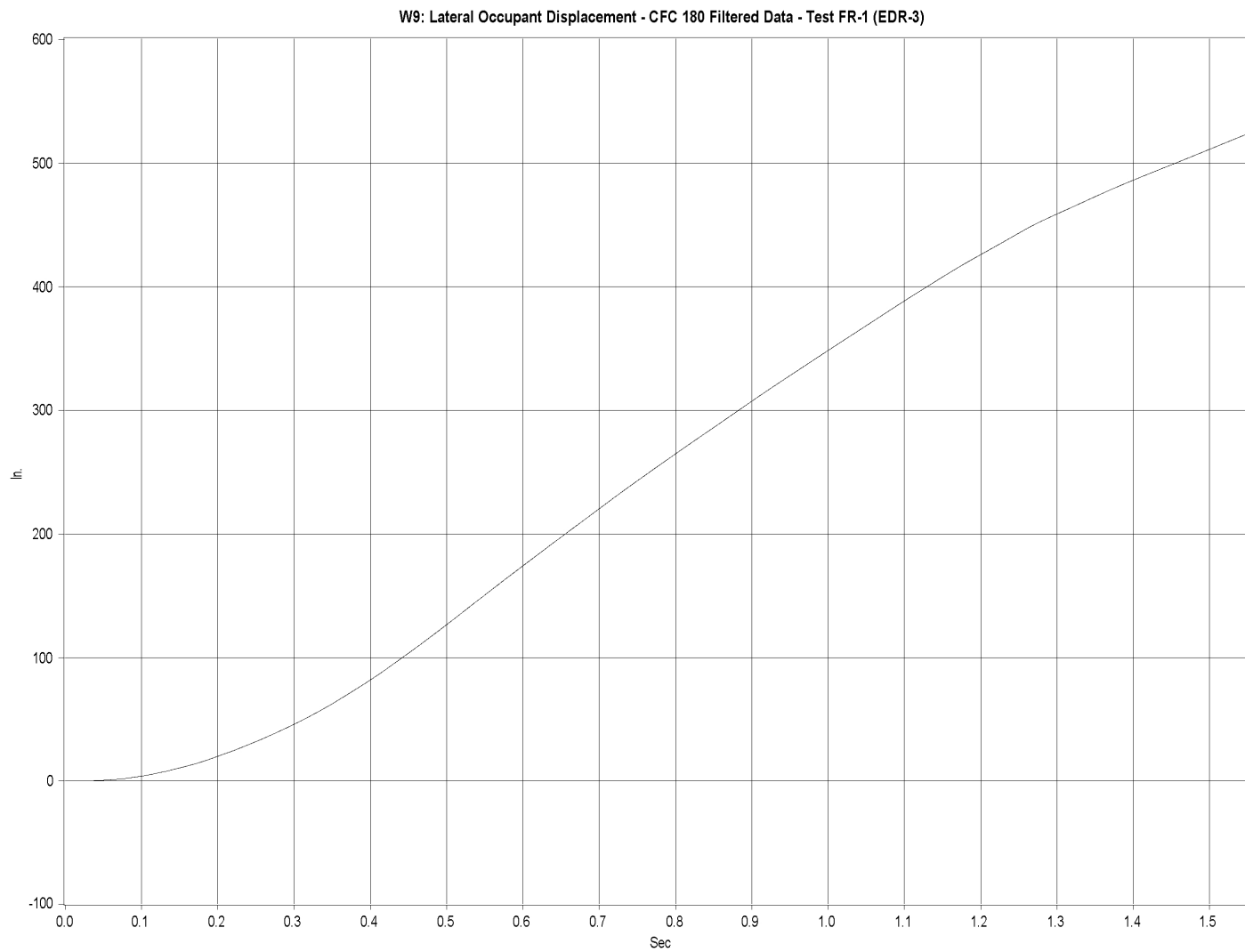


Figure D-6. Graph of Lateral Occupant Displacement, Test FR-1

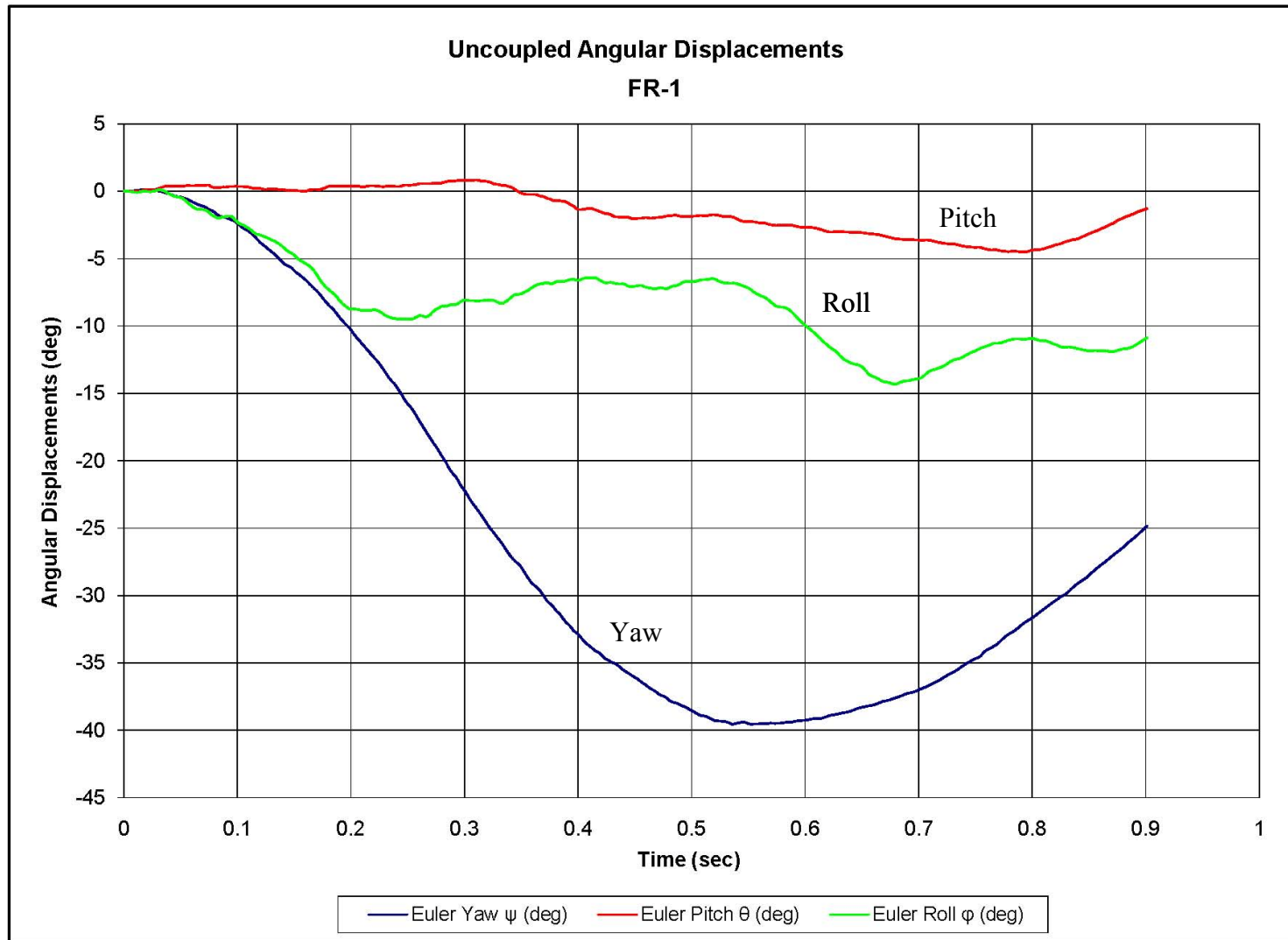


Figure D-7. Graph of Lateral Occupant Displacement, Test FR-1

APPENDIX E

SYSTEM DRAWINGS - DESIGN NO. 2

- Figure E-1. System Details, Design No. 2 (Metric)
- Figure E-2. Rail Details, Design No. 2 (Metric)
- Figure E-3. Post Details, Design No. 2 (Metric)
- Figure E-4. Anchorage Details, Design No. 2 (Metric)
- Figure E-5. Anchorage Details, Design No. 2 (Metric)
- Figure E-6. Anchorage Details, Design No. 2 (Metric)
- Figure E-7. System Details, Design No. 2 (English)
- Figure E-8. Rail Details, Design No. 2 (English)
- Figure E-9. Post Details, Design No. 2 (English)
- Figure E-10. Anchorage Details, Design No. 2 (English)
- Figure E-11. Anchorage Details, Design No. 2 (English)
- Figure E-12. Anchorage Details, Design No. 2 (English)

Figure E-1. System Layout, Design No. 2 (Metric)

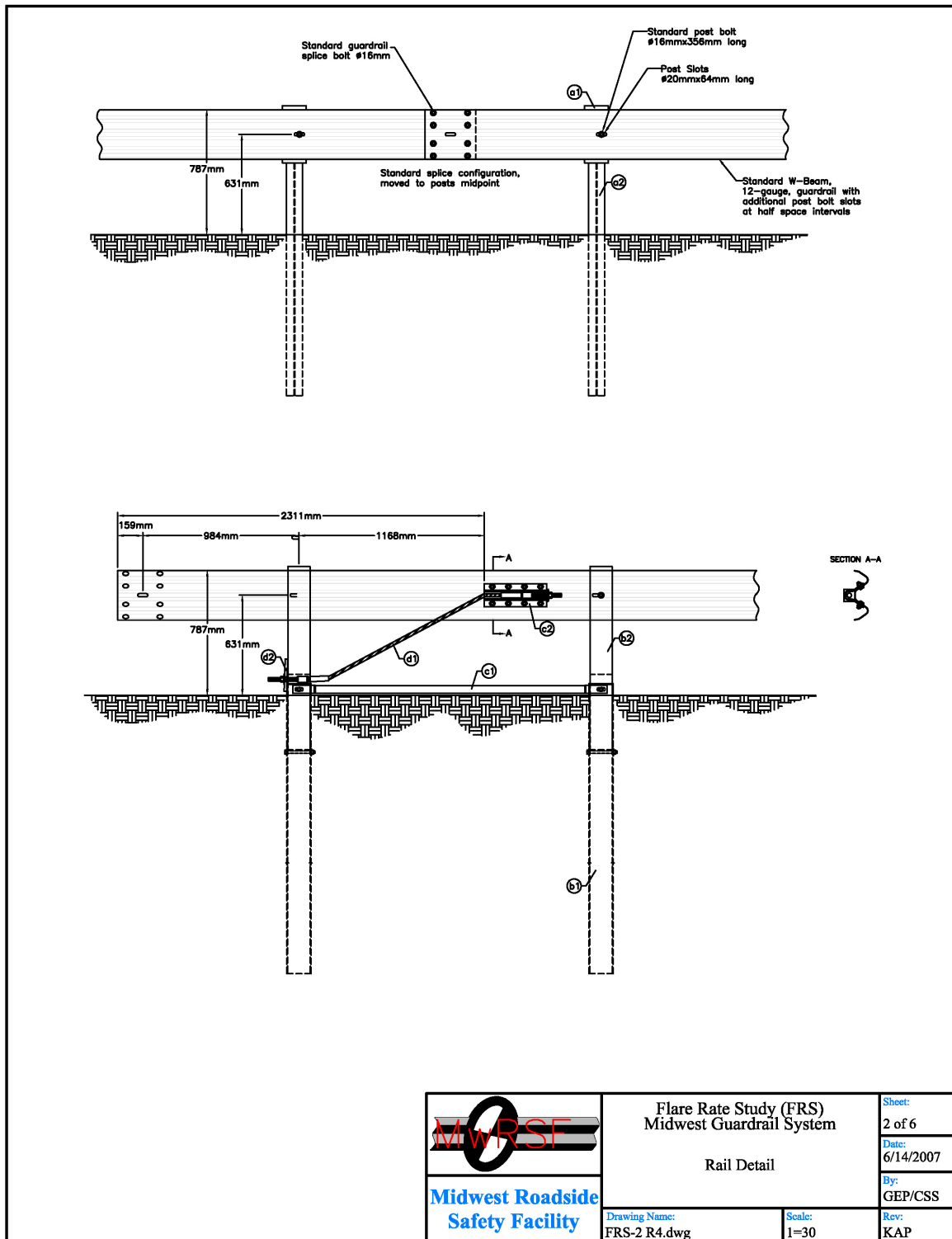


Figure E-2. Rail Details, Design No. 2 (Metric)

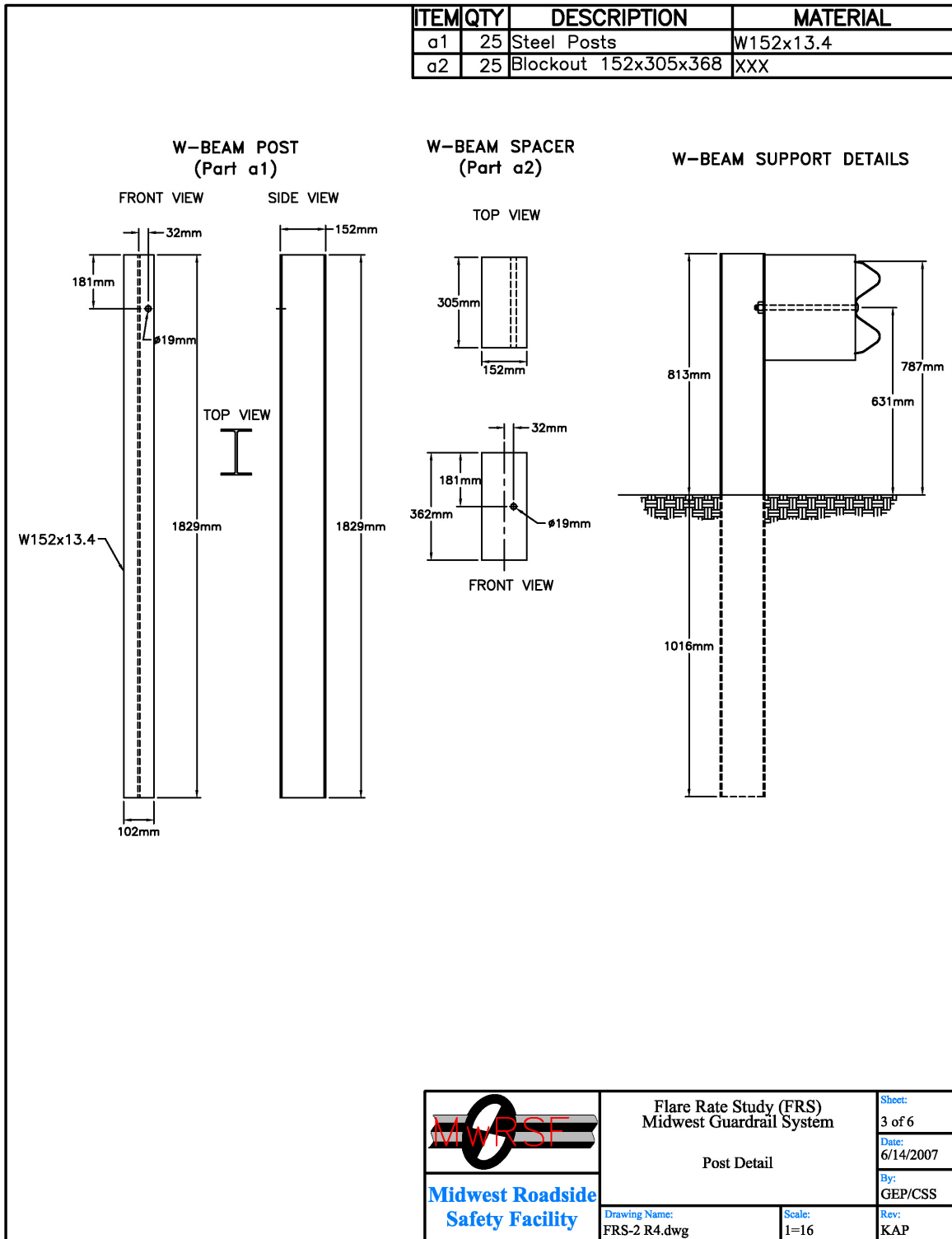


Figure E-3. Post Details, Design No. 2 (Metric)

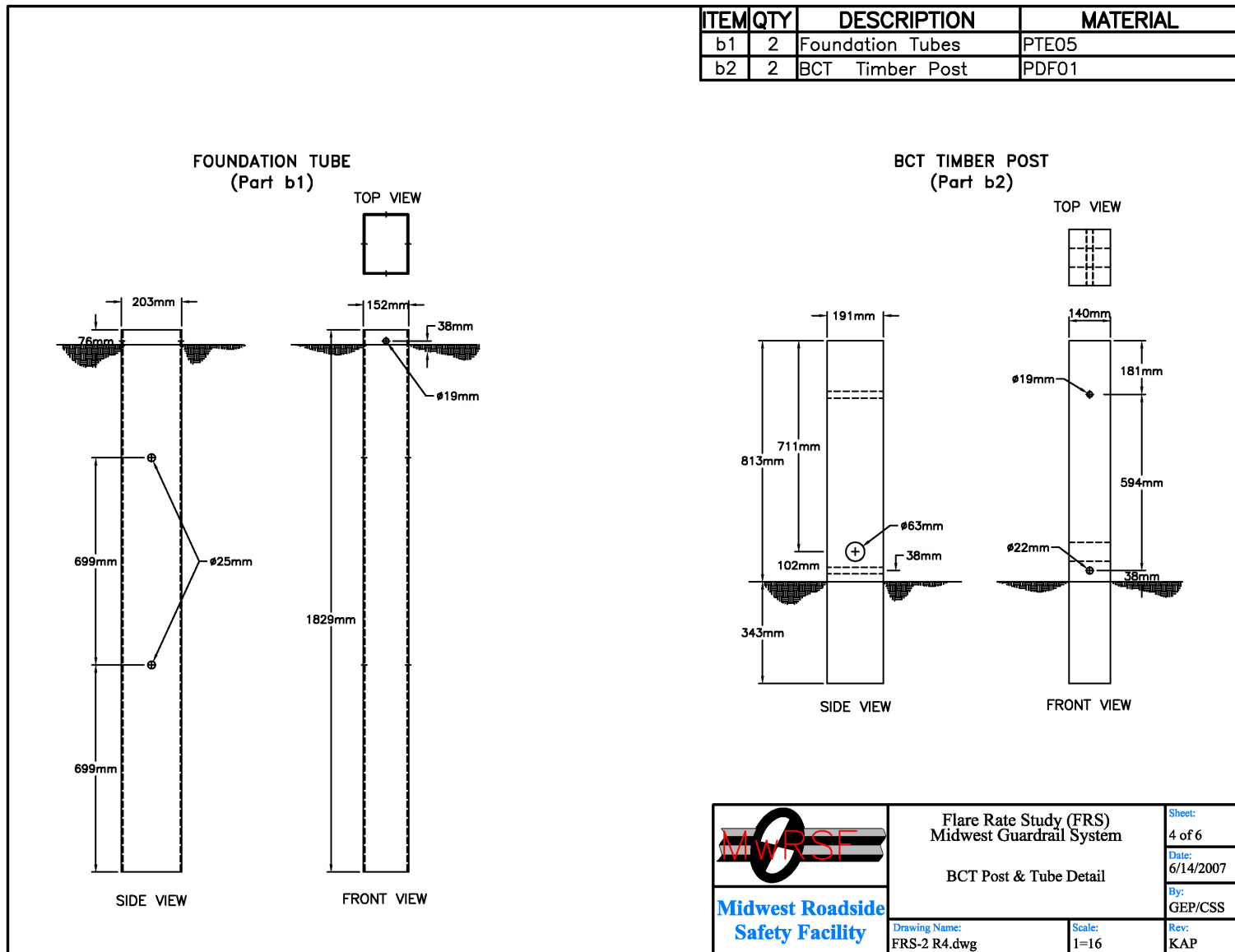


Figure E-4. Anchorage Details, Design No. 2 (Metric)

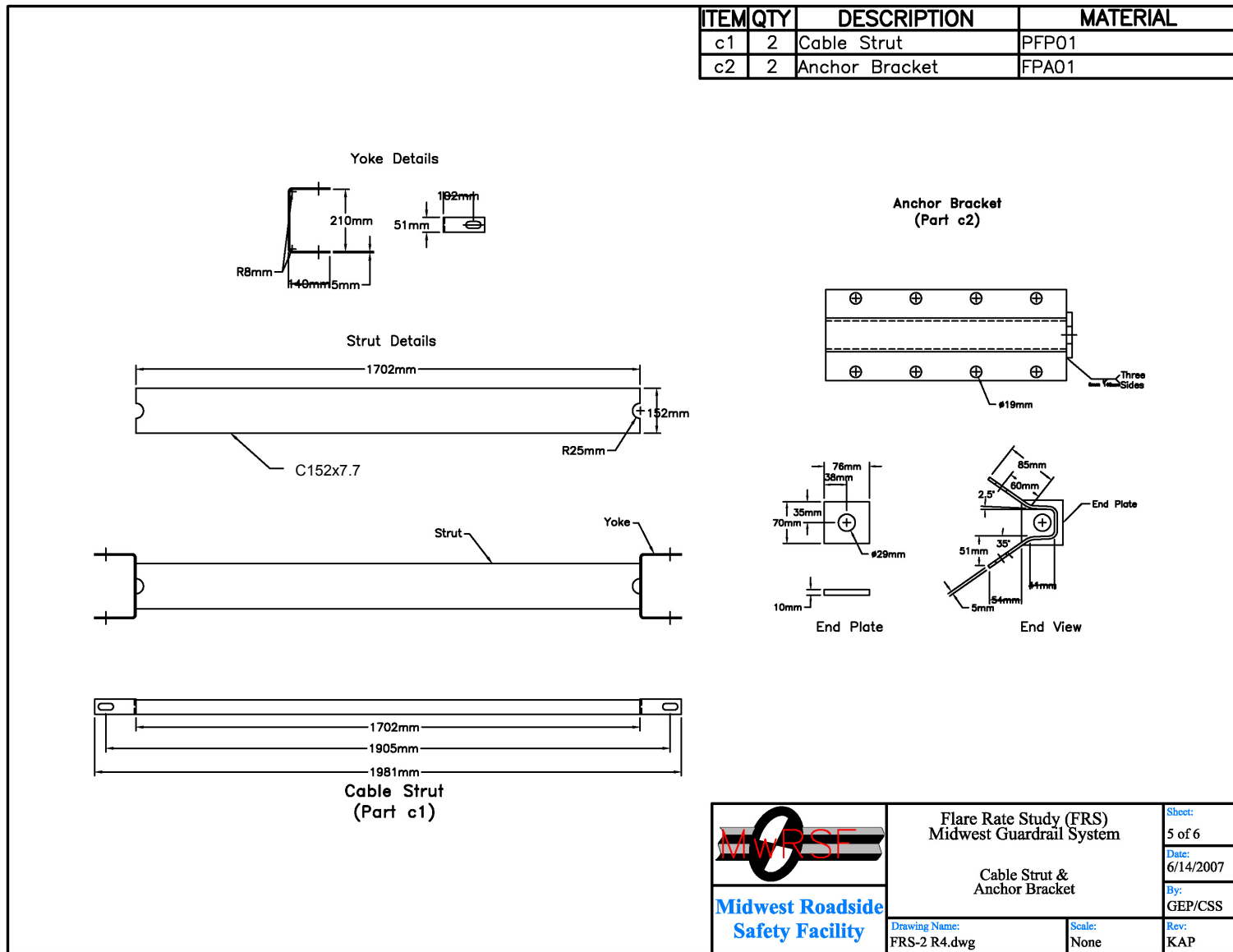


Figure E-5. Anchorage Details, Design No. 2 (Metric)

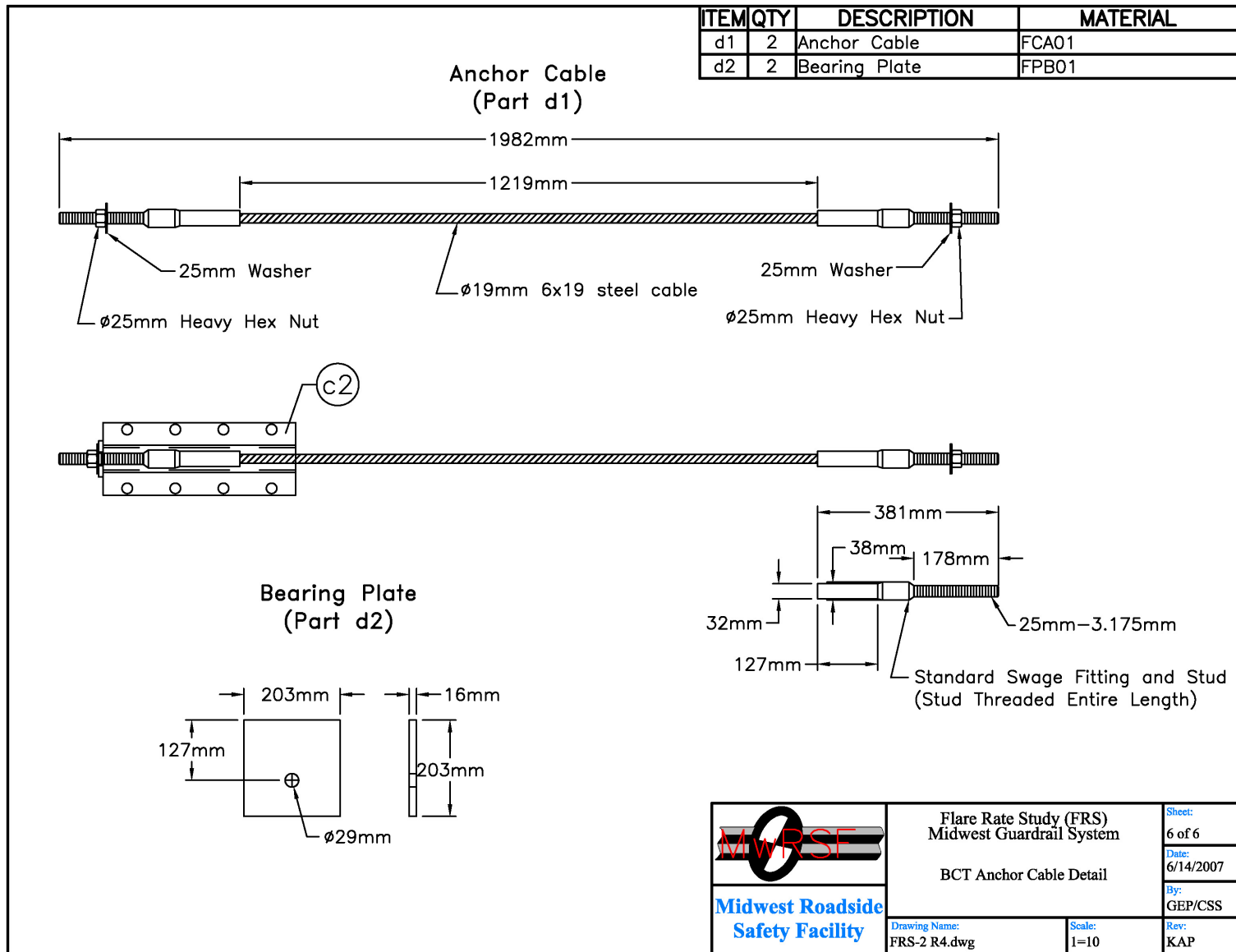


Figure E-6. Anchorage, Design No. 2 (Metric)

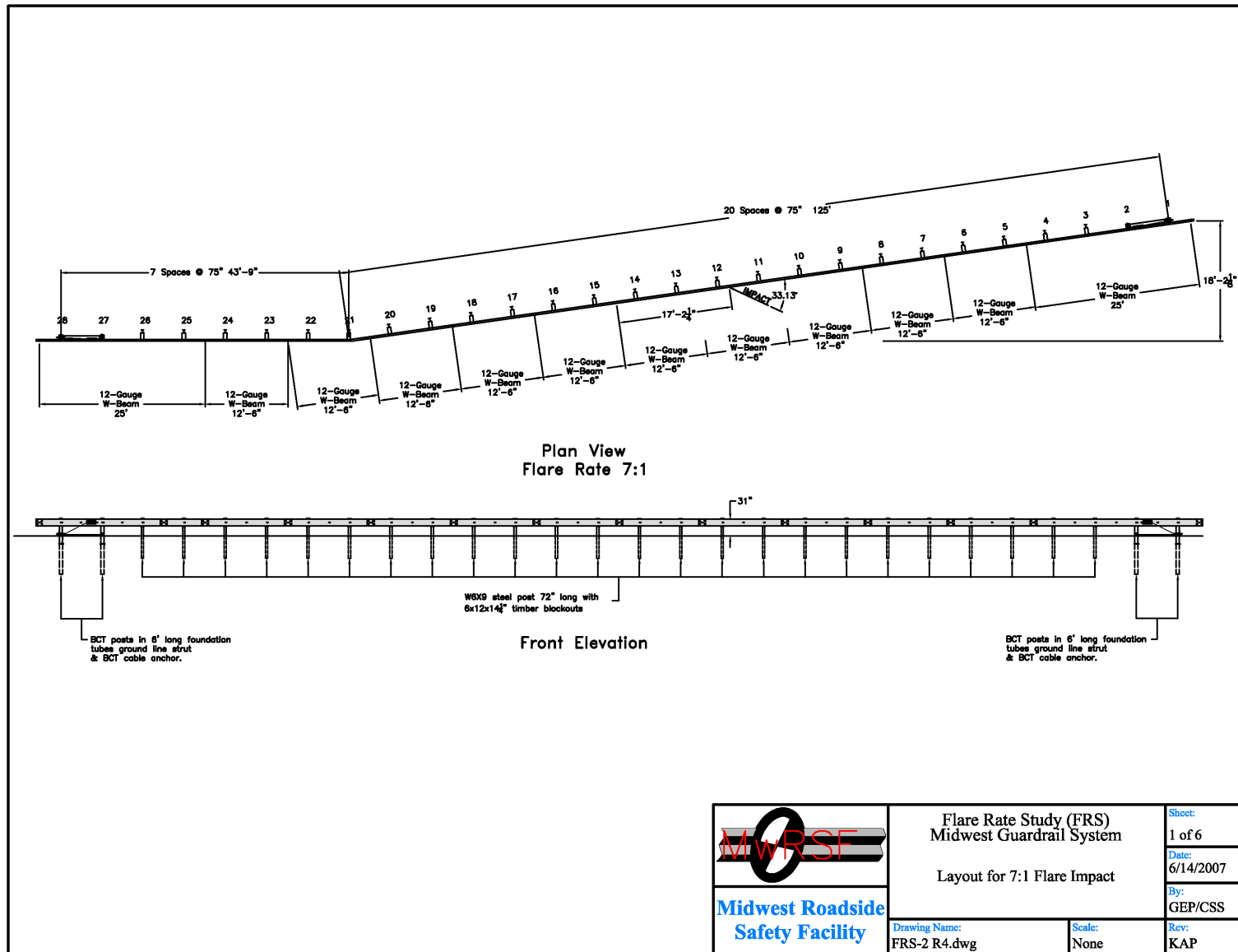


Figure E-7. System Layout, Design No. 2 (English)

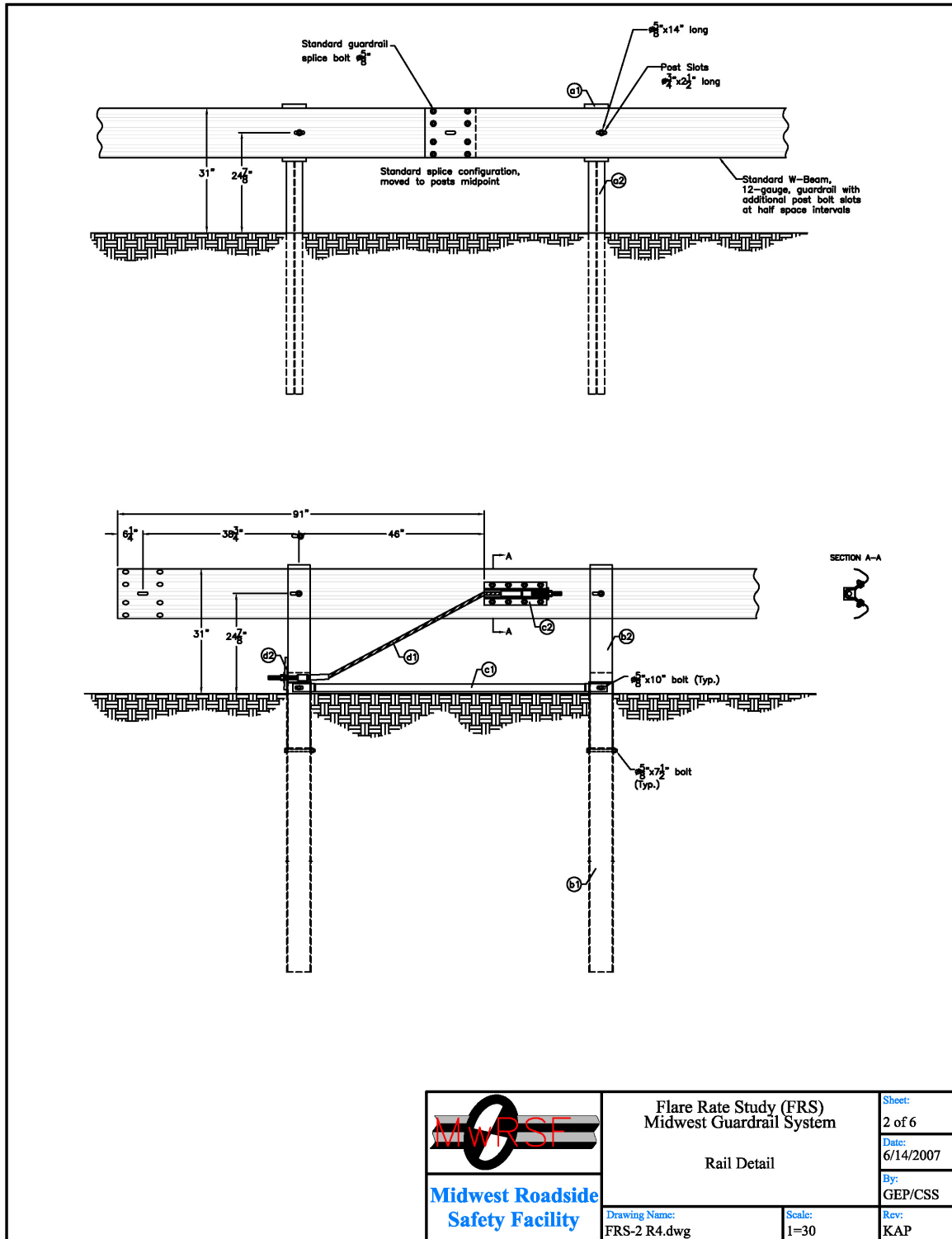


Figure E-8. Rail Details, Design No. 2 (English)

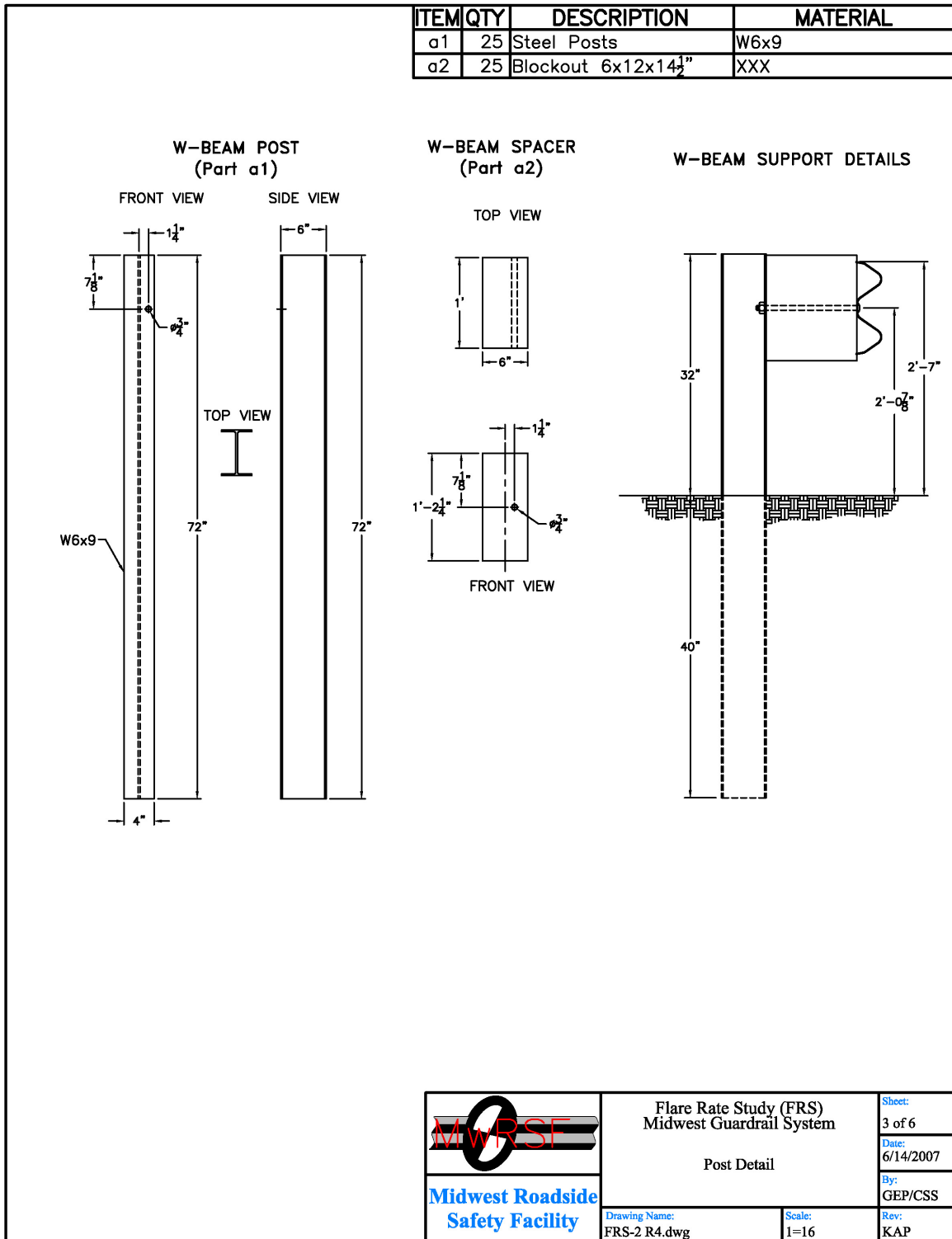


Figure E-9. Post Details, Design No. 2 (English)

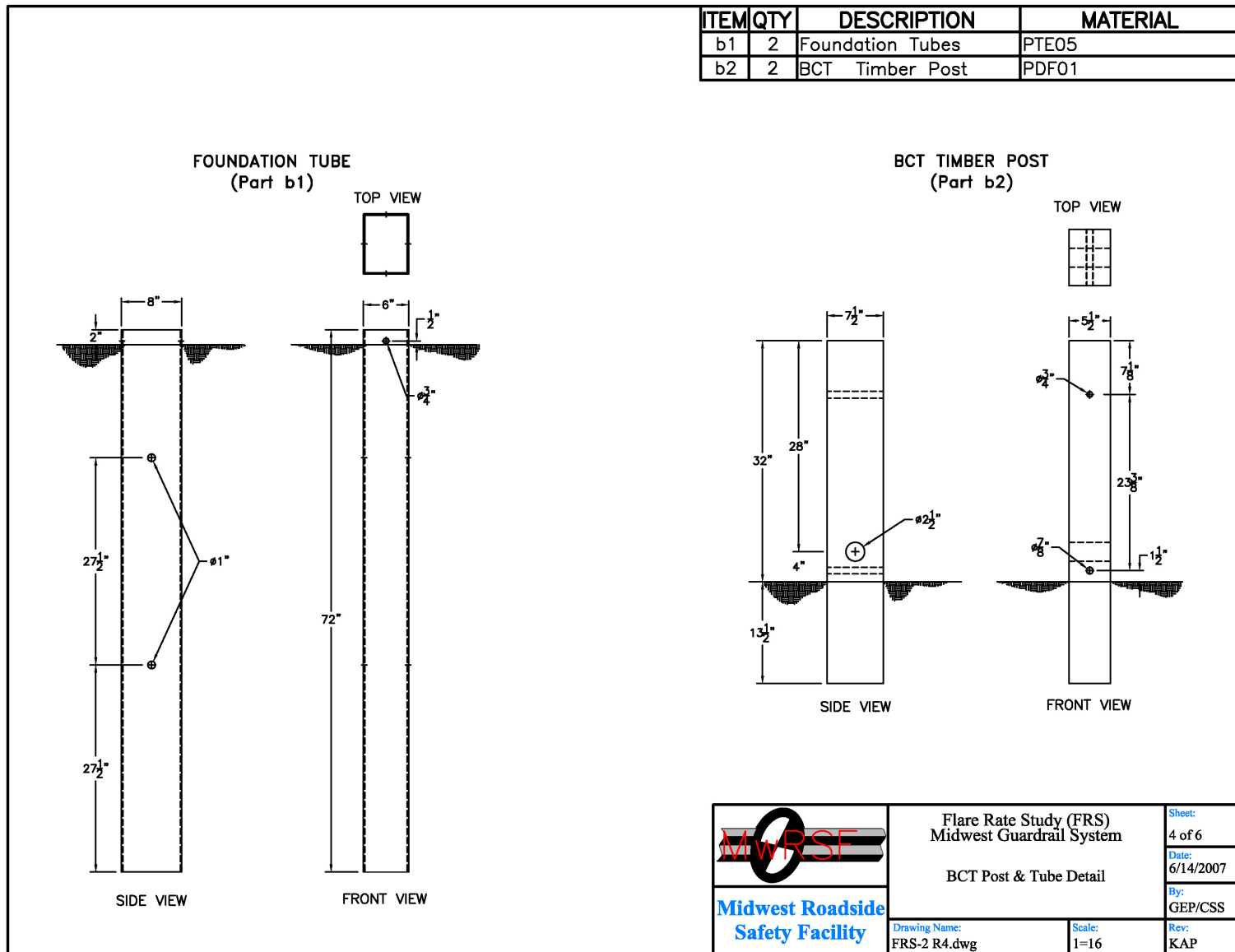


Figure E-10. Anchorage Details, Design No. 2 (English)

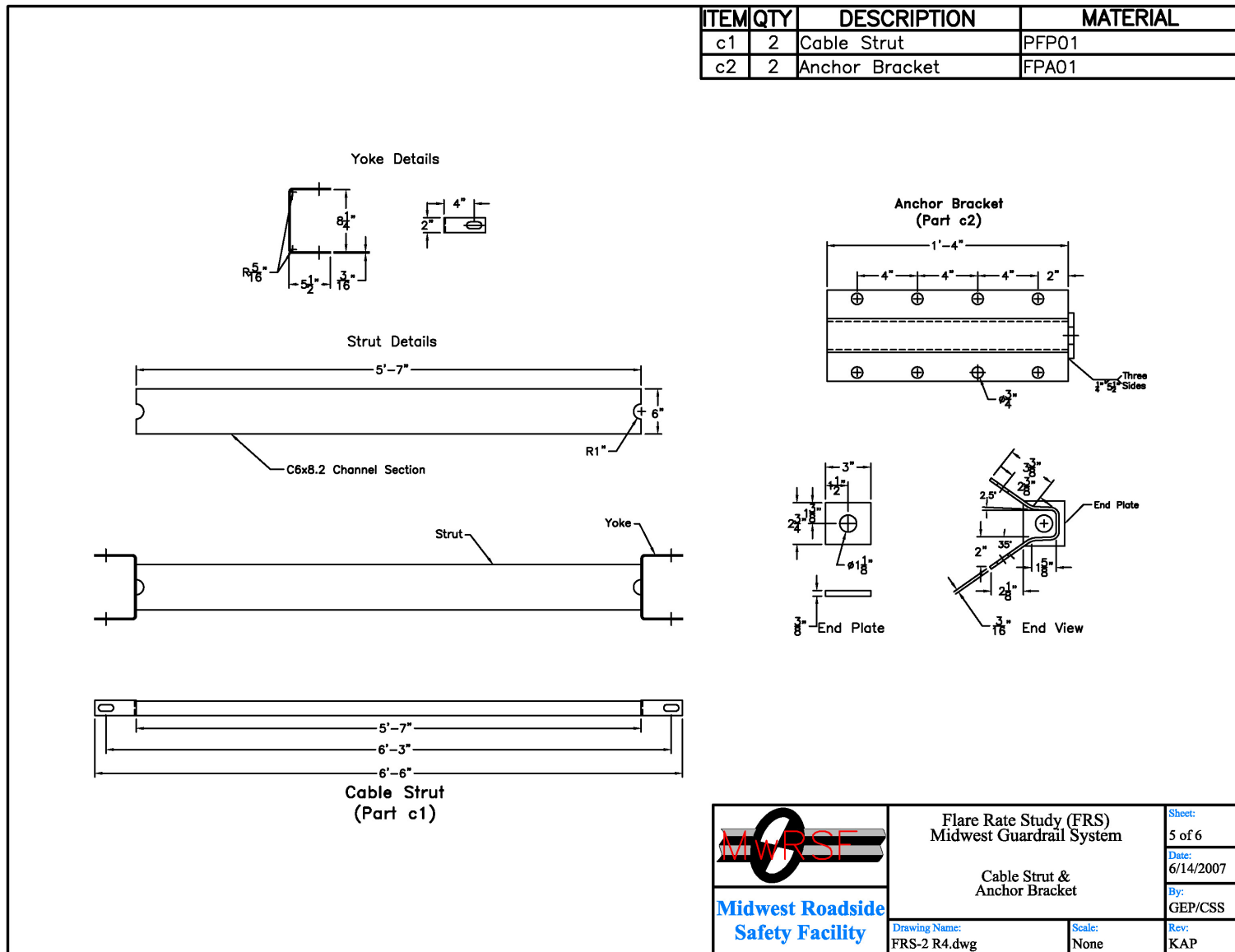


Figure E-11. Anchorage Details, Design No. 2 (English)

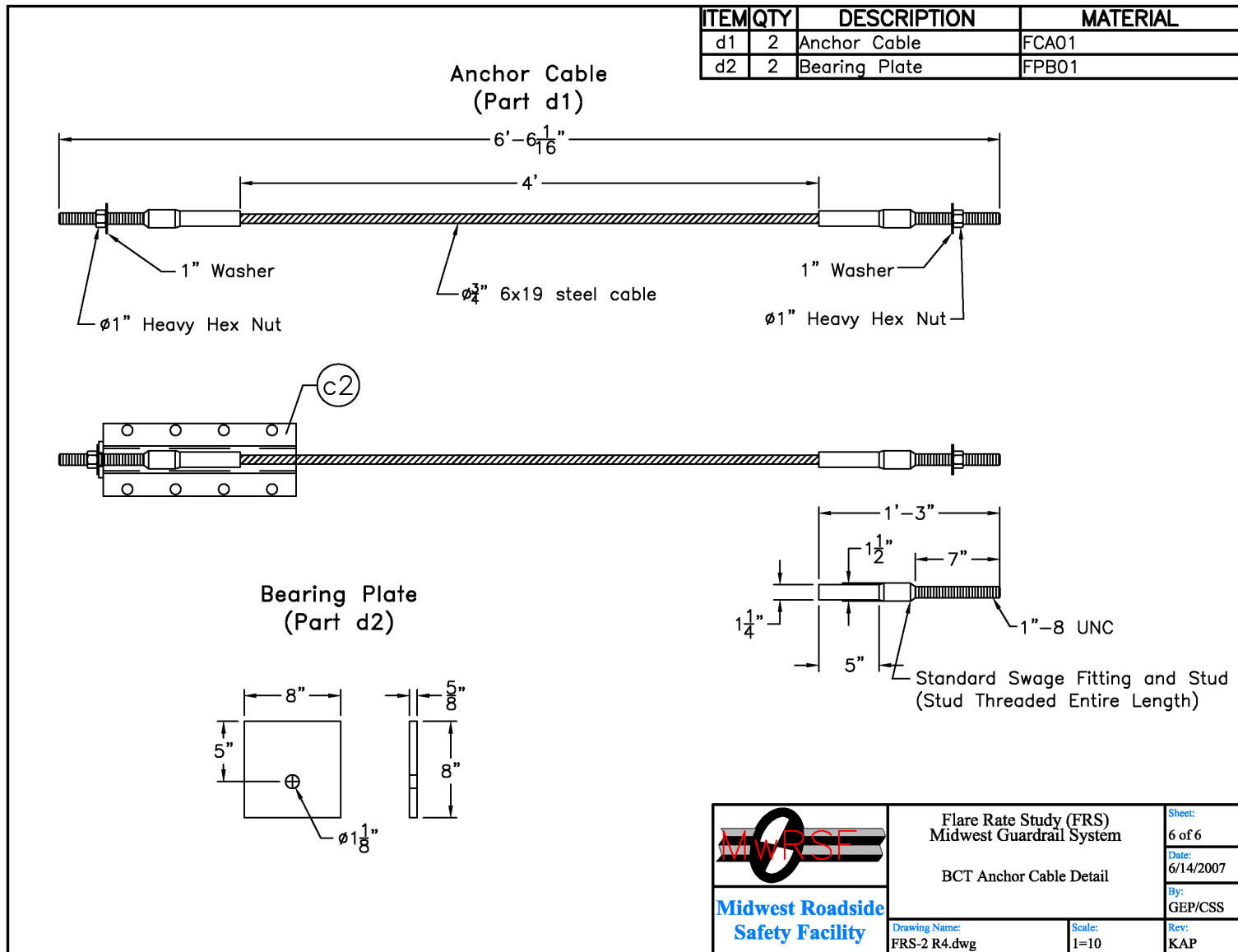


Figure E-12. Anchorage Details, Design No. 2 (English)

APPENDIX F

OCCUPANT COMPARTMENT DEFORMATION DATA, TEST FR-2

Figure F-1. Occupant Compartment Deformation Data - Set 1, Test FR-2

Figure F-2. Occupant Compartment Deformation Data - Set 2, Test FR-2

Figure F-3. Occupant Compartment Deformation Index (OCDI), Test FR-2

VEHICLE PRE/POST CRUSH INFO
Set-1

TEST: FR-2
VEHICLE: 2000p

Note: If impact is on driver side need to
enter negative number for Y

POINT	X	Y	Z	X'	Y'	Z'	DEL X	DEL Y	DEL Z
1	56.5	11.5	-1.75	56.75	11.25	-1.75	0.25	-0.25	0
2	57.75	15.75	-2.25	57.75	15.75	-2	0	0	0.25
3	58	20	-2.25	58	19.75	-2.5	0	-0.25	-0.25
4	58	25	-2	57.75	24.75	-1.75	-0.25	-0.25	0.25
5	57.25	29	-1.5	57	28.75	-1.5	-0.25	-0.25	0
6	54	11.5	-5.25	54	11.25	-5	0	-0.25	0.25
7	54.5	16	-4.5	54.75	15.5	-4.5	0.25	-0.5	0
8	54.75	20.5	-4.75	54.75	20.25	-4.75	0	-0.25	0
9	54.5	25.25	-4.75	54.5	25	-4.75	0	-0.25	0
10	54.5	29.5	-4.75	54.5	29.5	-4.75	0	0	0
11	49	10.75	-7	49	10.5	-6.75	0	-0.25	0.25
12	49	15	-7.25	49	14.5	-7.25	0	-0.5	0
13	49.5	19.75	-7.5	49.5	19.25	-7.25	0	-0.5	0.25
14	49.75	25	-7.25	49.75	24.75	-7.25	0	-0.25	0
15	51	30.5	-6.5	51	30.25	-6.5	0	-0.25	0
16	45.25	11	-7.5	45.25	10.75	-7	0	-0.25	0.5
17	45.25	14.75	-7.5	45.25	14.5	-7.25	0	-0.25	0.25
18	45	19.5	-7.5	44.75	19	-7.5	-0.25	-0.5	0
19	44.75	24.75	-7.5	44.75	24.5	-7.5	0	-0.25	0
20	44.75	29.5	-8	44.75	29.25	-8	0	-0.25	0
21	40.75	10.75	-7.25	40.75	10.75	-7.25	0	0	0
22	41.25	15	-7.5	41.5	15	-7.5	0.25	0	0
23	41	19.25	-7.5	41	19	-7.5	0	-0.25	0
24	40.75	24.25	-7.5	40.75	24.25	-7.5	0	0	0
25	41	29.25	-8	40.75	29.25	-8.25	-0.25	0	-0.25
26	35.75	10.75	-7.5	36	10.75	-7.25	0.25	0	0.25
27	36.75	18.75	-7.75	36.75	18.5	-7.5	0	-0.25	0.25
28	36	27.25	-8	36	27.5	-8	0	0.25	0
29									
30									

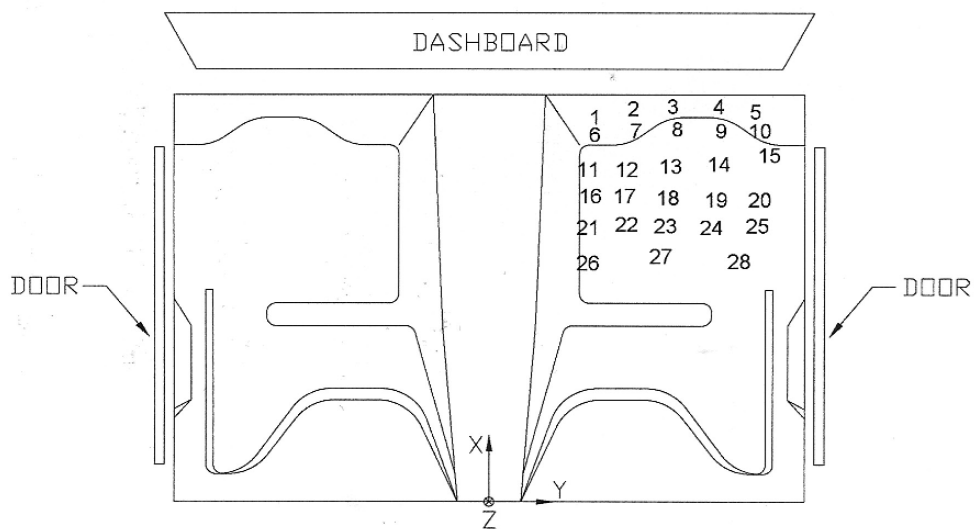


Figure F-1. Occupant Compartment Deformation Data - Set 1, Test FR-2

VEHICLE PRE/POST CRUSH INFO
Set-2

TEST: FR-2
VEHICLE: 2000p

Note: If impact is on driver side need to
enter negative number for Y

POINT	X	Y	Z	X'	Y'	Z'	DEL X	DEL Y	DEL Z
1	50	20.5	-1.5	50.25	20.25	-1.5	0.25	-0.25	0
2	51.25	24.75	-1.75	51.25	24.75	-1.5	0	0	0.25
3	51.5	29	-1.75	51.5	28.75	-1.5	0	-0.25	0.25
4	51.5	34	-1	51.25	33.75	-1	-0.25	-0.25	0
5	50.75	38	-0.5	50.5	37.75	-0.5	-0.25	-0.25	0
6	47.5	20.5	-4.75	47.5	20.25	-4.5	0	-0.25	0.25
7	48	25	-4	48.25	24.5	-4	0.25	-0.5	0
8	48.25	29.5	-4	48.25	29.25	-4	0	-0.25	0
9	48	34.25	-4	48	34	-4	0	-0.25	0
10	48	38.5	-3.75	48	38.5	-3.75	0	0	0
11	42.5	19.75	-6.75	42.5	19.5	-6.5	0	-0.25	0.25
12	42.5	24	-7	42.5	23.5	-6.75	0	-0.5	0.25
13	43	28.75	-6.75	43	28.25	-6.5	0	-0.5	0.25
14	43.25	34	-6.25	43.25	33.75	-6.25	0	-0.25	0
15	44.5	39.5	-5.5	44.5	39.25	-5.5	0	-0.25	0
16	38.75	20	-7	38.75	19.75	-6.75	0	-0.25	0.25
17	38.75	23.75	-7	38.75	23.5	-6.75	0	-0.25	0.25
18	38.5	28.5	-7	38.25	28	-6.75	-0.25	-0.5	0.25
19	38.25	33.75	-6.5	38.25	33.5	-6.5	0	-0.25	0
20	38.25	38.5	-7	38.25	38.25	-7	0	-0.25	0
21	34.25	19.75	-7	34.25	19.75	-6.75	0	0	0.25
22	34.75	24	-7.25	35	24	-7	0.25	0	0.25
23	34.5	28.25	-7	34.5	28	-6.75	0	-0.25	0.25
24	34.25	33.25	-6.75	34.25	33.25	-6.75	0	0	0
25	34.5	38.25	-7	34.25	38.25	-7	-0.25	0	0
26	29.25	19.75	-7.25	29.5	19.75	-7	0.25	0	0.25
27	30.25	27.75	-7	30.25	27.5	-6.75	0	-0.25	0.25
28	29.5	36.25	-7	29.5	36.5	-7	0	0.25	0
29									
30									

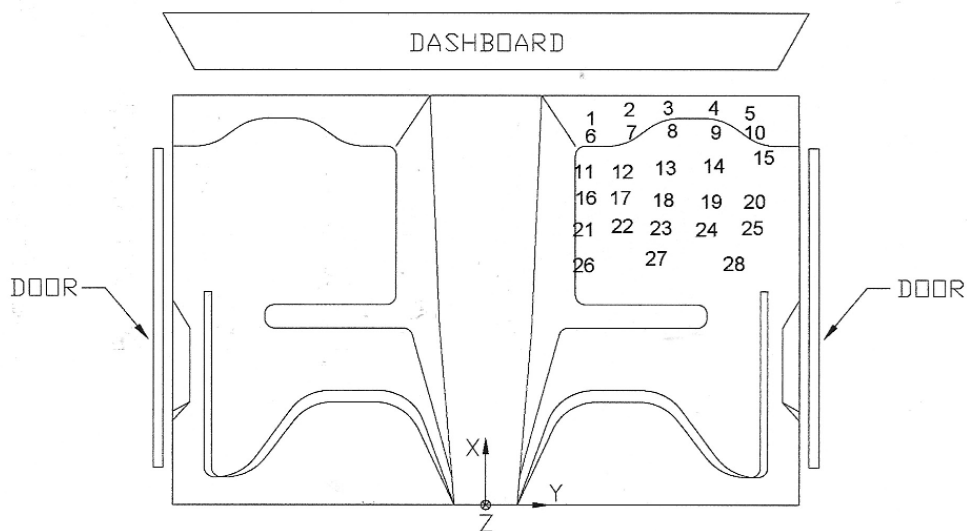


Figure F-2. Occupant Compartment Deformation Data - Set 2, Test FR-2

Occupant Compartment Deformation Index (OCDI)

Test No. FR-2
Vehicle Type: 2000P

OCDI = XXABCDEFGHI

XX = location of occupant compartment deformation

A = distance between the dashboard and a reference point at the rear of the occupant compartment, such as the top of the rear seat or the rear of the cab on a pickup

B = distance between the roof and the floor panel

C = distance between a reference point at the rear of the occupant compartment and the motor panel

D = distance between the lower dashboard and the floor panel

E = interior width

F = distance between the lower edge of right window and the upper edge of left window

G = distance between the lower edge of left window and the upper edge of right window

H = distance between bottom front corner and top rear corner of the passenger side window

I = distance between bottom front corner and top rear corner of the driver side window

Severity Indices

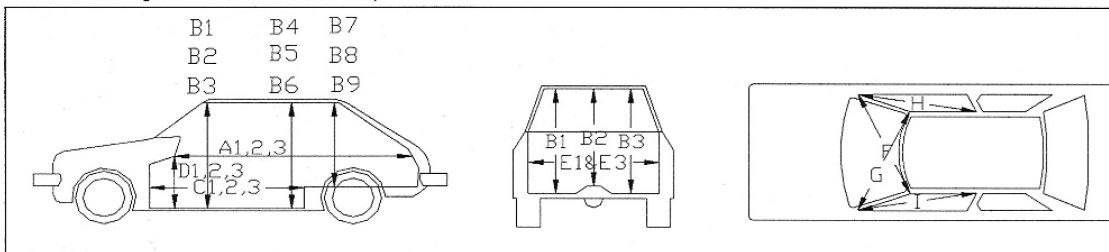
0 - if the reduction is less than 3%

1 - if the reduction is greater than 3% and less than or equal to 10 %

2 - if the reduction is greater than 10% and less than or equal to 20 %

3 - if the reduction is greater than 20% and less than or equal to 30 %

4 - if the reduction is greater than 30% and less than or equal to 40 %



where,
1 = Passenger Side
2 = Middle
3 = Driver Side

Location:

Measurement	Pre-Test (in.)	Post-Test (in.)	Change (in.)	% Difference	Severity Index
A1	39.50	39.50	0.00	0.00	0
A2	40.25	40.50	0.25	0.62	0
A3	39.50	39.50	0.00	0.00	0
B1	46.75	46.50	-0.25	-0.53	0
B2	42.00	41.75	-0.25	-0.60	0
B3	47.50	47.25	-0.25	-0.53	0
C1	58.50	58.50	0.00	0.00	0
C2	52.25	52.25	0.00	0.00	0
C3	57.00	57.00	0.00	0.00	0
D1	15.25	15.25	0.00	0.00	0
D2	14.75	14.75	0.00	0.00	0
D3	22.00	22.25	0.25	1.14	0
E1	62.50	62.25	-0.25	-0.40	0
E3	63.75	63.50	-0.25	-0.39	0
F	58.75	58.75	0.00	0.00	0
G	58.75	59.00	0.25	0.43	0
H	41.75	41.50	-0.25	-0.60	0
I	41.75	41.75	0.00	0.00	0

Note: Maximum severity index for each variable (A-I) is used for determination of final OCDI value

Final OCDI: XXABCDEFGHI
RF 0 0 0 0 0 0 0 0 0

Figure F-3. Occupant Compartment Deformation Index (OCDI), Test FR-2

APPENDIX G

ACCELEROMETER AND RATE TRANSDUCER DATA ANALYSIS, TEST FR-2

- Figure G-1. Graph of Longitudinal Deceleration, Test FR-2
- Figure G-2. Graph of Longitudinal Occupant Impact Velocity (OIV), Test FR-2
- Figure G-3. Graph of Longitudinal Occupant Displacement, Test FR-2
- Figure G-4. Graph of Lateral Deceleration, Test FR-2
- Figure G-5. Graph of Lateral Occupant Impact Velocity (OIV), Test FR-2
- Figure G-6. Graph of Lateral Occupant Displacement, Test FR-2
- Figure G-7. Graph of Roll, Pitch, and Yaw Angular Displacements, Test FR-2

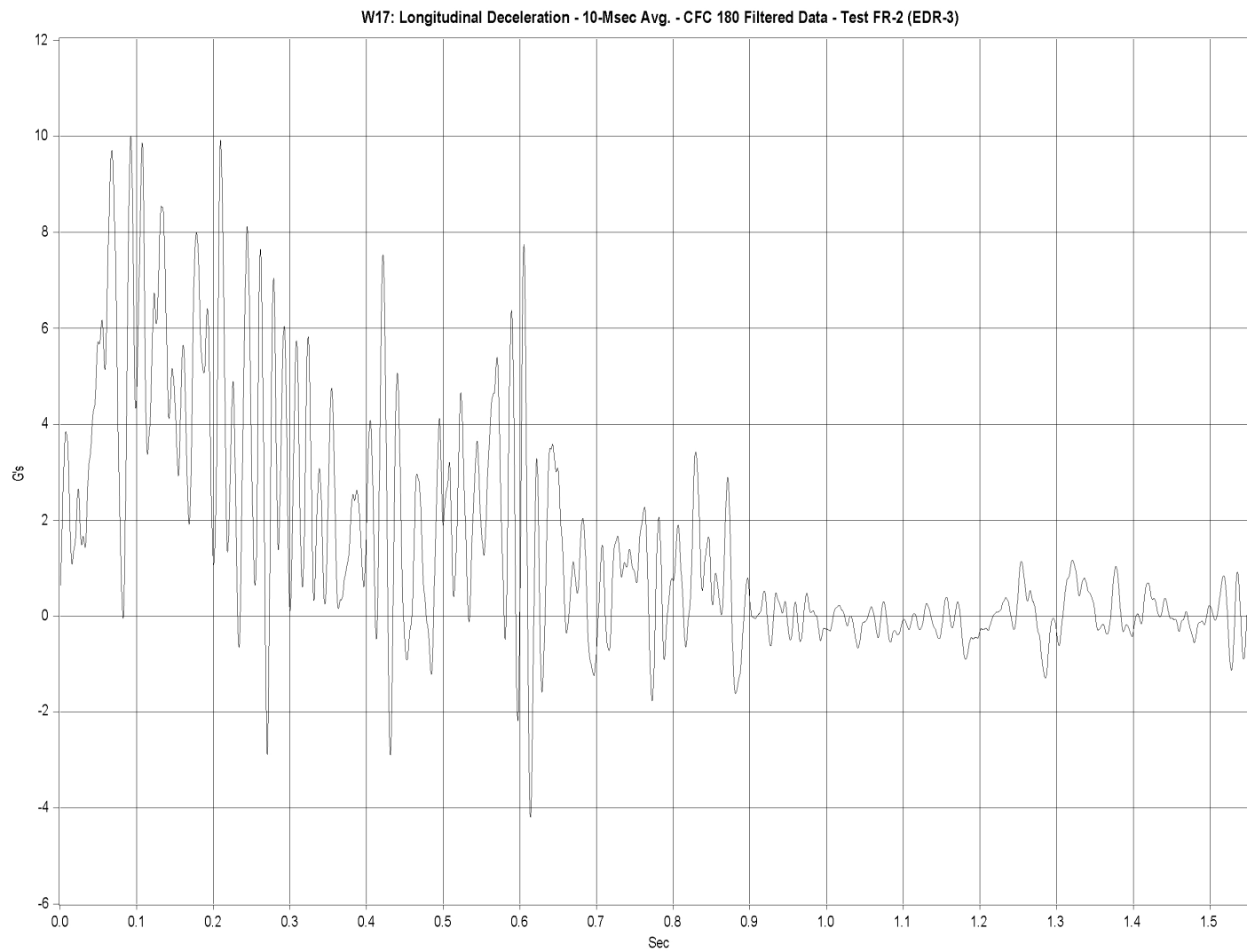


Figure G-1. Graph of Longitudinal Deceleration, Test FR-2

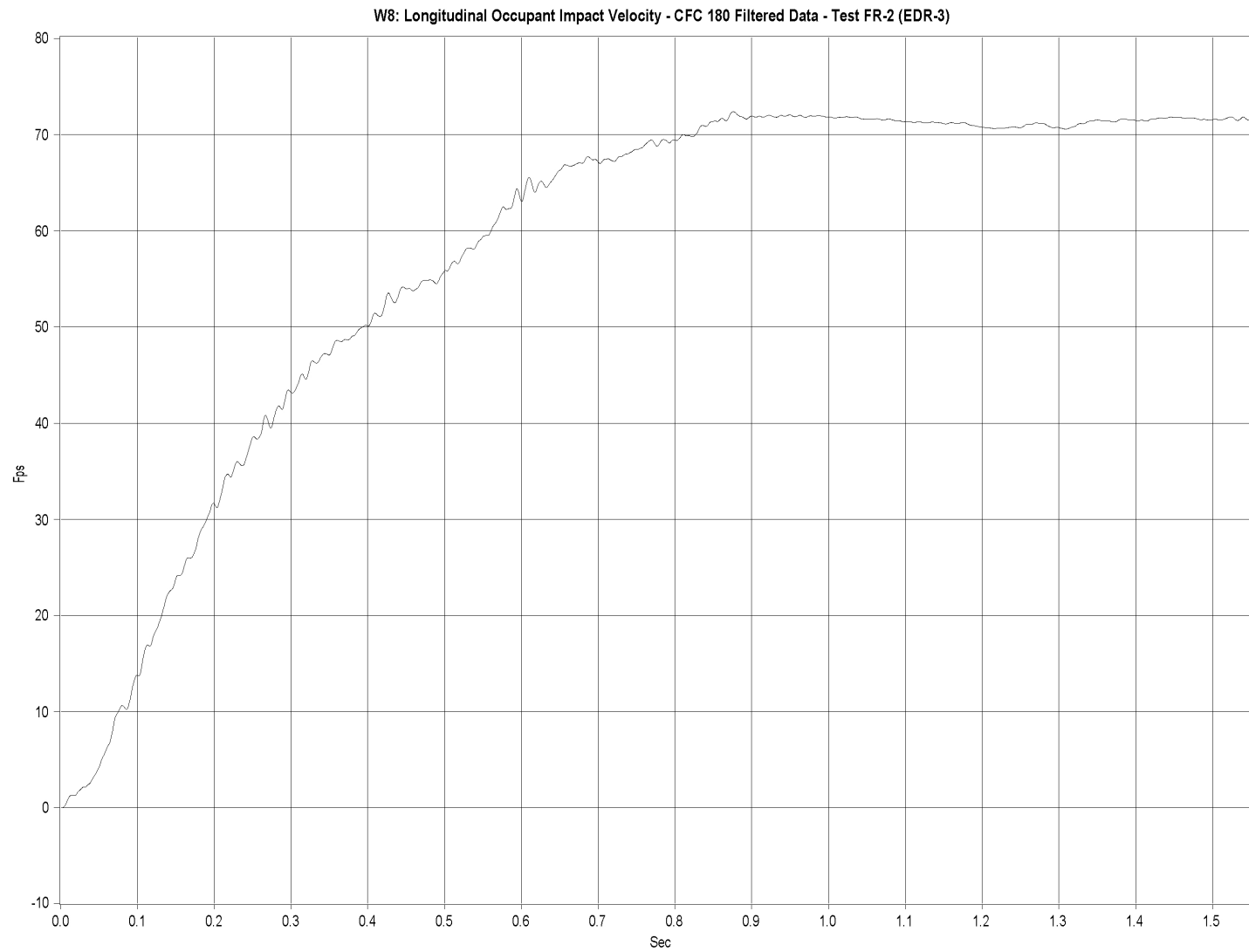


Figure G-2. Graph of Longitudinal Occupant Impact Velocity (OIV), Test FR-2

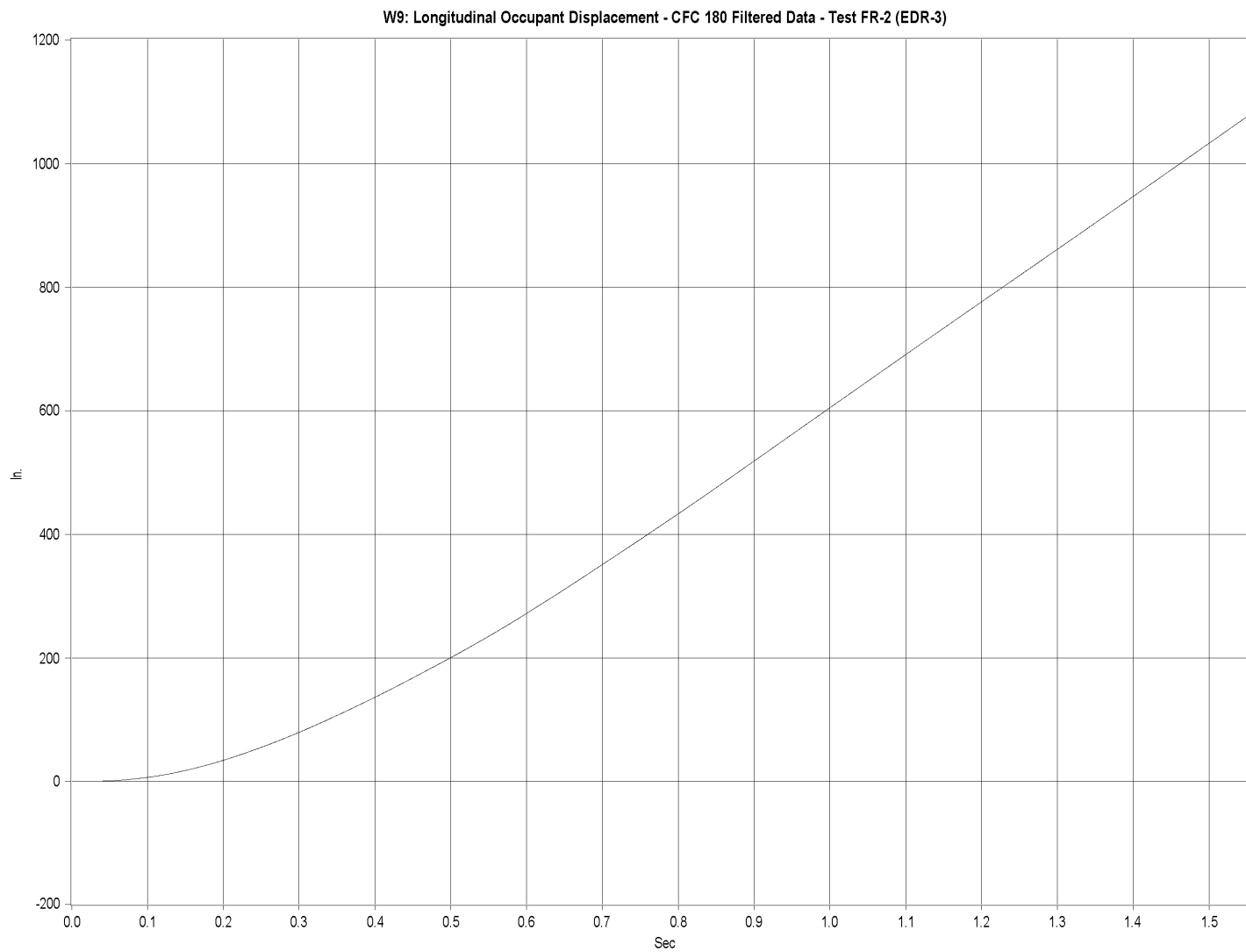


Figure G-3. Graph of Longitudinal Occupant Displacement, Test FR-2

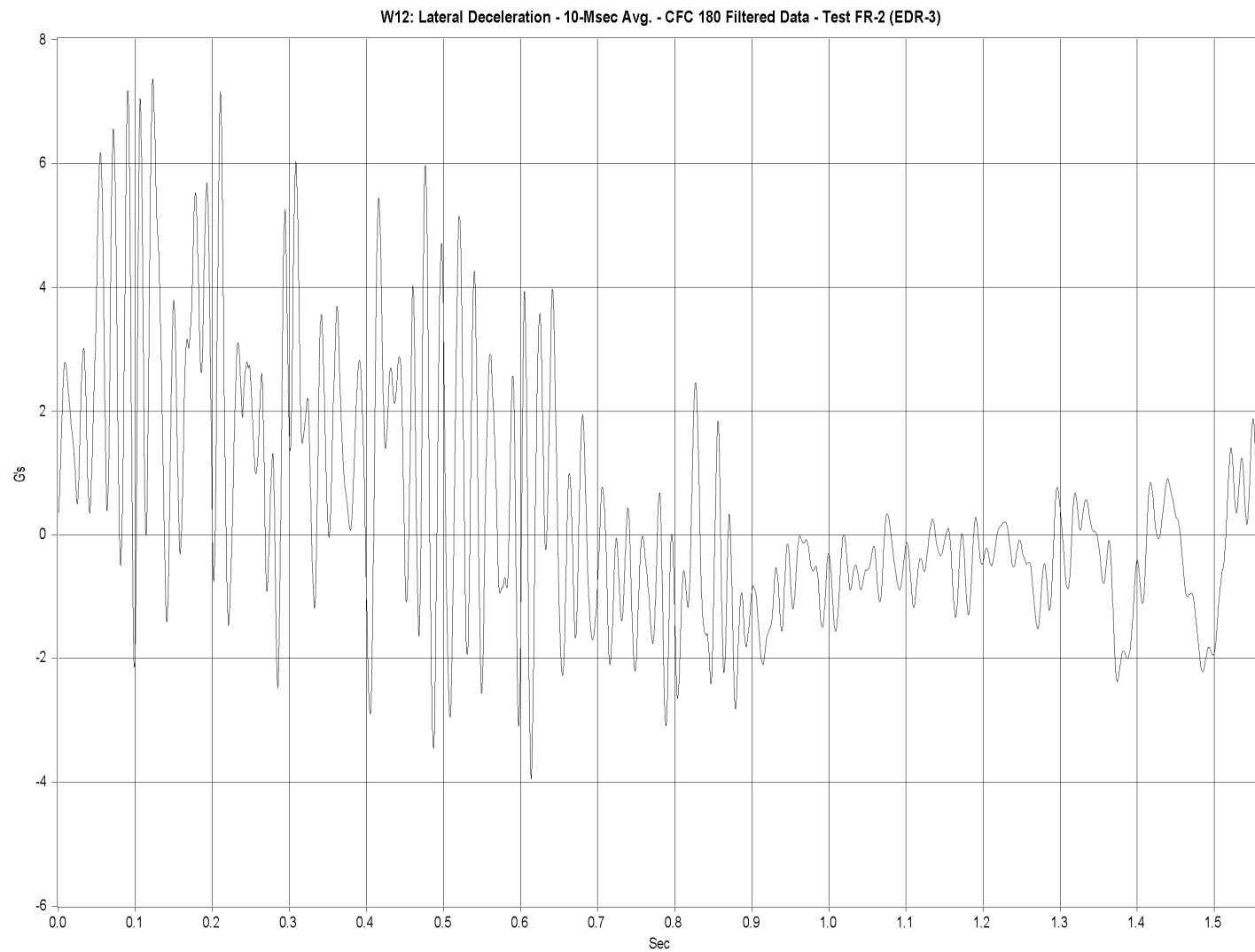


Figure G-4. Graph of Lateral Deceleration, Test FR-2

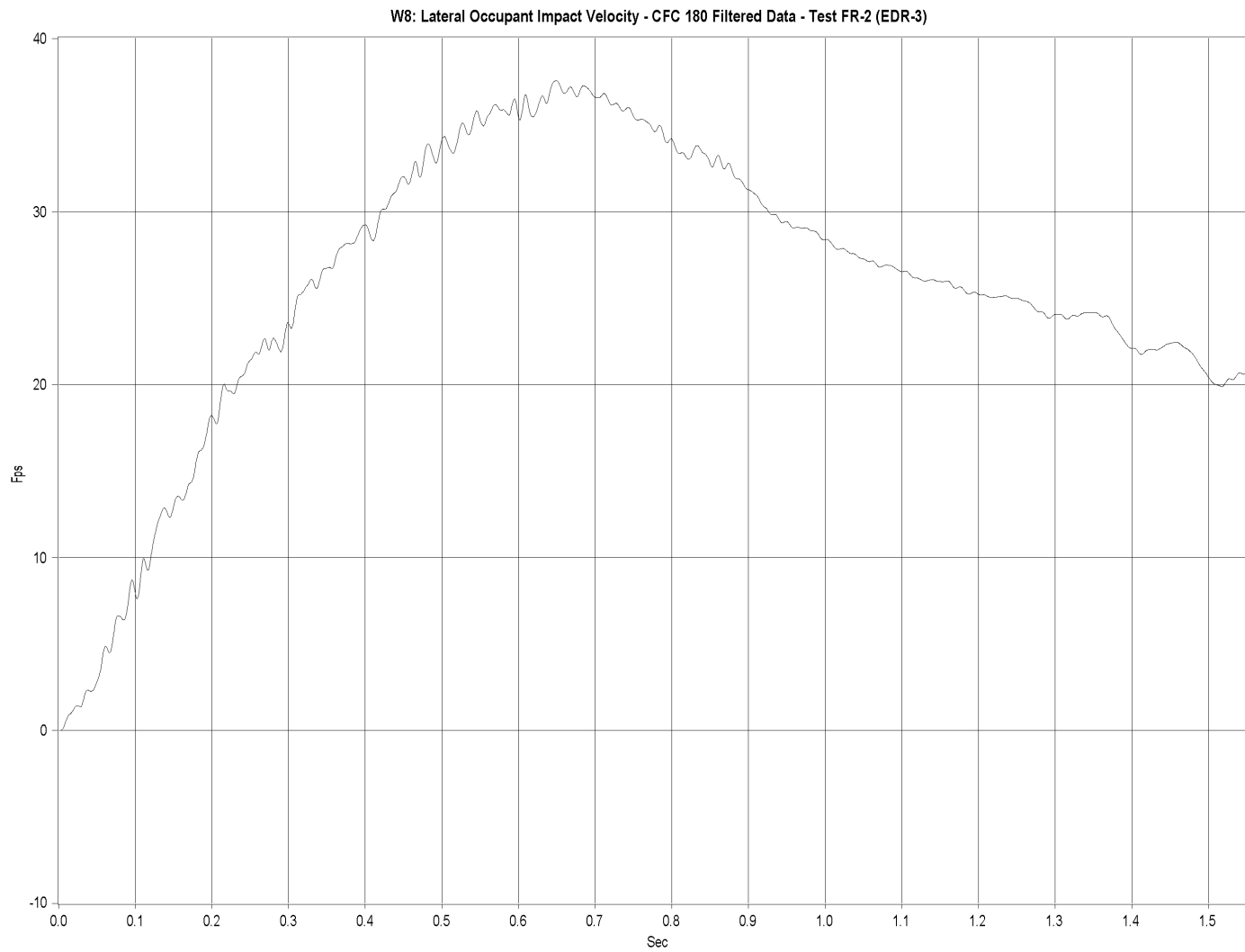


Figure G-5. Graph of Lateral Occupant Impact Velocity (OIV), Test FR-2

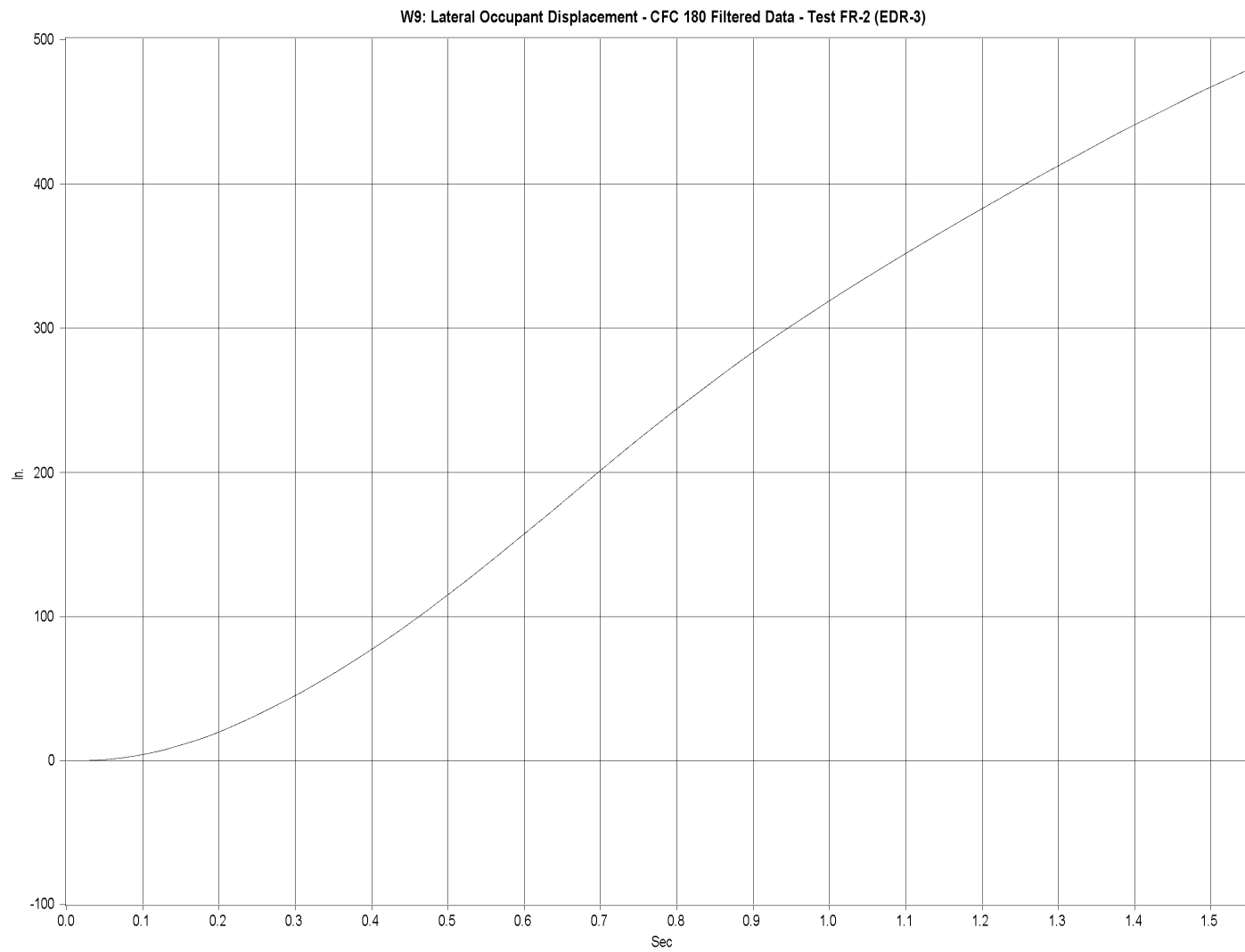


Figure G-6. Graph of Lateral Occupant Displacement, Test FR-2

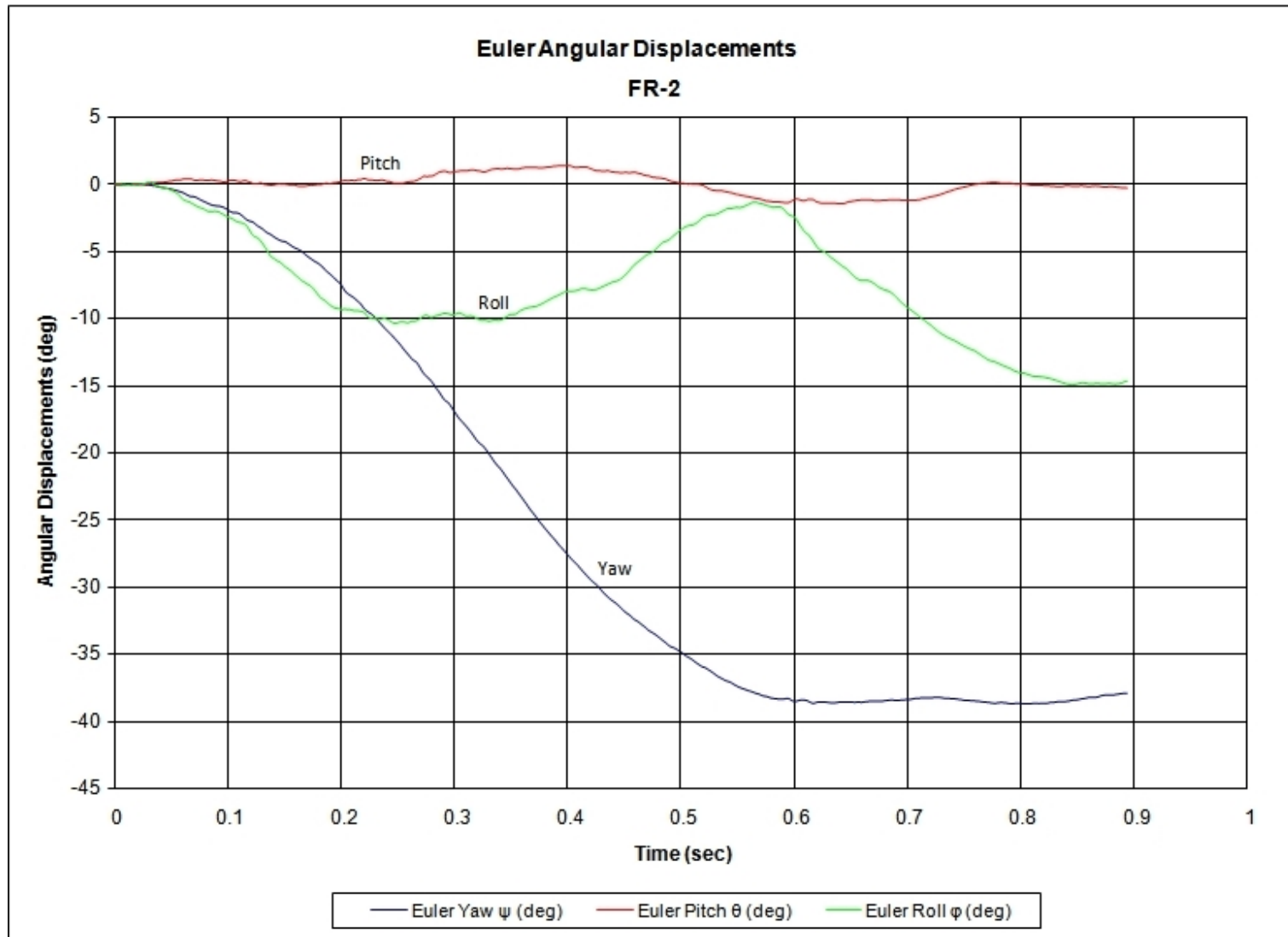


Figure G-7. Graph of Roll, Pitch, and Yaw Angular Displacements, Test FR-2

APPENDIX H

OCCUPANT COMPARTMENT DEFORMATION DATA, TEST FR-3

Figure H-1. Occupant Compartment Deformation Index (OCDI), Test FR-3

Occupant Compartment Deformation Index (OCDI)

Test No. FR-3
Vehicle Type: 820c

OCDI = XXABCDEFGHI

XX = location of occupant compartment deformation

A = distance between the dashboard and a reference point at the rear of the occupant compartment, such as the top of the rear seat or the rear of the cab on a pickup

B = distance between the roof and the floor panel

C = distance between a reference point at the rear of the occupant compartment and the motor panel

D = distance between the lower dashboard and the floor panel

E = interior width

F = distance between the lower edge of right window and the upper edge of left window

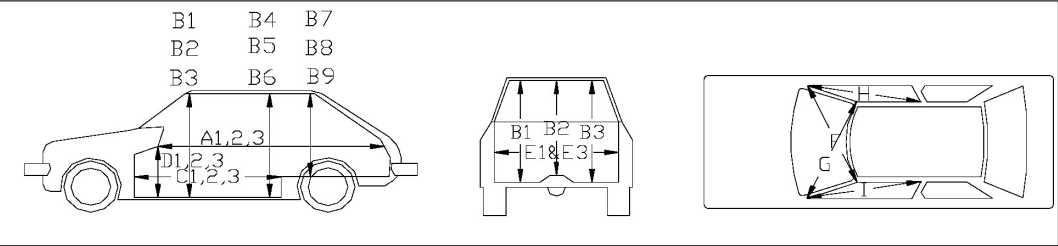
G = distance between the lower edge of left window and the upper edge of right window

H = distance between bottom front corner and top rear corner of the passenger side window

I = distance between bottom front corner and top rear corner of the driver side window

Severity Indices

- 0 - if the reduction is less than 3%
- 1 - if the reduction is greater than 3% and less than or equal to 10 %
- 2 - if the reduction is greater than 10% and less than or equal to 20 %
- 3 - if the reduction is greater than 20% and less than or equal to 30 %
- 4 - if the reduction is greater than 30% and less than or equal to 40 %



where,
1 = Passenger Side
2 = Middle
3 = Driver Side

Location:

Measurement	Pre-Test (in.)	Post-Test (in.)	Change (in.)	% Difference	Severity Index
A1	45.50	45.50	0.00	0.00	0
A2	44.50	44.25	-0.25	-0.56	0
A3	45.25	45.00	-0.25	-0.55	0
B1	40.00	40.00	0.00	0.00	0
B2	40.25	40.50	0.25	0.62	0
B3	41.00	41.25	0.25	0.61	0
C1	55.75	55.75	0.00	0.00	0
C2	58.75	59.00	0.25	0.43	0
C3	55.00	53.75	-1.25	-2.27	0
D1	18.25	18.25	0.00	0.00	0
D2	12.00	12.25	0.25	2.08	0
D3	12.25	12.50	0.25	2.04	0
E1	49.25	49.25	0.00	0.00	0
E3	49.50	49.50	0.00	0.00	0
F	47.50	47.75	0.25	0.53	0
G	48.00	48.00	0.00	0.00	0
H	39.75	40.00	0.25	0.63	0
I	39.75	39.75	0.00	0.00	0

Note: Maximum severity index for each variable (A-I) is used for determination of final OCDI value

Final OCDI: XX A B C D E F G H I
RF 0 0 0 0 0 0 0 0 0

Figure H-1. Occupant Compartment Deformation Index (OCDI), Test FR-3

APPENDIX I

ACCELEROMETER AND RATE TRANSDUCER DATA ANALYSIS, TEST FR-3

Figure I-1. Graph of Longitudinal Deceleration, Test FR-3

Figure I-2. Graph of Longitudinal Occupant Impact Velocity (OIV), Test FR-3

Figure I-3. Graph of Longitudinal Occupant Displacement, Test FR-3

Figure I-4. Graph of Lateral Deceleration, Test FR-3

Figure I-5. Graph of Lateral Occupant Impact Velocity (OIV), Test FR-3

Figure I-6. Graph of Lateral Occupant Displacement, Test FR-3

Figure I-7. Graph of Roll, Pitch, and Yaw Angular Displacements, Test FR-3

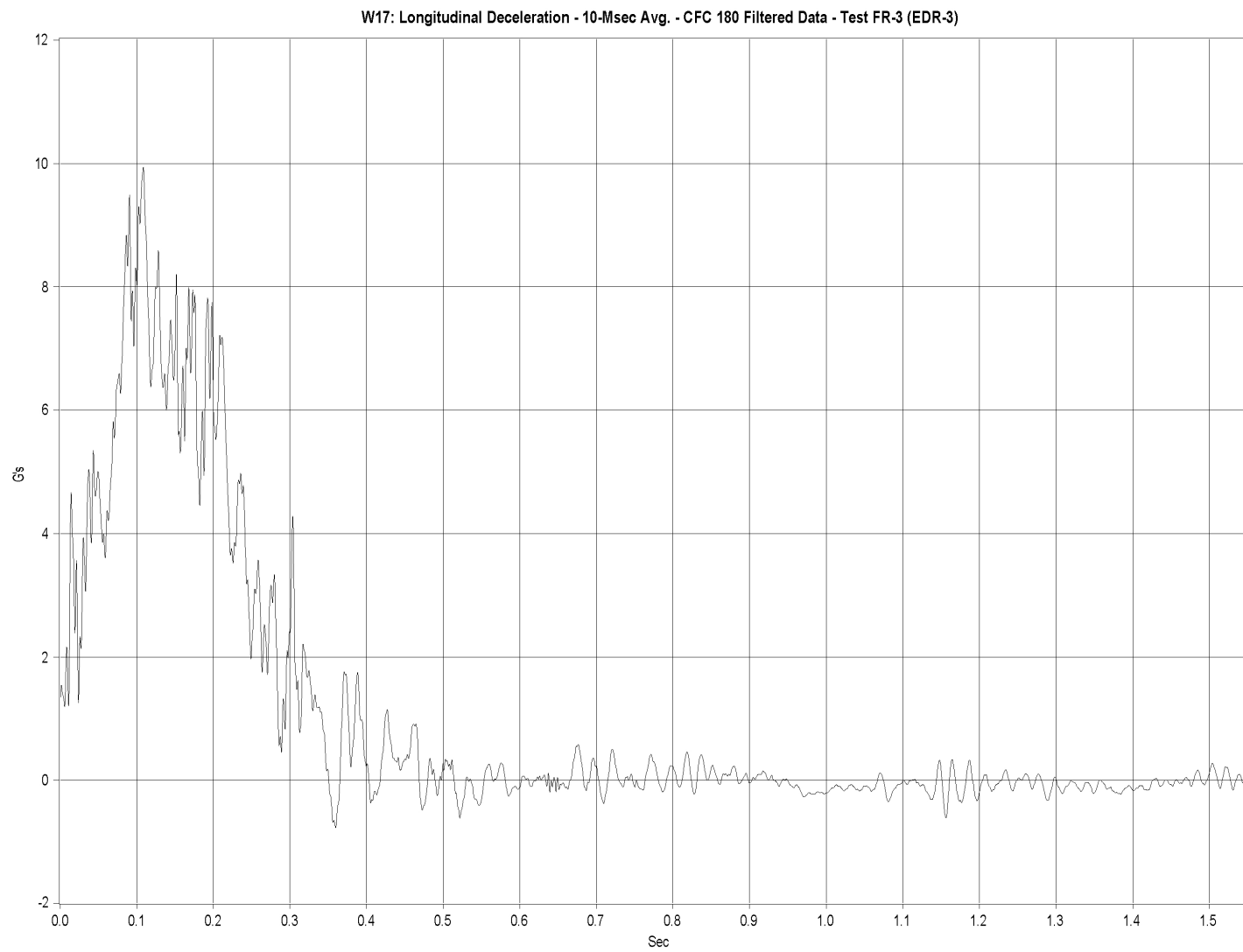


Figure I-1. Graph of Longitudinal Deceleration, Test FR-3

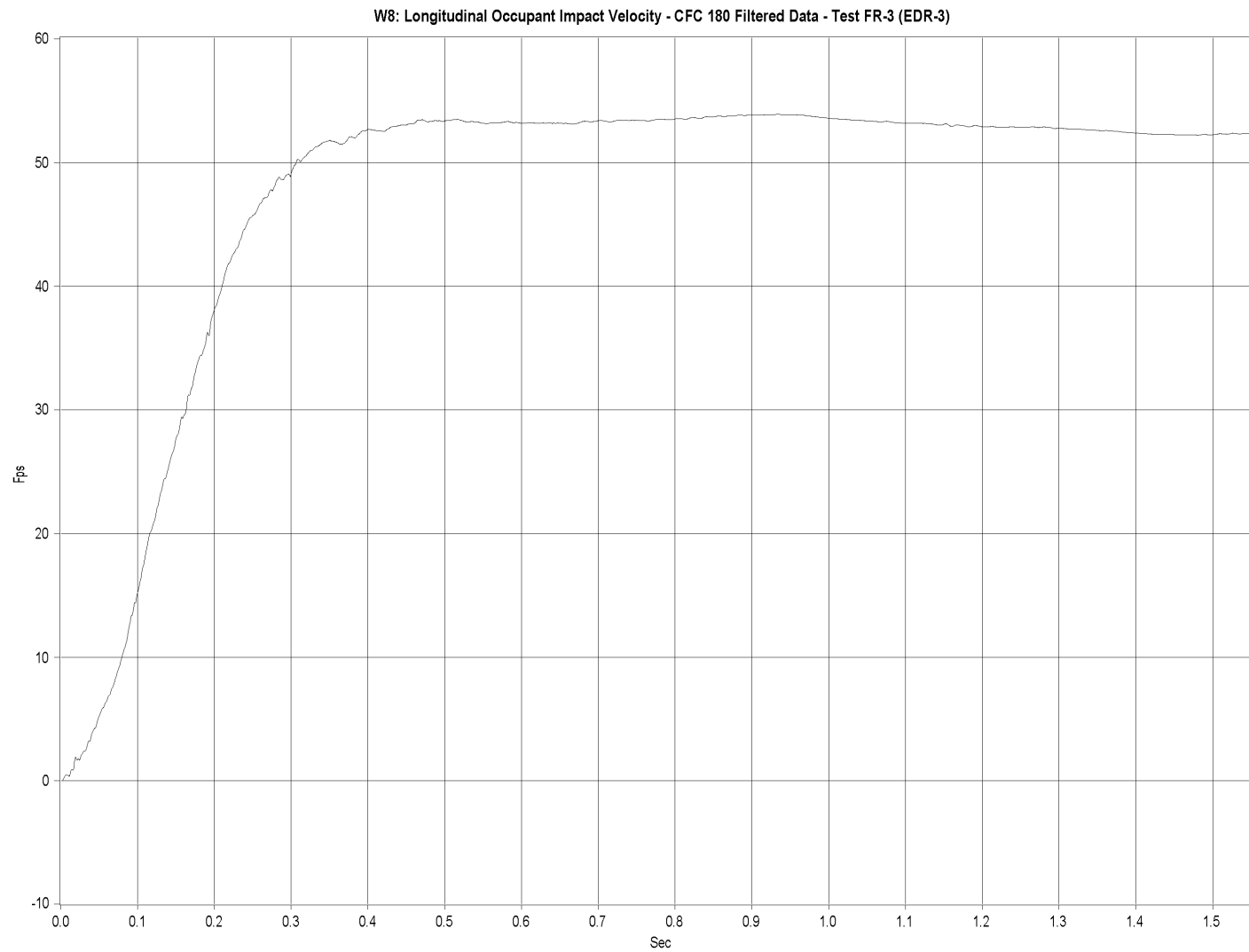


Figure I-2. Graph of Longitudinal Occupant Impact Velocity (OIV), Test FR-3

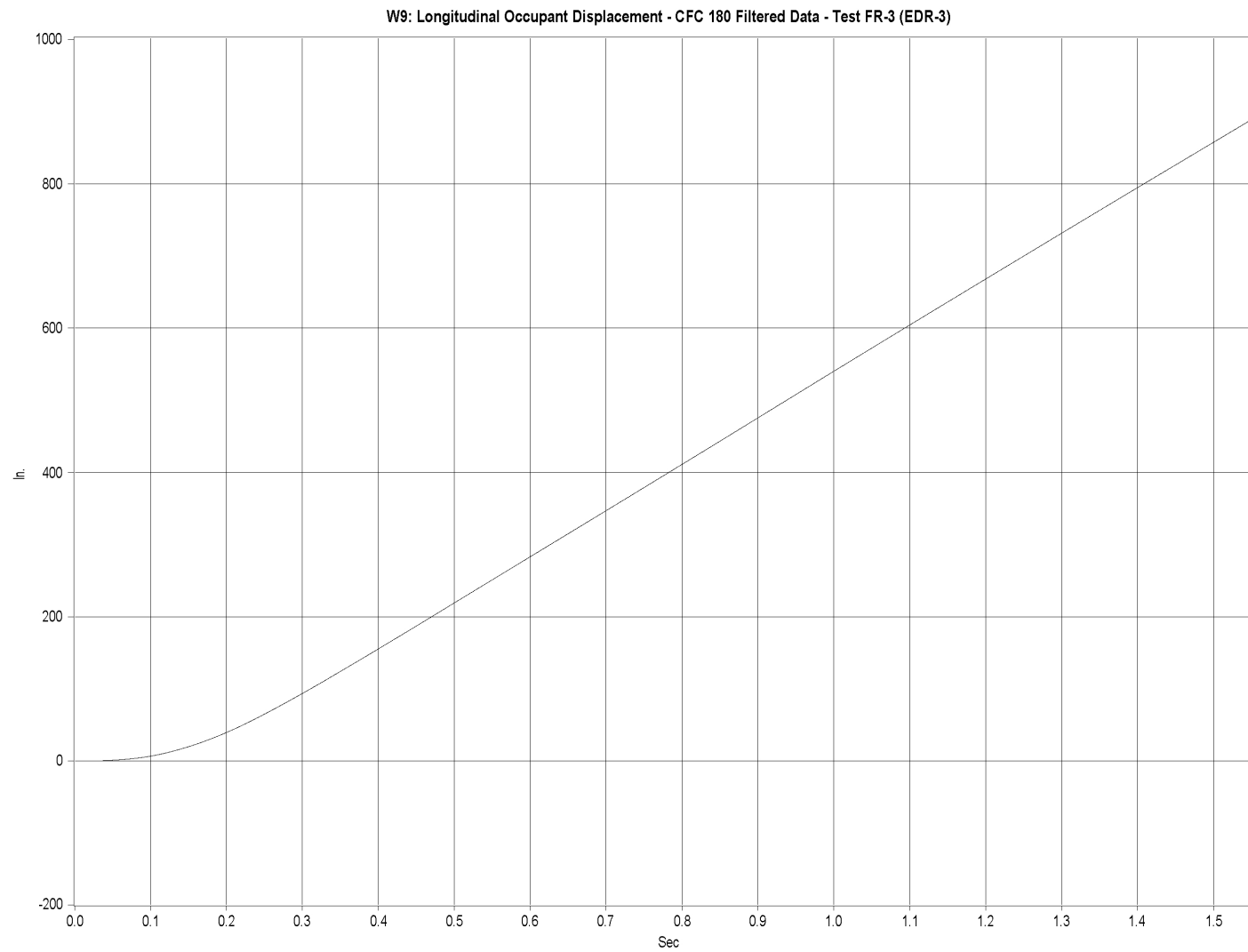


Figure I-3. Graph of Longitudinal Occupant Displacement, Test FR-3

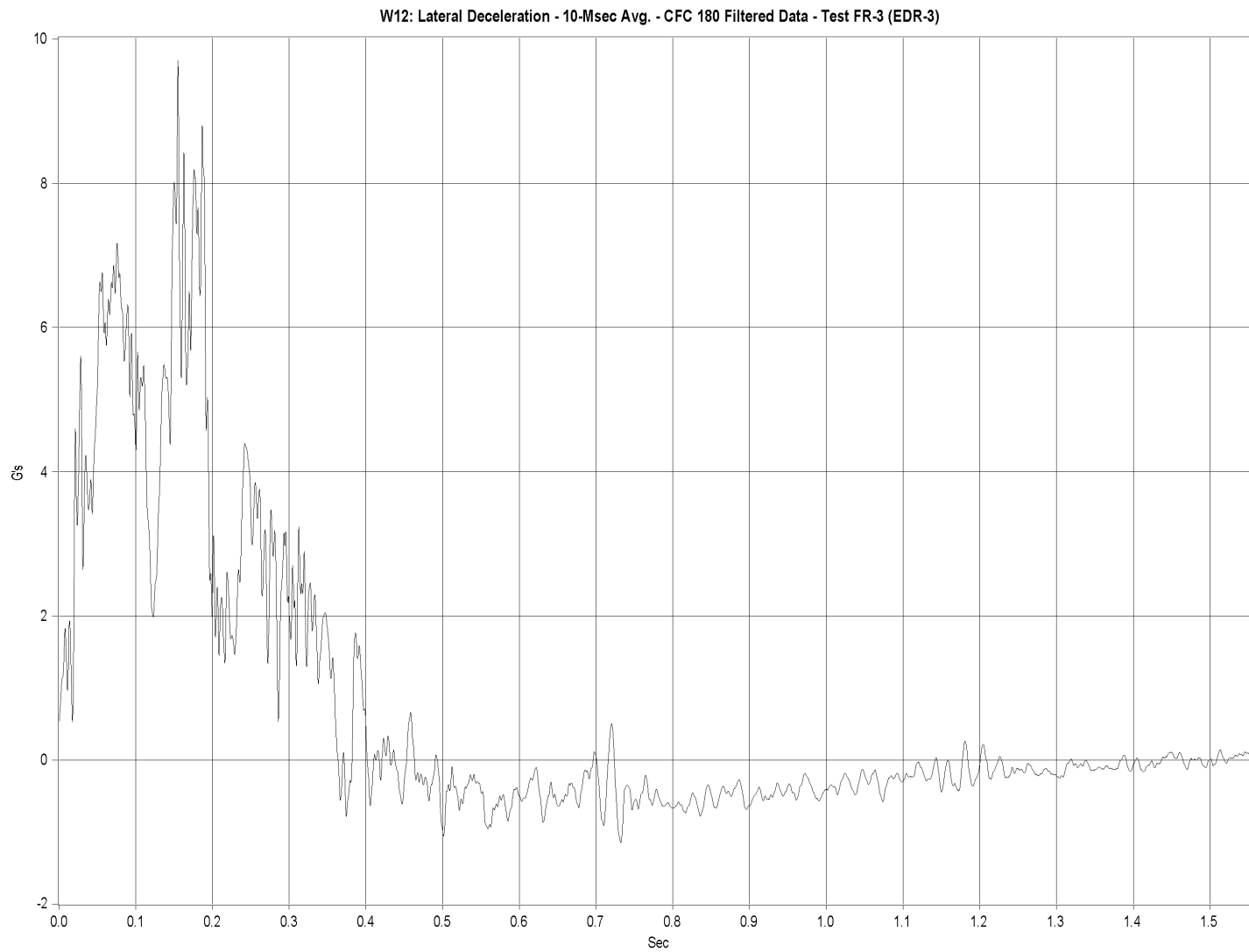


Figure I-4. Graph of Lateral Deceleration, Test FR-3

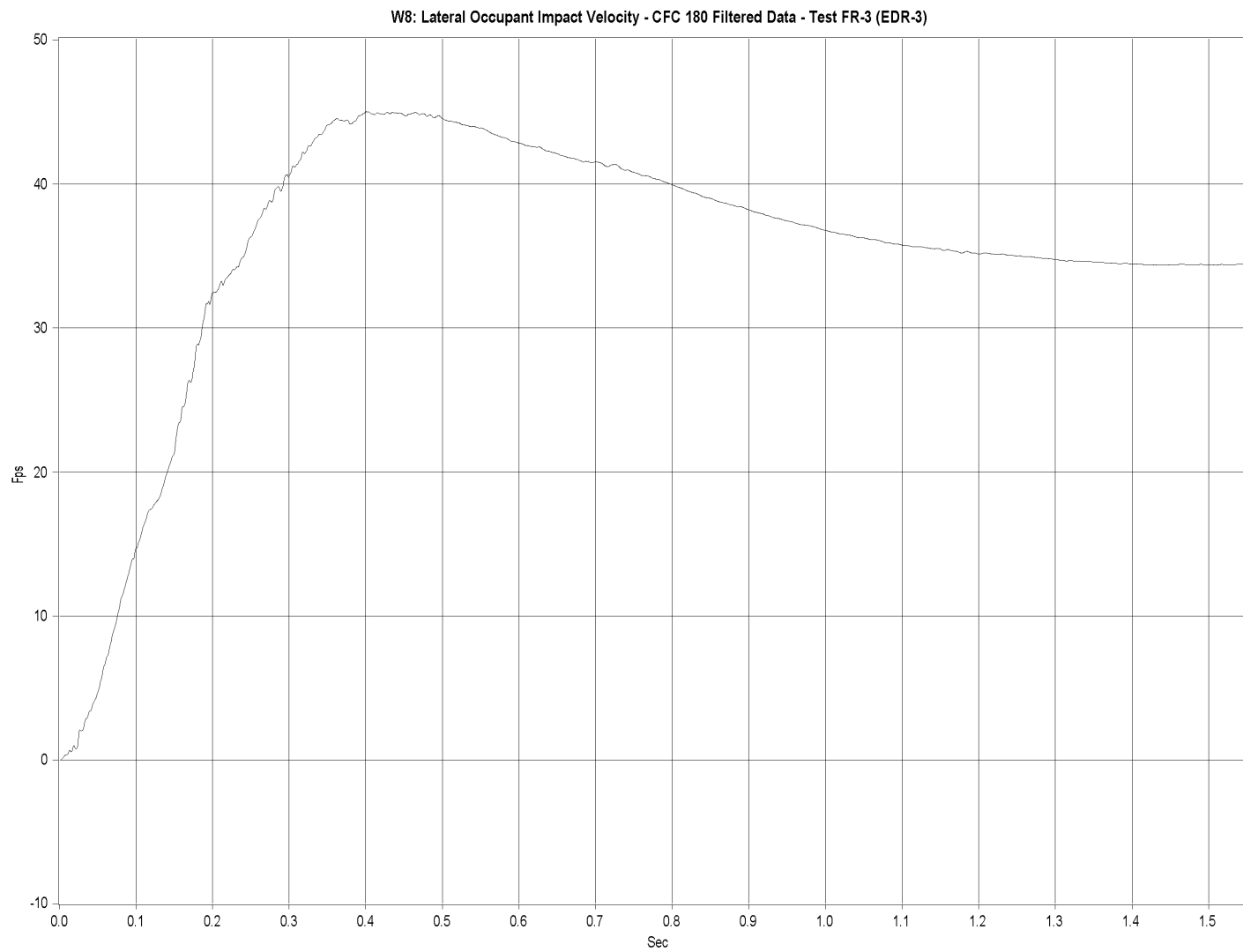


Figure I-5. Graph of Lateral Occupant Impact Velocity (OIV), Test FR-3

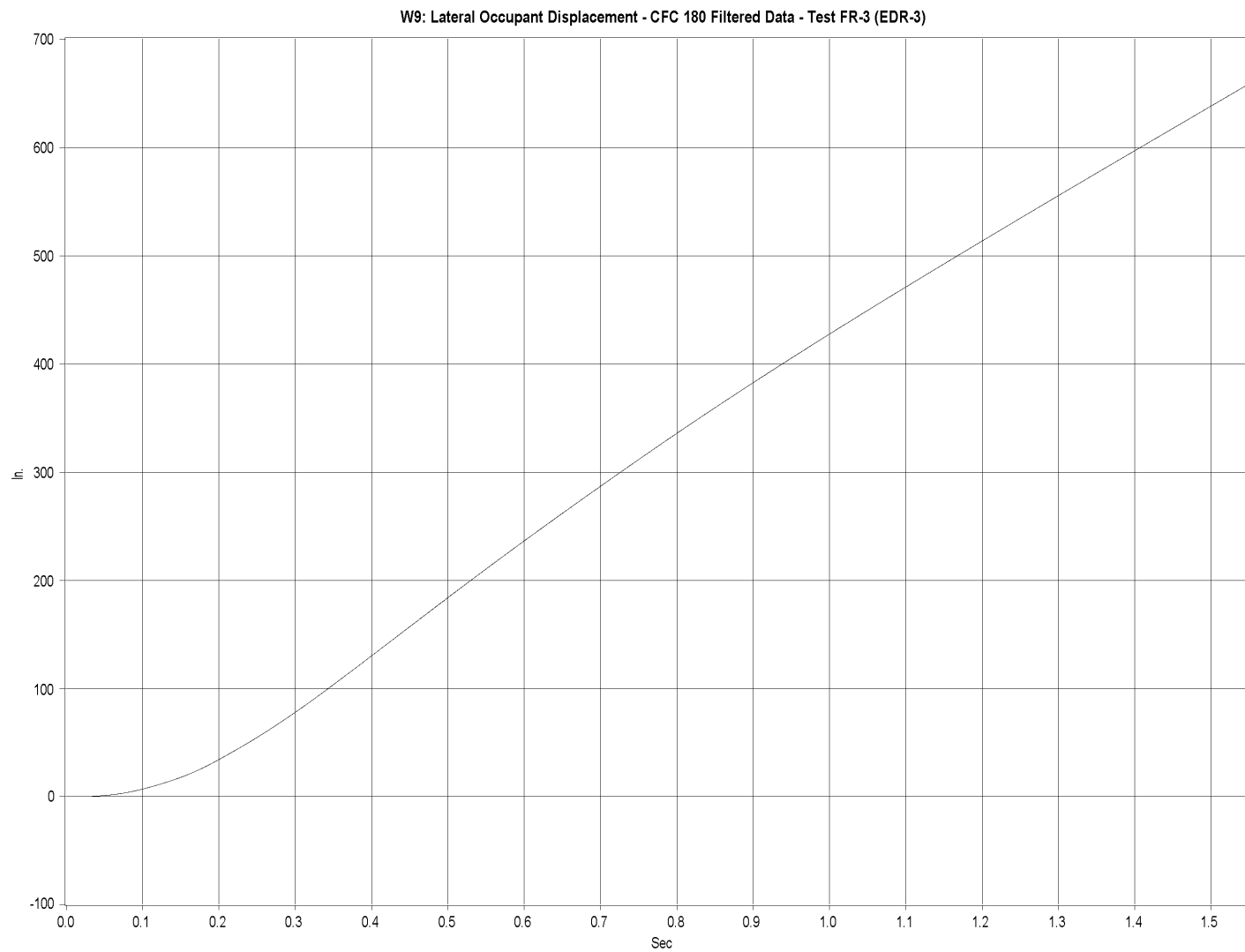


Figure I-6. Graph of Lateral Occupant Displacement, Test FR-3

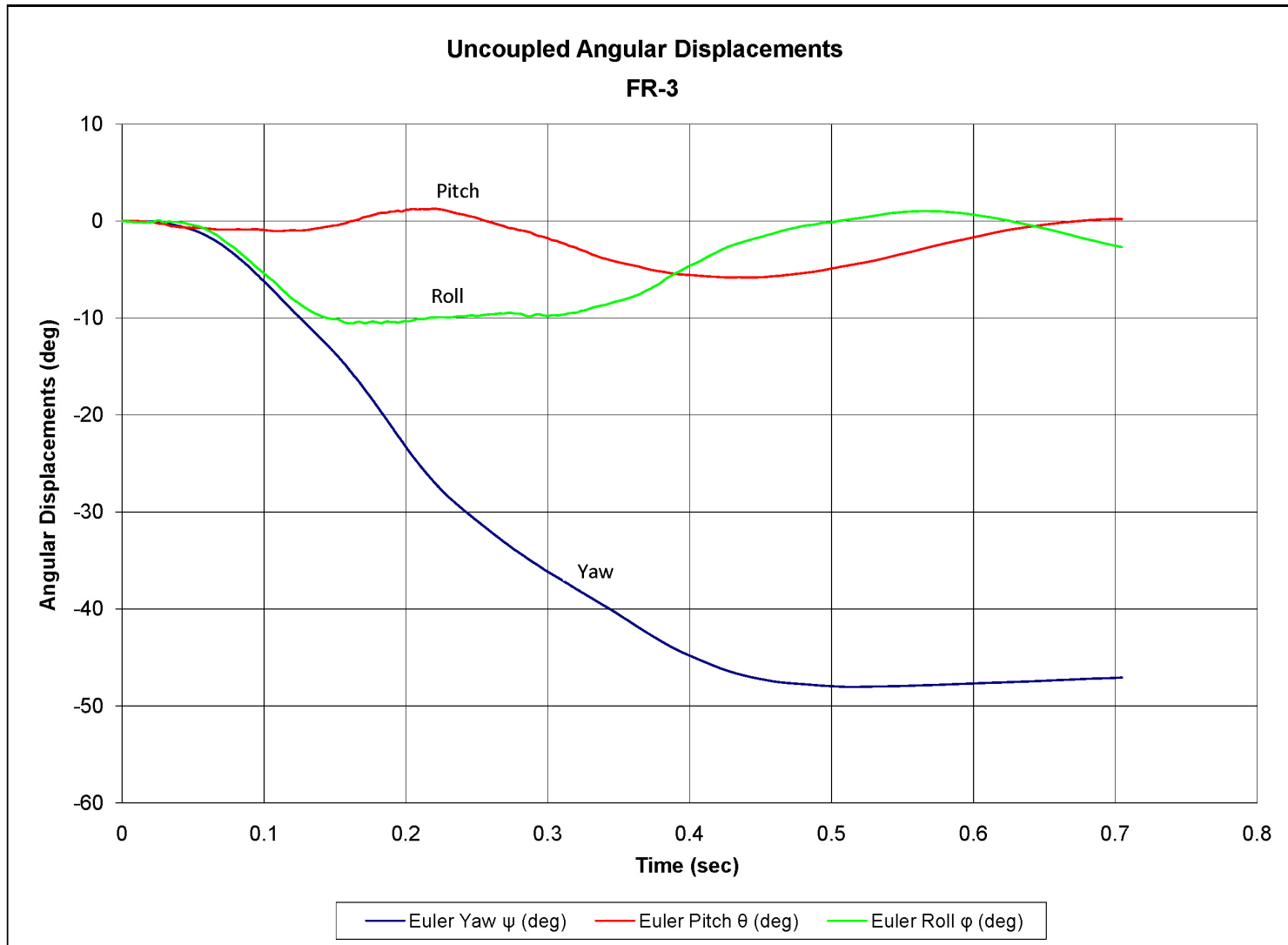


Figure I-7. Graph of Roll, Pitch, and Yaw Angular Displacements, Test FR-3

APPENDIX J

SYSTEM DRAWINGS - DESIGN NO. 3

- Figure J-1. System Details, Design No. 3 (Metric)
- Figure J-2. Rail Details, Design No. 3 (Metric)
- Figure J-3. Post Details, Design No. 3 (Metric)
- Figure J-4. Anchorage Details, Design No. 3 (Metric)
- Figure J-5. Anchorage Bracket Details, Design No. 3 (Metric)
- Figure J-6. Anchorage Details, Design No. 3 (Metric)
- Figure J-7. Rail Bend Details, Design No. 3 (Metric)
- Figure J-8. System Details, Design No. 3 (English)
- Figure J-9. Rail Details, Design No. 3 (English)
- Figure J-10. Post Details, Design No. 3 (English)
- Figure J-11. Anchorage Details, Design No. 3 (English)
- Figure J-12. Anchorage Bracket Details, Design No. 3 (English)
- Figure J-13. Anchorage Details, Design No. 3 (English)
- Figure J-14. Rail Bend Details, Design No. 3 (English)

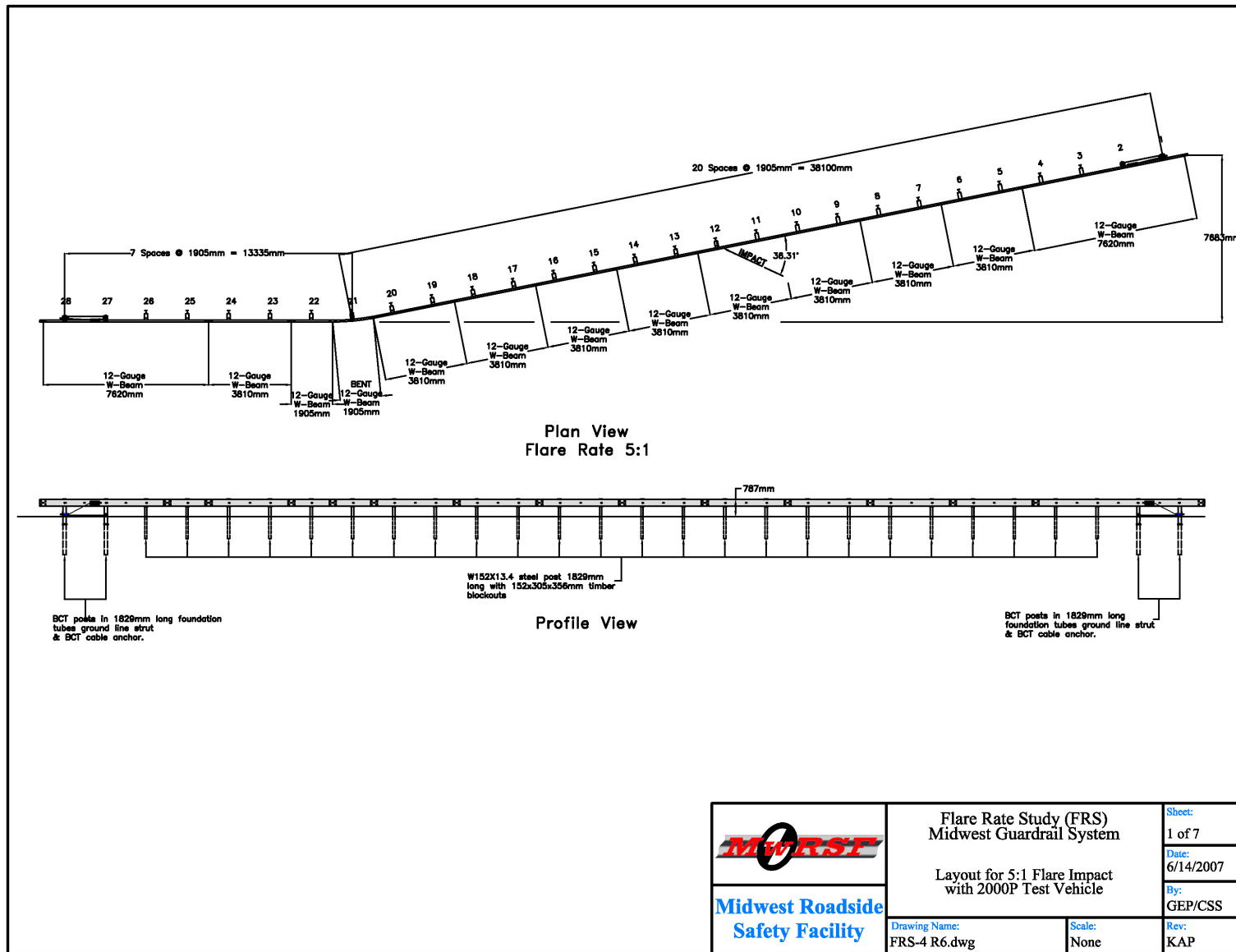


Figure J-1. System Layout, Design No. 3 (Metric)

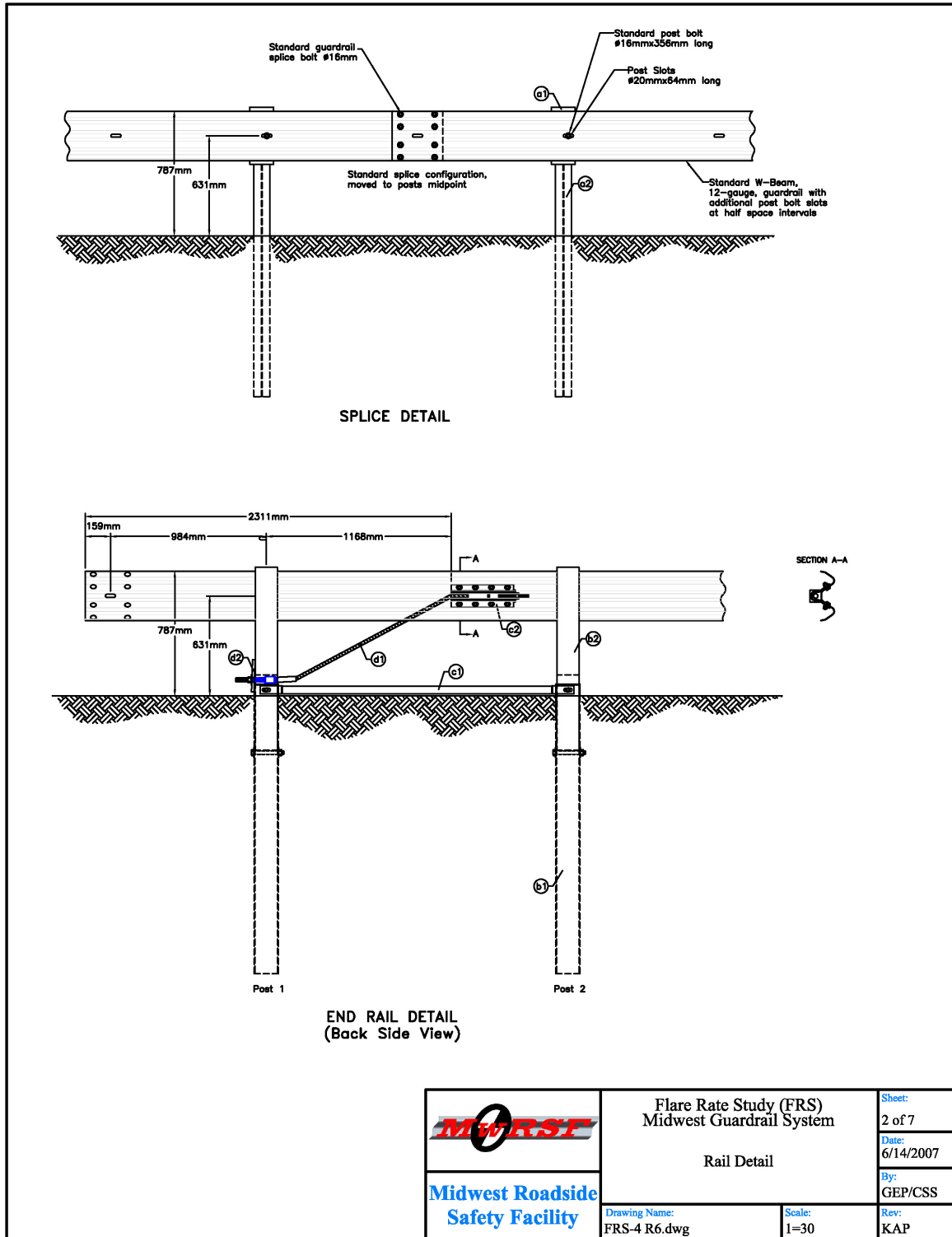


Figure J-2. Rail Details, Design No. 3 (Metric)

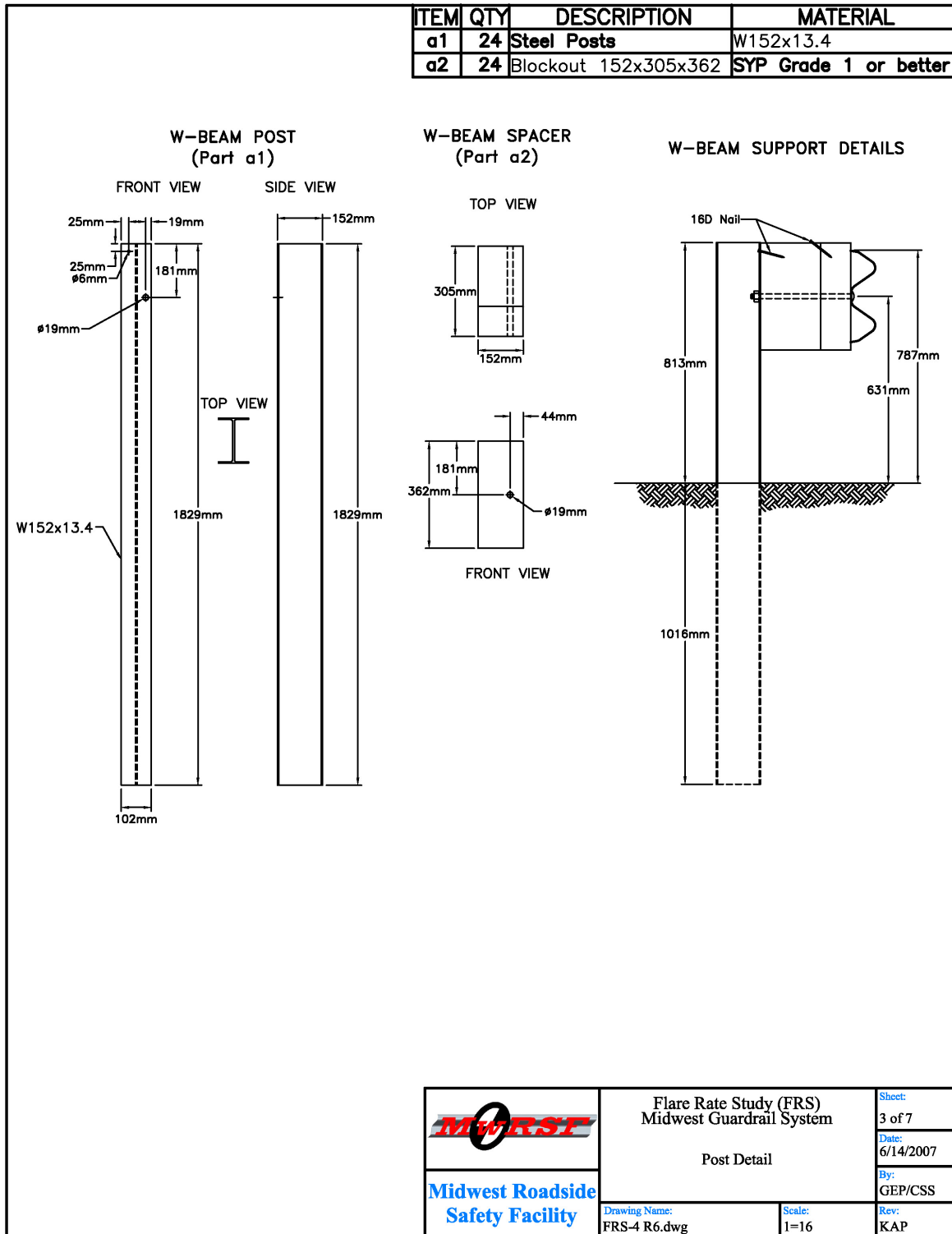


Figure J-3. Post Details, Design No. 3 (Metric)

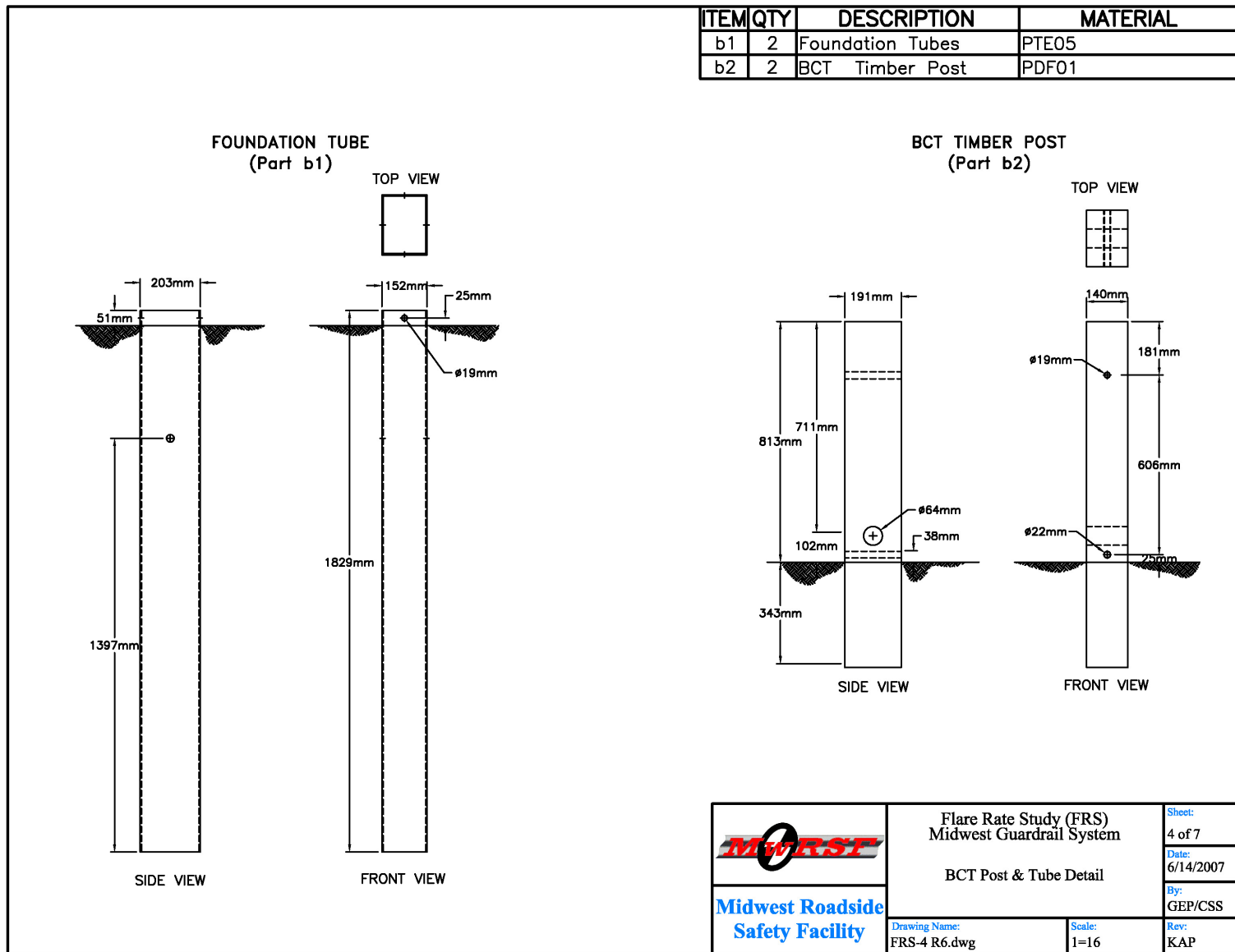


Figure J-4. Anchorage Details, Design No. 3 (Metric)

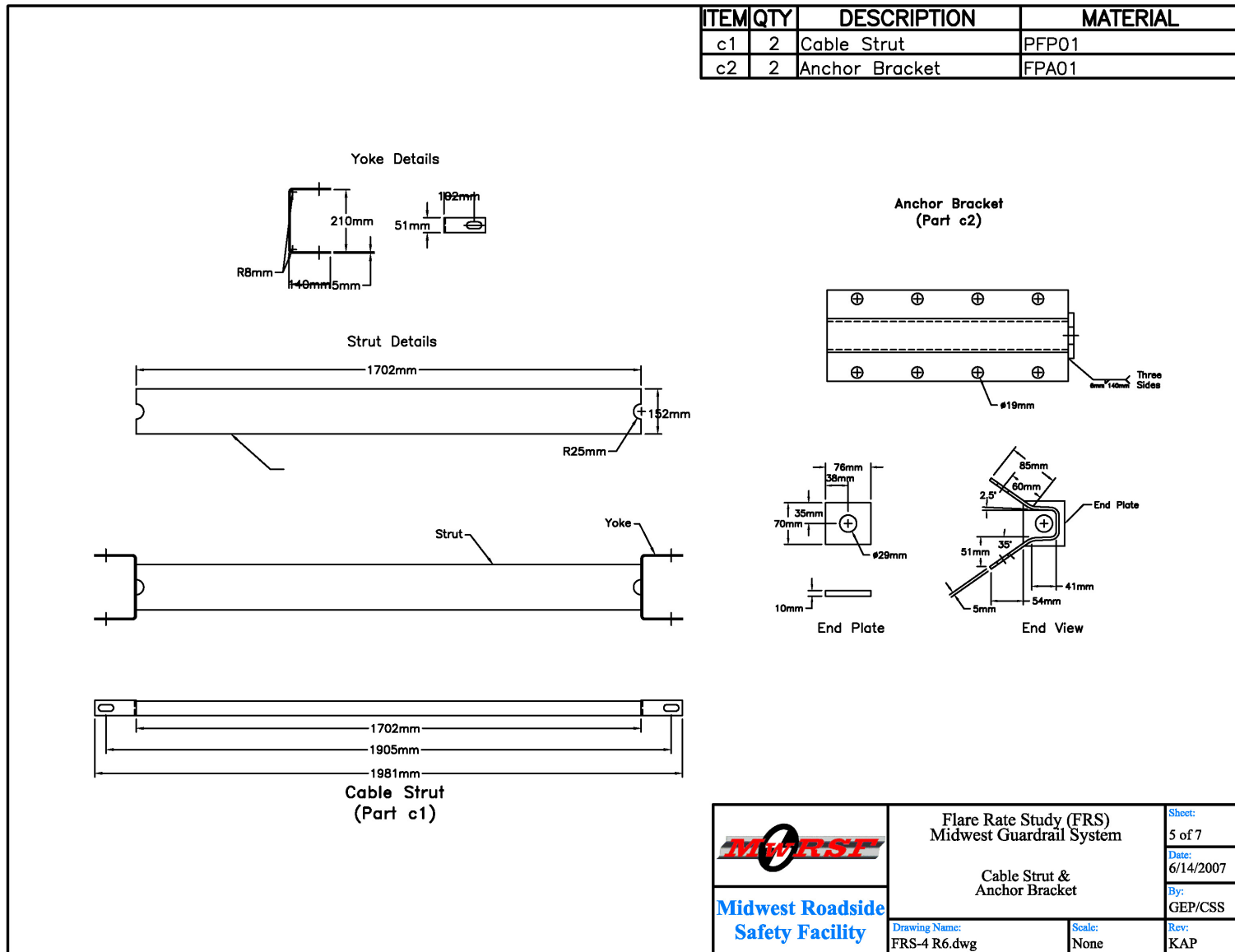


Figure J-5. Anchorage Details, Design No. 3 (Metric)

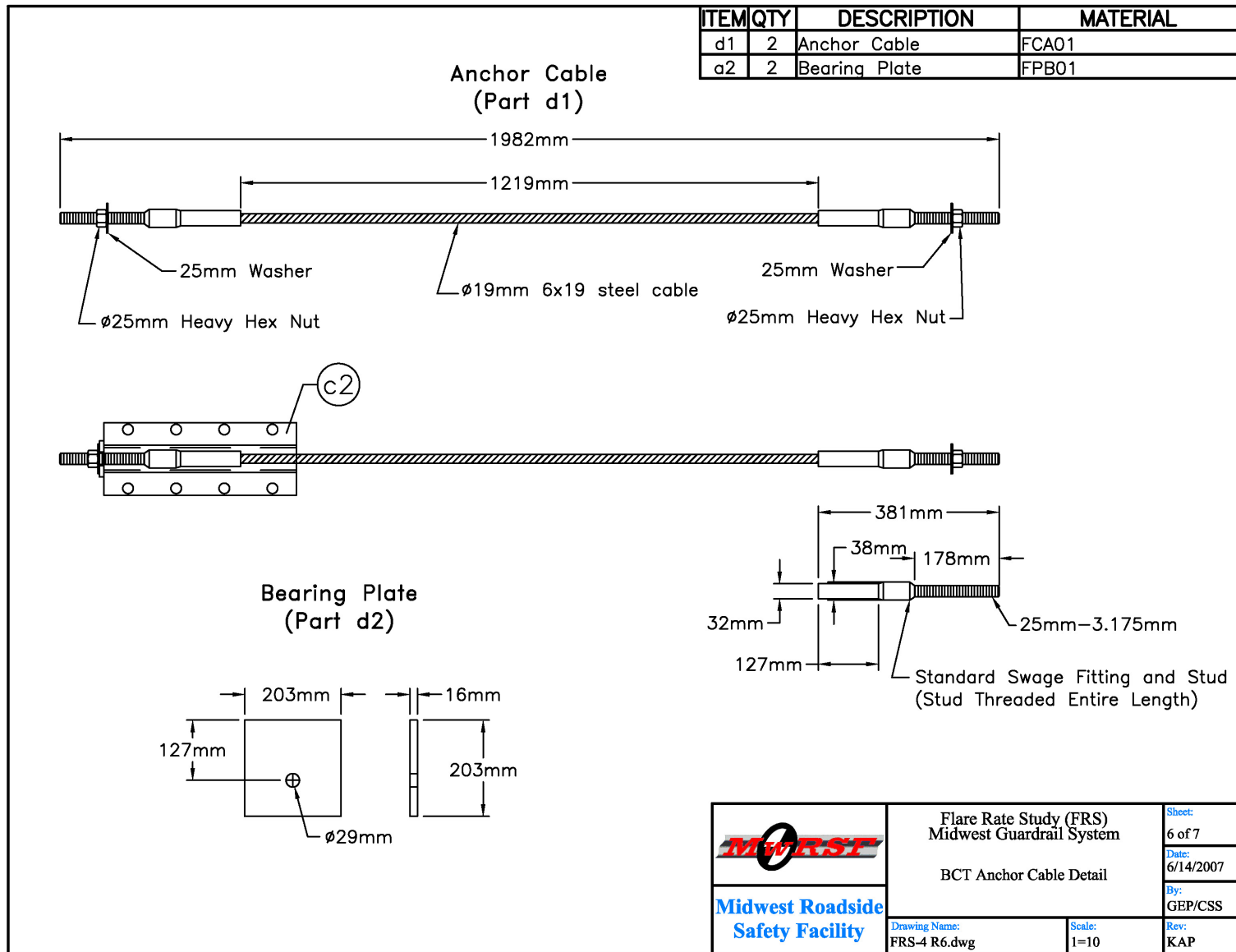
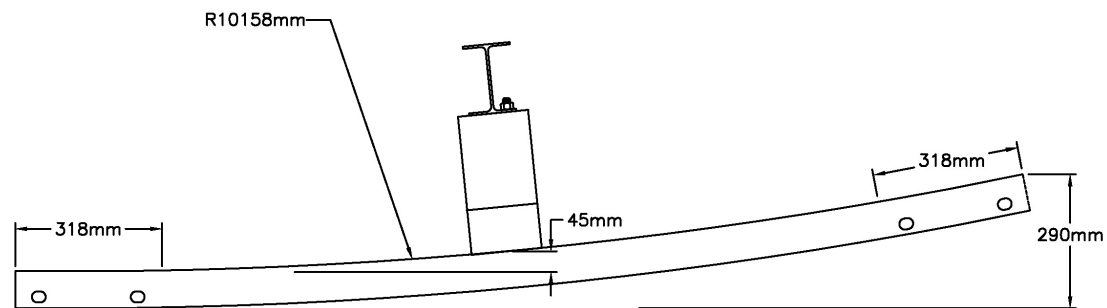


Figure J-6. Anchorage Details, Design No. 3 (Metric)




	Flare Rate Study (FRS) Midwest Guardrail System		Sheet: 7 of 7
	6'-3" Rail Section Bend Detail		Date: 6/14/2007
Midwest Roadside Safety Facility	Drawing Name: FRS-4 R6.dwg		By: GEP/CSS
	Scale: 1=10		Rev: KAP

Figure J-7. Rail Bend Details, Design No. 3 (Metric)

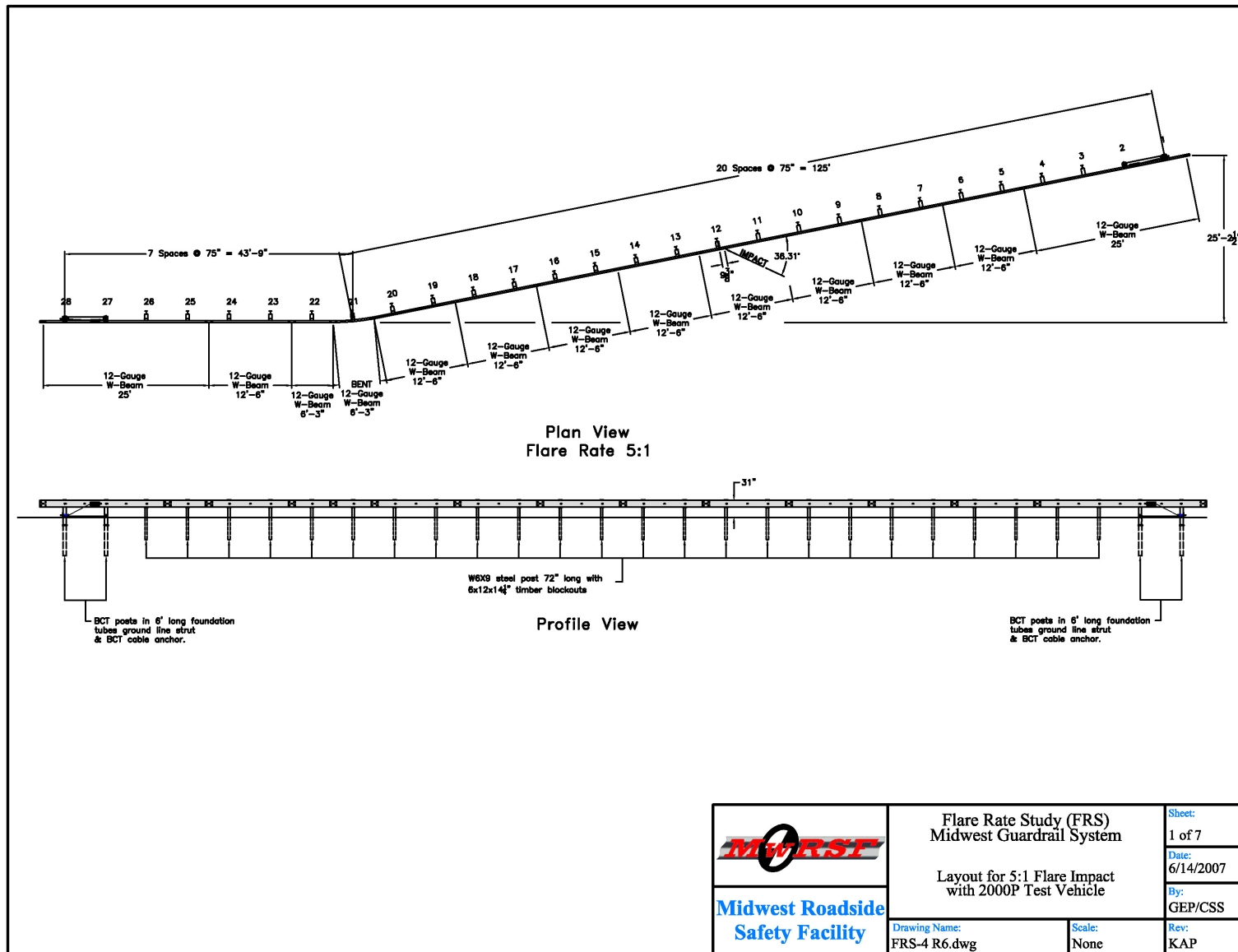


Figure J-8. System Layout, Design No. 3 (English)

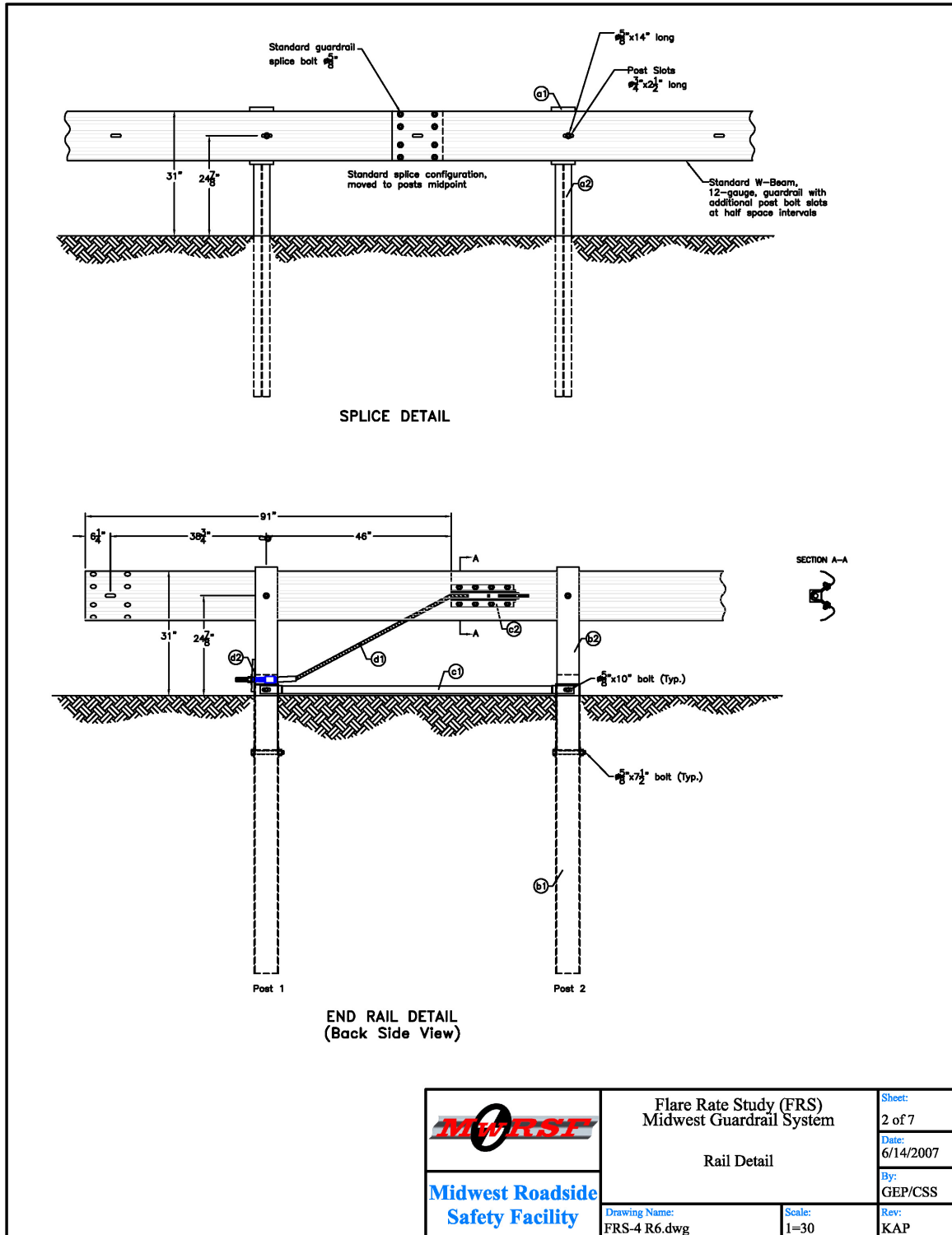


Figure J-9. Rail Details, Design No. 3 (English)

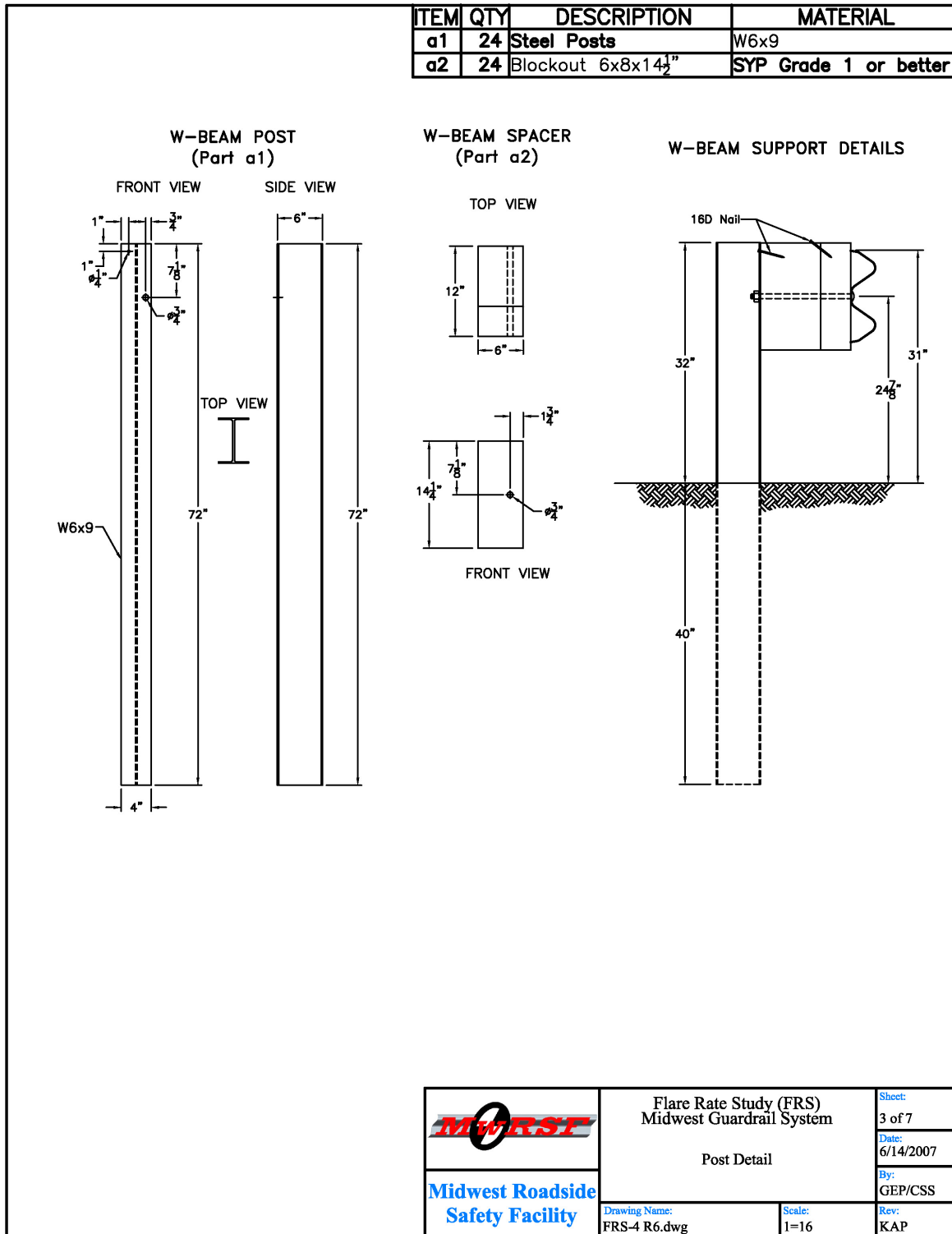


Figure J-10. Post Details, Design No. 3 (English)

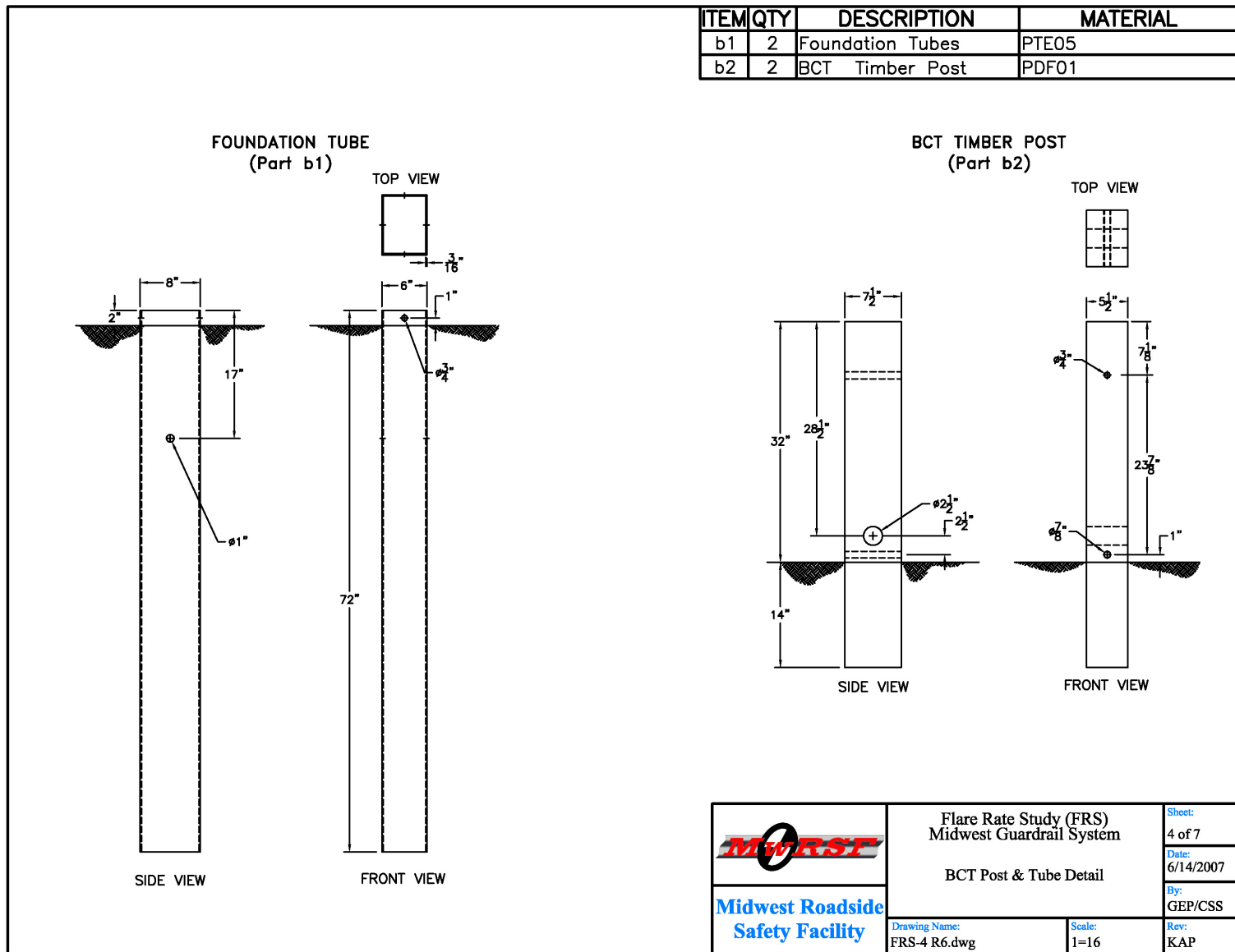


Figure J-11. Anchorage Details, Design No. 3 (English)

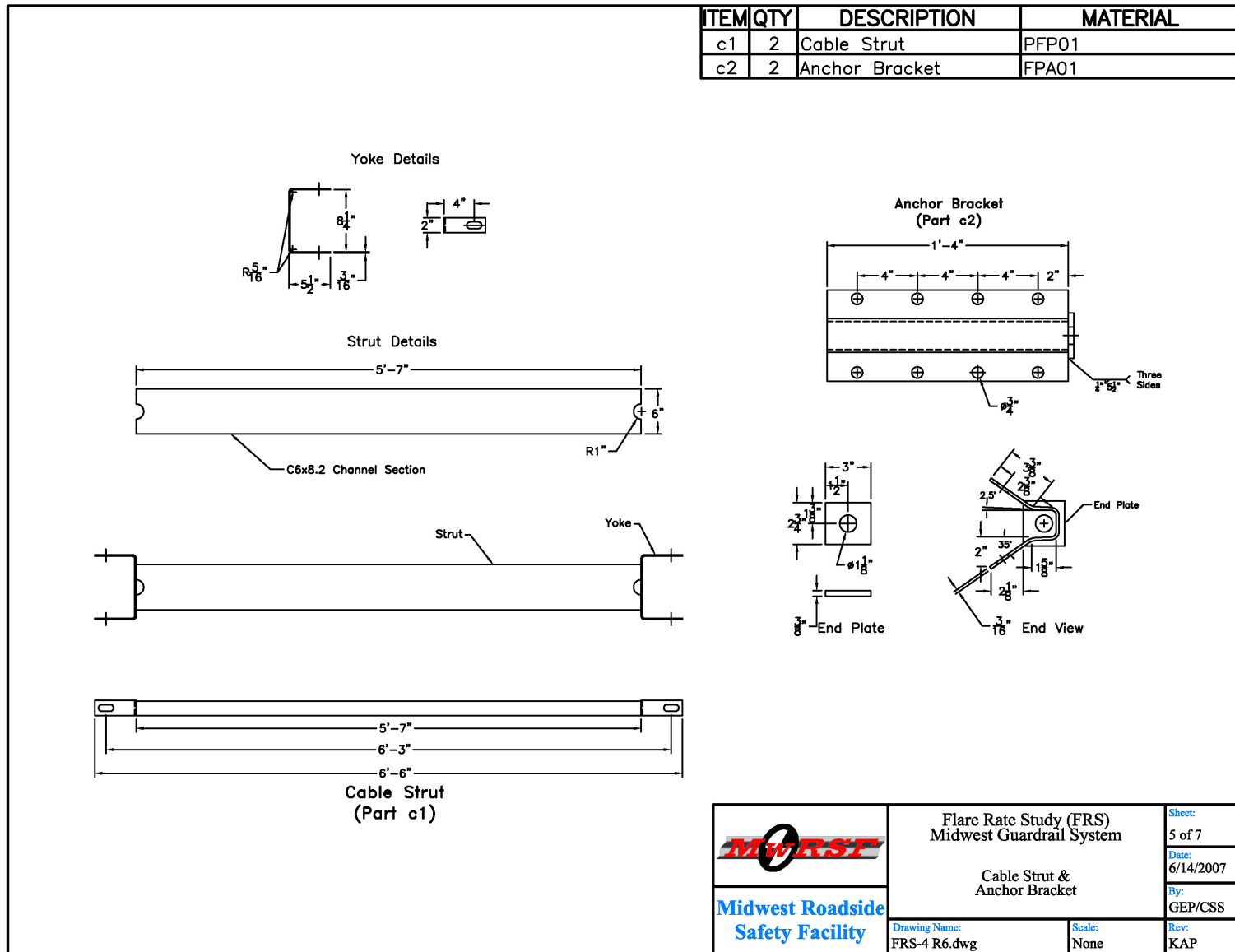


Figure J-5. Anchorage Details, Design No. 3 (English)

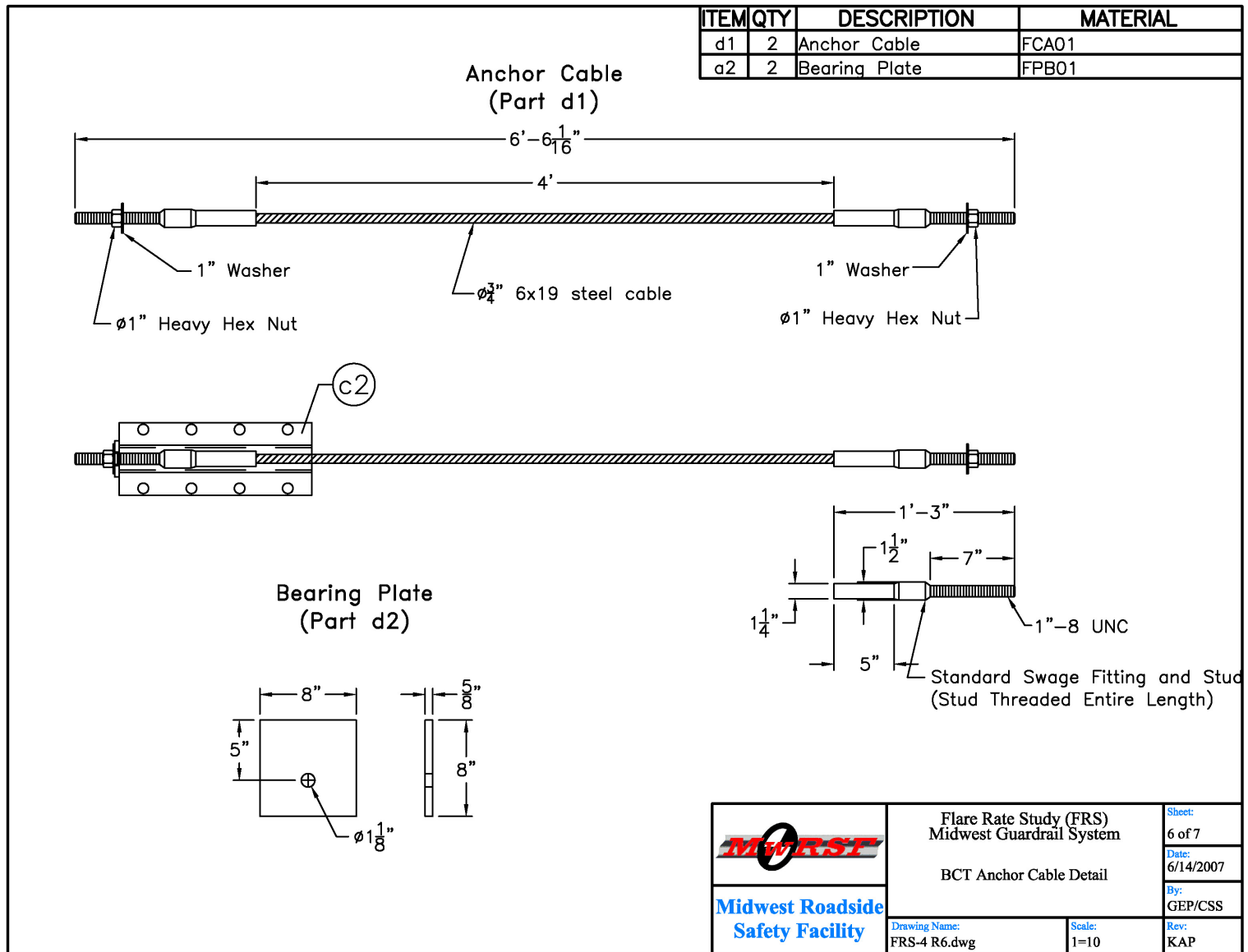
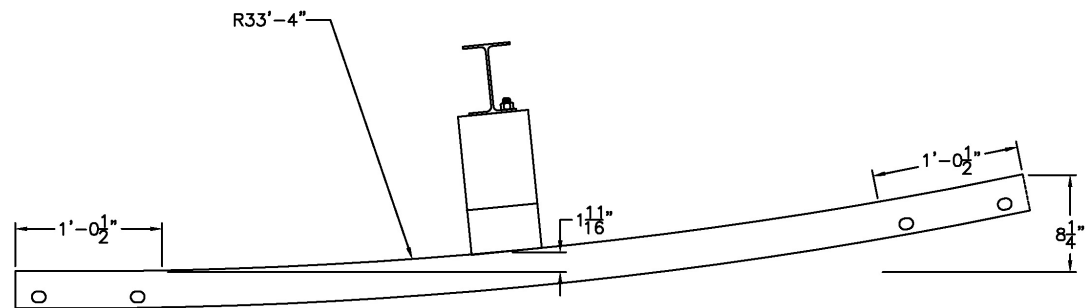


Figure J-13. Anchorage Details, Design No. 3 (English)




	Flare Rate Study (FRS) Midwest Guardrail System 6'-3" Rail Section Bend Detail		Sheet: 7 of 7
	Drawing Name: FRS-4 R6.dwg		Date: 6/14/2007 By: GEP/CSS Rev: KAP

Figure J-14. Rail Bend Details, Design No. 3 (English)

APPENDIX K

OCCUPANT COMPARTMENT DEFORMATION DATA, TEST FR-4

Figure K-1. Occupant Compartment Deformation Data - Set 1, Test FR-4

Figure K-2. Occupant Compartment Deformation Data - Set 2, Test FR-4

Figure K-3. Occupant Compartment Deformation Index (OCDI), Test FR-4

VEHICLE PRE/POST CRUSH INFO
Set-1

TEST: FR-4
VEHICLE: 2000p/1999 Chevy C2500

POINT	X	Y	Z	X'	Y'	Z'	DEL X	DEL Y	DEL Z
1	56.25	11.75	-2.75	56.5	11.25	-2.5	0.25	-0.5	0.25
2	57.5	16	-3.5	57.5	15.5	-3.5	0	-0.5	0
3	57.5	20.25	-3.75	57.5	19.5	-3.75	0	-0.75	0
4	58	24.25	-3.5	57.75	23.5	-3.5	-0.25	-0.75	0
5	57	29	-2.75	57	28.5	-2.5	0	-0.5	0.25
6	53.75	11.5	-6.75	53.75	11.5	-6.75	0	0	0
7	54	15.75	-6.5	54	15.25	-6.25	0	-0.5	0.25
8	54.25	20.25	-6.25	54.25	20	-6.25	0	-0.25	0
9	54.75	24.25	-5.75	54.75	24	-5.75	0	-0.25	0
10	54.75	28.75	-5.25	54.5	28.5	-5.25	-0.25	-0.25	0
11	49.75	11.75	-8.75	49.75	11.75	-8.5	0	0	0.25
12	50.25	15.25	-8.5	50	15.25	-8.5	-0.25	0	0
13	50.5	20	-8.5	50.5	19.75	-8.25	0	-0.25	0.25
14	51.25	24.5	-7.75	51	24.5	-8	-0.25	0	-0.25
15	50.75	28.75	-7.25	50.5	28.75	-7.25	-0.25	0	0
16	46.25	11.5	-8.75	46	12.25	-8.75	-0.25	0.75	0
17	46.5	15	-8.75	46.5	15.25	-8.75	0	0.25	0
18	47.5	19.25	-8.5	47.25	19.5	-8.5	-0.25	0.25	0
19	48	24.75	-8	48	24.75	-8.25	0	0	-0.25
20	48.5	28.75	-7.75	48.25	28.5	-7.75	-0.25	-0.25	0
21	42	11.5	-9	41.75	12	-8.75	-0.25	0.5	0.25
22	42.25	14.75	-9	42	15.25	-8.75	-0.25	0.5	0.25
23	43.5	19	-8.75	43.5	19.75	-8.5	0	0.75	0.25
24	43.25	23.75	-8.25	43.5	24.5	-8.25	0.25	0.75	0
25	43.75	27.5	-8.5	43.5	28.25	-8.5	-0.25	0.75	0
26	36	12.5	-9.25	35.75	12.25	-8.75	-0.25	-0.25	0.5
27	36.5	17.25	-8.75	36.5	17.5	-8.75	0	0.25	0
28	36.5	24	-8.75	36.5	24.5	-8.5	0	0.5	0.25
29									
30									

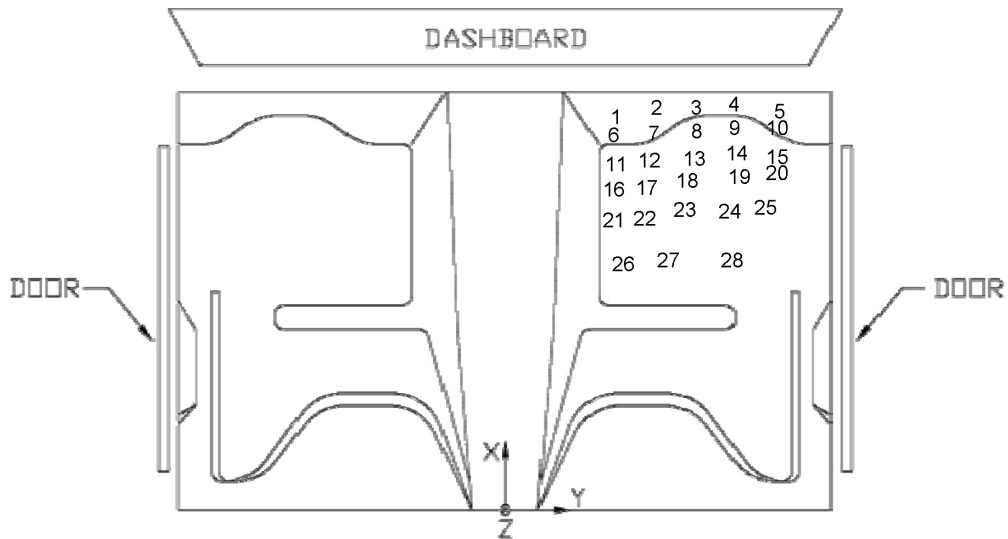


Figure K-1. Occupant Compartment Deformation Data - Set 1, Test FR-4

VEHICLE PRE/POST CRUSH INFO
Set-2

TEST:
VEHICLE:

POINT	X	Y	Z	X'	Y'	Z'	DEL X	DEL Y	DEL Z
1	49.75	20.25	-1.5	50	19.75	-1.5	0.25	-0.5	0
2	51	24.5	-2.5	51	24	-2.5	0	-0.5	0
3	51	28.75	-2.5	51	28	-2.75	0	-0.75	-0.25
4	51.5	32.75	-2.25	51.25	32	-2.25	-0.25	-0.75	0
5	50.5	27.5	-1.5	50.5	37	-1.5	0	9.5	0
6	47.25	20	-5.5	47.25	20	-5.75	0	0	-0.25
7	47.5	24.25	-5	47.5	23.75	-5.25	0	-0.5	-0.25
8	47.75	28.75	-5	47.75	28.5	-5.25	0	-0.25	-0.25
9	48.25	32.75	-4.5	48.25	32.5	-4.75	0	-0.25	-0.25
10	48.25	37.25	-4	48	37	-4.25	-0.25	-0.25	-0.25
11	43.25	20.25	-7.25	43.25	20.25	-7.25	0	0	0
12	43.75	23.75	-7.25	43.5	23.75	-7.5	-0.25	0	-0.25
13	44	28.5	-7.25	44	28.25	-7.25	0	-0.25	0
14	44.75	32.5	-6.75	44.5	33	-6.75	-0.25	0.5	0
15	44.25	37.25	-6.25	44	37.25	-6.25	-0.25	0	0
16	39.75	20	-7.5	39.5	20.75	-7.5	-0.25	0.75	0
17	40	23.5	-7.5	40	23.75	-7.5	0	0.25	0
18	41	27.75	-7.25	40.75	28	-7.5	-0.25	0.25	-0.25
19	41.5	33.25	-7	41.5	33.25	-7	0	0	0
20	42	37.25	-6.5	41.75	37	-6.75	-0.25	-0.25	-0.25
21	35.5	20	-7.75	35.25	20.5	-7.5	-0.25	0.5	0.25
22	35.75	23.25	-7.75	35.5	23.75	-7.5	-0.25	0.5	0.25
23	37	27.5	-7.5	37	28.25	-7.5	0	0.75	0
24	36.75	32.25	-7	37	33	-7.25	0.25	0.75	-0.25
25	37.25	36	-7.25	37	36.75	-7.5	-0.25	0.75	-0.25
26	29.5	21	-7.75	29.25	20.75	-7.5	-0.25	-0.25	0.25
27	30	25.75	-7.5	30	26	-7.5	0	0.25	0
28	30	32.5	-7.5	30	33	-7.5	0	0.5	0
29									
30									

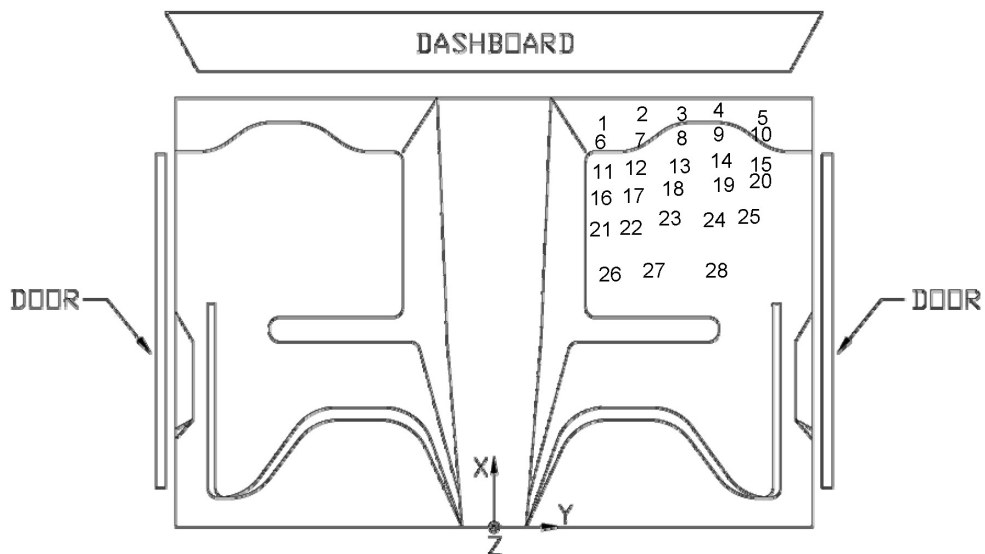


Figure K-2. Occupant Compartment Deformation Data - Set 2, Test FR-4

Occupant Compartment Deformation Index (OCDI)

Test No. FR-4
Vehicle Type: 2000p/Chevy C2500

OCDI = XXABCDEFGHI

XX = location of occupant compartment deformation

A = distance between the dashboard and a reference point at the rear of the occupant compartment, such as the top of the rear seat or the rear of the cab on a pickup

B = distance between the roof and the floor panel

C = distance between a reference point at the rear of the occupant compartment and the motor panel

D = distance between the lower dashboard and the floor panel

E = interior width

F = distance between the lower edge of right window and the upper edge of left window

G = distance between the lower edge of left window and the upper edge of right window

H = distance between bottom front corner and top rear corner of the passenger side window

I = distance between bottom front corner and top rear corner of the driver side window

Severity Indices

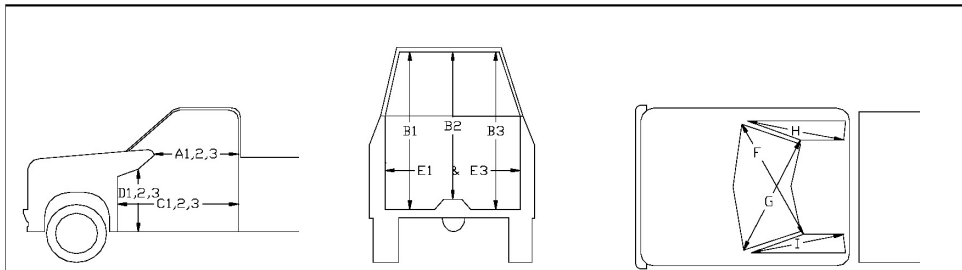
0 - if the reduction is less than 3%

1 - if the reduction is greater than 3% and less than or equal to 10 %

2 - if the reduction is greater than 10% and less than or equal to 20 %

3 - if the reduction is greater than 20% and less than or equal to 30 %

4 - if the reduction is greater than 30% and less than or equal to 40 %



where,
 1 = Passenger Side
 2 = Middle
 3 = Driver Side

Location:

Measurement	Pre-Test (in.)	Post-Test (in.)	Change (in.)	% Difference	Severity Index
A1	40.75	40.75	0.00	0.00	0
A2	42.00	41.75	-0.25	-0.60	0
A3	40.00	39.75	-0.25	-0.63	0
B1	48.50	48.25	-0.25	-0.52	0
B2	42.00	41.75	-0.25	-0.60	0
B3	47.00	46.75	-0.25	-0.53	0
C1	57.00	57.00	0.00	0.00	0
C2	52.75	52.75	0.00	0.00	0
C3	57.50	57.25	-0.25	-0.43	0
D1	15.25	15.00	-0.25	-1.64	0
D2	16.00	16.00	0.00	0.00	0
D3	18.50	18.50	0.00	0.00	0
E1	62.50	62.00	-0.50	-0.80	0
E3	64.00	64.00	0.00	0.00	0
F	58.00	58.00	0.00	0.00	0
G	58.00	58.00	0.00	0.00	0
H	41.00	40.75	-0.25	-0.61	0
I	41.50	41.50	0.00	0.00	0

Note: Maximum severity index for each variable (A-I) is used for determination of final OCDI value

Final OCDI: XX A B C D E F G H I
 RF 0 0 0 0 0 0 0 0 0

Figure K-3. Occupant Compartment Deformation Index (OCDI), Test FR-4

APPENDIX L

ACCELEROMETER AND RATE TRANSDUCER DATA ANALYSIS, TEST FR-4

Figure L-1. Graph of Longitudinal Deceleration, Test FR-4

Figure L-2. Graph of Longitudinal Occupant Impact Velocity (OIV), Test FR-4

Figure L-3. Graph of Longitudinal Occupant Displacement, Test FR-4

Figure L-4. Graph of Lateral Deceleration, Test FR-4

Figure L-5. Graph of Lateral Occupant Impact Velocity (OIV), Test FR-4

Figure L-6. Graph of Lateral Occupant Displacement, Test FR-4

Figure L-7. Graph of Roll, Pitch, and Yaw Angular Displacements, Test FR-4

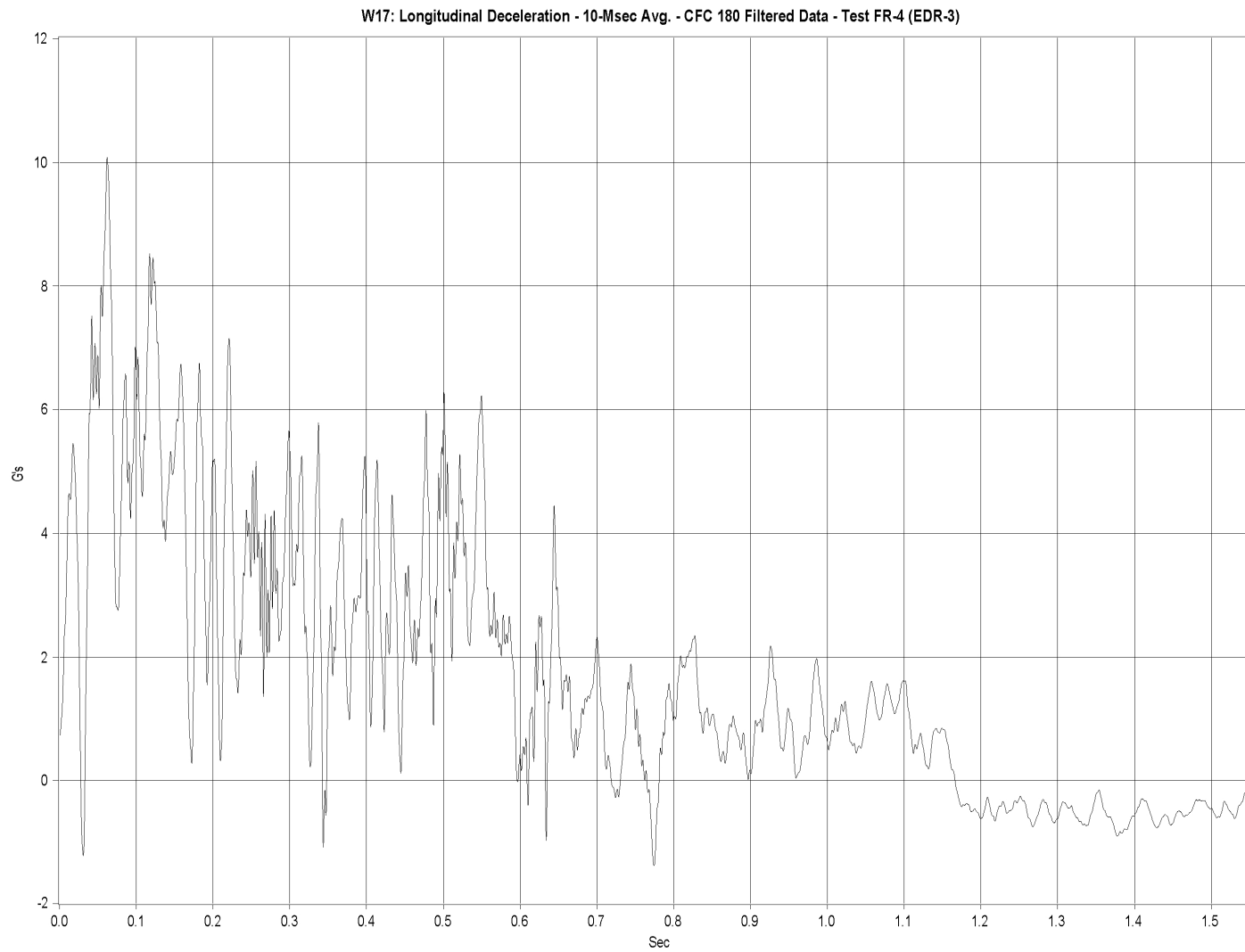


Figure L-1. Graph of Longitudinal Deceleration, Test FR-4

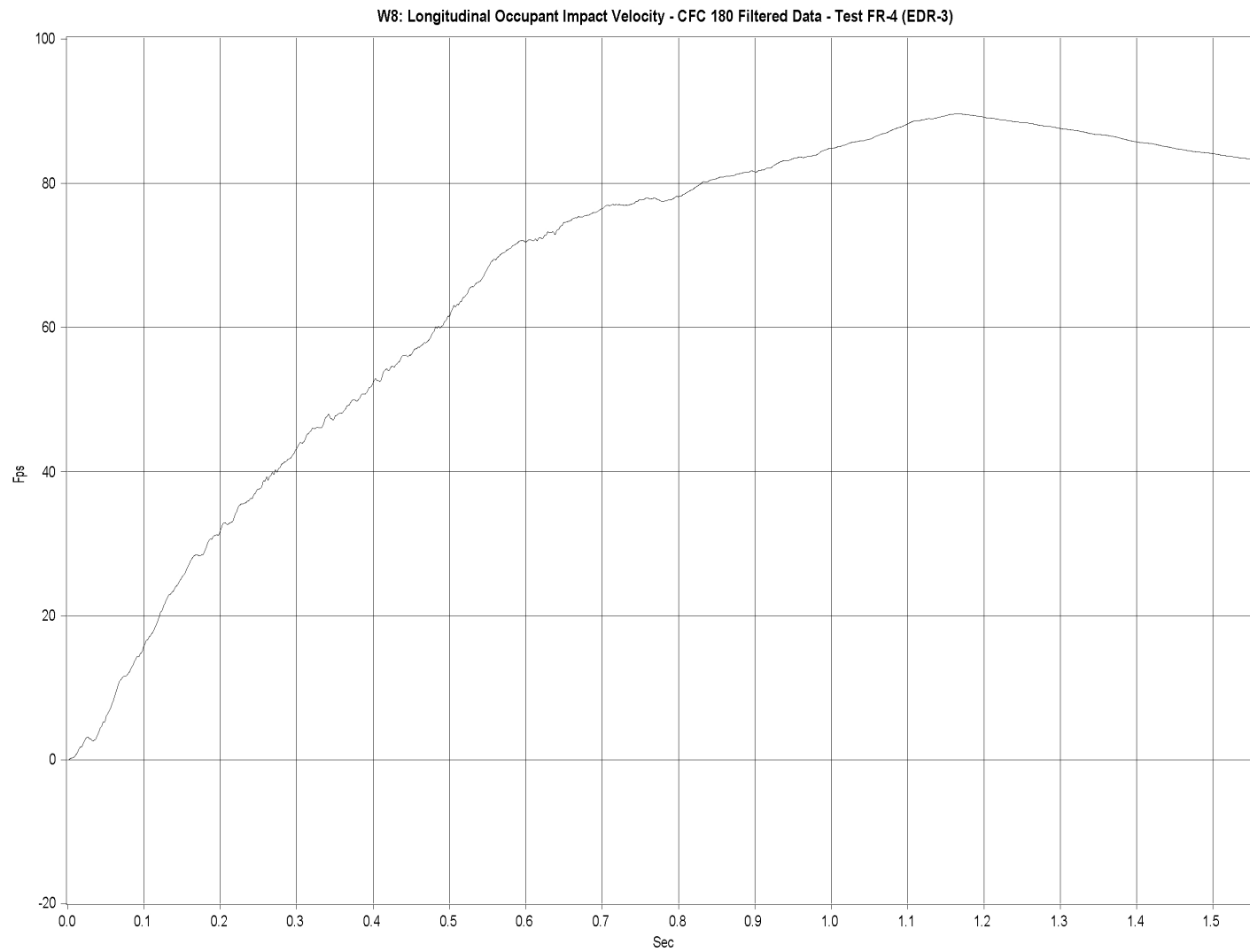


Figure L-2. Graph of Longitudinal Occupant Impact Velocity (OIV), Test FR-4

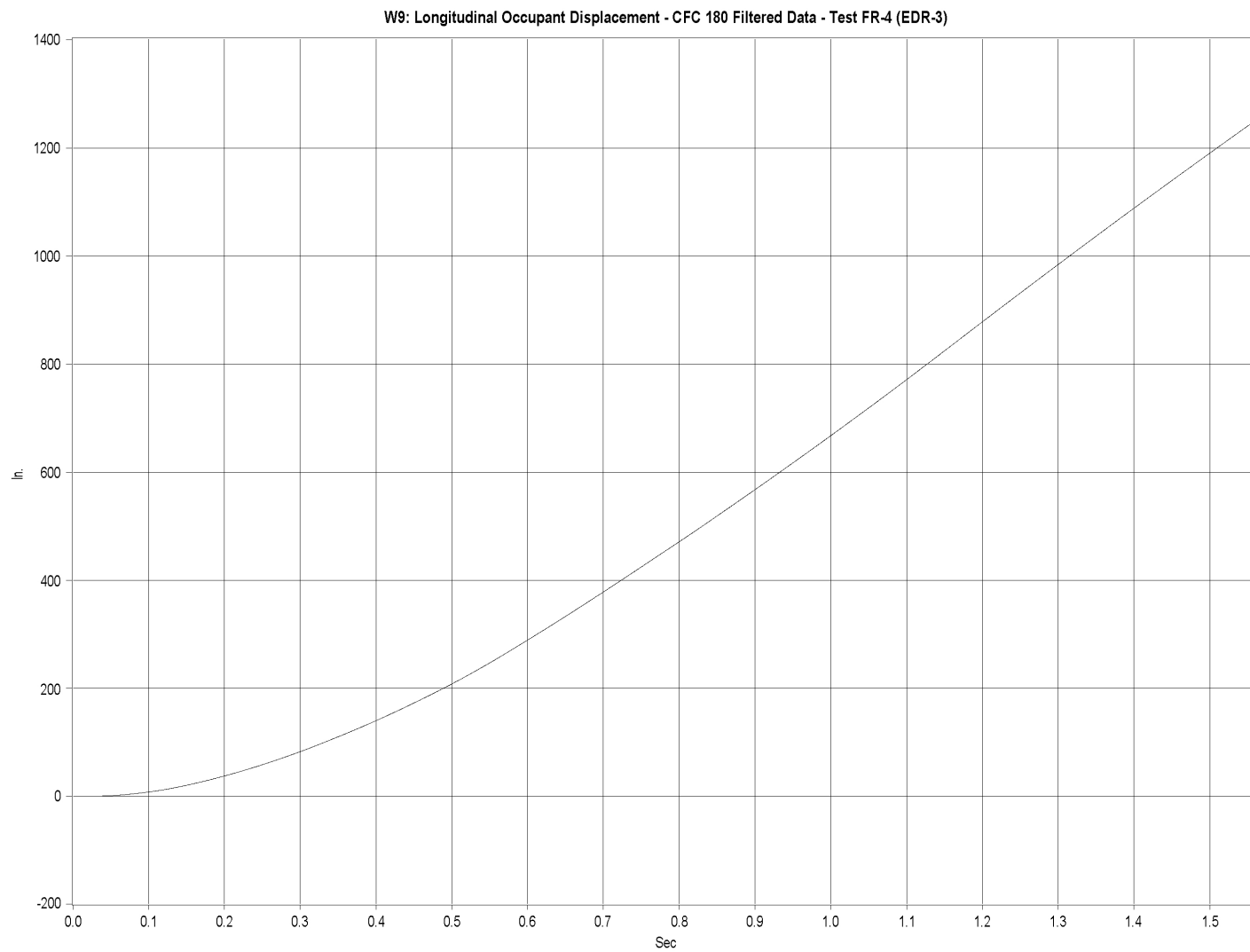


Figure L-3. Graph of Longitudinal Occupant Displacement, Test FR-4

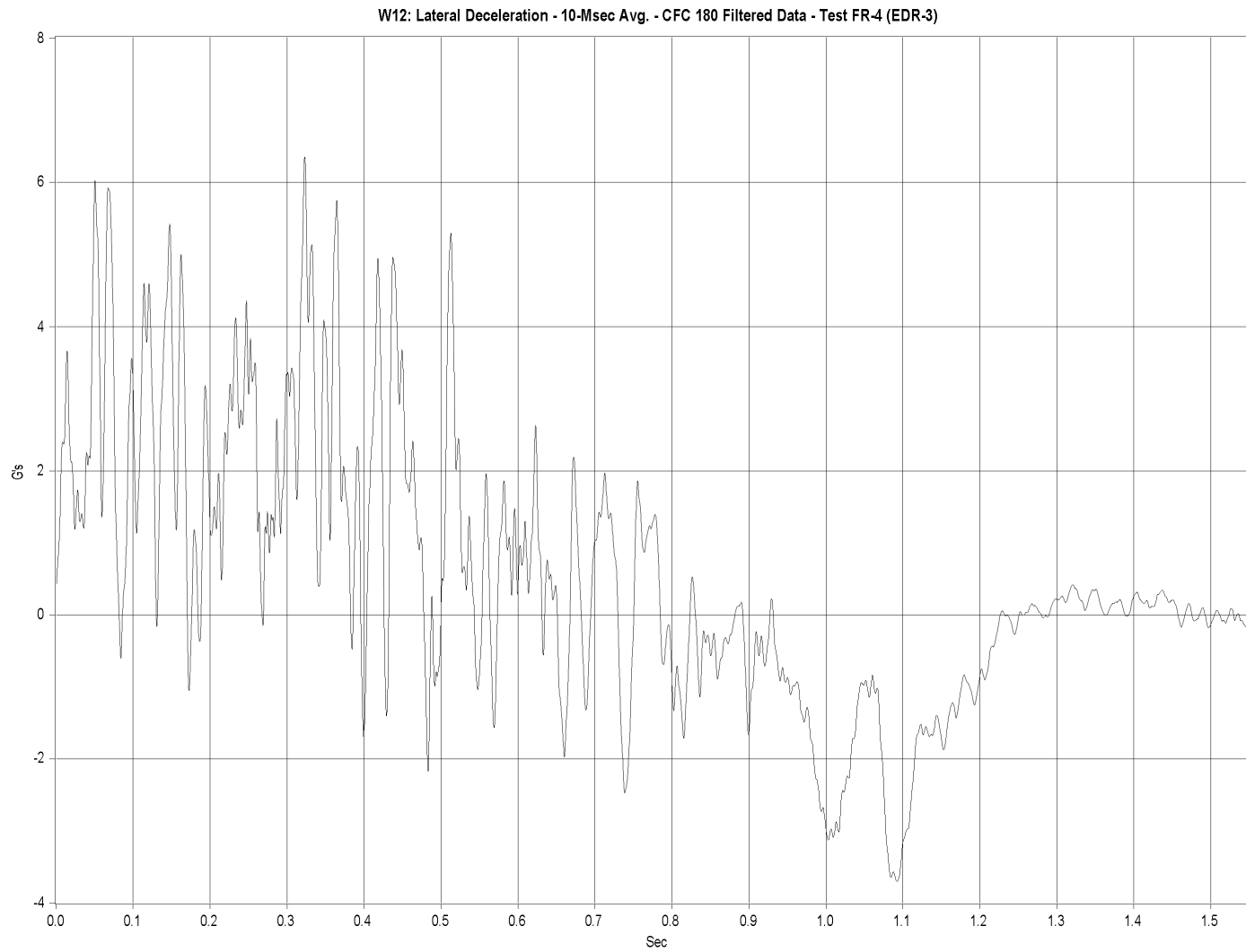


Figure L-4. Graph of Lateral Deceleration, Test FR-4

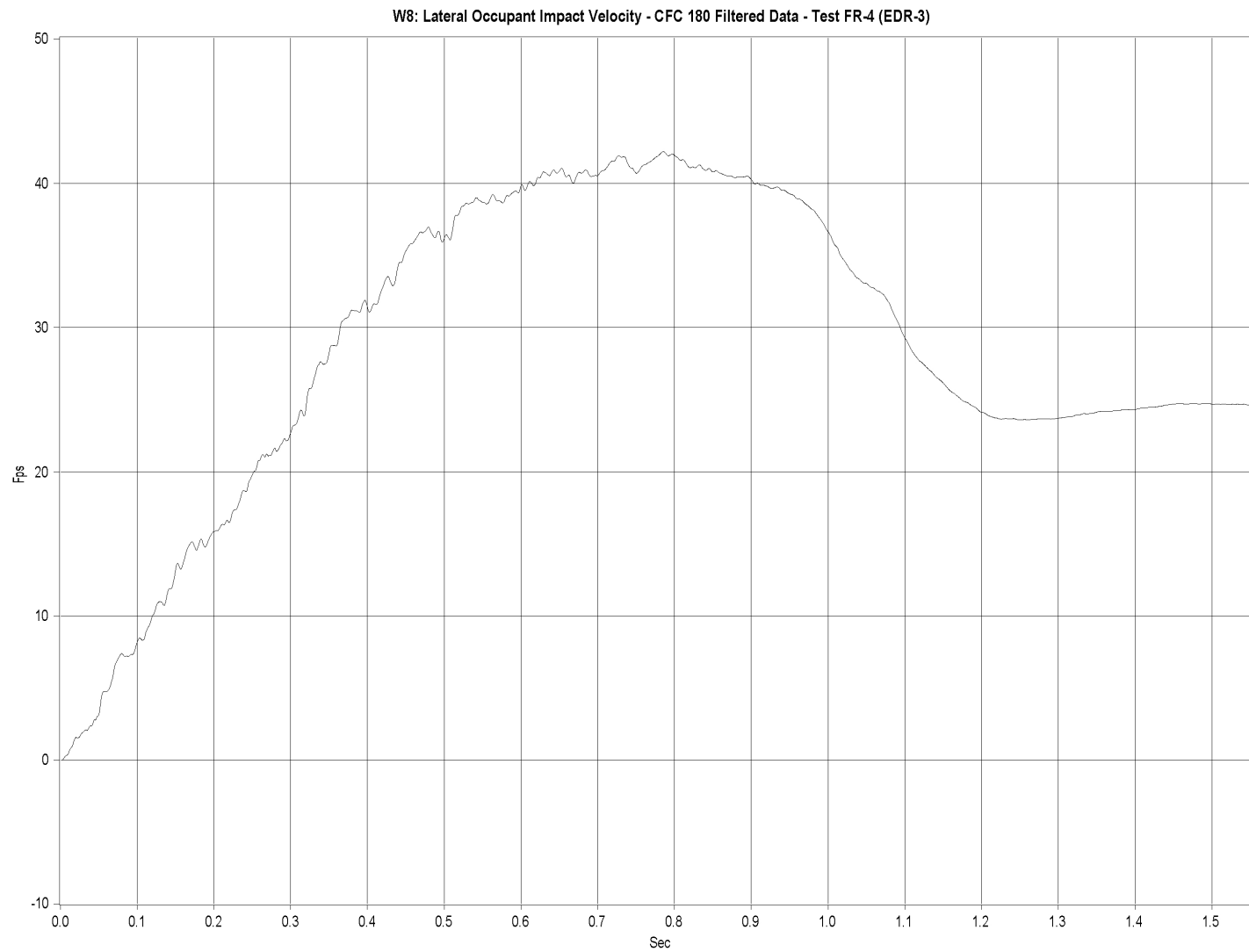


Figure L-5. Graph of Lateral Occupant Impact Velocity (OIV), Test FR-4

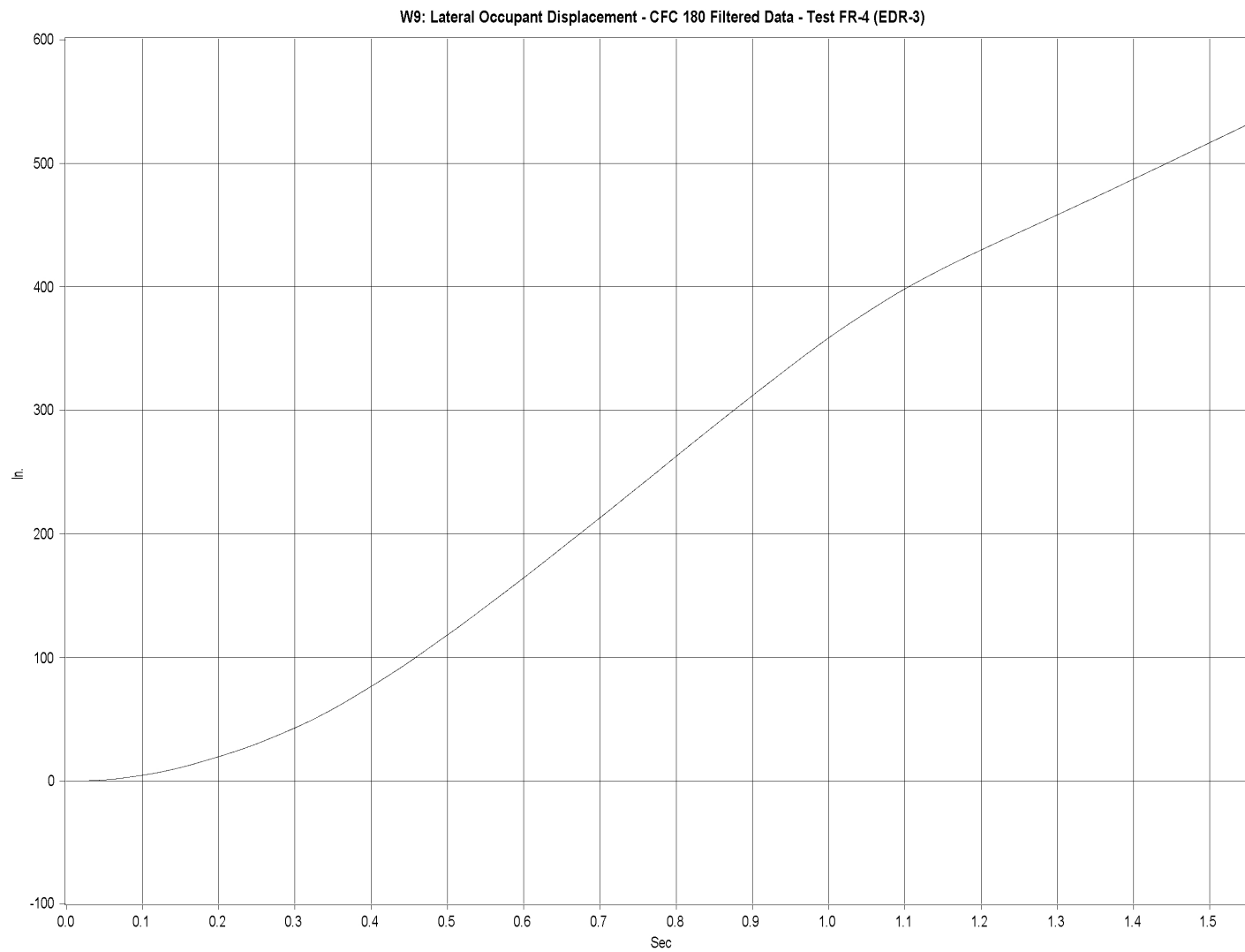


Figure L-6. Graph of Lateral Occupant Displacement, Test FR-4

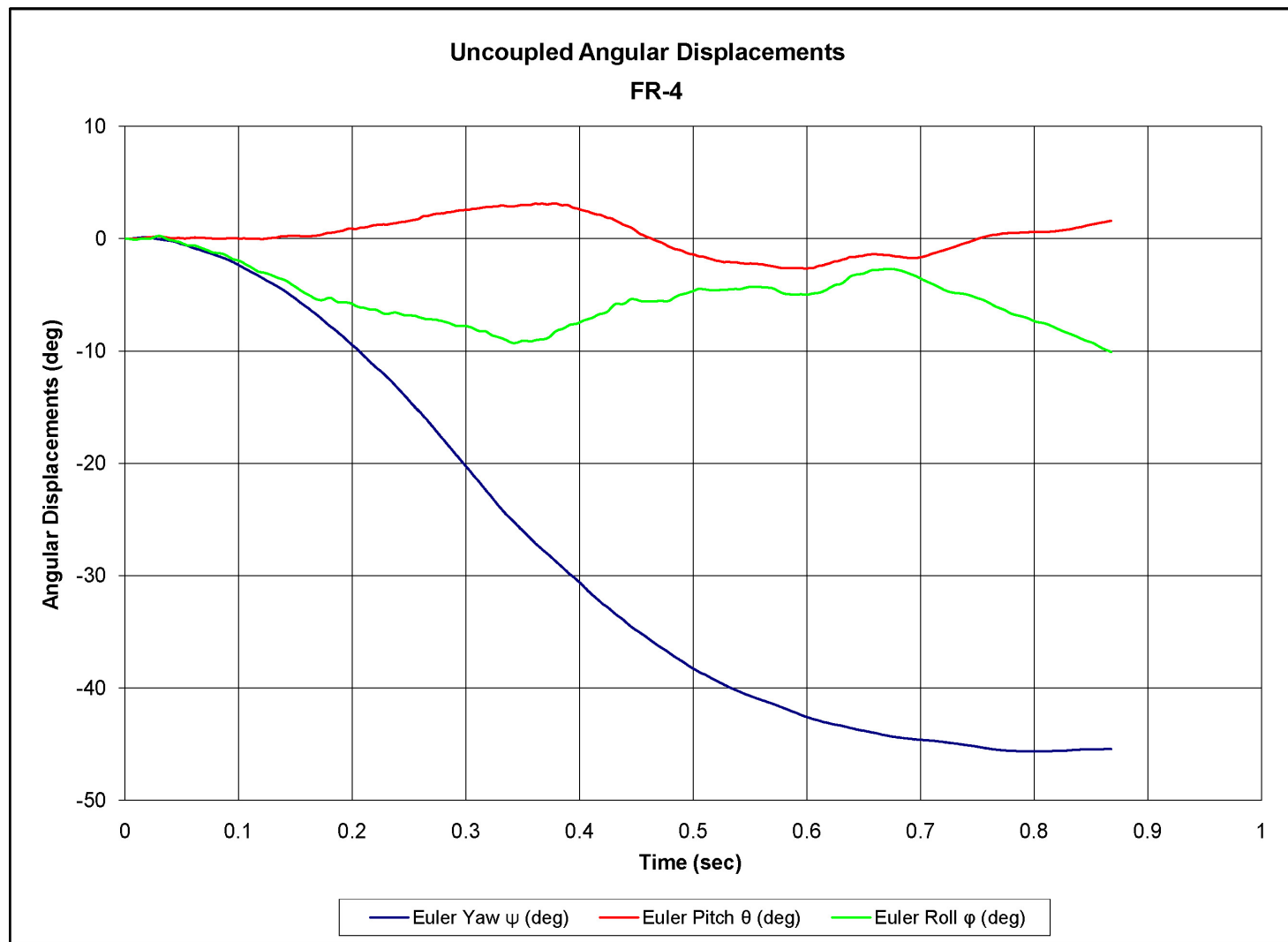


Figure L-7. Graph of Roll, Pitch, and Yaw Angular Displacements, Test FR-4

APPENDIX M

OCCUPANT COMPARTMENT DEFORMATION DATA, TEST FR-5

Figure M-1. Occupant Compartment Deformation Index (OCDI), Test FR-5

Occupant Compartment Deformation Index (OCDI)

Test No. FR-5
Vehicle Type: 1998 chevy metro 2dr

OCDI = XXABCDEFGHI

XX = location of occupant compartment deformation

A = distance between the dashboard and a reference point at the rear of the occupant compartment, such as the top of the rear seat or the rear of the cab on a pickup

B = distance between the roof and the floor panel

C = distance between a reference point at the rear of the occupant compartment and the motor panel

D = distance between the lower dashboard and the floor panel

E = interior width

F = distance between the lower edge of right window and the upper edge of left window

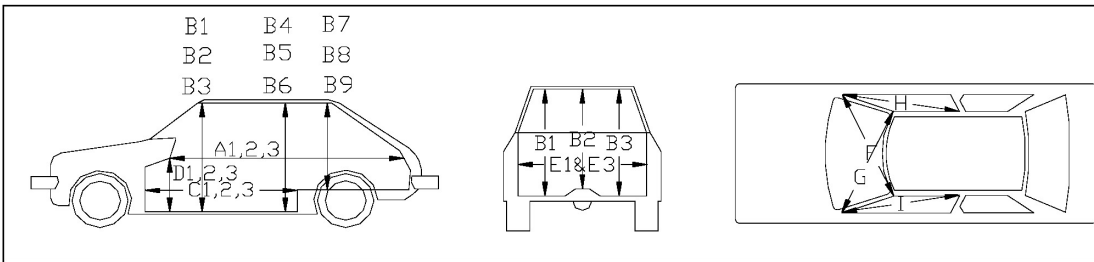
G = distance between the lower edge of left window and the upper edge of right window

H = distance between bottom front corner and top rear corner of the passenger side window

I = distance between bottom front corner and top rear corner of the driver side window

Severity Indices

- 0 - if the reduction is less than 3%
- 1 - if the reduction is greater than 3% and less than or equal to 10 %
- 2 - if the reduction is greater than 10% and less than or equal to 20 %
- 3 - if the reduction is greater than 20% and less than or equal to 30 %
- 4 - if the reduction is greater than 30% and less than or equal to 40 %



where,
 1 = Passenger Side
 2 = Middle
 3 = Driver Side

Location:

Measurement	Pre-Test (in.)	Post-Test (in.)	Change (in.)	% Difference	Severity Index
A1	48.50	48.75	0.25	0.52	0
A2	49.25	49.00	-0.25	-0.51	0
A3	50.25	50.25	0.00	0.00	0
B1	40.75	40.50	-0.25	-0.61	0
B2	38.00	37.75	-0.25	-0.66	0
B3	40.00	40.25	0.25	0.63	0
C1	56.50	56.75	0.25	0.44	0
C2	61.25	61.25	0.00	0.00	0
C3	56.75	55.25	-1.50	-2.64	0
D1	17.50	17.50	0.00	0.00	0
D2	9.50	9.50	0.00	0.00	0
D3	18.00	18.00	0.00	0.00	0
E1	49.75	48.75	-1.00	-2.01	0
E3	50.75	50.75	0.00	0.00	0
F	48.50	48.50	0.00	0.00	0
G	48.25	48.00	-0.25	-0.52	0
H	37.75	37.75	0.00	0.00	0
I	36.50	36.50	0.00	0.00	0

[Note: Maximum severity index for each variable (A-I) is used for determination of final OCDI value]

Final OCDI: XX A B C D E F G H I
 0 0 0 0 0 0 0 0 0

Figure M-1. Occupant Compartment Deformation Index (OCDI), Test FR-5

APPENDIX N

ACCELEROMETER AND RATE TRANSDUCER DATA ANALYSIS, TEST FR-5

- Figure N-1. Graph of Longitudinal Deceleration, Test FR-5
- Figure N-2. Graph of Longitudinal Occupant Impact Velocity (OIV), Test FR-5
- Figure N-3. Graph of Longitudinal Occupant Displacement, Test FR-5
- Figure N-4. Graph of Lateral Deceleration, Test FR-5
- Figure N-5. Graph of Lateral Occupant Impact Velocity (OIV), Test FR-5
- Figure N-6. Graph of Lateral Occupant Displacement, Test FR-5
- Figure N-7. Graph of Roll and Yaw Angular Displacements, Test FR-5

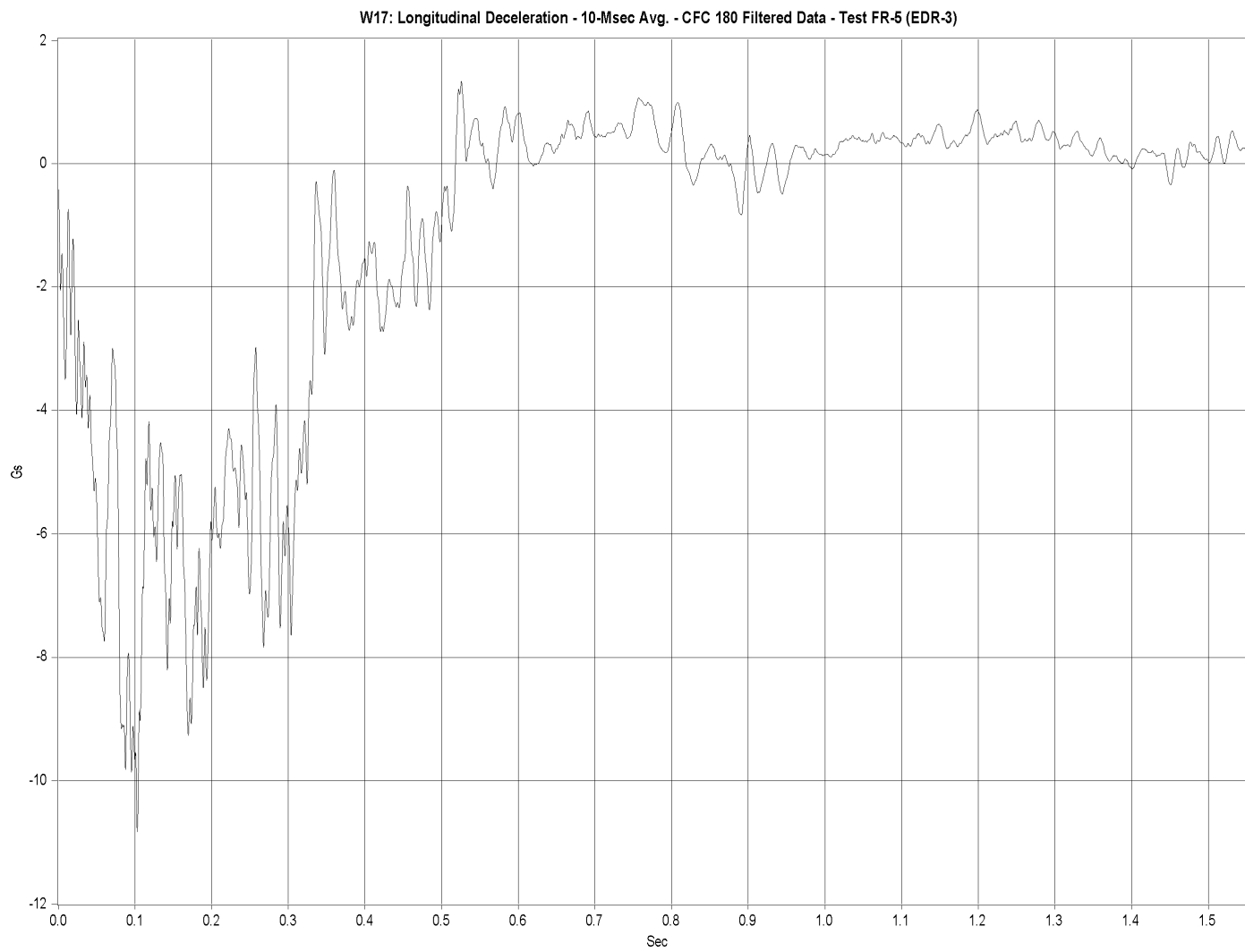


Figure N-1. Graph of Longitudinal Deceleration, Test FR-5

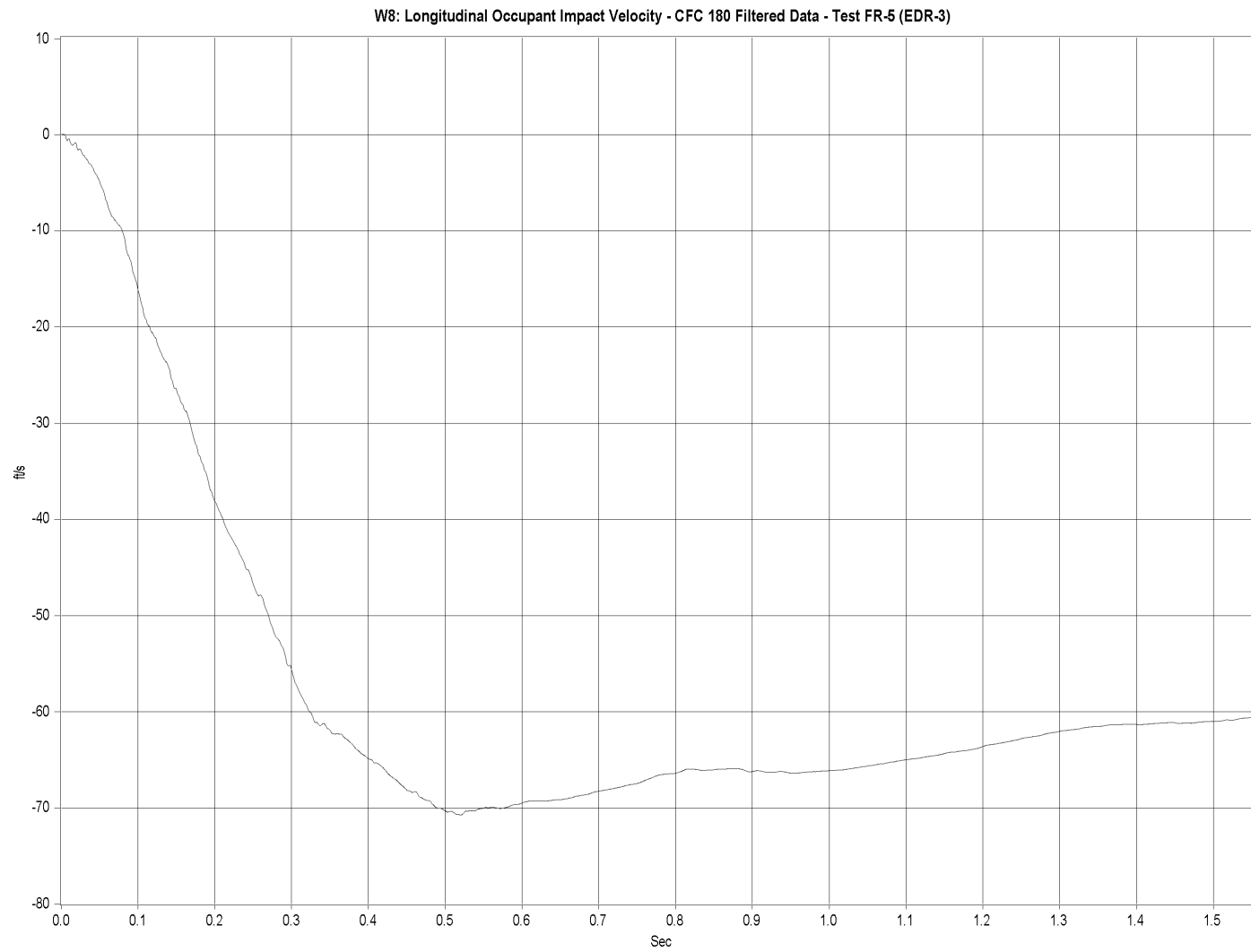


Figure N-2. Graph of Longitudinal Occupant Impact Velocity (OIV), Test FR-5

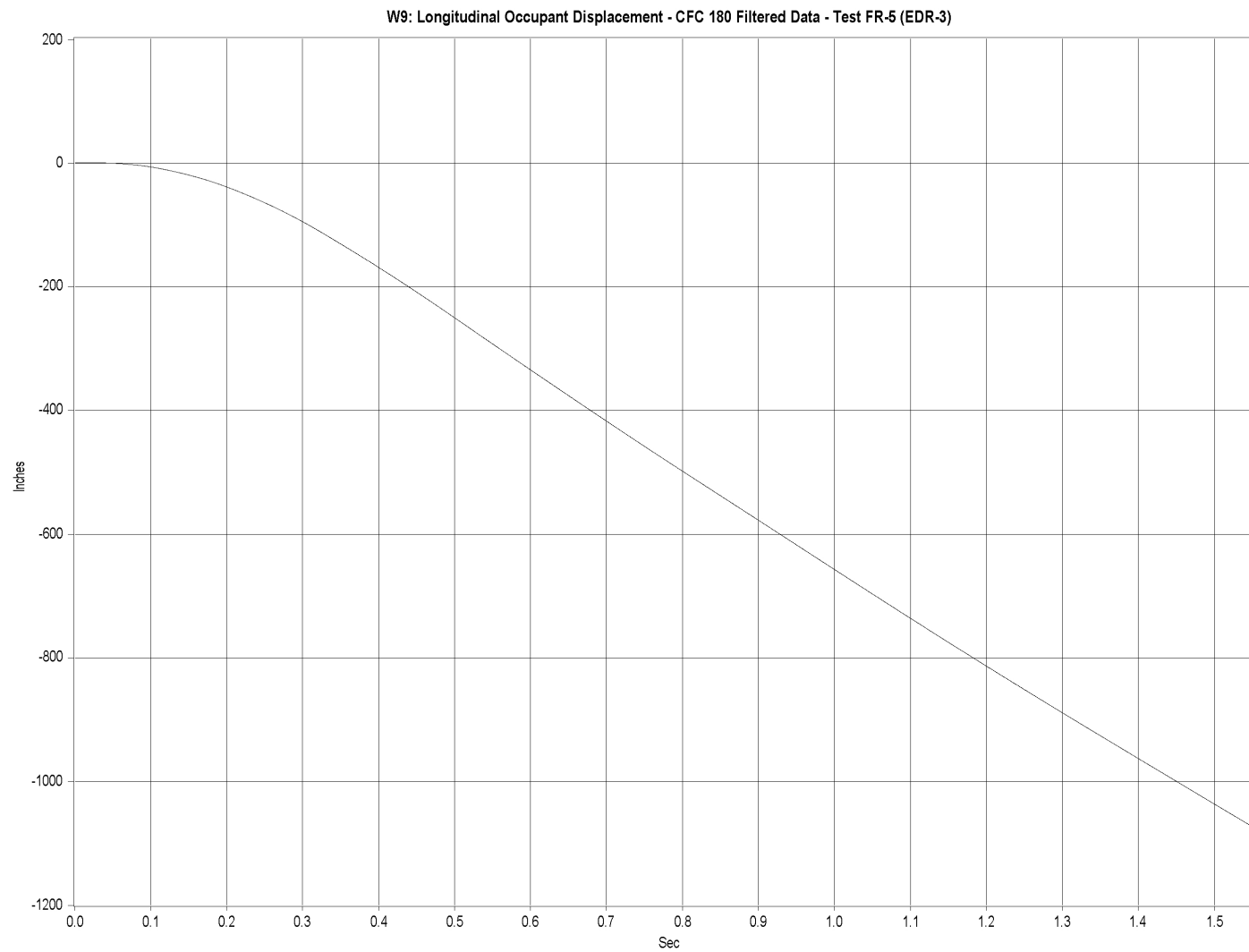


Figure N-3. Graph of Longitudinal Occupant Displacement, Test FR-5

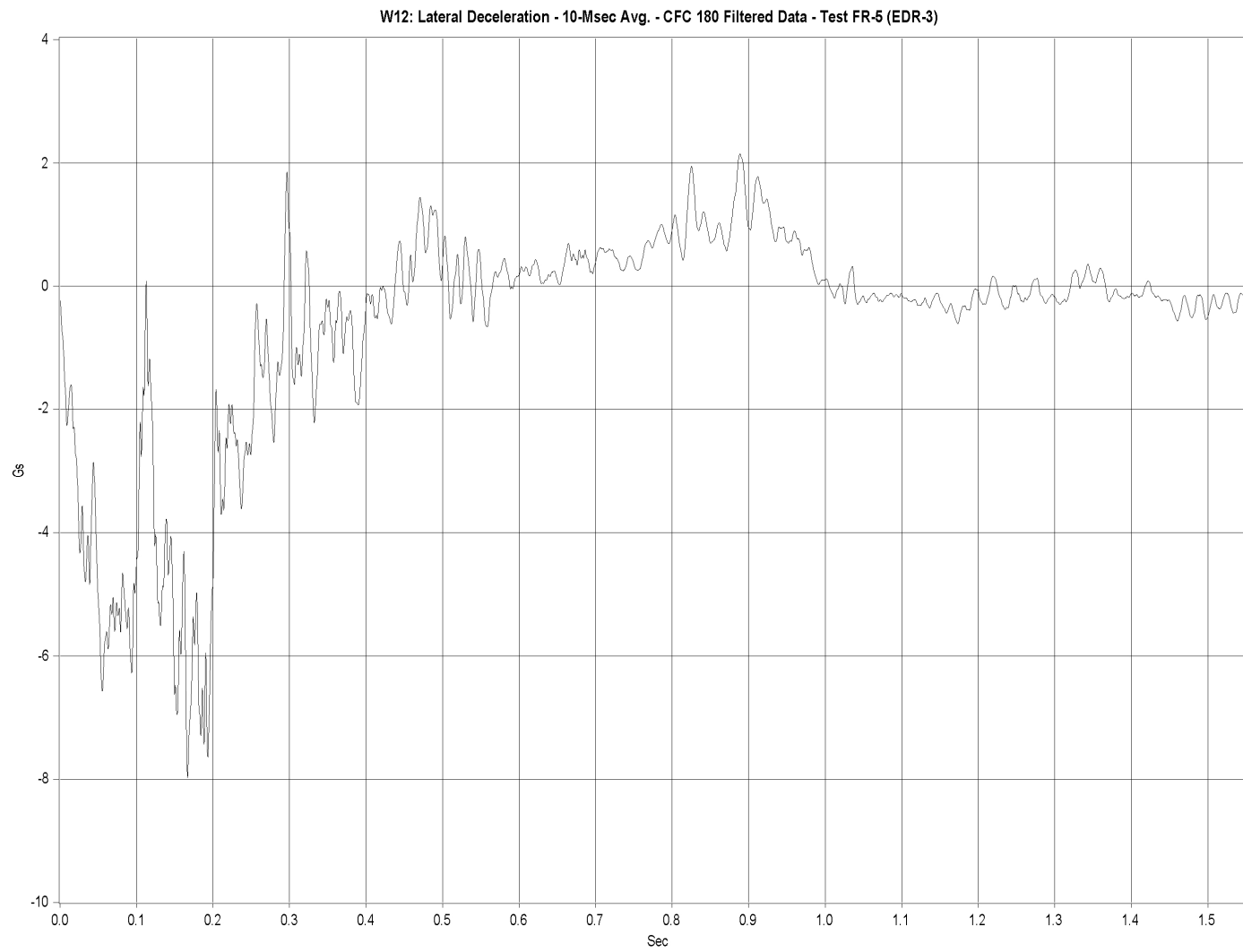


Figure N-4. Graph of Lateral Deceleration, Test FR-5

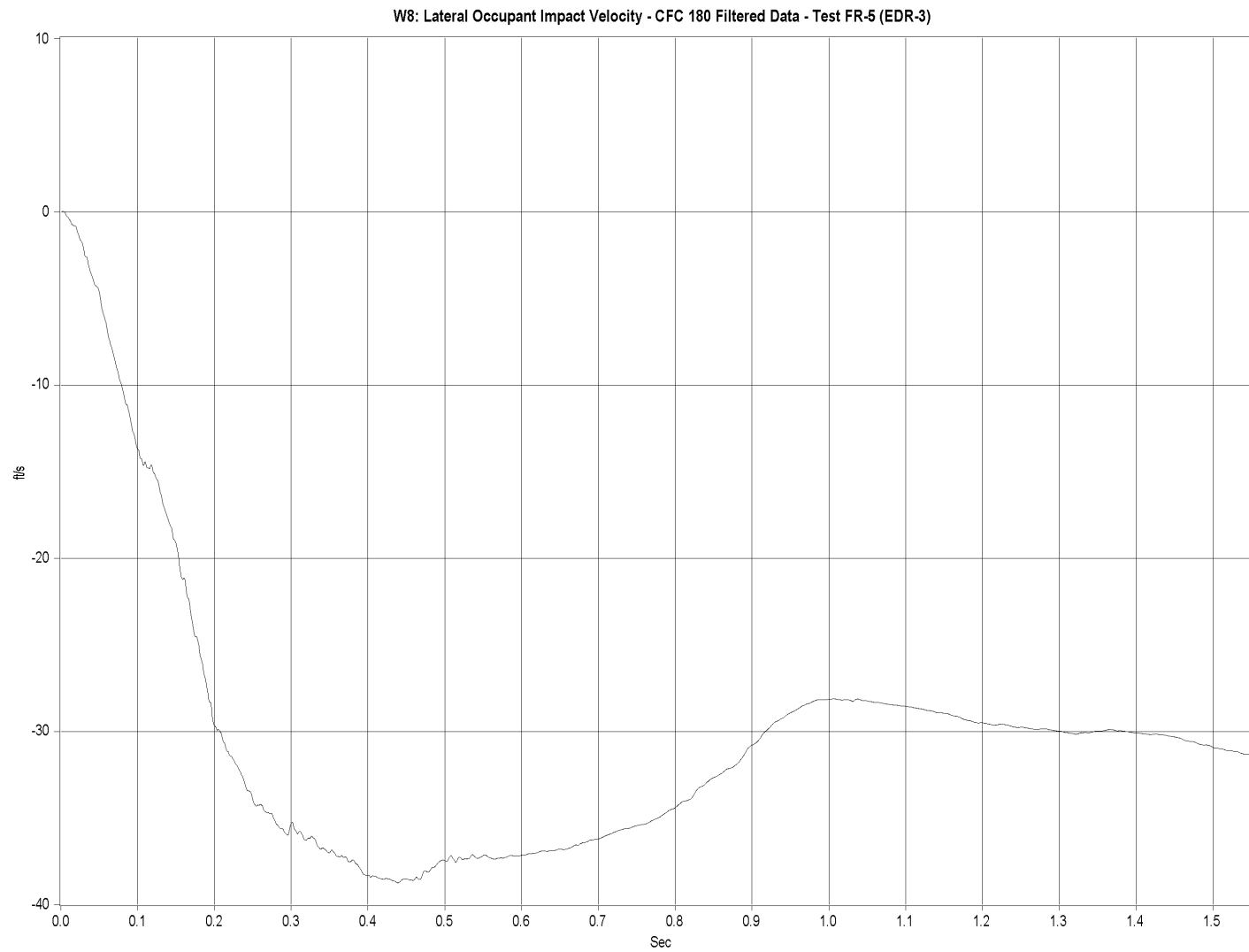


Figure N-5. Graph of Lateral Occupant Impact Velocity (OIV), Test FR-5

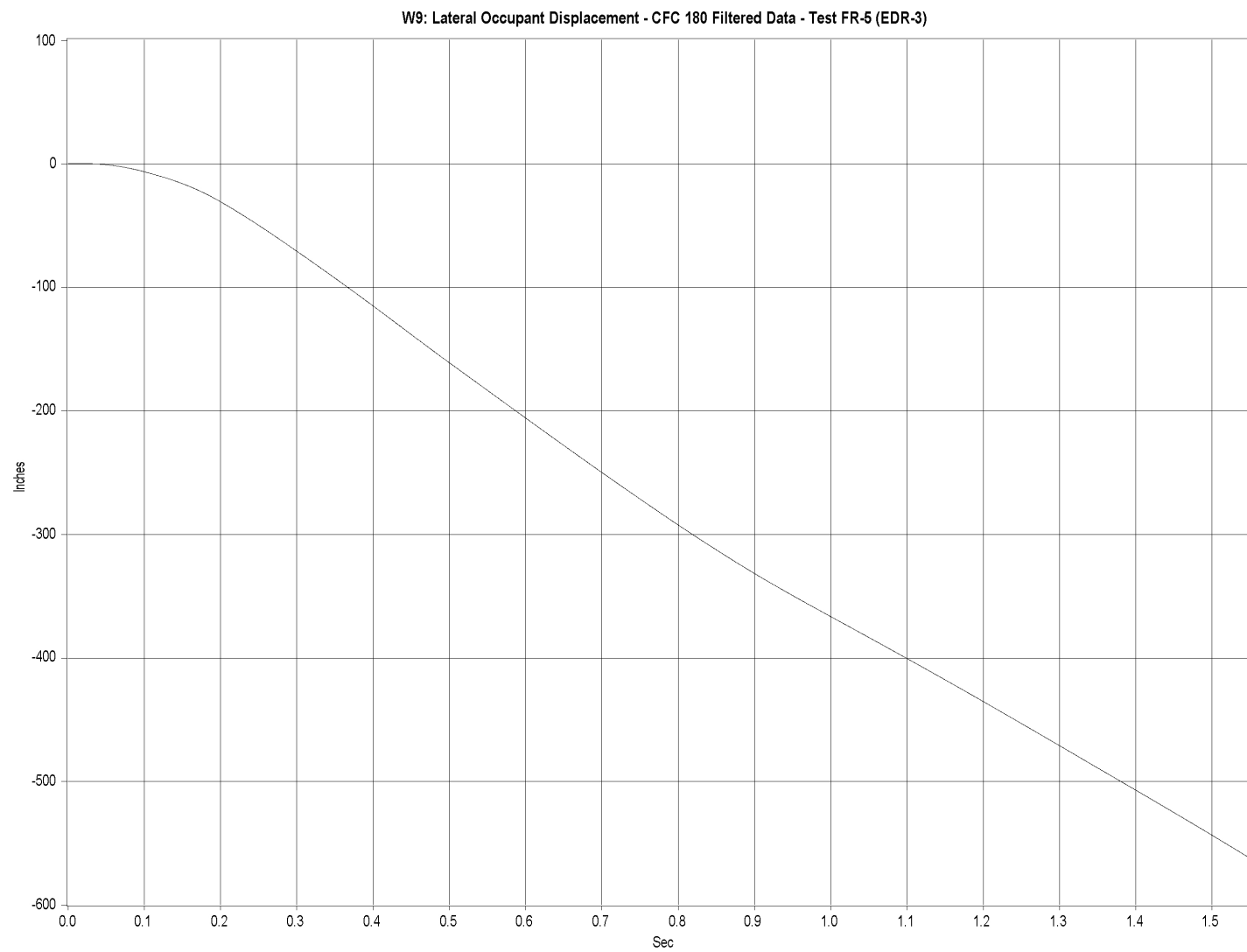


Figure N-6. Graph of Lateral Occupant Displacement, Test FR-5

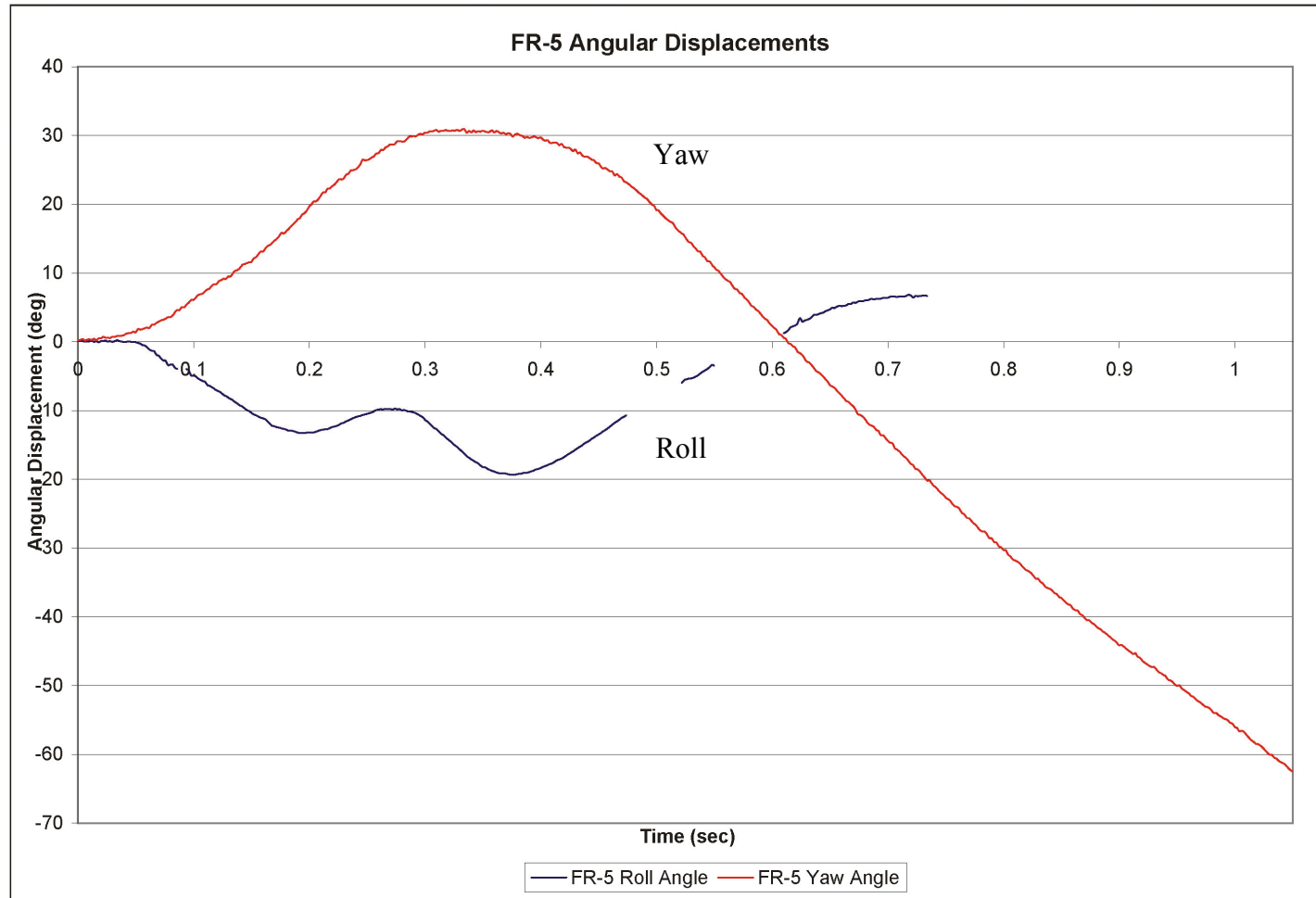


Figure N-7. Graph of Roll and Yaw Angular Displacements, Test FR-5